

Evaluation and Model Development

Grass Erosion Test at the Rhine dike

Andre van Hoven
Henk Verheij
Gijs Hoffmans
Jentsje van der Meer



1207811-002

Titel
Evaluation and Model Development

Opdrachtgever RWS	Project 1207811-002	Kenmerk 1207811-002-HYE-0007- svb	Pagina's 137
-----------------------------	-------------------------------	--	------------------------

Trefwoorden
Dikes (Rivierenland), Grass erosion, Transitions/objects, Wave overtopping and run-up

Samenvatting
This report deals with an evaluation of experimental tests at two locations Nijmegen and Millingen aan de Rijn. Models are here further developed to predict the consequences of wave overtopping on the strength of landward slopes. Also relations are established for estimating the effects of wave run-up on outer slopes.

Measured flow velocities and flow depths on a landward slope due to overtopping waves are discussed in relation to the steady state theory of overflow. The flow velocities accelerate from the crest to the toe of the dike and are calculated adequately provided the friction factor is relatively small (i.e. $f = 0.01$). Although the computed flow depths are too small they are not needed as the cumulative overload method depends on flow velocities and critical flow velocities.

The cumulative overload method is an erosion model based on the force balance in which load and strength are represented through velocities. The load of the waves is expressed by an empirical relation and predicts the flow velocities reasonable for a steepness of 1V:3H. The strength is modelled by the turf-element model.

The cumulative overload method is extended with a load factor to simulate the erosion at transitions and vertical objects. The load factor represents the load increase or the load decrease. Conceptual models are developed and evaluated by using experimental data obtained from prototype dikes. The cumulative overload method is also modified with a strength factor to model strength changes at edges.

The cumulative overload method assumes that damage will occur also for wave run-up only, if the velocities of wave run-up are high enough. This is the situation for sea dikes where the impact zone is protected with a hard revetment and large wave run-up may be expected above the impact zone. This report validates the cumulative overload method for wave run-up.

Pluto calculations, dynamic load tests and pressure measurements in the field are performed to evaluate the turf-element model. Experimental results show that the load penetration in the subsoil is very fast. Therefore, the starting points used in the turf-element model are adequately, that is, the load acts on the top of the grass sods and not on the side walls.

Turf tensile tests are carried out to evaluate the turf-element model. These experiments show that the critical tensile force occurs directly after deformations of 5 mm to 15 mm. This relation between force and deformation is used to estimate the grass strength on the landward slope. The fatigue strength is estimated by rule of thumbs.

At present the flow velocities on the landward slope can be predicted satisfactory with the theories. The prediction of the flow depths could be improved if the effects of air are included in the steady state theory. The cumulative overload method can be used for estimating the

Titel
Evaluation and Model Development

Opdrachtgever
RWS

Project
1207811-002

Kenmerk
1207811-002-HYE-0007-
svb

Pagina's
137

erosion growth on both landward slopes and seaward slopes. The critical flow velocity of grass revetments can be calculated with the turf-element provided the parameters are specified adequately.

Although different load factors are deduced for describing the strength changes at transitions and near obstacles these engineering tools should be validated by experiments/observations collected from the past few years and reported in the various SBW-WTI reports (period 2007 – 2013).

A 'quick and dirty' analysis is carried out to approximate the fatigue strength of grass revetments. It is needed to validate these first estimations in relation to the available experimental data.

It is recommended to study both the mean bed shear stress and the bed turbulence with for example the model Open Foam to validate the load on the landward slope. If the mean bed shear stress increases in the streamwise direction more erosion is expected halfway the slope and near the toe of the dike. The critical mean bed shear stress represents the resistance against erosion and depends on the soil properties only. However, if the strength is expressed by a critical flow velocity then U_c could be influenced by the bed turbulence. These computations should give insight in the load-strength interaction.

Versie	Datum	Auteur	Paraaf	Review	Paraaf	Goedkeuring	Paraaf
1	nov. 2013	Gijs Hoffmans		Mark Klein Breteler		Leo Voogt	
		Andre van Hoven					
		Henk Verheij					
		Jentsje van der Meer					
2	Dec 2013	Gijs Hoffmans		Mark Klein Bretelet		Leo Voogt	

Status
concept

Dit document is een concept en uitsluitend bedoeld voor discussiedoeleinden. Aan de inhoud van dit rapport kunnen noch door de opdrachtgever, noch door derden rechten worden ontleend.

Contents

1 Introduction	1
1.1 General	1
1.2 Readers guidance	2
2 Overview of erosion model	5
2.1 Introduction	5
2.2 Cumulative overload model	5
2.3 Flow velocity	5
2.4 Critical flow velocity	7
2.5 Load factor	8
2.6 Strength factor	10
2.7 Summary	12
3 Evaluation wave overtopping tests Nijmegen and Millingen	13
3.1 Introduction	13
3.2 Predictions	13
3.3 Measurements	14
3.4 Analysis of the critical flow velocity	16
3.5 Conclusions	20
4 Hydraulic load on the landward slope	25
4.1 Introduction	25
4.2 Flow velocity and flow thickness measurements	27
4.3 Load penetration in turf	38
4.4 Transitions and objects	46
4.5 Conclusions	60
5 Hydraulic load on the seaward slope	63
5.1 Introduction and objective	63
5.2 Overload method for run-up versus guidelines for wave impacts	65
5.3 Overload method for run-up against Delta flume tests	69
5.4 Conclusions	70
6 Erodibility of turf	71
6.1 Introduction	71
6.2 Grass strength	71
6.3 Turf-tensile tests	73
6.4 Deformations	75
6.5 Force transmission	77
6.6 Fatigue strength	77
6.7 Conclusion	81
7 Conclusions and recommendations	83
8 Relevant symbols	89
9 References	91

- Appendix A Load parameters on the dike**
 - Predictions of flow thickness and flow velocity
 - Measurements and data processing
 - Experimental results of flow thickness and flow velocity

- Appendix B Grass properties**
 - Introduction
 - Sample preparation
 - Dynamic load tests
 - Permeability tests
 - Pore pressure response
 - Symbols and references

- Appendix C Load factor at revetment transitions**
 - Introduction
 - Current over smooth and rough strip beds
 - Analysis
 - Symbols and references

- Appendix D Load factor at geometrical transitions**
 - Introduction
 - Analysis
 - Symbols and references

- Appendix F Pressure measurements**

- Appendix G Turf-tensile tests**

1 Introduction

1.1 General

In the Netherlands, primary sea and flood defences along the coast and inland waters have to be assessed periodically. Although developments were realised in the past few years, still knowledge gaps are unsolved. The WTI-2017 program (“Statutory Safety Assessment to Water Defences”) aims to improve the assessment tools in order to achieve a better estimate of the safety of the hinterland. The program is funded by the Dutch Ministry of Environment and Infrastructure, delegated to the Rijkswaterstaat (WVL) and, again, delegated to Deltares.

One of the projects within the WTI program is the project “Wave Overtopping and Grass Revetment Stability”. In the planning 2012/2013 research activities were defined that should result in an upgrading of the guidelines for wave overtopping, grass and asphalt revetment. The latest developments about the erodibility of grass revetments and the effects of transitions and vertical objects are here discussed.

At the start of the WTI program in 2007 a project group (consisting of Deltares, Van der Meer Consulting, Infram and Alterra) was initiated to answer several research questions regarding the grass cover strength in case of wave overtopping. Tests were carried out with the wave overtopping simulator on several Dutch and Belgium dikes in the winter season. A closed grass sod proved to be very resilient against the erosive forces of massive wave overtopping volumes, whereas rough herbal growth and open patches can make grass sods vulnerable to erosion, see also RWS 2012 where the research results are summarized.

The research in the period 2007-2012 was not unambiguous on the effect of vertical objects and transitions in the slope geometry and transitions from a grass cover to other (hard) revetment types. Also the wave run-up zone was not yet covered. The report at hand starts a next research period which will continue until 2015 and where the aim will be to incorporate the aspects as noted above.

Erosion of grass sods occurs owing to pressure gradients inside the sod. In case of wave overtopping, the water volumes give a highly turbulent flow over the slope surface, generating pressure fluctuations. The pressure fluctuations are transmitted, damped and delayed, into the soil below the slope surface. The differences between the pressure-fluctuations at the slope surface and at some depth result in pressure gradients. An accurate prediction method for outward directed pressure gradients will help to model grass erosion on a slope, but also at transitions to other types of revetments and structures or other objects.

The research questions concerning grass erosion are approached in a cyclic way (Fig. 1.1; www.thesis.nl/kolb). The current report ‘Evaluation and Model development’ aims to describe the state of the art models and ways to enhance insight in the process of erosion of grass at objects and transitions. Moreover, the predictions and the measurements of the tests carried out in Nijmegen and Millingen aan de Rijn are evaluated. The next step will be to implement the models in software codes to be used in the WTI-2017 program.

As this report is written in the English language also foreign researchers are welcomed to analyze/use the research results generated within the WTI-2017 program and to contact Deltares or Rijkswaterstaat. Interaction and feedback on the use of the results are much appreciated. It must be noted that the prediction models and experiences obtained by the

prototype tests with the wave overtopping simulator are based on the Dutch and Belgium circumstances, grasses and substrates. Grasses and substrate can be very similar in the wider region; however, they can also differ.

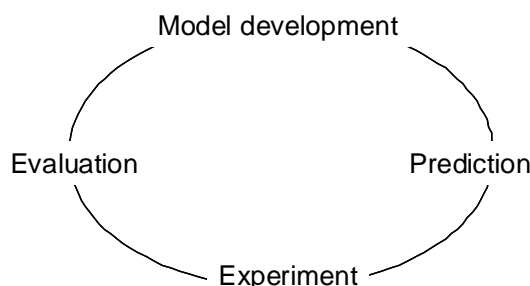


Figure 1.1 Cyclic research approach

1.2 Readers guidance

The report at hand contains the ‘evaluation’ and ‘model development’ steps in the cyclic research approach. The following aspects about erosion of grass are covered by the report.

- The overload method is a model for predicting the erodibility of grass revetments. **Chapter 2** discusses the latest developments about the load factor which represents the increase of the load at transitions or at vertical objects on dikes. The load factor multiplies the depth averaged maximum velocity during a wave overtopping event, in the case of an object in the grass cover, or a geometrical transition from slope to horizontal.
- **Chapter 3** presents a brief overview of the predicted values of both the critical depth-averaged flow velocity and the load factors related to different transitions and obstacles. These predictions refer to the prototype experiments conducted in Nijmegen and Millingen aan de Rijn during the winter 2012-2013. By using both the overload method and observations the critical flow velocities are calculated for all tests and evaluated with the predicted ones. Also qualitative conclusions are drawn about the predicted load factors in relation to the observed erosion near transitions and obstacles.
- Flow velocities and flow thicknesses on the crest and on the landward slope were measured and evaluated with theories (**Chapter 4**). Chapter 4 also argues the load penetration in the sub soil due to bed turbulence in order to validate the assumptions in the turf-element model. Tested samples were taken from a dike along the river Rhine near Millingen to determine soil parameters. During overtopping tests pressures on top and below the slope surface were measured to validate the outcome of the consolidation analyses. Engineering approaches for the load factor are discussed and evaluated with prototype data of revetment transitions, geometrical transitions and vertical objects at prototype scale.
- The cumulative overload method has been applied to wave run-up. This method assumes that damage will occur also for wave run-up only, if the velocities of wave run-up are high enough. This is the situation for sea dikes where the impact zone is protected with a hard revetment and large wave run-up may be expected above the impact zone. **Chapter 5** validates the cumulative overload method for wave run-up.

- The grass sod tensile strength was determined directly by conducting experiments with a developed tensile test device. The strength parameter in the erosion model represents a critical flow velocity. A relation between the critical flow velocity and grass parameters was not yet established. Determining the tensile strength directly from the field and connecting the load parameter (flow velocity) to pressure gradients over the grass sod can yield a better understanding of the critical flow velocity and to an improvement of the modelling. This approach also opens the way to model the effect of transitions and objects in the grass cover. **Chapter 6** describes the latest developments about the strength of grass.
- Each of the chapters ends with conclusions; they are summarized in **chapter 7**.

2 Overview of erosion model

2.1 Introduction

Surface erosion is erosion of fines from the top layer whereas block erosion represents erosion of turf (or grass sods). The initiation of erosion can be approximated by different models. Dean et al (2010) developed an erosion approach by using the energy balance, that is, work above a critical value. The block erosion model is based on the shear stress concept as proposed by Grass (1970) and semi-empirical equations deduced from the systematic research on scour carried out by Deltares in 1960s and 1970s. Van der Meer et al (2010) applied the force balance to express the erosion on the inner slope of dikes. As these three models are all based on physical backgrounds they yield similar results (Hoffmans 2012).

This Chapter discusses the cumulative overload method and the extensions to represent a load increase (or load decrease), for example, due to transitions and a strength reduction, for instance, at edges.

2.2 Cumulative overload model

The force balance (force is proportional to U^2) is used which can be written as (also known as the cumulative overload method)

$$\sum_{i=1}^N (U_i^2 - U_c^2) = D \quad \text{for } U_i > U_c \quad (2.1)$$

where

initial damage	$D < 500 \text{ m}^2/\text{s}^2$
damage at various locations	$500 \text{ m}^2/\text{s}^2 < D < 1500 \text{ m}^2/\text{s}^2$
dike failure	$D > 3500 \text{ m}^2/\text{s}^2$

in which D is the damage number (Fig. 2.1), U_i is the representative flow velocity of the overtopping wave (Section 2.3), U_c is the critical (depth-averaged) flow velocity (Section 2.4), N is the number of the waves in which $U_i > U_c$. The damage number is determined by considering the number of waves and the flow velocities of the largest wave volumes as well as from observations after the hydraulic measurements.

To include the effects of transitions and obstacles on dikes Eq. 2.1 is modified

$$\sum_{i=1}^N (\alpha_M U_{i,crest}^2 - \alpha_s U_c^2) = D \quad \text{for } U_i > U_c \quad (2.2)$$

where α_M is the load factor (Section 2.5) and α_s is the strength factor (Section 2.6). The first term on the left side is a measure for the load and the second term represents the measure for strength. Equation 2.2 represents a hypothesis which is evaluated with prototype experiments (see Chapters 3 and 4).

2.3 Flow velocity

For overtopping waves the flow velocity at the transition of the crest of the dike to the landward slope can be approximated by (SBW 2012-2)



Initial damage



Damage at various locations or multiple open spots



Failure



Non-failure after testing

Figure 2.1 Different definitions of damage and failure (Van der Meer et al. 2010)

$$U_{i,crest} = \alpha_v V_i^{\beta_v} \quad (2.3)$$

where V is the wave volume (expressed in m^3) and $\alpha_v (= 4.5)$ and $\beta_v (= 0.3)$ are dimensional coefficients. The flow on the landward slope accelerates and can be computed with the model as developed by Schüttrumpf and Oumeraci (2005). A first estimation can be given with α_a as an acceleration factor by

$$U_{i,slope} = \alpha_a U_{i,crest} \quad (2.4)$$

In Nijmegen, measurements showed that the erosion occurs faster if the slope is steeper than 1V:3H. The acceleration factor varies from 1.25 to 1.5 close to the toe of the dike. Hence, if the velocity is calculated by using Eq. 2.4 then the magnitude of D obtained from the cumulative overload method increases with a factor of 3 to 6, see also Chapter 3 where the evaluation of U_c is discussed.

2.4 Critical flow velocity

The turf element model describes the forces acting on a turf cube with a length scale of 10 cm. As the vertical equilibrium of the cube is considered just before block erosion occurs the sum of forces in the vertical direction equals nil. The upward directed force (or the load) is determined by the maximum under pressures as a result of bed turbulence. The downward directed (resisting) forces are characterised by shear forces acting on the side walls and a normal force at the bottom due to the strength of roots. The submerged weight of the cube is marginal with respect to the critical mean grass normal stress at the surface. Therefore, this force is excluded in the modelling.

Working out the vertical force balance and by using both the equation of Chézy and the definition of the bed shear stress the critical flow velocity can be estimated by (Table 2.1 where indicative values of U_c are presented) (Hoffmans et al. 2008, Hoffmans et al 2010, Hoffmans 2012)

$$U_c = 2r_0^{-1} \sqrt{\Psi_c (\sigma_{grass,c}(0) - p_w) / \rho} \quad (2.5)$$

where r_0 is the relative (depth-averaged) turbulence intensity, ρ is the water density, $\sigma_{grass,c}(0)$ is the critical mean grass normal stress at the ground level (i.e. perpendicular to the ground surface) and Ψ_c is the critical Shields parameter. The strength parameter $\sigma_{grass,c}(0)$ depends on the root area ratio (or root intensity), the critical root tensile strength and the root diameter, see also Chapter 6 where $\sigma_{grass,c}(0)$ is related to the experimental results of the turf-tensile tests. The pore water pressure (p_w) represents the suction pressure in the sub soil. The suction pressure has a negative sign which decreases with time after infiltration.

The suction pressure in the core of a dike can vary from 0 kN/m² (fully saturated) to rarely more than 50 kN/m². During winter conditions p_w varies from 0 kN/m² to -10 kN/m². The suction pressure is inversely proportional to the particle diameter or to the dimensions of the capillaries, thus the suction pressure increases with a decreasing hydraulic conductivity. The suction pressure also depends on how much water is in the soil, see also Section 6.2 where more information is given about the relation between the suction pressure and the water contents.

Table 2.1 Indicative values of U_c and $\sigma_{grass,c}(0)$ for grass (Hoffmans 2012)

Quality of grass	$\sigma_{grass,c}(0)$ (kN/m ²)	⁽¹⁾ U_c (m/s)	⁽²⁾ U_c (m/s)
very poor	< 3.0	< 3.0	< 6.2
poor	3.0 – 5.3	3.0 – 4.0	6.2 – 6.8
average	5.3 – 7.5	4.0 – 4.7	6.8 – 7.2
good	> 7.5	> 4.7	> 7.2

⁽¹⁾ computed by using Eq. 2.5 with $p_w = 0$ kN/m², $r_0 = 0.2$ (steepness of slope is about 1V:3H) and $\Psi_c = 0.03$

⁽²⁾ computed by using Eq. 2.5 with $p_w = -10$ kN/m², $r_0 = 0.2$ and $\Psi_c = 0.03$

If the turbulence increases the critical flow velocity decreases as the critical bed shear stress is independent of the flow characteristics. For example, if the flow depth decreases then the Chézy coefficient also decreases and thus r_0 increases whence follows that erosion will occur easier (see also Hoffmans 2012).

2.5 Load factor

Experiments show that erosion at revetment transitions (Fig. 2.2), at geometrical transitions (Fig. 2.3) and at side-wall structures (e.g. at trees; Fig. 2.4) differs with respect to erosion at e.g. slopes or horizontal grass revetments. This difference can be ascribed to both an increase of the load and a reduction of the grass strength. Usually the load is expressed in forces which are proportional to the flow velocity squared. Defining (see also Eqs. 2.1 and 2.2)

$$\alpha_M = \frac{F_m}{F} = 1 + \frac{dF}{F} \quad (2.6)$$

where dF is the increase of the shear (or normal) force at the transition or obstacle, F which is related to $(U_i)^2$, represents the shear (or normal) force under flow conditions on a regular slope and F_m is the maximum shear (or normal) force.

As the load factor is expressed in relative forces the load increase of a combined transition can be predicted. Consider an asphalt road on the crest of a dike and a grass revetment on the landward slope, the total load factor is

$$\alpha_{M-tot} = \alpha_{M-asphalt/grass} + \alpha_{M-horz/slope} \quad (2.7)$$

At transitions from a dike slope to a horizontal berm, a downward directed centripetal force acts at the transition which results in an increase of the normal force. At transitions from the horizontal crest to the inner slope the normal force reduces as the centripetal force is directed upwards. Also at side-wall structures there is a down-flow just before the stagnation zone giving an increase of the normal force at the bed.



Figure 2.2 Revetment transitions from grass to asphalt and from asphalt to grass



Figure 2.3 Geometrical transitions (Kattendijke)



Figure 2.4 Erosion at tree; width of test section is 4 m

For revetment transitions, the load increase is determined by the roughness difference of the beds (see also Chapter 4 and Appendix C). For geometrical transitions, the magnitude of the centripetal force depends on the steepness of the inner slope (see also Chapter 4 and Appendix D). For vertical objects and side-wall structures, the impact force is dependent on the form of the object (see also Chapter 4).

For example, Table 2.2 demonstrates the experimental values of wave characteristics versus damage number for the test section at the Vechtdijk. If $\alpha_M = 1.0$ (no obstacle) then it follows from Table 2.2 that after 40 waves the damage number is $D \approx 1000 \text{ m}^2/\text{s}^2$. In such cases, at

several locations erosion occurs which is acceptable since the residual strength is not yet applied. If $\alpha_M = 1.5$ due to obstacles, for example the tree as shown in Fig. 2.4 then $D \approx 1700 \text{ m}^2/\text{s}^2$ (Table 2.2) and so more erosion is expected. Assuming that $\alpha_M = 2$ the erosion/damage increases significantly. However, failure will most likely not occur ($D \approx 2500 \text{ m}^2/\text{s}^2$).

2.6 Strength factor

Typically, objects at dikes have a front, a back side and two side walls relative to overtopping flow direction. Along these side walls the erodibility is stronger because on one side the roots do not intersect due to the foundation of the object. Based on turf-tensile tests (Fig. 2.5) the strength factor lies in the range of 0.82 to 0.97 with a mean value of $\alpha_s = 0.89$ (see Chapter 6). Following Pijpers (2013) the strength reduction (viz. critical flow velocity) is $\alpha_s = 0.95$.



Figure 2.5 Turf-tensile apparatus



Figure 2.6 Reduction of grass strength along concrete wall (on the left side)

Table 2.2 Experimental values Vechtdijk V (wave volume (ℓ/m), U and $U_c = 4$ m/s and computational results of the overload method (α_M and D)

N	V (ℓ/m)	U (m/s)	$\alpha_M = 1.00$	$\alpha_M = 1.25$	$\alpha_M = 1.50$	$\alpha_M = 1.75$	$\alpha_M = 2.00$
1	200	2.89					0.70
2	200	2.89					0.70
3	200	2.89					0.70
4	400	3.66		0.74	4.09	7.44	10.79
5	400	3.66		0.74	4.09	7.44	10.79
6	400	3.66		0.74	4.09	7.44	10.79
7	600	4.20	1.64	6.05	10.46	14.87	19.28
8	600	4.20	1.64	6.05	10.46	14.87	19.28
9	600	4.20	1.64	6.05	10.46	14.87	19.28
10	800	4.63	5.44	10.80	16.16	21.51	26.87
11	800	4.63	5.44	10.80	16.16	21.51	26.87
12	800	4.63	5.44	10.80	16.16	21.51	26.87
13	800	4.63	5.44	10.80	16.16	21.51	26.87
14	1000	5.00	9.00	15.25	21.50	27.75	34.00
15	1000	5.00	9.00	15.25	21.50	27.75	34.00
16	1000	5.00	9.00	15.25	21.50	27.75	34.00
17	200	2.89					0.70
18	1000	5.00	9.00	15.25	21.50	27.75	34.00
19	1000	5.00	9.00	15.25	21.50	27.75	34.00
20	1000	5.00	9.00	15.25	21.50	27.75	34.00
21	2000	6.33	24.07	34.09	44.10	54.12	64.14
22	2000	6.33	24.07	34.09	44.10	54.12	64.14
23	2000	6.33	24.07	34.09	44.10	54.12	64.14
24	3000	7.26	36.71	49.88	63.06	76.24	89.42
25	3000	7.26	36.71	49.88	63.06	76.24	89.42
26	3000	7.26	36.71	49.88	63.06	76.24	89.42
27	4000	8.01	48.16	64.20	80.24	96.28	112.32
28	4000	8.01	48.16	64.20	80.24	96.28	112.32
29	4000	8.01	48.16	64.20	80.24	96.28	112.32
30	5000	8.64	58.65	77.31	95.97	114.64	133.30
31	5000	8.64	58.65	77.31	95.97	114.64	133.30
32	5000	8.64	58.65	77.31	95.97	114.64	133.30
33	5500	8.93	63.74	83.68	103.62	123.55	143.49
34	5500	8.93	63.74	83.68	103.62	123.55	143.49
35	5500	8.93	63.74	83.68	103.62	123.55	143.49
36	1000	5.00	9.00	15.25	21.50	27.75	34.00
37	2000	6.33	24.07	34.09	44.10	54.12	64.14
38	3000	7.26	36.71	49.88	63.06	76.24	89.42
39	4000	8.01	48.16	64.20	80.24	98.28	112.32
40	5000	8.64	58.65	77.31	95.97	114.64	133.30
Damage number (m^2/s^2)			951	1323	1703	2083	2466

It should be remarked that the range $0.82 < \alpha_s < 0.97$ was not validated by applying prototype experiments, for example as shown in Fig. 2.6. Hence, more research is needed to evaluate the strength factor (see also Chapter 4).

2.7 Summary

The overload method is discussed including the extensions to predict the load increase or the load decrease at transitions and obstacles. In this study these effects are expressed by a load factor. When a down-flow occurs the load factor is greater than 1. The load decreases provided there is an up-flow resulting in a load factor that lies in the range of 0 to 1. The reduction of the strength is here modelled by a strength factor which reduces the critical depth-averaged flow velocity.

3 Evaluation wave overtopping tests Nijmegen and Millingen

3.1 Introduction

Wave-overtopping tests in February/March (2013) were conducted. These experiments aim to understand the failure mechanism of grass revetments, especially near transitions and objects. Moreover, they are needed for validating “the state of the art” models.

This Chapter gives an overview of the predictions and measurements of the experiments carried out in Nijmegen and Millingen aan de Rijn. The predictions are based on the loading supplied by the wave overtopping simulator, consisting of a series of overtopping volumes based on the theory for each simulated storm as discussed in the prediction report of Deltares (SBW 2012-2). The simulated loading is a sequence of storms: 6 hours 1 ℓ/s per m, 6 hours 10 ℓ/s per m, 6 hours 50 ℓ/s per m, 6 hours 100 ℓ/s per m and 6 hours 200 ℓ/s per m based on a wave height of $H_s = 1$ m.

A way to validate both the critical flow velocity and the cumulative overload method as discussed in Chapter 2, is to perform short tests with only large overtopping waves. In such a case, overtopping wave volumes with flow velocities lower or close to the critical flow velocities are left out of the load series and only overtopping wave volumes which may contribute to erosion/damage are - a priori – selected. The evaluation of the critical flow velocity is here presented for all the tests.

The load factors and the times at which initial damage at several locations and failure of the grass cover occur are here briefly described. The evaluation of the predicted and modified load factors is given in Chapter 4 for different experiments.

3.2 Predictions

This Section deals with the predictions of both the critical flow velocity and the load factors with respect to the different transitions and obstacles. The predicted critical flow velocities of grass for the test locations were based on the following assumptions

- During winter conditions the suction pressure (p_w) lies in the range of -5 kPa to -10 kPa (Van Ooijen et al 1996). Here, p_w was assumed to be $p_w = -7.5$ kPa;
- On the crest of the dike the relative depth-averaged turbulence intensity was $r_0 = 0.2$;
- For non-cohesive soils the critical Shields parameter depends on the Reynolds number and varies from 0.03 to 0.06. For cohesive soils the critical Shields parameter was $\Psi_c = 0.03$;
- Based on a root investigation (counting roots according to the Dutch assessment guidelines) Alterra reported that the grass quality at Millingen aan de Rijn and Nijmegen was moderate (resulting $\sigma_{grass,c}(0) = 7.5$ kPa, see also Table 2.1) and poor ($\sigma_{grass,c}(0) = 6.0$ kPa) respectively (see also SBW-2012-2; Section 4.3).

The predictions of the critical flow velocity were 7 m/s at the river dike in Millingen and 6 m/s at the Hollands-Duits pumping station in Nijmegen (see also Chapter 6 and SBW- 2012-2).

As less information was available to predict the erodibility of grass at transitions and at obstacles the cumulative overload method is extended with a load factor (α_M) (see also Chapter 2). The relations to predict the load factor are based on scouring models and simple expressions/expert judgement, see also SBW-2012-2 where the modelling is discussed. Here, the predicted values of the load factors are summarised.

The flow at obstacles is somewhat stronger than expected which results in larger load factors, see also Chapter 4 where the predictions of different load factors are evaluated. For a tree with a diameter of 1 m, α_M was estimated by

$$\alpha_{M-tree} = 1.2 \quad (3.1)$$

If the form is rectangular for example for a vertical plate/wall the load factor measured

$$\alpha_{M-wall} = 1.4 \quad (3.2)$$

Considering a slope with a steepness of 1V:2H α_M for geometrical transitions was assumed

$$\alpha_{M-slope/berm} = 1.3 \quad (3.3)$$

If the steepness measured 1V:3H then the load factor was

$$\alpha_{M-slope/berm} = 1.1 \quad (3.4)$$

As there was no conceptual model to predict α_M for transitions from grass to concrete a first approximation was given for the Hollands Duits pumping station, that is

$$\alpha_{M-general} = 1.3 \quad (3.5)$$

In the erosion predictions two characteristic events are distinguished (see also Chapter 2). When multiple damage spots are observed the damage number reaches a value of $D = 1000 \text{ m}^2/\text{s}^2$. The grass cover fails provided $D = 3500 \text{ m}^2/\text{s}^2$. The predictions are carried out with the following assumptions, see Table 3.1 where the predicted parameters (times, velocities and load factors) are presented.

- Cumulative overload method is applied (see also Eq. 2.2);
- Flow velocities are estimated by Eq. 2.3 (see Chapter 2);
- Theory of acceleration of the flow velocity on the slope was used. The acceleration multiplier on U measured 1.25 ($\alpha_a = 1.25$) (see also Eq. 2.4 in Chapter 2).

3.3 Measurements

This Section deals with the predictions and measurements for having a first impression of the computational results. The evaluation of both the critical flow velocities and the load factors for the different tests are discussed in Section 3.4 and Chapter 4 respectively.

Table 3.1 gives the experimental results of the wave overtopping tests conducted in Nijmegen and Millingen aan de Rijn. Observations (photos) and the definitions for multiple damage spots ($D = 1000 \text{ m}^2/\text{s}^2$) and failure of the grass cover ($D = 3500 \text{ m}^2/\text{s}^2$) are used to determine the two times at which these events occurred for the different tests (Infram 2013).

For the test Nijmegen N2 the predictions agree approximately with the measurements. However, for the test Nijmegen N1 the calculated times are about 30% too high which could be ascribed to the steepness of the slope. For overtopping waves, the relation between flow velocity and wave volume is based on a steepness of about 1V:3H (see also Chapter 2). At section N1 in Nijmegen, the dike slope measures 1V:2H. As the predicted flow velocities were

most likely too low for this steep slope the calculated times for reaching damage and failure were greater than the measured ones. Therefore, it is recommended to extend the relation between flow velocity and wave volume with the steepness of the dike (thus Eq. 2.3 should include the angle of the landward slope).

Table 3.1 Predictions and measured results of damage and failure during wave overtopping tests at Nijmegen and Millingen Rijn

Location	Predictions			Measurements	
	α_M	Time (reached in storm) ($D=1000 \text{ m}^2/\text{s}^2$)	Time (reached in storm) ($D=3500 \text{ m}^2/\text{s}^2$)	Time (reached in storm) ($D=1000 \text{ m}^2/\text{s}^2$)	Time (reached in storm) ($D=3500 \text{ m}^2/\text{s}^2$)
Nijmegen 1					
Slope (1V:2H)	1.0	6.0 h - 100 $\ell/\text{s}/\text{m}$	2.0 h - 200 $\ell/\text{s}/\text{m}$	2.0 h - 50 $\ell/\text{s}/\text{m}$	1.0 h - 100 $\ell/\text{s}/\text{m}$
Geom. transition	1.3	6.0 h - 50 $\ell/\text{s}/\text{m}$	2.0 h - 100 $\ell/\text{s}/\text{m}$	6.0 h - 10 $\ell/\text{s}/\text{m}$	4.0 h - 50 $\ell/\text{s}/\text{m}$
Construction //		not predicted	not predicted	2.5 h - 50 $\ell/\text{s}/\text{m}$	6.0 h - 50 $\ell/\text{s}/\text{m}$
Revet. transition		not predicted	not predicted	1.0 h - 100 $\ell/\text{s}/\text{m}$	n.a.
berm – concrete slab					
Nijmegen 2					
Slope (1V:3H)	1.0	6.0 h - 100 $\ell/\text{s}/\text{m}$	2.0 h - 200 $\ell/\text{s}/\text{m}$	6.0 h - 100 $\ell/\text{s}/\text{m}$	1.5 h - 200 $\ell/\text{s}/\text{m}$
Geom. transition	1.1	3.0 h - 100 $\ell/\text{s}/\text{m}$	1.0 h - 200 $\ell/\text{s}/\text{m}$	4.0 h - 50 $\ell/\text{s}/\text{m}$	4.0 h - 100 $\ell/\text{s}/\text{m}$
Side-wall structure	1.4	4.0 h - 50 $\ell/\text{s}/\text{m}$	2.0 h - 100 $\ell/\text{s}/\text{m}$	1.0 h - 50 $\ell/\text{s}/\text{m}$	n.a.
Rough vegetation	-	not predicted	not predicted	not reported	1.0 h - 50 $\ell/\text{s}/\text{m}$
Nijmegen 3 (Short tests)					
Slope	1.0	not predicted	not predicted	after UC5	after UC6
Geom. transition	1.1	not predicted	not predicted	n.a.	n.a.
Millingen 1					
Slope	1.0	>6.0h - 200 $\ell/\text{s}/\text{m}$	>6.0h - 200 $\ell/\text{s}/\text{m}$	6.0 h - 100 $\ell/\text{s}/\text{m}$?
Geom. transition	1.1	1.0 h - 200 $\ell/\text{s}/\text{m}$	5.0 h - 200 $\ell/\text{s}/\text{m}$	6.0 h - 100 $\ell/\text{s}/\text{m}$?
Revet. transition (road- grass)	-	not predicted	not predicted	6.0 h - 10 $\ell/\text{s}/\text{m}$	2.0 - 50 $\ell/\text{s}/\text{m}$
Revet. transition (grass – road)	-	not predicted	not predicted	> 6.0 - 50 $\ell/\text{s}/\text{m}$	
Millingen 2 (Short tests)					
Slope	-	not predicted	not predicted	after UC5	after UC6
Geom. transition	-	not predicted	not predicted	n.a.	n.a.

Note that for the predictions the following assumptions were made.

Nijmegen: $U_c = 6 \text{ m/s}$ and Millingen $U_c = 7 \text{ m/s}$ and acceleration factor is $\alpha_a = 1.25$.

In Millingen the predicted times for the two characteristic events ($D = 1000 \text{ m}^2/\text{s}^2$ and $D = 3500 \text{ m}^2/\text{s}^2$) are much higher than the measured times. Most likely, the predicted critical flow velocity is too high as the influence of suction pressure was included, see also Section 3.4.

For both the geometrical transitions and the side-wall structure the calculated times are higher. So far, a first impression is given between the measured and predicted times with respect to the events multiple damage spots and failure of the grass cover for various tests. Next, the predictions of the critical depth-averaged flow velocities for both Nijmegen and Millingen aan de Rijn are evaluated (Section 3.4). Chapter 4 discusses the evaluation of the load factors for geometrical transitions, revetment transitions and side-wall structures.

3.4 Analysis of the critical flow velocity

General

In the prediction phase the critical flow velocity for the test section (= strength parameter of the slope) can be obtained from the clay and grass investigations (see also Section 2.4 and Chapter 6). This section discusses the critical flow velocity computed by applying both the cumulative overload method (Chapter 2) and the load series of the five tests carried out in Rivierenland (N1, N2, N3, M1 and M2). This value is here considered as a measurement.

First, the critical flow velocity is determined for two short tests (N3 and M2). Each short test consists of three subtests (UC4, UC5 and UC6; number of waves for each subtest is 150). In this analysis also the effects of the accelerated flow on the damage number is examined. Next, the critical flow velocity for the conventional tests is evaluated (N1, N2 and M1; number of waves for these tests lies in the range of 3,000 to 4,000).

For all overtopping wave volumes the flow velocity and the flow thickness at the crest are approximated by

$$U = 4.5V^{0.3} \quad (U \text{ in m/s; } V \text{ in m}^3/\text{m; coefficient 4.5 is not dimensionless}) \quad (3.6)$$

$$h = 0.1V^{0.75} \quad (h \text{ in m; } V \text{ in m}^3/\text{m; coefficient 0.1 is not dimensionless}) \quad (3.7)$$

The flow velocities and flow thicknesses that are produced by the simulator are known (see also SBW report (2012-2)). In this report also the theory for steady state overflow at a slope is described and compared with measured flow velocities and flow thicknesses. The analysis showed that by applying a friction factor of $f = 0.01$ in the theoretical formulae a good reproduction of the measured values was obtained (see also Chapter 4). These formulae will then be used to give the damage number further down the slope.

Infram (2013) described the experimental results of the testing. The pictures/photos are here further analysed. To deduce the critical flow velocity as discussed above the following definitions for the damage number are used for the three events (see also Chapter 2). First damage corresponds to $D = 500 \text{ m}^2/\text{s}^2$. More open spots occur if $D = 1000 \text{ m}^2/\text{s}^2$ and failure is defined if $D = 3500 \text{ m}^2/\text{s}^2$.

Short tests

To determine the critical flow velocity (and validating the overload method) short tests with only large overtopping waves were performed. In such a case, overtopping wave volumes with flow velocities lower or close to the critical flow velocity are left out and only overtopping wave volumes which may contribute to erosion/damage are - a priori - selected.

Overtopping volumes larger than 1.5 m^3 per unit width contribute to the damage number if $U_c = 4 \text{ m/s}$. The test with a overtopping discharge $q = 100 \text{ l/s}$ per unit width in Nijmegen and Millingen had a maximum of about 2.5 m^3 per unit width. The first subtest started with

overtopping wave volumes of 1.5, 2.0 and 2.5 m³ per unit width. These three overtopping wave volumes have a total damage number of 44 m²/s² at the crest and 124 m²/s² at 10 m down the slope (based on $U_c = 4$ m/s) (Table 3.2).

By repeating these three overtopping wave volumes the damage number increases (Table 3.3). With 50 repeats of the three overtopping wave volumes a damage number of about 2200 m²/s² is reached at the crest and more than 6000 m²/s² at 10 m down the slope by using a critical flow velocity of 4 m/s. If the slope indeed fails within this test, the critical flow velocity is lower than 4 m/s. If the slope does not fail, the test is continued with larger overtopping wave volumes. This first subtest contained 150 waves and was called the $U_c = 4$ m/s test.

It is noted that Tables 3.2 and 3.3 also give the damage number for larger critical flow velocities than 4 m/s. These data are required as the damage number of this subtest has to be included in the damage number by further tests. An increase of the critical flow velocity from 4 m/s to 5 m/s gives a decrease in damage number from 2181 m²/s² (= 5 x 436) to 831 m²/s² (= 5 x 166). This value reduces to zero if a critical flow velocity of 6.3 m/s is taken.

Table 3.2 Damage number for 3 overtopping wave volumes and for 3 critical velocities

V (l/m)	D (m ² /s ²) ($U_c = 4$ m/s)		D (m ² /s ²) ($U_c = 5$ m/s)		D (m ² /s ²) ($U_c = 6.3$ m/s)	
	at crest	at 10 m	at crest	at 10 m	at crest	at 10 m
	1500	10	32	1	23	-
2000	15	42	6	33	-	18
2500	19	50	10	41	-	26
sum	44	124	17	97	-	53

Table 3.3 Damage number for subtest $U_c = 4$ m/s by repeating 3 overtopping wave volumes of 1500, 2000 and 2500 l/m

V (l/m)	D (m ² /s ²) ($U_c = 4$ m/s)		D (m ² /s ²) ($U_c = 5$ m/s)		D (m ² /s ²) ($U_c = 6.3$ m/s)	
	at crest	at 10 m	at crest	at 10 m	at crest	at 10 m
repeat 10x	436	1239	166	969	-	529
repeat 20x	872	2479	332	1939	-	1057
repeat 30x	1308	3718	498	2908	-	1586
repeat 40x	1744	4958	664	3878	-	2115
repeat 50x	2181	6197	831	4847	-	2644

Tables 3.4 and 3.5 give the computational results for the second subtest. Damage numbers are calculated for both a critical flow velocity of $U_c = 5$ m/s and $U_c = 6.3$ m/s. The subtest is called $U_c = 5$ m/s. The fourth and fifth columns of Table 3.4 present the damage number after the subtest $U_c = 5$ m/s, but including the damage number of the preceding subtest $U_c = 4$ m/s. The damage number for this subtest at the crest is 2068 m²/s² and this increases to 2899 m²/s² (= 2068 + 831) if the previous subtest is included. The damage number for $U_c = 5$ m/s of 2068 m²/s² reduces to 683 m²/s² if the critical flow velocity is increased to $U_c = 6.3$ m/s (Table 3.6).

If the slope has not failed after the two subtests as described then the critical flow velocity is probably greater than about $U_c = 5$ m/s. It is then possible to continue with a third subtest with even higher velocities. Tables 3.6 and 3.7 give these three larger overtopping wave volumes, which include the maximum volume of 5.5 m³ per unit width (called the subtest $U_c = 6.3$ m/s).

Table 3.4 Damage number for 3 overtopping wave volumes and for 2 critical flow velocities

V (ℓ/m)	D (m^2/s^2) ($U_c = 4$ m/s)		D (m^2/s^2) ($U_c = 5$ m/s)		D (m^2/s^2) ($U_c = 6.3$ m/s)	
	at crest	at 10 m	at crest	at 10 m	at crest	at 10 m
2000			6	33		18
3000			14	48	3	34
4000			22	62	11	48
sum			41	143	14	99

Table 3.5 Damage number for subtest $U_c = 5$ m/s by repeating 3 overtopping wave volumes of 2000, 3000 and 4000 ℓ/m . The second column includes the load by subtest $U_c = 4$ m/s

V (ℓ/m)	D (m^2/s^2) ($U_c = 5$ m/s)		Including previous tests ($U_c = 4$ m/s)		D (m^2/s^2) ($U_c = 6.3$ m/s)	
	at crest	at 10 m	at crest	at 10 m	at crest	at 10 m
repeat 10x	414	1434	1244	6281	137	993
repeat 20x	872	2868	1658	7715	273	1987
repeat 30x	1241	4302	2071	9149	410	2980
repeat 40x	1654	5736	2485	10583	547	3973
repeat 50x	2068	7170	2899	12017	683	4967

The damage number for this subtest $U_c = 6.3$ m/s only amounts to 1848 m^2/s^2 and this increases to 2531 m^2/s^2 if the previous subtests are included (Table 3.7). Actually, this is still smaller than the value of 3500 m^2/s^2 , a value that gives "failure of the slope". Table 3.8 presents a summary of the 'measured' critical flow velocities.

Table 3.6 Damage numbers for 3 overtopping wave volumes and a critical flow velocity of $U_c = 6.3$ m/s

V (ℓ/m)	D (m^2/s^2) ($U_c = 4$ m/s)		D (m^2/s^2) ($U_c = 5$ m/s)		D (m^2/s^2) ($U_c = 6.3$ m/s)	
	at crest	at 10 m	at crest	at 10 m	at crest	at 10 m
4000					7	48
5000					13	60
5500					17	66
sum					37	174

Table 3.7 Damage numbers for subtest $U_c = 6.3$ m/s by repeating 3 overtopping wave volumes of 4000, 5000 and 5500 ℓ/m . The last two columns includes the load by subtests $U_c = 4$ m/s and 5 m/s

V (ℓ/m)	D (m^2/s^2) ($U_c = 4.0$ m/s)		D (m^2/s^2) ($U_c = 6.3$ m/s)		Including previous tests ($U_c = 4$ m/s and 5 m/s)	
	at crest	at 10 m	at crest	at 10 m	at crest	at 10 m
repeat 10x			370	1738	1053	9348
repeat 20x			739	3476	1423	11086
repeat 30x			1109	5213	1792	12824
repeat 40x			1478	6951	2162	14561
repeat 50x			1848	8689	2531	16299

Until now analysis on the damage number was focused on the velocities at the crest. This was also the case in this section described so far. It is only very recently that it became clear that for a landward slope steeper than 1V:5H the velocities on the slope increase significantly

down the slope. Probably this is the reason why most of the damages observed in testing with the wave overtopping simulator appeared to be on the lower half of the slope and not directly after the crest. The recent validation of the theory of steady overflow with measurements on the Tholen dike and also the hydraulic measurements at the Millingen dike, showed clearly this increase in velocity (see also Chapter 4).

Table 3.8 'Measured' critical flow velocities

Location Nijmegen N3	Definition	State of testing	Damage number (m ² /s ²)		
			U _c = 4.0 m/s	U _c = 5 m/s	U _c = 6.3 m/s
short test	first damage more open spots large damage, no failure	- after U _c = 5 m/s after U _c = 6 m/s	-	2899 -	683 2531

Conclusion: damage definition reached for about U_c = 6.3 m/s. Failure was not reached.

Location Millingen M2	Definition	State of testing	Damage number (m ² /s ²)		
			U _c = 4.0 m/s	U _c = 5 m/s	U _c = 6.3 m/s
short test	first damage more open spots large damage	after U _c = 5 m/s after U _c = 6.3 m/s	-	3257 -	801 2649 -

This test section received first the overtopping volumes for the hydraulic measurements of flow velocity and flow thickness. This pre-loading give a cumulative overload of respectively, 595 m²/s²; 358 m²/s²; and 118 m²/s² for critical velocities of 4 m/s; 5 m/s; and 6.3 m/s. This preloading was added to the loading during the short test. Conclusion: critical flow velocity close to U_c = 6.3 m/s, or even somewhat higher. Failure was not reached.

If the critical flow velocity is assumed constant then the damage number increases along the slope and depends on the steepness of the slope and the location on the slope. A steeper slope gives higher flow velocities and these flow-velocities increase along the slope.

Below a first estimation is given of the damage number at a location of 10 m down the slope by using the subtests. Table 3.9 gives an overall view of the damage numbers which was taken from data in Tables 3.2 - 3.8. For the U_c = 4 m/s subtest the damage number from the crest to 10 m down the slope increases from 2181 m²/s² to 6197 m²/s², which is almost a factor of three. For subtest U_c = 5 m/s, including the previous subtest, the damage number increases from 2899 m²/s² to 12017 m²/s², which is more than a factor of four. The final subtest U_c = 6.3 m/s, including both other subtests, gives an increase from 2531 m²/s² to 16299 m²/s², which is more than a factor of six. It is very clear that the location on the slope and also the cumulative effect of the subtests, have a large impact on the calculated damage number.

If the flow velocities accelerate then the turbulence intensities decrease which results most likely in an increase of the critical flow velocity as the load is the product of velocity and turbulence. However, this hypothesis is here not investigated in greater detail. If the critical flow velocity is independent of the turbulence a re-analysis of all data may give values for the damage definitions that are probably much larger than used now.

Table 3.9 Damage numbers after three subtests, at the crest and 10 m down the slope

Subtest	Used U_c (m/s)	D (m^2/s^2) (for used U_c)		Including previous Subtests	
		at crest	at 10 m	at crest	at 10 m
$U_c = 4$ m/s	4	2181	6197		
$U_c = 5$ m/s	5	2068	7170	2899	12017
$U_c = 6.3$ m/s	6.3	1848	8689	2531	16299

Conventional tests

In order to make an analysis of the tests carried out in Rivierenland the damage number for each subtest including the accumulation of the subtests, has to be established for the conventional tests N1, N2 and M1. Next, they can be compared with the damage numbers of the short tests as described in the previous subsection. First this will be done at the crest, directly after release of the overtopping wave volume from the wave overtopping simulator.

Table 3.10 presents the damage number at the crest for critical velocities of $U_c = 4, 5$ and 6.3 m/s (values used in earlier analyses) and for single tests with the given overtopping discharge and for a duration of 1 hour. The test sequence was $q = 1, 10, 50, 100$ and 200 ℓ/s per unit width with a subtest duration of 6 hours. It is also possible to calculate the total damage number after each subtest, including the previous subtests. The data in Table 3.10 have been used for this and the results are shown in Table 3.11. If $U_c = 6.3$ m/s then there will hardly be any damage as $D \approx 5$ m^2/s^2 .

Where possible the three damage definitions were determined at a certain stage of testing. Then the damage number is calculated for that stage of testing. The 'measured' critical flow velocities for each test vary from 3.5 m/s to 5 m/s (Table 3.12).

Table 3.10 Damage number (m^2/s^2) for various discharges and critical velocities and for a duration of 1 hour (assuming $H_s = 1$ m). Location: at the crest

q	0.1	1	5	10	30	50	75	100	150	200
	ℓ/s per m	ℓ/s per m	ℓ/s per m	ℓ/s per m	ℓ/s per m	ℓ/s per m	ℓ/s per m	ℓ/s per m	ℓ/s per m	ℓ/s per m
$U_c = 4$				2	36	127	335	648	1542	2812
$U_c = 5$						2	14	43	180	461
$U_c = 6.3$										5

Table 3.11 Total cumulative overload (m^2/s^2) for a sequence of 5 subtests with various critical velocities and for a duration of 6 hours for each subtest (assuming $H_s = 1$ m). Location: at the crest

q				10		50		100		200
				ℓ/s per m		ℓ/s per m		ℓ/s per m		ℓ/s per m
$U_c = 4$				12		774		4662		21534
$U_c = 5$						12		270		3036

3.5 Conclusions

The overall conclusion is that there seems to be a difference between the short tests and the conventional tests. For the conventional tests the critical flow velocity for sections N1 and N2 were 3.5 m/s and 5 m/s, respectively, and for section M1 this was 4.5 m/s. The critical flow velocity from the short tests (sections N3 and M2) was 6.3 m/s or even higher. A reason for the low critical flow velocity of 3.5 m/s at section N1 might be that the damage occurred at a very steep slope of about 1V:2H, which means that the velocity must have increased

enormously compared to the velocity at the crest. But even then the conventionally tested slopes showed critical velocities of about 5 m/s or lower, compared to 6.3 m/s or higher for the short tests.

Table 3.12 'Measured' critical flow velocity

Location Nijmegen N1	Definition	State of testing	Damage number (m ² /s ²)		
			$U_c = 4.0$ m/s	$U_c = 5$ m/s	$U_c = 6.3$ m/s
Conventional	first damage	-	-	-	-
Test	more open spots	2.0 h - 50 ℓ/s per m	266	5	-
	failure	1.0 h - 100 ℓ/s per m	1422	65	-

Conclusion: damage definition reached before limits for $U_c = 4$ m/s. Actual critical flow velocity in this test was U_c around 3.5 m/s. Damage was on the very steep 1V:2H slope.

Location Nijmegen N2	Definition	State of testing	Damage number (m ² /s ²)		
			$U_c = 4.0$ m/s	$U_c = 5$ m/s	$U_c = 6.3$ m/s
Conventional	first damage	6.0 h - 100 ℓ/s per m	4662	270	-
Test	more open spots	1.5 h - 200 ℓ/s per m	8880	962	-
	failure	-	-	-	-

Conclusion: damage definition reached for about $U_c = 5$ m/s. Failure was not reached.

Location Millingen M1	Definition	State of testing	Damage number (m ² /s ²)		
			$U_c = 4.0$ m/s	$U_c = 5$ m/s	$U_c = 6.3$ m/s
Conventional test	between first damage and more open spots	6.0 h - 100 ℓ/s per m	4662	270	-

Conclusion: the damage reached would need a damage number of 750 m²/s². This means that the critical flow velocity was around $U_c = 4.5$ m/s.

Consequently, one may not conclude that the short tests gave similar results as the longer conventional tests. This conclusion will not change if the damage number would be calculated by the actual velocities at the location of the damage. The reason is that the test sections were more or less similar and the damage occurred more or less at the same location for most cases. This might be different for the first test at N1, where a very steep slope was tested.

Owing to the steep slope at the location N1 the computed flow velocities (obtained from Eq. 3.6) are most likely too low. Hence, by using the cumulative overload model including the definitions of damage and failure the critical flow velocity is probably also too low. Therefore, the measured critical flow velocity should be higher than 3.5 m/s. It is recommended to modify Eq. 3.6 for steep slopes (steeper than 1V:3H).

Table 3.13 presents the predicted and 'measured' critical flow velocities for the test locations Nijmegen and Millingen aan de Rijn. To predict the critical flow velocity 5 parameters have to

be known (see also Section 2.4). The ‘measured’ U_c is based on measurements/observations and determined by using the cumulative overload method (so it cannot be considered as a 100% measurement). Below the evaluation is given between the predictions and ‘measurements’.

Table 3.13 demonstrates that the predicted and ‘measured’ U_c have approximately the same values for the short tests. However, for the conventional tests the ‘measured’ critical flow velocities are significantly lower, which could be ascribed to the more wetted soil (suction pressures are lower), to the lower fatigue strength (more load repetitions) and to the bed roughness (acceleration effects on the landward slope).

Table 3.13 Overview of predicted and ‘measured’ critical flow velocities for the test sections in Rivierenland

Test location	Type of test	Predictions (conditions halfway slope)		‘Measurements’ (crest conditions)	
		U_c (m/s)	α_a (-)	U_c (m/s)	α_a (-)
Nijmegen N1	conventional	6	1.25	3.5	1.00
Nijmegen N2	conventional	6	1.25	5.0	1.00
Nijmegen N3	short	6	1.25	6.3	1.00
Millingen M1	conventional	7	1.25	4.5	1.00
Millingen M2	short	7	1.25	> 6.3	1.00

The total test duration for the conventional tests was approximately 18 hours. The test duration for the total short tests was only 4 hours. When the soil becomes wetter the suction pressure decreases so the critical flow velocities for the tests N1, N2 and M1 may be smaller than the critical flow velocities for the short tests (N3 and M2).

Also the fatigue strength (see also Chapter 6) influences the magnitude of U_c . The longer the tests the smaller the critical flow velocity becomes. Therefore, U_c for the conventional tests is smaller as there were more load repetitions (see also Chapter 6).

Heterogeneity refers to the fact that turf consists of clay, roots and many different things. As they are not mixed evenly throughout the soil (humus, sand particles, clay particles, root structure) the standard deviation of the grass strength can be large, see also Chapter 6 where experimental results of the turf-tensile apparatus are discussed. Hence, the minimum value of the strength determines the magnitude of U_c as well.

There is more to evaluate. Measurements showed that the flow velocities increased on the landward slope (see also SBW 2012-2 and Chapter 4). For large wave volumes the maximum value of the acceleration factor is approximately 1.5, thus the maximum flow velocity at the lower part of the landward slope, is 1.5 times the flow velocity at the crest of the dike. Before the experiments started, the prediction for the acceleration factor was carried out with expert judgement resulting in $\alpha_a = 1.25$. If the predictions $U_c = 6$ m/s and $\alpha_a = 1.25$ are used then more open spots occur at 6.0 h - 100 l/s/m and the grass cover fails at 2.0 h - 200 l/s/m for the test location Nijmegen N2. These two predicted times are about in agreement with the measured times (Table 3.14). Hence, if α_a increases (or if the turbulence decreases) then U_c also increases. As this hypothesis is not examined thoroughly for all the tests it is recommended to study this more in detail in 2014.

At present the effects of the fatigue strength, heterogeneity and turbulence on erosion are processes which are still not fully understood, see also Chapters 4 and 6. The evaluation of

the load and strength factors for different transitions and obstacles are discussed in relation to the measured U_c (see Chapter 4) as less information was available about the modelling.

Table 3.14 Predicted and measured times regarding two characteristic events

Nijmegen N2	Predictions (about halfway the landward slope: $r_0 \approx 0.15$)			'Measurements' (crest conditions: $r_0 \approx 0.2$)		
	U_c (m/s)	α_a (-)	predicted time	U_c (m/s)	α_a (-)	'measured' time
	(see Table 3.13)		(see Table 3.1)	(see Table 3.13)		(see Table 3.1)
more open spots	6.0	1.25	6.0 h - 100 l/s/m	5.0	1.0	6.0 h - 100 l/s/m
failure grass cover	6.0	1.25	2.0 h - 200 l/s/m	5.0	1.0	1.5 h - 200 l/s/m

4 Hydraulic load on the landward slope

4.1 Introduction

Flow velocities of overtopping wave volumes over the crest of a dike, including turbulence, are considered as the main cause for damage of the grass cover and the under laying clay. Recently, specific instruments were developed to measure both flow velocities and flow thicknesses (or flow depths) on the crest and on the landward slope of dikes (see also Van der Meer 2011 and SBW 2012-1 for more details).



Figure 4.1 First surfboard on the middle of the road and second at the start of the landward slope



Figure 4.2 Surfboards 1, 2, 4 and 6 with paddle wheels 3, 5 and 7 at the grass surface

A paddle wheel meter consists of a small impeller which was here used to measure the flow velocities. The flow thicknesses were measured by applying surf boards as shown in Figs. 4.1 and 4.2. Usually one or two paddle wheels were mounted on a surfboard, measuring the flow velocity on top of an overtopping wave. Sometimes a paddle wheel was mounted up-side down on a plate to measure the velocities at 2 cm to 3 cm above the ground surface.

Section 4.2 deals with the measured flow depths and flow velocities for different wave volumes at the test locations Nijmegen and Millingen aan de Rijn. These experimental results are compared with the predictions obtained from the theory of steady state overtopping as developed by Schüttrumpf and Oumeraci (2005). As the turbulence intensity is related to the friction factor as used in the above-mentioned model simple relations for predicting the turbulence are applied to evaluate the computations.

A prediction method for outward directed pressure gradients gives insight in the modelling of grass erosion on a slope, at transitions of revetments and near objects on dikes. The near-bed turbulence energy (k_b) (or turbulent kinetic energy close to the bed) represents the magnitude of the maximum pressure fluctuation (p_m) (or the maximum upward or downward pressure gradient). Emmerling (1973) examined the instantaneous structure of the wall pressure under a turbulent flow in air and found $p_m \approx 6\rho k_b$ (with ρ is the density of water). According to Nezu (1977) this relation is also valid for supercritical flow in water (say Froude number is greater than 2).

Figure 4.3 shows that near the bed (at $z/d_{f50} = 0$) the turbulence intensity ($k_b/(u_*^2)$ with u_* is the bed shear velocity) is at maximum (= 100%). For non-cohesive materials the load penetration into the soil decreases significantly with the depth. Measurements of Klar (2005) demonstrate that for gravel with a mean grain size of 1 cm the dimensionless turbulence energy ($k_b/(u_*^2)$) is about 10% at five times the grain size (i.e. at $z/d_{f50} = -5$). Hence, at 5 cm below the ground surface the load acting on gravel may be neglected. This reduction of the pressure fluctuation will probably be even more for sand or clay.

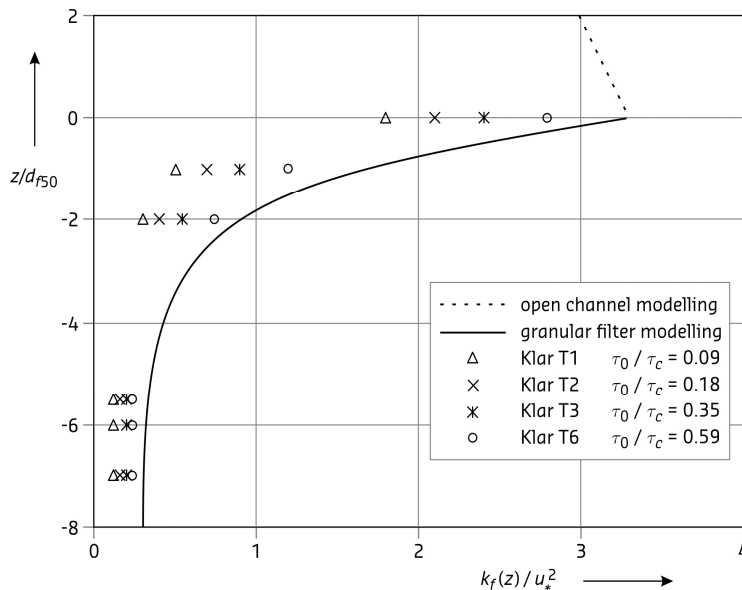


Figure 4.3 Dimensionless load versus relative depth (Klar 2005)
 (τ_0 is the bed shear stress and τ_c is the critical bed shear stress)

The grass revetment consists of roots, clay and/or sand. As no information was available of the load penetration in cohesive soils here experimental research and desk studies are carried out. Section 4.3 deals with the load on grass revetments and the load penetration both in an analytical and experimental way in order to evaluate the assumptions in the turf-element model (see also Chapter 6).

Hinze and Nezu (Nezu and Nakagawa 1993) found experimentally that up-flows (i.e. upward flowing current) occurred over smooth-bed strips, whereas down-flows occurred over rough-bed strips for air and water flows. In the down-flow region over the rough bed the bed shear stress and the turbulence reach a maximum value immediately downstream from smooth to rough bed conditions. Beyond this location, the bed shear stress decreases in the streamwise direction to its equilibrium value, see also Appendix C where more information is given regarding the influence of up-flows and down-flows on the revetment transitions.

Erosion by wave overtopping at dike transitions is a major cause of dike damage or failure during severe overtopping events. When the flow of the waves is directed from a smooth to a rough bed the load increases. In the direction from rough to smooth the load decreases. These effects are here expressed by a load factor (see also Chapter 2). The damage at transitions can be predicted by the cumulative overload method in which the load is corrected by the load factor. Section 4.4 deals with the load factor for revetment transitions, geometrical transitions and vertical objects.

Section 4.5 provides conclusions with respect to both the load near the ground surface and the load penetration in the subsoil.

4.2 Flow velocity and flow thickness measurements

Introduction

The theory of steady state overtopping as developed by Schüttrumpf and Oumeraci (2005) (see also SBW 2012-1; Section 2.1) is used for predicting the flow velocities and flow thicknesses. All hydraulic measurements from 2008 to 2012 were re-analysed, giving (new) relations between overtopping wave volume (V) and flow velocity (U) as well as V and flow thickness (h) at the crest of the dike (point of release of the overtopping wave). Also the development of the flow velocity and the flow thickness along the landward slope was analysed and compared with the theory.

The conclusion was that for slopes steeper than 1V:5H the flow velocity increases. By using the aforementioned theory the friction factor of $f = 0.01$ yields velocities which agree with measurements. At the lowest part of the slope (say after 10 m - 15 m) the overtopping duration may increase, causing deviations from the theory, such as slowing down of velocity where the flow thickness remains similar.

The objectives of the hydraulic measurements at Millingen were

- Measure the flow velocity and thickness along the landward slope;
- Compare the $V - U$ and $V - h$ relations on the horizontal crest with measurements, before the gravitational acceleration and friction of the grass can change the flow velocity and thickness on the landward slope. The current formulae are given in SBW (2012-1). Note that the German model holds for 'real' waves. As the waves are simulated by the wave simulator differences may occur between calculations and measurements.

- Validate the use of $f = 0.01$ in the theory as described in Section 2.1 of SBW, 2012-1 with these measurements.

Test set-up

Infram (2013) presented an overall view of tests and measurements at Rivierenland. The hydraulic measurements on the landward slope of the dike at Millingen were performed with the wave overtopping simulator placed on the crest and just 0.15 m on the asphalt road on top of the dike. The asphalt road is 3.1 m wide. In order to have a more smooth transition from the asphalt road to the landward slope a heavy geotextile was placed on the top of an impermeable plastic sheet (Fig. 4.2). Five surfboards (SP1, SP2, SP4, SP6 and SP8) were placed, one halfway the road, one just at the start of the slope and three along the landward slope. The outer crest line (start of the landward slope) was taken as the zero line, which means that the outflow of the simulator was at -4.15 m. Each surfboard had a paddle wheel to measure velocities. Three paddle wheels (numbers SM3, SM5 and SM7, Fig. 4.4) were placed upside down in a plate on the ground surface with the paddle wheel 3 cm above the surface.

The measurements were concentrated on the top part of the slope, as in that area the largest developments of flow velocity and flow thickness were expected. The locations of surfboards and paddle wheels are given in Fig. 4.4 (see also Table A1 in Appendix A). The landward slope is about 1V:3H between surfboards 2 and 8 and is somewhat gentler near the toe of the dike.

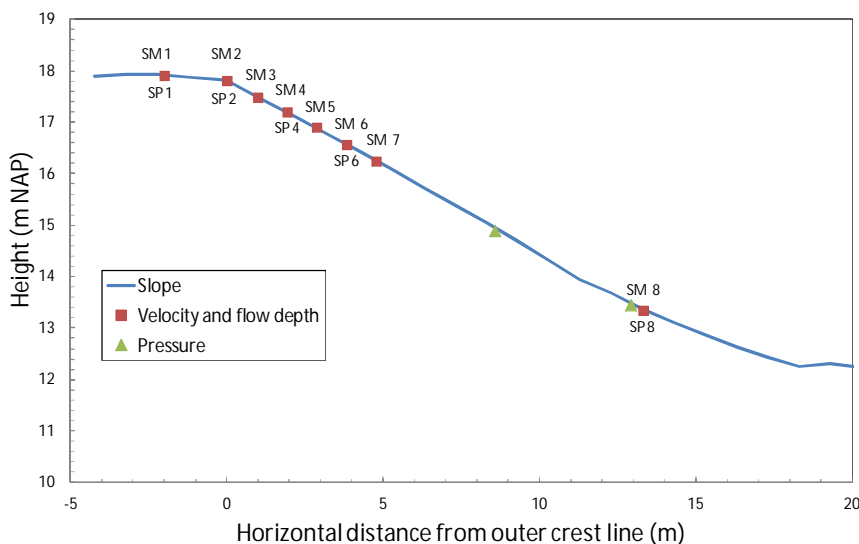


Figure 4.4 Set-up of hydraulic measurements at Millingen
SM refers to paddle wheel (PW); SP refers to surfboard

Error-analysis of measurements

A first analysis was performed by analysing the individual records of flow velocity and flow thickness as given in Appendix A. Three observations are made. The first one is that the flow thickness on the crest (SB1) is relatively large. The second one is that SB2 (flow thickness at location 2) did not function properly. Therefore, these measurements are doubtful. The last observation is that for test series 3 some instruments did not work: PW3, PW5, PW7, PW8 and SB8. The first two observations are here described in greater detail.

Figures 4.5 and 4.6 demonstrate the flow thicknesses and flow velocities for overtopping wave volumes of 800 ℓ/m and 5000 ℓ/m . Figure 4.5 also shows that the flow thickness measured at SB1, that is halfway the crest, is more than twice as large as the flow thicknesses measured by the other instruments which can be ascribed to the rounding of the asphalt road (see also Figs. 4.2 and 4.4).

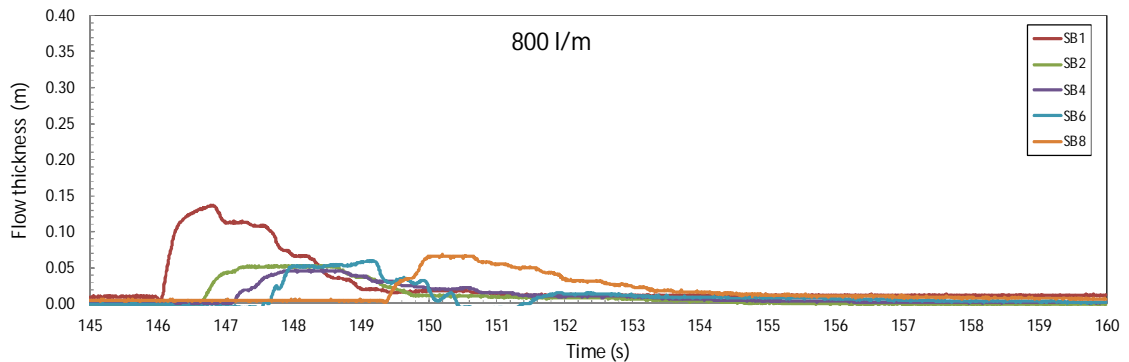


Figure 4.5 Records of flow thickness for a wave overtopping volume release of 800 ℓ/m

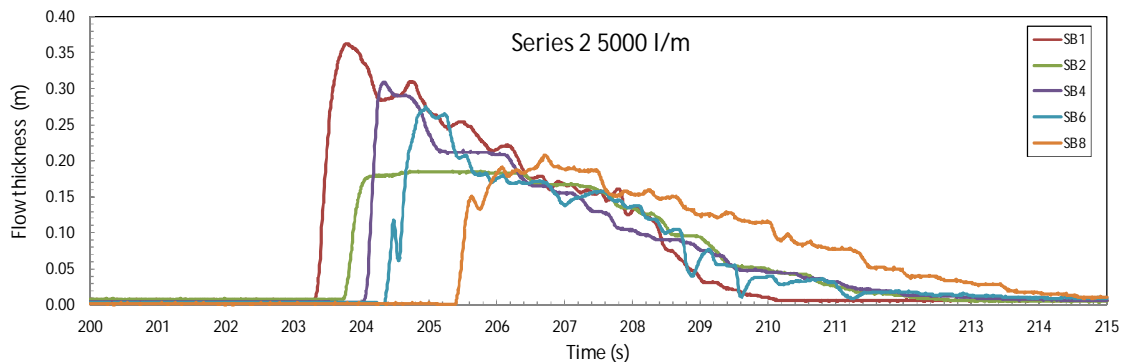


Figure 4.6 Records of flow thickness for a wave overtopping volume release of 5000 ℓ/m

The released water must lift before it flows in the streamwise direction. For small overtopping volumes this results in a decrease of the flow velocity and therefore, to satisfy the equation of continuity in an increase of the flow thickness. This effect is negligible when large overtopping wave volumes are released, as shown in Fig. 4.6. The influence of the rounding is only visible for small overtopping wave volumes.

When the experimental values recorded at SB1 are omitted the differences between the flow thicknesses at SB1, SB3 and SB4 become smaller. Of course the flow thickness at SB1 is largest as the flow velocity at the slope increases. Hence, the flow thickness has to decrease. However, by omitting SB1 the difference is only about 15% and not more than 50% as can be seen in Fig. 4.5. Comparing flow thicknesses in SB1 on the crest with earlier measurements will probably give outliers for these measurements (will be validated further on).

Another observation was that the SB2 recorder, just at the outer crest line and at the start of the landward slope, measures low values of the flow thickness compared to the other records (see also Fig. 4.6). Moreover, the green curve is flat. The records also starts relatively late

(not close enough to SB1). Overall it can be concluded that the measurements obtained by SB2 are not reliable. Therefore, they are here not further analysed.

A reason to repeat series 2 and series 3 was that the hinge of the surfboards was not correctly mounted. It was assumed that this would not have influence the measurements. Figure 4.7 shows the comparison of flow thicknesses for series 2 and 3. The measurements at the same locations correspond well and there is no bias so series 2 and 3 can be used for further analysis.

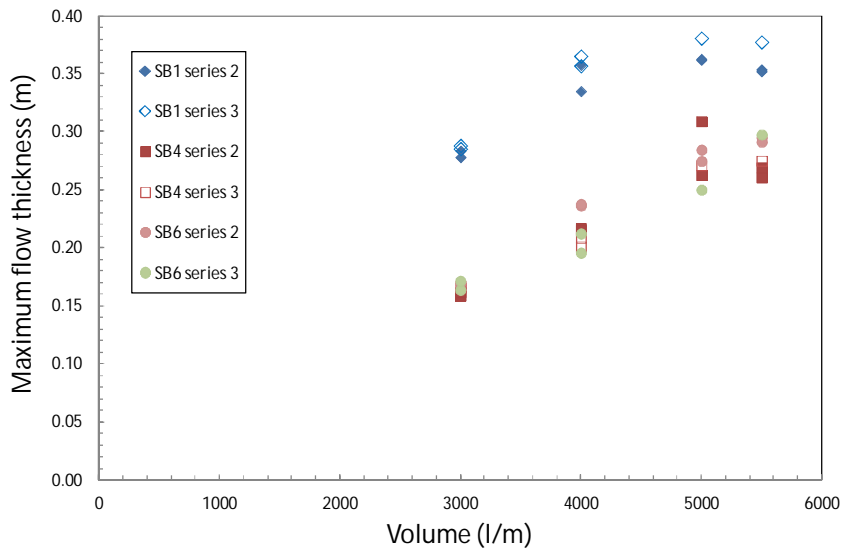


Figure 4.7 Comparison of flow thicknesses for series 2 and 3

The first objective was to compare the velocities on the crest with earlier measurements and relations. Figures 4.8 and 4.9 present the flow velocity and the flow thickness halfway the crest for PW1 and PW2 or SB1. The measured flow velocities as shown in Fig. 4.8 are lower than the relation (SBW-2012) and correspond well with the measurements in Belgium. One reason may be that only one paddle wheel was used in the surfboard and that the real maximum was not always recorded. Another reason might be that the middle of the crest is higher than the position of the outflow of water. Nevertheless, the difference is small and acceptable.

As expected the measured flow thicknesses as presented in Figure 4.9 are larger than the predicted ones. For the largest overtopping wave volumes ($V > 5000 \text{ l/m}$) the agreement is satisfactory.

Figure 4.10 shows all measured flow velocities. It is clear that the flow velocities increase with increasing released overtopping wave volume as well as along the slope. The velocities PW1 and PW2 on the crest are the lowest and the velocity at PW10 at 10 m downstream of the crest is by far the largest. A closer look at PW3, PW5 and PW7 for released wave volumes of about 3000 l/m and larger gives the observation that these measurements give lower velocities than expected. They are not in agreement with the surrounding instruments. These instruments were the paddle wheels that were mounted on a plate on the surface. It might well be that with larger velocities (around 7 m/s and more) the flow is too turbulent close to

the surface and that the paddle wheels do not longer work properly. These measurements are here disregarded (see also Table A4 in Appendix A).

Figure 4.11 presents the maximum flow thickness as function of the wave volume and shows a similar trend as the flow velocities (see also Fig. 4.10). As shown in Fig. 4.9 the flow thickness on the crest (SB1) is somewhat too large. Except for overtopping wave volumes of 5000 ℓ/m and 5500 ℓ/m . Flow thicknesses measured at SB4, SB6 and SB8 are quite similar. For small volumes, smaller than about 2000 ℓ/m , the flow thickness at SB8 (14 m down the slope) is somewhat larger than at SB4 and SB6. Probably further down the slope these smaller volumes lead to slow down of the process and a longer overtopping duration. For the largest volumes of 5000 ℓ/m and 5500 ℓ/m there is a clear trend of decreasing flow thickness along the slope with increasing velocity (see Fig. 4.10).

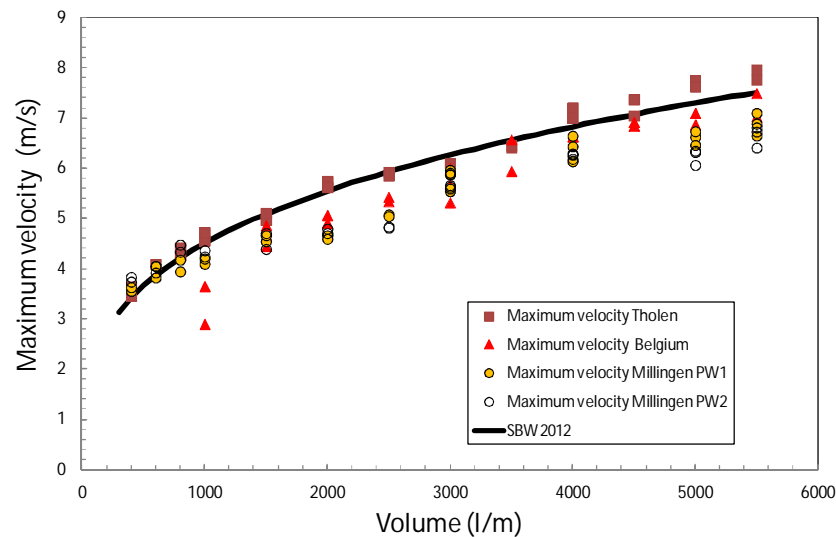


Figure 4.8 Flow velocity on the crest compared with earlier measurements

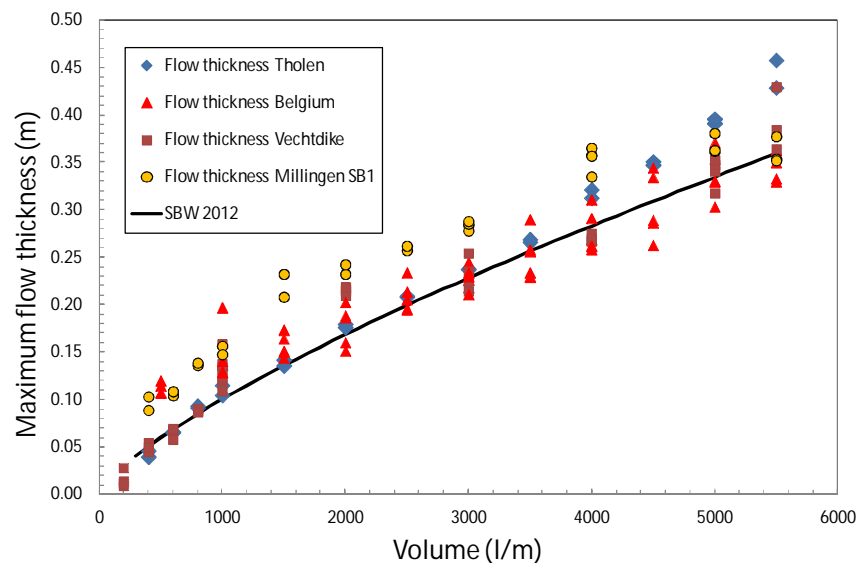


Figure 4.9 Flow thickness on the crest compared to earlier measurements

A better evaluation of Figs. 4.10 and 4.11 can be made if for selected overtopping wave volumes the development of flow velocity and thickness along the slope is given. Such graphs can also be compared with the theoretical curves as shown in Appendix A. (Figures A1-A4 were given for initial velocities of 4, 5, 6 and 7 m/s, respectively, and were calculated with a friction factor of $f = 0.01$. If trends found for the measurements are in agreement with the trends given in Figures A1 - A4, then this would be a validation of the value of $f = 0.01$ for the friction factor). Three cases are here selected, see also Figure 4.10, with $u_o = 4, 5$ and 6 m/s and corresponding overtopping wave volumes of 1000, 2500 and 4000 ℓ/m .

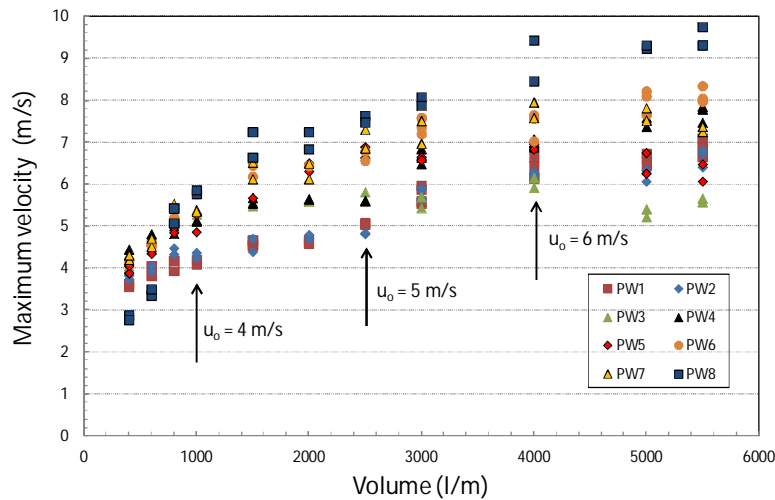


Figure 4.10 All measured velocities as function of released overtopping volume and location

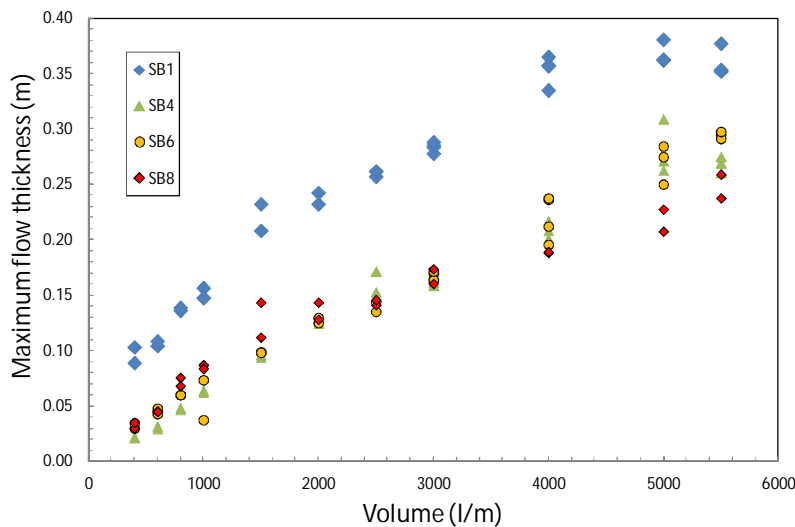


Figure 4.11 All measured flow thicknesses as function of released overtopping volume and location

Computational results

Figures 4.12 to 4.14 give the development of the flow velocity and Figures 4.15 to 4.17 presents the flow thickness as function of the streamwise direction. Note that in the last case with $u_o = 6$ m/s, a slightly higher velocity was present in the measurements (between 6.14 and 6.64 m/s).

Overall, the trends of the velocities agree between theory and measurements (Figs. 4.12 to 4.14). Measured data is scattered around the theoretical trend and there is no bias. This means that with respect to flow velocity the friction factor of $f = 0.01$ has been validated by these measurements.

Analysis of the flow thicknesses (Fig. 4.15 to 4.17) is given below. First of all h_o at SB1 is too high, as concluded earlier. Secondly, on a similar level SB2 did not measure correctly, which means that there is no correct measured h_o . Actually, the trend can only be judged from SB3 to SB5, where SB5 is much further down the slope. Figure 4.15 gives a fairly good match for SB3 and SB4 and theory. The flow thickness for this relatively small overtopping wave volume at SB5 further down the slope increases a little. As said earlier, slowing down of the overtopping process might be a reason for this.

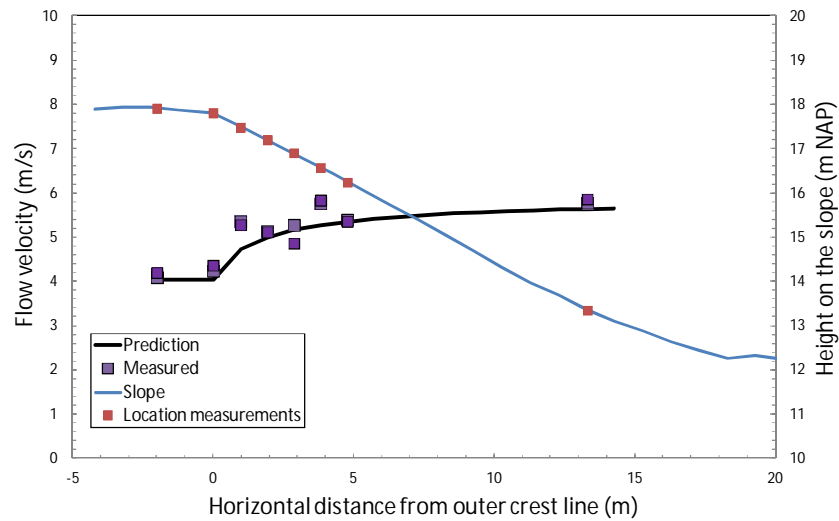


Figure 4.12 Measured and calculated velocity along the slope for $u_o = 4 \text{ m/s}$ ($V = 1000 \text{ l/m}$)

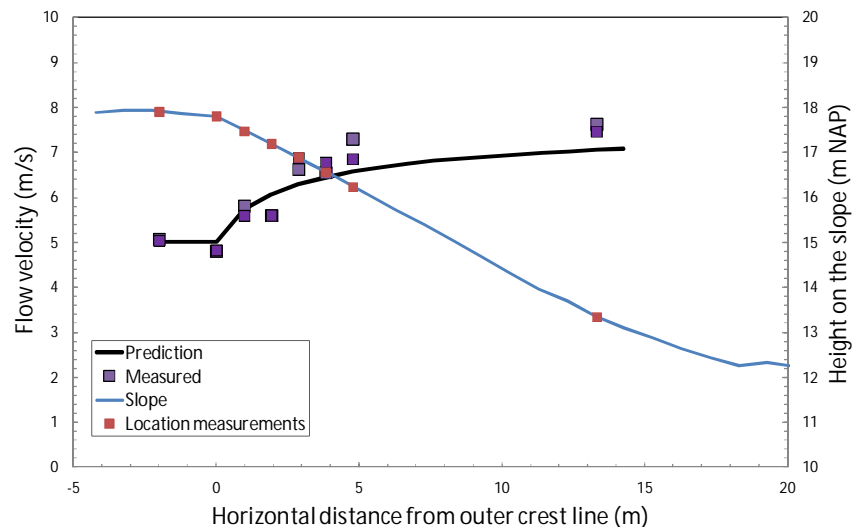


Figure 4.13 Measured and calculated velocity along the slope for $u_o = 5 \text{ m/s}$ ($V = 2500 \text{ l/m}$)

The measured flow thicknesses as shown in Figures 4.16 and 4.17 do not match the theoretical lines. Although there is a similar trend, the theoretical line gives much smaller flow thicknesses than measured. With increasing flow velocity at the crest the flow thickness increases too, but faster than the velocity. For instance, if the flow velocity at the crest is increased from 5 m/s to 6 m/s (20% increase, see Fig. 4.16) then the flow thickness increases from 0.13 m to 0.20 m (50% increase). Now the points for SB3 to SB5 fall well between the theoretical lines.

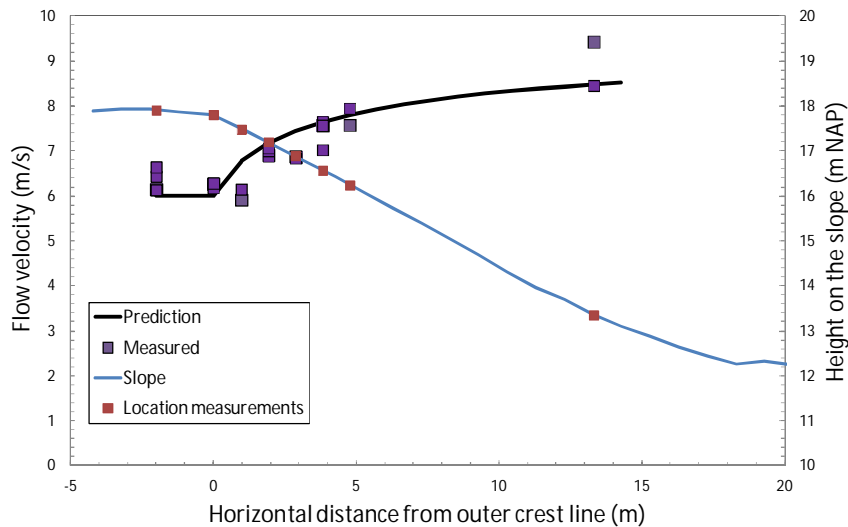


Figure 4.14 Measured and calculated velocity along the slope for $u_o = 6$ m/s ($V = 4000$ l/m)

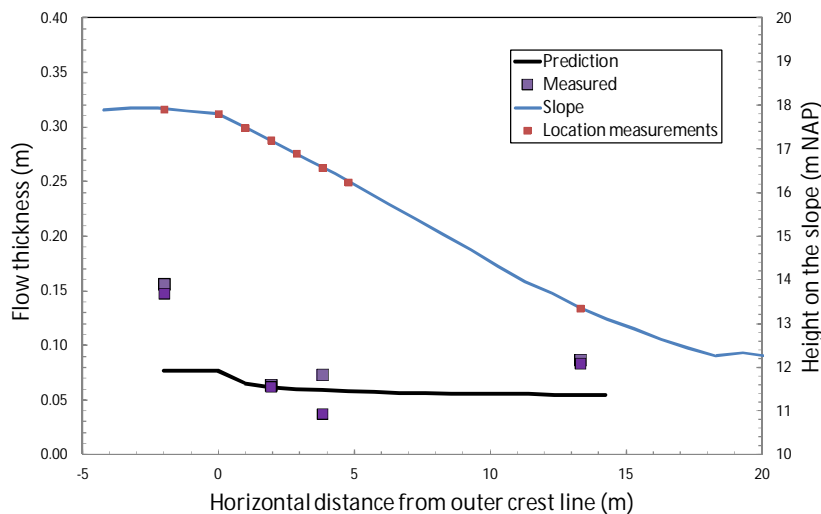


Figure 4.15 Measured and calculated flow thickness along the slope for $u_o = 4$ m/s ($V = 1000$ l/m)

Also in Fig. 4.17 the prediction, i.e. $u_o = 6$ m/s and a theoretical line for $u_o = 7$ m/s are given. Though the velocity at the crest was really close to 6 m/s and not to 7 m/s the measured flow thicknesses of SB3 to SB5 are closer to the 7 m/s line. It is unclear why the measured points are higher than expected. Nevertheless, the *trend* of theory and measurements is similar, a

decrease between SB3 and SB4. This decrease should theoretically (for steady state overflow!) continue for SB5, which is not the case. The slowdown of the overtopping process (increased overtopping duration), which cannot be modelled by steady state, may be the reason for this.

In general one may conclude that a friction factor of $f = 0.01$ leads to the correct trends for both flow velocity and flow thickness. The actual values for the flow velocity are well predicted by the theory of steady state. It is more difficult to predict the correct flow thickness. But the flow velocities are governing in the cumulative overload, which makes the prediction of flow thicknesses less relevant.

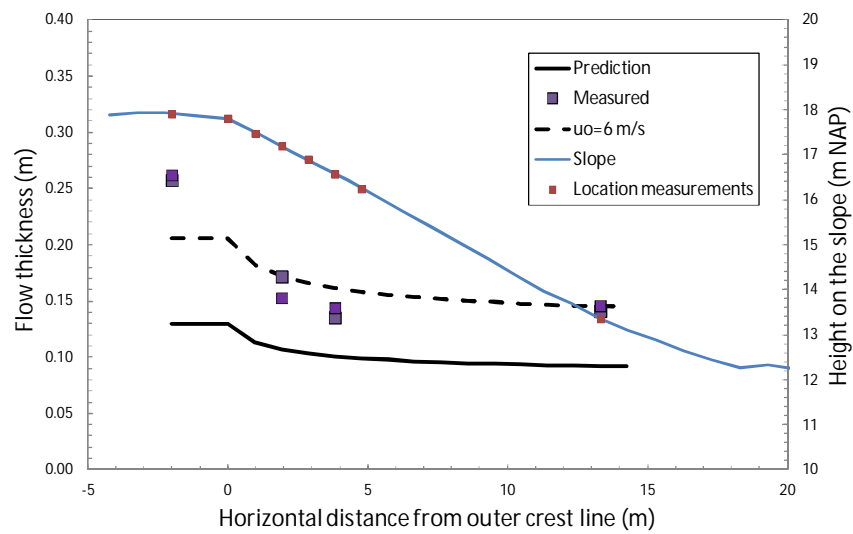


Figure 4.16 Measured and calculated flow thickness along the slope for $u_o = 5$ m/s ($V = 2500$ l/m)

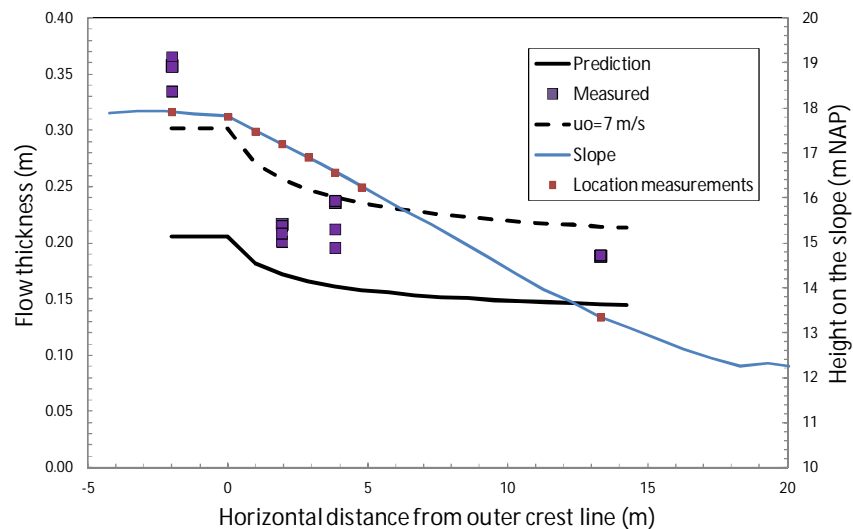


Figure 4.17 Measured and calculated flow thickness along the slope for $u_o = 6$ m/s ($V = 4000$ l/m)

Friction factor and turbulence

Based on the equations of continuity and motion Schüttrumpf and Oumeraci (2005) deduced a model for predicting the flow velocities and flow thicknesses on the landward slope of dikes. Both the effects of acceleration and deceleration of the overtopping waves can be simulated. Computational results show that the acceleration on the slope can be described well provided $f = 0.01$. However, by using $f = 0.01$ the predicted flow thicknesses are too small.

Turbulence parameters are related to friction factors. In the literature different parameters can be found to express the friction close to the bed, for example, Chézy coefficient (C), friction factor (f) as proposed by Schüttrumpf and Oumeraci (2005) and Manning coefficient (n_M).

Table 4.1 shows the relation between these friction factors and the depth-averaged relative turbulence intensity (r_0) for uniform flow conditions (SBW-2012-1).

Table 4.1 Friction factors versus turbulence intensities (uniform flow conditions)

r_0 (-)	0.06	0.08	0.12	0.18
f (-)	0.0058	0.01	0.02	0.045
C ($m^{0.5}/s$)	60	45	32	21
n_M ($s/m^{1/3}$)	0.014	0.018	0.03	0.054

Following Schüttrumpf and Oumeraci (2005) the friction factor is $f = 0.0058$ yielding $C = 60$ $m^{0.5}/s$ (or $r_0 = 0.06$ or $n_M = 0.014$ $s/m^{1/3}$). If $f = 0.01$ then $C = 45$ $m^{0.5}/s$ (or $r_0 = 0.08$ or $n_M = 0.018$ $s/m^{1/3}$). These values of the friction factor seem too low because they result in too high values of C . For example, for rivers with ripples and sand dunes values of 35 $m^{0.5}/s$ to 40 $m^{0.5}/s$ are applied. Moreover, this value of f is considerably lower than the value mentioned in the literature for grass in floodplains where n_M is about $n_M = 0.03$ (corresponding with $C \approx 32$ $m^{0.5}/s$). For turbulent flow conditions the normal turbulence is approximately $r_0 = 0.1$.

However, owing to acceleration effects on the landward slope and the smoothness of grass lower turbulence intensities might be possible which is discussed below. The Chézy equation reads (e.g. Graf 1998)

$$U = C\sqrt{h\sin\theta} \quad (4.1)$$

where the turbulence intensity can be approximated by (e.g. Hoffmans 2012)

$$r_0 = 1.2\sqrt{g} / C \quad (4.2)$$

If air is included then r_0 can be written as (e.g. Hoffmans 2012)

$$r_0 = 1.2\sqrt{gh(1-\eta_a)\sin\theta} / U \quad (4.3)$$

where C is the Chézy coefficient, g is the acceleration of gravity, h is the flow depth, U is the flow velocity, r_0 is the depth-averaged relative turbulence intensity, θ is the angle of the slope and η_a is the air content .

Two locations on the dike, i.e., on the crest and near the toe (or at the lowest measuring point) are considered. Table 4.2 presents the measured flow depths and flow velocities which are obtained from Figs. 4.9 to 4.11. Table 4.2 also provides the computational results of the

friction factors (C and f) and the turbulence parameter r_0 . On the crest, the flow is significant turbulent as r_0 lies in the range of $0.15 < r_0 < 0.2$ whereas near the toe the turbulence decreases to uniform flow conditions, that is, $r_0 \approx 0.1$. The computations also show that the turbulence decreases with increasing wave volumes (see also Fig. 4.18).

Table 4.2a Experimental results on the crest and computed frictions factors and turbulence

V (ℓ)	h (m)	U (m/s)	C ($m^{0.5}/s$)	f (-)	$^{(1)} r_0$ (-)	$^{(2)} r_0$ (-)
1000	0.16	3.9	17.8	0.062	0.211	0.177
2500	0.25	5.1	18.6	0.057	0.202	0.169
4000	0.32	6.0	19.4	0.052	0.194	0.162

⁽¹⁾ computed by using Eq. 4.3 without air ⁽²⁾ computed by using Eq. 4.3 with air ($\eta_a = 0.3$); $\sin\theta = 0.3$

Table 4.2b Experimental results near the toe of the dike and computed frictions factors and turbulence

V (ℓ)	h (m)	U (m/s)	C ($m^{0.5}/s$)	f (-)	$^{(1)} r_0$ (-)	$^{(2)} r_0$ (-)
1000	0.08	5.5	35.5	0.016	0.106	0.089
2500	0.15	7.7	36.3	0.015	0.104	0.087
4000	0.18	9.0	38.7	0.013	0.097	0.081

⁽¹⁾ computed by using Eq. 4.3 without air ⁽²⁾ computed by using Eq. 4.3 with air ($\eta_a = 0.3$); $\sin\theta = 0.3$

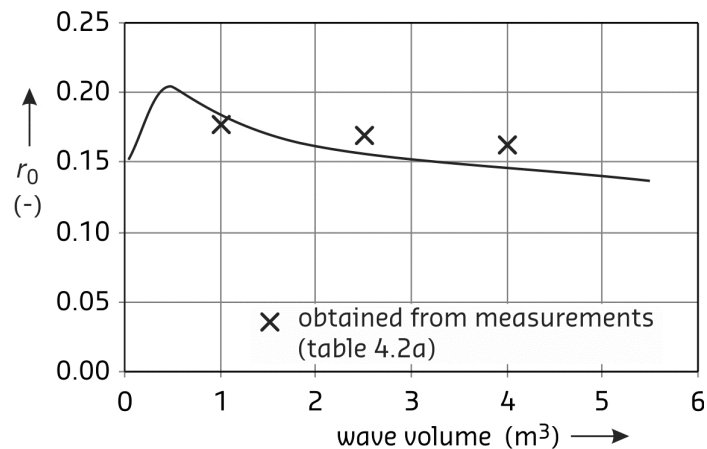


Figure 4.18 Turbulence intensity (best guess values) as function of the wave volume on the crest of the dike (Hoffmans 2012)

When the overtopping waves are released on the crest of the dike the flow on the landward slope accelerates. Measurements show that the equilibrium flow depth is achieved close to the toe of the dike, that is, approximately 20 m downstream of the crest (see also Appendix A). When the new-boundary layer reattaches the water surface the flow is in equilibrium, i.e. at a distance (L) of 20 to 50 times the flow depth. By using $h = 0.25$ m it follows that L varies from 4 m to 10 m. Hence, the turbulence intensity on the landward slope can decrease to uniform flow conditions.

Based on the aforementioned comparison between values for $f \leq 0.01$ recommended by Schüttrumpf and Oumeraci (2005) it should be concluded that the value of the friction factor is too low given the corresponding values for r_0 , C and n_M . However, measured flow velocities

can be predicted well with a value of $f = 0.01$. Note that if $f = 0.06$ is used then the computed flow on the landward slope not accelerates but decelerates. Most likely the German model predicts relative small values of f as the influence of air is not taken into account.

When the effects of air are included in the German model the flow depth must increase to satisfy the equilibrium equations. As there are air bubbles in the flow the water density is lower. In order to correct the normal force the flow depth has to increase which results by using Eq. 4.1 in a decrease of the Chézy coefficient (or in an increase of the friction factor). Note that the predicted flow thickness as shown in Figs. 4.15, 4.16 and 4.17 are too small with respect to the measured h . Hence, it is recommended to investigate the relation between air content and friction factor in greater detail.

4.3 Load penetration in turf

Introduction

On the landward slope, the current of overtopping waves causes pressure fluctuations or pressure gradients near the bed. Figure 4.19 shows a simplification of the hydrostatic and fluctuating pressures as function of time. The soil absorbs over pressures (or pressure gradients directed downward) whereas the roots are mainly loaded by under pressures (or pressure gradients directed upward).

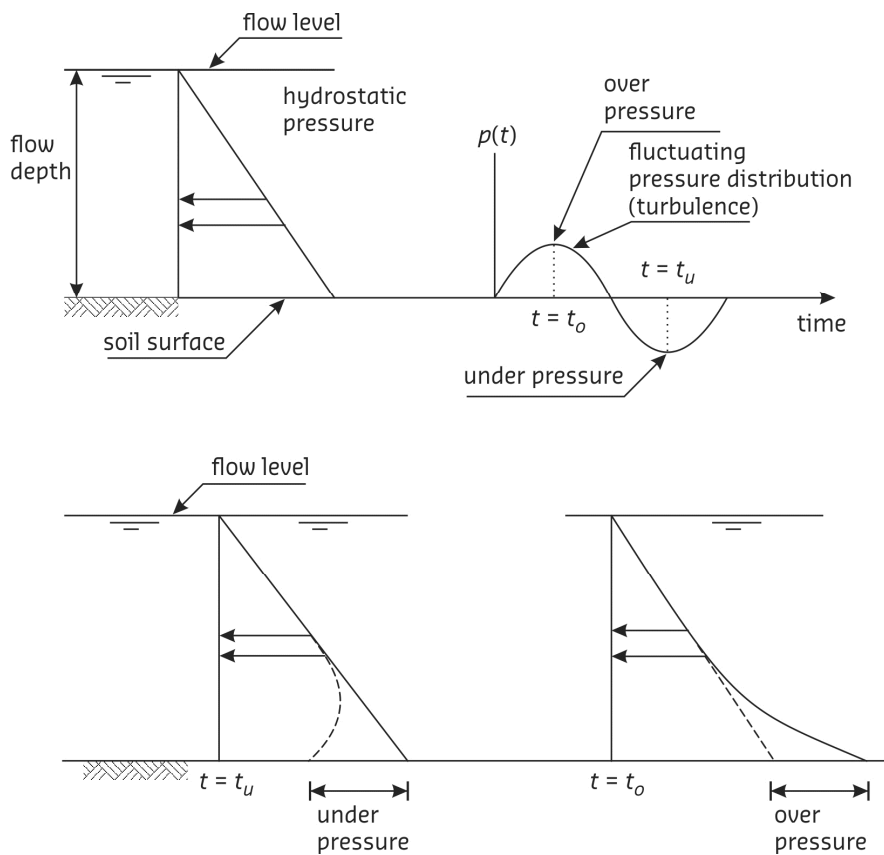


Figure 4.19 Hydrostatic and fluctuating pressures as function of time

This Section deals with the load penetration in the subsoil. In Millingen aan de Rijn pressure fluctuations (or pore pressures as function of the time) are measured both near the bed and at 10 cm depth. The measured pressure fluctuations at the bed are used to determine the relative depth-averaged turbulence intensity. These computational results are discussed in relation to the friction factor (see also Section 4.2).

In the laboratory dynamic load tests are conducted to determine the pressures fluctuations at the bottom of the sample. Soil parameters are determined from grass sods taken from the test location in Millingen aan de Rijn and used for Pluto calculations. Both computational and experimental results are discussed for evaluating the assumptions in the Turf-element model (see also Chapter 2 and Hoffmans 2012).

Pressure measurements

Physically, the turbulence energy (k) is characterised by measured (RMS) flow velocity fluctuations. As pressure fluctuations are related to flow velocity fluctuations they are also correlated to the turbulence energy. Klar (2005) measured the flow velocity fluctuations with a laser doppler anemometer in the open pores of the filter layer. Figure 4.3 shows that the turbulence energy (and thus also the pressure fluctuations) decreases significantly with depth as the bed pressure fluctuations depend on both time and place. If the contribution to the fluctuating soil stresses at about 10 cm below is negligible or if the soil stress is determined by the suction pressures which is dependent on the local soil properties then the damping of the load penetration is very fast.

In Millingen aan de Rijn pressure fluctuations were measured on two locations, i.e., at the ground surface and at about 10 cm below. The four pressure sensors measured signals with a frequency of 100 Hz. As the wave period is about 10 s the total number of signals is 1000 per wave. These tests were carried out at approximately halfway the dike slope for different wave volumes. The distance between the recorder instruments was about 5 m (Fig. 4.4). Before the tension apparatus was positioned below the surface the soil in the inclined hole was carefully removed (Fig. 4.20).

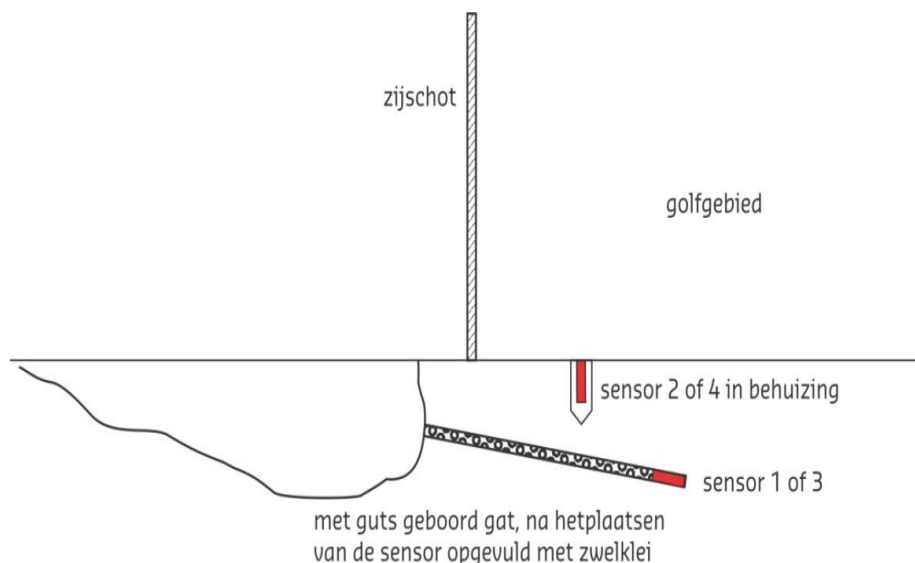


Figure 4.20 Pressure sensors

Figure 4.21 shows the measured pressure fluctuations at the ground level and the measured pore pressures in the soil for both small and large waves ($V = 400\ell$ and $5,000\ell$), see also Appendix E where more details of the experimental results are shown.

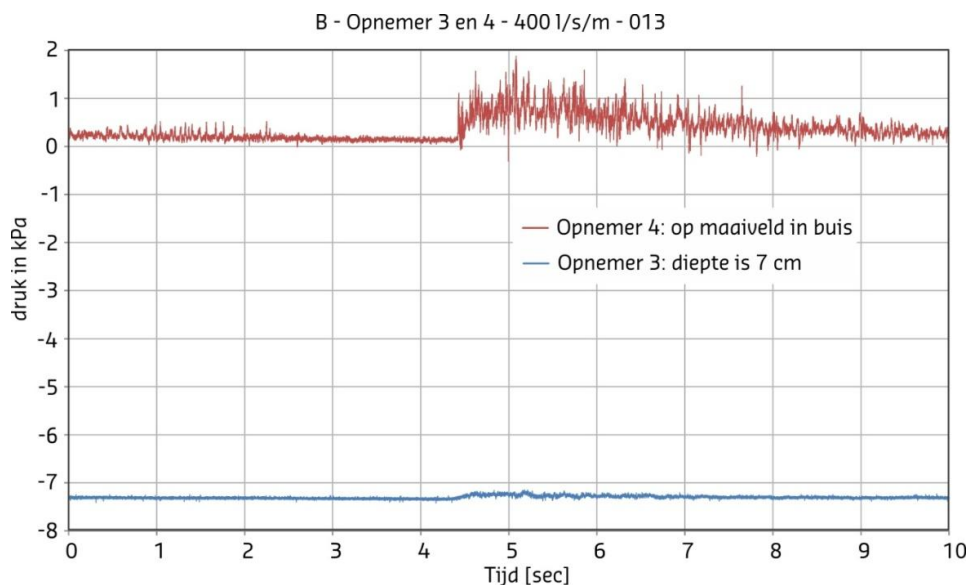


Figure 4.21a Pressure distributions as function of time at the surface and about 10 cm below for $V = 400 \ell/s$ per m (Location B)

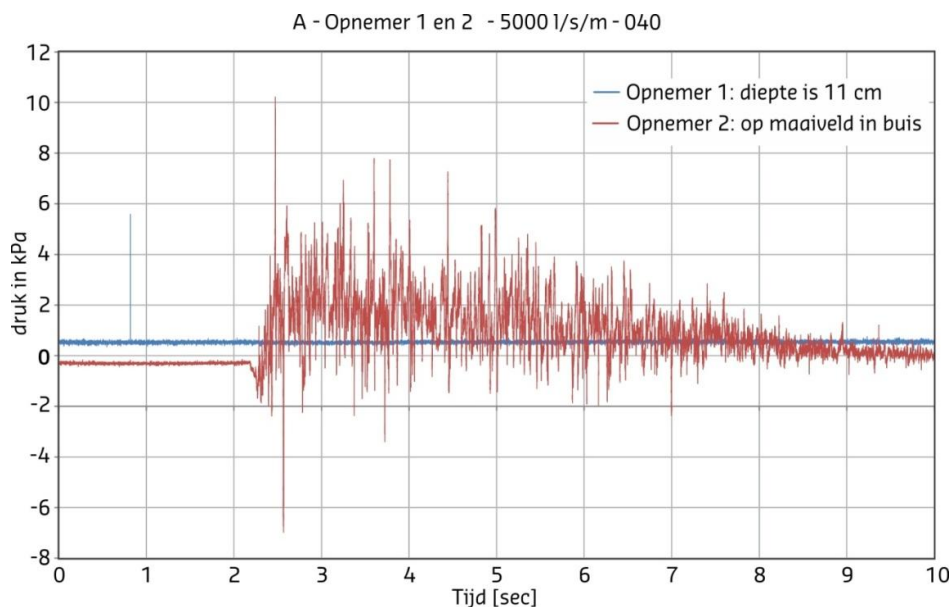


Figure 4.21b Pressure distributions as function of time at the surface and about 10 cm below for $V = 5000 \ell/s$ per m (Location A; series 2)

At about 10 cm below the surface, the measured pore pressures varied from 0 kPa to -7.5 kPa. When the experiments in Millingen aan de Rijn started the measurements showed that the pore pressures were about -7.5 kPa with a small response (Fig. 4.21a). Most likely, the suction pressures were active when the soil was not wet enough. Later, when the soil was saturated (probably fully saturated) the suction pressures reduced to zero (thus p_w reduced from -7.5 kPa to 0 kPa during the experiment; see also Figs. 4.21a and 4.21b).

The measurements also show that there is hardly a correlation between the pressure fluctuations at the ground surface and at 10 cm below (see also Fig. 4.21c). Moreover, the amplitude at 10 cm depth is marginal. Hence, the load at this reference level is mainly determined by the suction pressures, which is dependent on the local soil properties and not by the bed turbulence at the ground surface.

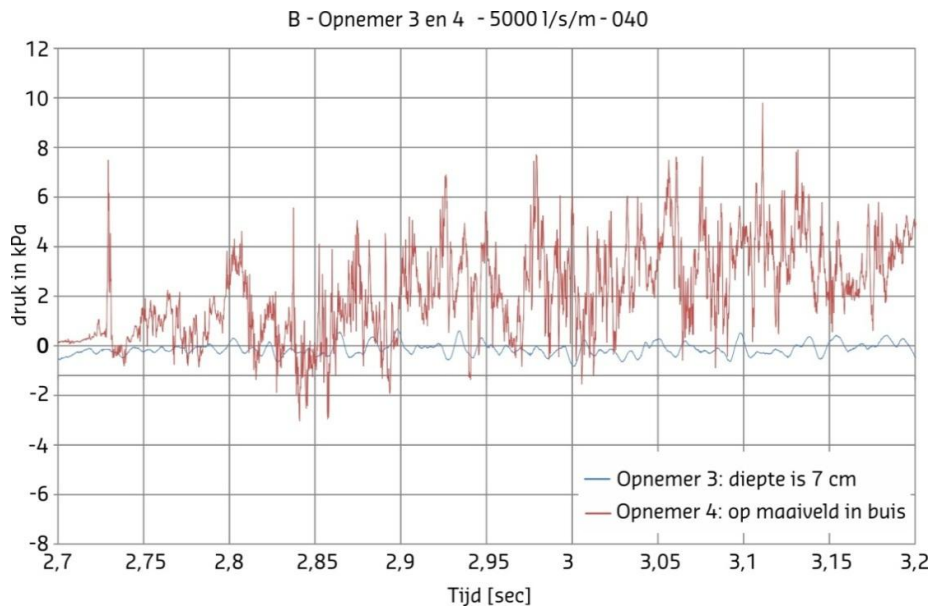


Figure 4.21c Pressure distributions as function of time at the surface and about 10 cm below for $V = 5000$ l/s per m (Location A; series 2)

Turbulence measurements on the river dike along the Vecht, the steepness of which is about 1V:4H, demonstrated that the pressure fluctuation is at maximum where the flow depth is at maximum. These measurements also showed that with an increasing wave volume (V) the flow depths and flow velocities increase. Although r_0 gradually decreases if V (and thus also h and U) increase as can be seen in Fig. 4.18 the values of r_0 obtained from measurements (Table 4.2a) are about constant.

Table 4.3 presents the measured maximum pressure fluctuations or the peak values of the maximum over and under pressures for a wave volume of 5 m^3 halfway the landward slope. Also the local maximum values of both the under and over pressures are given. These values represent the actual bed load as they are corrected for the hydrostatic pressures (estimated flow depth was 0.25 m).

The depth-averaged relative turbulence intensity can be computed by (e.g. Hoffmans 2012)

$$r_0 = \frac{1}{U} \sqrt{\frac{p_m}{12.6\rho}} \quad (4.4)$$

Table 4.3 Experimental results of peak values (amplitude) (see also Appendix E)

Recorder	Measurements (incl. flow depth)		Measurements (excl. flow depth of 25 cm)	
	Max. over pressure (kPa)	Max. under pressure (kPa)	Max. over pressure (kPa)	Max. under pressure (kPa)
2	10.0	-5.8	7.5	-8.3
2	10.2	-6.8	7.7	-9.3
4	10.0	-4.5	7.5	-7.0
4	9.8	-5.2	7.3	-7.7
		mean values	7.5	-8.1

If a wave volume of $V = 5 \text{ m}^3$ is considered halfway the landward slope with a flow depth of $h = 0.25 \text{ m}$ (see also Fig. 4.11), flow velocity of $U = 8 \text{ m/s}$ (note that the flow velocity is increased from 6 m/s (crest conditions) to about 8 m/s , see also Fig. 4.10), maximum under pressure fluctuation $p_m = 8 \text{ kPa}$ and an aeration content of $\eta_a = 0.3$ at a dike slope of 1V:3H ($\sin\theta = 0.3$) then it follows that for this wave volume the computed turbulence is about $r_0 \approx 0.1$ (or $f = 0.014$) which is significantly lower than the turbulence intensity on the crest of the dike.

The turbulence period (T) of the largest eddies with the highest energy varies from 0.01 s to 0.05 s for super critical flow as can be seen in Fig. 4.21c. Usually such eddies have a length scale which equals the flow depth. Hence, if these eddies are advected with the mean flow, then the time interval for it to pass is given by $T = h/U$. By using $h = 0.25 \text{ m}$ and $U = 8 \text{ m/s}$ it follows that $T = 0.03 \text{ s}$.

This analysis also demonstrates that the computed turbulence halfway the landward slope obtained from measured parameters (see Eqs. 4.3 and 4.4) agree with the turbulence corresponding to uniform flow. Therefore, the friction factor $f = 0.01$ as discussed in Section 4.2 can certainly be used to predict the flow velocities on the landward slope.

Dynamic load tests

The soil properties in the upper 10 cm are characterised by the soil structure, fissures, roots and worm holes. To determine soil parameters just beneath the slope surface, turf samples were taken from a dike along the river Rhine near Millingen (Greeuw 2013). The following soil parameters are experimentally determined, namely the hydraulic conductivity (K), the bulk density of soil (ρ_n), the one-dimensional stiffness parameter (M with dimensions of Pa) ($M = E_{oed}$ is the oedometric modulus of deformation or $M = 1/m_v$, where m_v is the coefficient of volume compressibility). The consolidation coefficient (c_v) is computed by using the Terzaghi formula (e.g. Barends 1992)

$$c_v = \frac{KM}{\rho g} \quad (4.5)$$

where g is the acceleration of gravity. The resulting values of the hydraulic conductivity (20°C) are (see also Appendix B where the laboratory tests are described) $K = 2.1 \cdot 10^{-4} \text{ m/s}$ (test 1) and $K = 1.7 \cdot 10^{-4} \text{ m/s}$ (test 2). For a field temperature of 10°C , a multiplication factor of 0.8 has to be applied as the kinematic viscosity of water is higher and thus the hydraulic conductivity is lower at lower temperatures. After the permeability tests the samples were

dismounted and weighed. The bulk densities of the saturated samples are $\rho_n = 1500 \text{ kg/m}^3$ (test 1) and $\rho_n = 1430 \text{ kg/m}^3$ (test 2).

Dynamic load tests (Fig. 4.22) were conducted in order to determine the stiffness parameter of turf. Substituting the aforementioned values of K and an averaged value of the stiffness parameter $M = 150 \text{ kPa}$ (see also Appendix B) in Eq. 4.5 yields $c_v = 3.4 \cdot 10^{-3} \text{ m}^2/\text{s}$ (test 1) and $2.6 \cdot 10^{-3} \text{ m}^2/\text{s}$ (test 2).



Fig.4 22a Preparing the bottom side by picking off clay parts and application of gravel layer

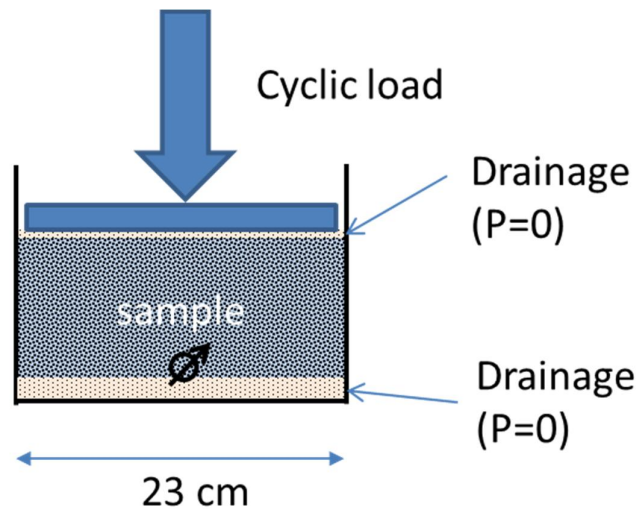


Fig.4 22b Schematic side view of dynamic test principle

The turf samples were subjected to a cyclic load in which the pressure amplitude was about $p_m = 2 \text{ kPa}$ with a pressure period $T = 0.2 \text{ s}$ which is about 10 times larger than the measured pressure period at the test location Millingen aan de Rijn (see also Fig. 4.21c). Figure 4.23

shows experimental results of the displacement, the sample pressure (p_{top}) on the top and the pore pressure ($p_{w,b}$) at the bottom, see also Appendix B where additional measurements are presented. The ratio between the pressure fluctuations on top of the grass sample and the pressure fluctuations at the bottom of the grass sample lies in the range of 80% to 100%. Hence, the load penetration of water overpressures is very slowly. The differences between the laboratory and the prototype results can most likely be ascribed to the different load on the top of the sample/ground surface and the differences in the force transmission.

In the laboratory the pressure was modelled by a sinusoidal time function, whereas in the prototype situation the bed pressure fluctuations depend on both time and place. Moreover, the frequency of the relevant eddies in the turbulent flow was about 10 times larger. In the laboratory the side walls were made frictionless while the friction forces at the test location in Millingen aan de Rijn depend on the soil properties. Therefore, the laboratory and prototype experiments may not be compared.

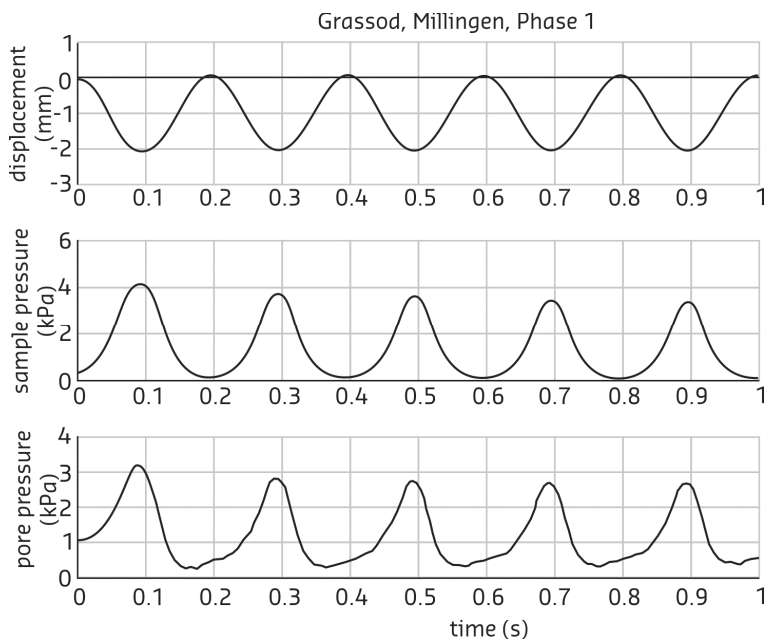


Figure 4.23 Pore pressure (at bottom of sample) , sample pressure (on top) and displacement as function of time (Phase 1)

Pluto calculations

PLUTO is a finite elements program designed for deformation analysis by using non-linear stationary algorithms and consolidation analysis by using quasi-static or time dependent algorithms. The geotechnical problems, which can be solved with this program, include elastic and/or plastic deformation analysis, groundwater flow and the combination of these for consolidation analysis (Teunissen 2010).

For problem schematisation purposes the soil can be constructed by using multiple layers or material groups. Each layer or group can be defined with its own constitutive model and appropriate stiffness and strength parameters. The problem can be defined by either prescribed displacements or by loads. To simulate bed turbulence on the landward slope of dikes as a result of wave overtopping the following starting points are made:

- Grid domain is 1 m long and 1 m deep;
- Grass shear stresses are excluded (thus the effects of roots along the side walls are neglected). In other words, a free-slip condition is used along the side-walls similar to the dynamic load tests;
- Horizontal groundwater flow is not modelled;
- Effects of turbulence are modelled by a sinusoidal pressure function with an amplitude of $p_m = 5$ kPa;
- Pressure period representing the bed turbulence is $T = 0.2$ s;
- Pressure fluctuations caused by the flow act on the soil;
- Bulk density measures $\rho_n = 1500$ kg/m³;
- Porosity is estimated to be $n = 0.4$;
- Compressibility of water (β) varies from $1.6 \cdot 10^{-3}$ (kPa)⁻¹ to $2.0 \cdot 10^{-4}$ (kPa)⁻¹;
- Poisson ratio (ν) lies in the range of 0 to 0.3.

Figure 4.24 shows computational results of Pluto where the effective fluctuating soil stress is given as function of the vertical coordinate. The maximum value of the effective fluctuating soil stress is 5 kPa and occurs near the surface. At 5 cm depth the effective fluctuating soil stress is approximately 1 kPa. At 10 cm depth the effective fluctuating soil stress measures about 0.5 kPa. The computations also demonstrate that the influence of the magnitude of both the compressibility of water and the Poisson ratio on the damping of soil stresses is negligible.

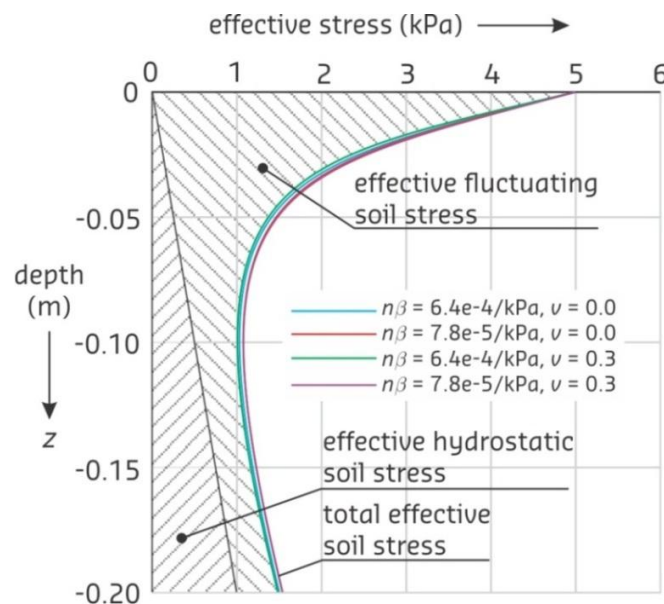


Figure 4.24 Effective soil normal stresses as function of the vertical (over pressure)
(Pluto calculations)

In the Pluto calculations and the dynamic load tests similar assumptions are used so these computational and experimental results are comparable. If traveling waves are included in the calculations (thus the effects of both dp/dx and dp/dt are taken into account) then the load penetration is somewhat faster. However, this computed load penetration still differs with the measured one as shown in Fig. 4.21. Most likely the differences can be ascribed to the different pressure periods (Pluto: $T = 0.2$ s and Millingen aan de Rijn: $T = 0.03$ s). Hence, it is recommended to make new computations with Pluto where a pressure period $T = 0.03$ s.

Based on a one-dimensional approach, Barends (1992) (see also De Groot et al. 1996) deduced for the characteristic length (L) of the effect of consolidation under cyclic loading

$$L = \sqrt{\frac{c_v T}{2\pi}} \quad (4.11)$$

By using a vertical consolidation coefficient of $c_v = 0.8 \times 3 \cdot 10^{-3} = 2.4 \cdot 10^{-3} \text{ m}^2/\text{s}$ (where the factor 0.8 represents a correction for the field temperature 10^0 C) and a pressure period of $T = 0.03 \text{ s}$ (corresponding to super critical flow) the characteristic length is $L = 0.33 \text{ cm}$. Hence, the measured pressure variations at 5 cm depth are marginally influenced by the effect of cyclic consolidation and thus one of the assumptions made in the turf-element model is correct, i.e., the load can be considered as acting on the surface (and not on the side walls).

4.4 Transitions and objects

Introduction

Erosion by wave overtopping at dike transitions is a major cause of dike damage or failure during severe overtopping events. For example, when the flow of the waves is directed from a smooth to a rough bed the load increases. In the direction from rough to smooth the load decreases. These effects are here expressed by a load factor. The damage at transitions can be predicted by the cumulative overload method in which the load is corrected by the load factor. This Section deals with the load factor for revetment transitions (Fig. 4.25), geometrical transitions and vertical objects.



Figure 4.25 Revetment transition from asphalt to grass (Millingen aan de Rijn)

Revetment transitions

As the flow at transitions is complex some assumptions are made. In the analysis the following starting points are used (see also Chapter 3 and Appendix C which provide insight in the load modelling at (dike) transitions between revetments with different roughness, perpendicular to the general flow direction).

- Load increase or load decrease is modelled by a down-flow or an up-flow; see also Appendix C) and is determined from the flow velocities outside the internal boundary layer at a vertical distance $\delta = 0.3h$ (not from the velocities in the inner region);
- Effects of eddies and turbulence are neglected;
- Bed shear velocity is computed by using the Shields approach;
- Nikuradse roughness is proportional to the particle diameter;
- Longitudinal flow velocity as function of the vertical is modelled by a log-function;
- Manning coefficient is used for predicting the roughness of the revetments at the transition, as this coefficient is broadly accepted in hydraulic engineering.

When the flow is directed from a smooth to a rough revetment the load factor (α_M) can be written as (Box A gives a working out of the load factor at revetment transitions; complete derivation is given in Appendix C)

$$\alpha_M = 2 - \left(\frac{n_{M,s}}{n_{M,r}} \right)^6 \left(\frac{\ln \frac{10h}{(8\sqrt{g}n_{M,s})^6}}{\ln \frac{10h}{(8\sqrt{g}n_{M,r})^6}} \right)^2 \quad (4.12)$$

where g is the acceleration of gravity, h is the flow depth and n_M is the Manning coefficient (subscripts r and s refer to rough bed and smooth bed).

Box A Working out of load factor at revetment transitions

At transitions when the flow is directed from a smooth to a rough bed the maximum shear force ($F_{s,m}$) can be written as

$$F_{s,m} = F_{s,r} + dF_{s,r} \quad (A1)$$

where $F_{s,r}$ is the mean shear force (or friction force) at the rough bed under uniform flow conditions and $dF_{s,r}$ is the increase of the mean shear force at the transition. By applying the friction factor (e.g. Hoffmans 2012) Eq. A1 can be rewritten as

$$f_r F_{n,m} = f_r F_{n,r} + f_r dF_{n,r}$$

or

$$F_{n,m} = F_{n,r} + dF_{n,r} \quad (A2)$$

where f_r represents the friction factor related to the rough bed, $F_{n,r}$ is the mean normal force at the rough bed far downstream of the transition and $dF_{n,r}$ is the increase of the mean normal force at the transition.

Note that F_s is related to the (mean) bed shear stress and F_n is correlated to the weight of the water. As there is a down-flow at the rough bed (see also Appendix C) the mean normal force at the transition increases with $dF_{n,r}$.

Box A (continued)

Note that F_s is related to the (mean) bed shear stress and F_n is correlated to the weight of the water. As there is a down-flow at the rough bed (see also Appendix C) the mean normal force at the transition increases with $dF_{n,r}$.

Figure A1 shows the experimental and computational results of the bed shear stress as function of the streamwise direction (Nezu and Nakagawa 1993). At the transition the bed shear stress is about twice as large as the bed shear stress far downstream of the transition. Hence, when the bed shear stress upstream of the transition at the smooth bed is marginal, e.g. in case of extreme smooth conditions, it follows that $F_{s,m} \approx 2F_{s,r}$ or $dF_{s,r} \approx F_{s,r}$.

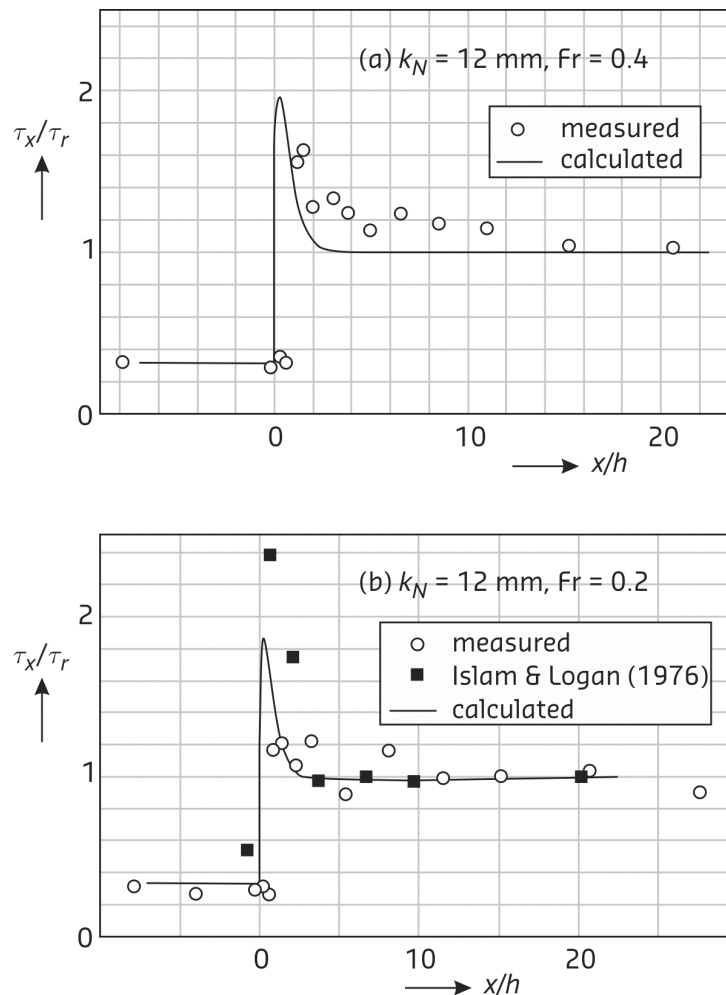


Figure A1 Overshooting property of bed shear stress in open channel flows (Nezu and Nakagawa 1993)

Fr is the Froude number; k_N is the Nikuradse roughness, τ_x is the bed shear stress in the streamwise direction and τ_r is the bed shear stress at the rough bed under uniform flow

Box A (Continued)

In this study, the following assumption is made

$$dF_{s,r} = F_{s,r} - F_{s,s} \quad (\text{A3})$$

in which $F_{s,s}$ is the mean shear force at the smooth bed upstream of the transition and thus $F_{s,m}$ can be rewritten as (see also Eq. A1)

$$F_{s,m} = 2F_{s,r} - F_{s,s} \quad (\text{A4})$$

or

$$\alpha_M = 2 - \frac{F_{s,s}}{F_{s,r}} \quad (\text{A5})$$

so the load factor ranges from 1 to 2 depending on the roughness difference of the beds at the transition. In the opposite direction, i.e. from rough to smooth beds, the near-bed flow is upwards directed yielding a decrease of the mean shear force.

Consequently, the load factor varies from 1 (no transition) to 2 (extreme roughness difference at transition). When the flow is directed from a rough to a smooth bed the load factor could be written as (this has not been validated here, see also Appendix C))

$$\alpha_{M,r \rightarrow s} = 2 - \alpha_M \quad (4.13)$$

Below some examples are discussed (see also Table 4.4 where indicative values of the Manning coefficient are given for various boundaries).

Example 1: Consider the transition of an asphalt road on the crest of the dike and a grass revetment at the inner side of the dike. The Manning coefficient of asphalt is estimated by $n_{M,s} = 0.016$ (or $k_{N,s} \approx 4$ mm) and the roughness of grass is about $n_{M,r} = 0.025$ (or $k_{N,r} \approx 6$ cm), thus α_M varies from 1.7 to 1.8 depending on the flow depth ($0.1 \text{ m} < h < 0.5 \text{ m}$).

Example 2: If a horizontal transition is considered between a grass revetment ($k_{N,r} = 0.05 \text{ m}$) and a parking area of (smooth) bricks $n_{M,s} = 0.016$ (or $k_{N,s} \approx 4$ mm), thus the flow is directed from the grass revetment to the stones, the load factor ranges from 0.2 to 0.3 depending on the flow depth. Although the load decreases damage could occur as the strength or the critical flow velocity of stones could be less than the grass strength.

Figure 4.26 shows the time dependent erosion at the transition of an asphalt road on the crest of the dike to a grass revetment. This revetment transition was tested on a dike in Millingen during the winter 2012/2013. In the beginning of the test, slit erosion occurred, i.e., sand was washed out forming an unevenness at the transition which influence is not included in the modelling.

Most likely a horizontal eddy developed in the track during the testing. Hence, the near-bed velocities in the recirculation zone decrease. However, due to a mixing layer the bed turbulence increases. As the decrease of the near-bed velocities is greater than the increase

of the bed turbulence the total load decreases, more details are given by Hoffmans (2012). To improve the modelling on this topic more research is needed.

Table 4.4 Manning's roughness coefficients for various boundaries

The following Manning's roughness coefficient table is from the United States Department of Transportation – Federal Highway Administration: Hydraulic Engineering website:

<http://www.fhwa.dot.gov/engineering/hydraulics/pubs/08090/appb.cfm>

	Manning's coefficient
Rigid Boundary Channels	
Very smooth concrete and planed timber	0.011
Smooth concrete	0.012
Ordinary concrete lining	0.013
Wood	0.014
Vitrified clay	0.015
Shot concrete, untroweled, and earth channels in best condition	0.017
Straight unlined earth canals in good condition	0.020
Mountain streams with rocky beds	0.040 -0.050
MINOR STREAMS (top width at flood stage < 30 m)	
Streams on Plain	
1. Clean, straight, full stage, no rifts or deep pools	0.025–0.033
2. Same as above, but more stones and weeds	0.030–0.040
3. Clean, winding, some pools and shoals	0.033–0.045
4. Same as above, but some weeds and stones	0.035–0.050
5. Same as above, lower stages, more ineffective slopes and sections	0.040–0.055
6. Same as 4, but more stones	0.045–0.060
7. Sluggish reaches, weedy, deep pools	0.050–0.080
8. Very weedy reaches, deep pools, or floodways with heavy stand of timber and underbrush	0.075–0.150
Mountain Streams, no Vegetation in Channel, Banks Usually Steep, Trees and Brush Along Banks Submerged at High Stages	
1. Bottom: gravels, cobbles and few boulders	0.030–0.050
2. Bottom: cobbles with large boulders	0.040–0.070
Floodplains, Pasture, No Brush	
1. Short Grass	0.025–0.035
2. High Grass	0.030–0.050
Cultivated Areas	
1. No Crop	0.020–0.040
2. Mature Row Crops	0.025–0.045
3. Mature Field Crops	0.030–0.050
Brush	
1. Scattered brush, heavy weeds	0.035–0.070
2. Light brush and trees in winter	0.035–0.060
3. Light brush and trees in summer	0.040–0.080
4. Medium to dense brush in winter	0.045–0.110
5. Medium to dense brush in summer	0.070–0.160
Trees	
1. Dense willows, summer, straight	0.110–0.200
2. Cleared land with tree stumps, no sprouts	0.030–0.050
3. Same as above, but with heavy growth of sprouts	0.050–0.080
4. Heavy stand of timber, a few down trees, little undergrowth, flood stage below branches	0.080–0.120
5. Same as above, but with flood stage reaching branches	0.100–0.160

Table 4.4 (Continued)

MAJOR STREAMS (Topwidth at flood stage > 30 m)	
The n_M value is less than that for minor streams of similar description, because banks offer less effective resistance.	
Regular section with no boulders or brush	0.025–0.060
Irregular and rough section	0.035–0.100
Alluvial Sand-bed Channels (no vegetation)	
Tranquil flow, $Fr < 1$	
Plane bed	0.014–0.020
Ripples	0.018–0.030
Dunes	0.020–0.040
Washed out dunes or transition	0.014–0.025
Plane bed	0.010–0.013
Rapid Flow, $Fr > 1$	
Standing waves	0.010–0.015
Antidunes	0.012–0.020
Overland Flow and Sheet Flow	
Smooth asphalt	0.011
Smooth concrete	0.012
Cement rubble surface	0.024
Natural range	0.13
Dense grass	0.24
Bermuda grass	0.41
Light underbrush	0.40
Heavy underbrush	0.80

Damage at various locations ($D = 1000 \text{ m}^2/\text{s}^2$) was measured at $t = 6 \text{ h}$ in 10 l/s per m and failure near the transition ($D = 3500 \text{ m}^2/\text{s}^2$) was observed at 2 h in 50 l/s per m. Although a first estimation was made for the load increase at transitions, that is $\alpha_{M-general} = 1.3$ (see also Chapter 3) no prediction was given (see also Table 3.1). If the following assumptions are made

- Typically, the clay quality near the edges is less fat as the clay cover on the dike which can be ascribed to the sand layer below the asphalt road. Here, these effects are not considered;
- Eddies in the track and the influence of a geometrical transition, i.e. from the horizontal crest to the landward slope are neglected, see also next Section;
- Acceleration factor equals $\alpha_a = 1.0$ (see also Eq. 2.4);
- Load factor is $\alpha_M = 1.75$ (see also example 1 and Eq. 4.12);
- Critical flow velocity on slope is $U_c = 4.5 \text{ m/s}$ (see also Chapter 2);
- Strength factor is $\alpha_s = 0.9$ thus U_c reduces from 4.5 m/s to 4.0 m/s (see also Eq. 2.2 and Section 2.6).

then the predicted and measured times are about in agreement on which multiple open spots and failure of the grass cover occur.

Table 4.5 gives the calculated damage numbers of these events for three values of α_M . By using a load factor of $\alpha_M = 1.75$ the damage number at $t = 6 \text{ h}$ in 10 l/s per m for multiple open spots is $D = 771 \text{ m}^2/\text{s}^2$. For failure of the grass cover the predicted damage number is $D = 4241 \text{ m}^2/\text{s}^2$. These calculated values of D are in agreement with the defined values as discussed in Chapter 2.



Figure 4.26a Less damage at transition from asphalt road to grass revetment (after 6 h at the end of $q = 1$ l/s per m)



Figure 4.26b Multiple open spots at transition from asphalt road to grass revetment (after 12 h at the end of $q = 10$ l/s per m)



Figure 4.26c Failure of transition from asphalt road to grass revetment (after 14 h or after 2 h with $q = 50$ l/s per m)

Table 4.5 Effects of load factor on the erosion as function of time (U_c is related to crest conditions)

α_M (-)	U_c (m/s)	t_{measured} (hours)	Multiple open spots D (m^2/s^2)	t_{measured} (hours)	Failure grass cover D (m^2/s^2)
1.50	4.0	6 h – 10 l/s	330	2 h – 50 l/s	2320
1.75	4.0	6 h – 10 l/s	771	2 h – 50 l/s	4241
2.00	4.0	6 h – 10 l/s	1436	2 h – 50 l/s	6690

If the load factor is reduced by the effects of a geometrical transition (see also Eq. 4.13) then the strength factor should also decrease (or U_c must decrease). This analysis has not been done here.

The load factor for an asphalt road to a grass revetment lies in the range of 1.5 to 2.0 with a best guess value of $\alpha_M = 1.75$. The reduction of the strength, expressed by α_s is about 0.9 (see also Chapter 6). This value agrees approximately with the results of Pijpers (2013).

A conceptual model is discussed for predicting the load factor at revetment transitions (more details about the modelling can be found in Appendix C). The load factor represents the relative increase (or decrease) of the load. To determine the erosion/damage the extended overload method is used (see also Chapter 2).

Although the computational results are in the range of expectations it is recommended to validate the theoretical modelling by applying more (prototype) tests. Therefore, it is needed to select experiments where damage at transitions is/was observed. In addition, guidelines are needed for predicting the strength of different materials.

Furthermore, it is recommended to examine the work of, for example, Antonia and Luxton (1971) and Benson (2005). Here, a limited literature review is carried out. Moreover, it is recommended to make computations with mathematical flow models to investigate the effects of supercritical flow on the load factor (i.e., when the Froude number is greater than 1).

Geometrical transitions

The situation at a transition of a slope to a horizontal berm can be compared with a jet that normally occurs because of flow under, through or over hydraulic structures. In general, a jet lifts soil and transports it downstream of the impacted area. The jet impact area is transformed into an energy dissipater and a scour hole is formed (Fig. 4.27). Figure 4.27c shows a scour hole at the toe of the dike due to wave overtopping. Note that when a scour hole is formed deeper than 20 cm the grass revetment fails.

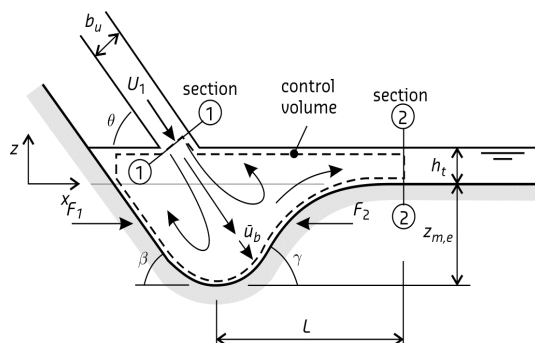


Figure 4.27a Scour due to plunging jets

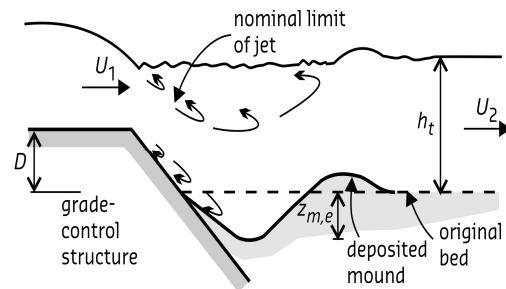


Figure 4.27b Scour downstream of grade control structure



Figure 4.27c Scour hole at the toe of the dike; sub soil consists of gravel (Kattendijke)

The following assumptions are made for estimating the load factor (see also Appendix D where more details about the modelling are given)

- Control volume is defined near the transition;
- Scouring is not considered;
- Force balance is applied to deduce the centripetal force at the transition;
- Load increase/decrease is defined as the ratio between the centripetal force and the maximum normal force;
- Maximum normal force is related to the energy grade line.

For geometrical transitions as shown in Fig. 4.27 the load factor (α_M) can be written as function of the steepness (θ) (see also Appendix D where the derivation of α_M is presented)

$$\alpha_M = 1 + \sin \frac{1}{2}\theta \quad (4.14)$$

The load factor depends on the steepness of the dike. If there is no geometrical transition or if $\theta = 0^\circ$ then $\alpha_M = 1$. If $\theta = 20^\circ$ (steepness is 1V:2.7H) then $\alpha_M = 1.17$. The predictions of the load factor were based on a scour approach (see also SBW 2012-2) and therefore they are less reliable. Nevertheless, Eq. 4.14 gives similar results for slopes with a steepness of 1V:3H. For a steeper slope, say 1V:2H, the load factor obtained from Eq. 4.14 is 10% smaller than the predicted value.

By using both the experimental data and the cumulative overload method the load factor varies from 1.25 to 1.35 for Nijmegen (N1 and N2) (see Table 4.6). For the steepest slope (N1) the load factor is 1.35. In Millingen multiple damage spots observed at the slope and at the geometrical transition occurred at the same time as the water could not flow away. Most likely the pool influenced/reduced the erosion process. Therefore, the load factor is $\alpha_M \approx 1$ (see also Chapter 2). By using Eq. 4.14 the predicted load factor lies in the range of 1.16 (Nijmegen N2) to 1.23 (Nijmegen N1).

Table 4.6 Load factor at the geometrical transition for Nijmegen and Millingen (U_c is related to crest conditions)

Location	α_M (-)	U_c (m/s)	t_{measured} (hours)	Multiple open spots D (m^2/s^2)	t_{measured} (hours)	Failure grass cover D (m^2/s^2)
Nijmegen (N1) - slope -	1.00	3.5	1.5h – 50 l/s	734	6.0h – 50 l/s	2636
Nijmegen (N1) - toe -	1.23	3.5	6.0h – 10 l/s	376	4.0h – 50 l/s	4324
Nijmegen (N1) - toe -	1.35	3.5	6.0h – 10 l/s	613	4.0h – 50 l/s	6061
Nijmegen (N2) - slope -	1.00	4.5	4.0h – 100 l/s	959	1.5h – 200 l/s	3280
Nijmegen (N2) - toe -	1.16	4.5	4.0h – 50 l/s	361	4.0h – 100 l/s	1589
Nijmegen (N2) - toe -	1.25	4.5	4.0h – 50 l/s	600	4.0h – 100 l/s	3977

Although there are differences between the measured and calculated load factors the relative error is less than 10%. The range of the load factor obtained from Eq. 4.14 is in agreement with other prototype measurements (see also SBW 2012-1). The load factor varied from 1.05 to 1.21 (Boonweg: $\alpha_M = 1.05$ and $U_c = 6.3$ m/s; St. Philipsland: $\alpha_M = 1.09$ and $U_c = 5.0$ m/s; Tholen: $\alpha_M = 1.21$ and $U_c = 4.0$ m/s).

If the flow is directed from a horizontal crest to a landward slope then the load factor is

$$\alpha_M = 1 - \sin \frac{1}{2}\theta \quad (4.15)$$

It is recommended validating this theoretical equation by using prototype experiments in greater detail.

Vertical objects and side-wall structures

The flow pattern at vertical objects can be divided into four characteristic features for sub-critical flow, namely the bow wave (or surface roller) due to the up-flow, the down-flow, the horseshoe vortex and the wake zone with the shed vortices (or vortex street) (Fig. 4.28).

The flow decelerates as it approaches the pier and comes to rest at the face of the pier. Near the surface, the deceleration is greatest, and decreases downwards. The down-flow reaches a maximum just below the bed level. The development of the scour hole at vertical objects also gives rise to a lee eddy, known as the horseshoe vortex. The horseshoe vortex is effective in transporting particles and extends downstream, past the sides of the pier.

Usually the flow separates at the sides of the object leading to the development of shed vortices in the interface between the flow and the wake. However, practical tests have shown that downstream of thick vertical objects there will be no directly mixing of water for super critical flow. Consequently, the load of the water along the tree is decisive with respect to the load downstream of the tree (Fig. 4.29).

The following starting points are made for modelling the erosion process at vertical objects (for example trees)

- Prototype tests at Dutch dikes have shown that the erosion process of grass covers is negligible at slender vertical objects (diameter is less than 15 cm);
- At relative thick vertical objects, whose thickness varies from 0.15 m to 1 m (e.g. tree on the Vechtdijk), erosion was observed after a series of storms, so these situations are further considered (Fig. 4.30);
- Erosion resistance of grass near trees and the erosion resistance of grass on the landward slope are assumed equal. In practice, due to shadow effects the grass strength near trees is less (see also Chapter 2);

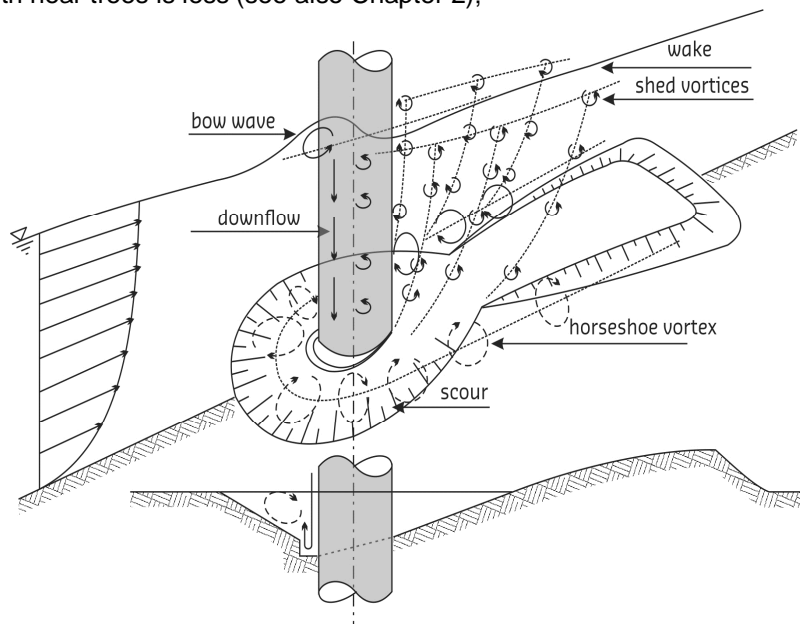


Figure 4.28 Characteristic flow zones at vertical obstacles (sub-critical flow)



Figure 4.29 Downstream of tree (there is no mixing downstream of the tree) for super critical flow



Figure 4.30 Erosion at tree; width of test section is 4 m

Based on expert judgement, the load factor (α_M) upstream of the vertical obstacle with C_D as the drag coefficient can be given by

$$\alpha_M = 1 + \frac{1}{4} C_D \quad (4.16)$$

The column on the left in Table 4.7 compares three-dimensional shapes like disks, cones, and spheres while the column on the right is for two-dimensional shapes like plates, wedges, and cylinders. Here, two-dimensional objects are considered. Therefore, the drag coefficient for piles, trees and houses varies from 1.2 to 2.3 depending on the shape.

Along the vertical obstacle, that is, in the acceleration zone the load factor is estimated by (basis is also expert judgement)

$$\alpha_M = 1.4 K_s \quad (4.17)$$

where the shape factor K_s varies from 0.8 to 1.2 (Table 4.8). For cylinder shaped objects (e.g. trees) the drag coefficient measures $C_D = 1.2$ ($K_s = 1.0$) yielding $\alpha_m = 1.3$ (Eq. 4.16) and $\alpha_m = 1.4$ (Eq. 4.17). For rectangular objects (for example side-wall structures, Fig. 4.31) holds $C_D = 2$ ($K_s = 1.2$) thus $\alpha_m = 1.5$ (Eq. 4.16) and $\alpha_m = 1.7$ (Eq. 4.17). Consequently, the load factor for vertical obstacles lies in the range of 1.3 to 1.7. Next, these predictors for the load factor are validated by using prototype tests.

In Nijmegen, a side-wall structure was tested on the horizontal berm as shown in Fig. 4.31. In the stagnation zone the grass revetment was reinforced with a concrete protection so at that location no erosion occurred. However, in the acceleration zone multiple damage spots were observed at $t = 1$ h in $q = 50$ ℓ/s . Subsequently, the acceleration zone was covered with a geotextile. The prediction was carried out with $U_c = 6$ m/s and $\alpha_M = 1.4$ yielding $t = 4$ h in $q = 50$ ℓ/s which is 3 hours later than the measured time. As the prediction of U_c is not correct the load factor at side-wall structures is evaluated with the following assumptions

Table 4.7 Drag coefficients for 2D (right side) and 3D (left side) objects for Reynolds numbers between 10^4 to 10^6 (source: <http://www.aerospaceweb.org/question/aerodynamics/q0231.shtml>)


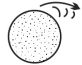
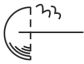


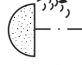

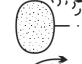





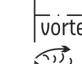





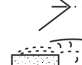

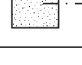
shape	C_B	shape	C_D
1  sting support	0.47	12 	1.17
2 	0.38	13 	1.20
3 	0.42	14 	1.16
4  3-4	0.59	15 	1.60
5  cube	0.80	16 	1.55
6  60°	0.50	17 	1.55
7  separation	1.17	18  vortex street	1.98
8  V	1.17	19  V	2.00
9  V	1.42	20  V	2.30
10  V	1.38	21  V	2.20
11  V cube	1.05	22  V	2.05

Table 4.8 Shape factor for different obstacles (Hoffmans and Verheij 1997)

Form of cross section		K_s
Horizontal	Lenticular	0.7 – 0.8
	Elliptic	0.6 – 0.8
	Circular	1.0
	Rectangular	1.0 – 1.2
	Rectangular with semi-circular nose	0.90
	Rectangular with chamfered corners	1.01
	Rectangular nose with wedge-shaped tail	0.86
	Rectangular with sharp nose 1:2 to 1:4	0.65 – 0.76
Vertical	Pyramid-like (narrowing upwards)	0.76
	Inverted pyramid (broadening upwards)	1.2

- Acceleration factor equals $\alpha_a = 1.0$ (see also Eq. 2.4);
- Load factor is $\alpha_M = 1.7$ ($K_s = 1.2$) (see also Eq. 4.17);
- Critical depth-averaged flow velocity is $U_c = 4.5$ m/s (see also Chapter 2);
- Strength factor $\alpha_s = 1.0$.

Hence, the calculated time at which initial damage at several locations occurs, is $t = 1$ h (in $q = 50$ l/s giving $D = 997$ m²/s²). This modification of the load factor agrees well with the

measurement; see also Table 4.9 where different load factors including the predicted one ($\alpha_M = 1.44$) are presented with corresponding damage numbers.

Table 4.9 Damage number versus load factor for side-wall structure at Nijmegen N2

α_a (-)	α_s (-)	α_M (-)	U_c (m/s)	t_{measured} (hours)	Multiple open spots D (m^2/s^2)
1.0	1.0	1.4	4.5	1h – 50 l/s	338
1.0	1.0	1.7	4.5	1h – 50 l/s	997
1.0	1.0	2.0	4.5	1h – 50 l/s	2102
1.0	1.0	2.3	4.5	1h – 50 l/s	3657

Following Pijpers (2013) the load factor is related to the wave volume and ranges from 1 (for the smallest waves) to 2.4 (for the largest waves). Although there are differences between his approach and the proposed modelling, this is here not further analysed. Moreover, it is recommended to investigate the erosion process near the tree at the Vechtdijk and compare that with the erosion results as presented in Table 4.9.

Two models based on expert judgment are discussed for predicting the load factor at vertical objects and side-wall structures. One relation characterizes the load increase just upstream of the obstacle and the other relation represents the relative load increase of the near-bed forces along the obstacle. To determine the erosion at the side-wall structure the cumulative overload method is recommended to use (see also Chapter 2).

Though the predicted time satisfies the measured time when multiple open spots near the side-wall structure occurred, it is recommended to validate the approaches by using more observations and/or to deduce theoretical models.

As the erodibility of grass near side-wall structures was tested in Nijmegen the dimensions of these structures were relatively small compared to the width of houses. Hence, additional research is needed to extrapolate the experimental results to prototype situations. At present there are still knowledge gaps, e.g. close to stairs the erosion is still not fully understood (Fig. 4.32).



Figure 4.31 Side-wall structure



Figure 4.32 Erosion close to stairs (Tholen)

4.5 Conclusions

Flow velocities and flow depths

The theory of steady state overtopping as developed by Schüttrumpf and Oumeraci (2005) is used for predicting the flow velocities and flow thicknesses. All hydraulic measurements from 2008 to 2012 were re-analysed, giving (new) relations between overtopping wave volume and flow velocity as well as overtopping wave volume and flow thickness at the crest of the dike. Also the development of the flow velocity and the flow thickness along the landward slope is analysed and compared with the theory.

In general one may conclude that a friction factor of $f = 0.01$ leads to the correct trends for both flow velocity and flow thickness. The actual values for the flow velocity are well predicted by the theory of steady state. It is more difficult to predict the correct flow thickness. But the flow velocities are governing in the cumulative overload, which makes the prediction of flow thicknesses less relevant.

Schüttrumpf and Oumeraci (2005) found a friction factor which most likely is too low given the corresponding values for the turbulence. However, measured flow velocities can be predicted well with a value of $f = 0.01$. Probably the German model predicts relative small values of f as the influence of air is not taken into account. It is recommended to investigate the relation between air content and friction factor in greater detail.

Load penetration in subsoil

At about 10 cm below the ground surface, the measured pore pressures varied from 0 kPa to -7.5 kPa. When the experiments in Millingen aan de Rijn started the measurements showed that the pore pressures were about -7.5 kPa with a small response. Most likely, the suction pressures were active when the soil was not wet enough. Later, when the soil was more saturated the suction pressures reduced to zero.

The pressure measurements at the test location Millingen aan de Rijn show that the load penetration in turf decreases very fast. This observation is also confirmed by the one-

dimensional consolidation theory. Hence, the relevant load for causing erosion/damage occurs mainly on top of the sample/ground surface.

As the load at a reference level of about 10 cm below is mainly determined by the suction pressures and not by the turbulence near the ground surface the assumption made in the turf-element model is adequate, i.e. the load acts on the top of the turf element and not on the side walls.

Laboratory tests and Pluto calculations demonstrate that the load penetration as a result of over pressures decreases slowly. Therefore, these results may not be compared with the measured load penetration obtained from the test location in Millingen. Most likely the differences can be ascribed to the different pressure periods. Therefore, it is recommended to make new Pluto calculations with a measured pressure period ($T = 0.03$ s).

Revetment transitions

A conceptual model is discussed for predicting the load factor at revetment transitions. The load factor represents the relative increase (or decrease) of the load. To determine the erosion/damage the cumulative overload method is used.

The load factor for an asphalt road to a grass revetment varies from 1.5 to 2.0 with a best guess value of $\alpha_M = 1.75$. The reduction of the strength, expressed by α_s is about 0.9. This value is approximately in agreement with the research results of Pijpers (2013).

Although the computational results are in the range of expectations it is recommended to validate the theoretical modelling by applying more (prototype) tests. Therefore, it is needed to select experiments where damage at transitions is/was observed. In addition, guidelines are needed for predicting the strength of different materials.

Furthermore, it is recommended to examine the literature on revetment transitions, e.g., Antonia and Luxton (1971) and Benson (2005). Here, a limited literature review is carried out. Moreover, it is recommended to make computations with mathematical flow models to investigate the effects of supercritical flow on the load factor (i.e., when the Froude number is greater than 1).

Geometrical transition

A conceptual model is discussed for predicting the load factor at geometrical transitions. The load factor represents the relative increase (or decrease) of the load. To determine the erosion/damage the cumulative overload method is used.

The load factor depends on the steepness of the dike. If there is no geometrical transition or if $\theta = 0^\circ$ then $\alpha_M = 1$. If $\theta = 20^\circ$ (steepness is 1V:2.7H) then $\alpha_M = 1.17$. The predictions of the load factor were based on a scour approach and therefore they are less reliable.

By using both the experimental data and the cumulative overload method the load factor varies from 1.25 to 1.35 for Nijmegen (N1 and N2). For the steepest slope (N1) the load factor is 1.35. In Millingen the multiple open spots at both the slope and at the transition of the slope-berm were observed at the same time as the water could not flow away. Most likely the pool at the berm reduced the erosion process. Therefore, the load factor is $\alpha_M \approx 1$.

By using the proposed conceptual model the predicted load factor lies in the range of 1.16 (Nijmegen N2) to 1.23 (Nijmegen N1). Although there are differences between the measured

and calculated load factors the relative error is less than 10%. The range of the load factor obtained from the conceptual model is in agreement with other prototype measurements. The load factor varied from 1.05 to 1.21 (Boonweg: $\alpha_M = 1.05$ and $U_c = 6.3$ m/s; St. Philipsland: $\alpha_M = 1.09$ and $U_c = 5.0$ m/s; Tholen: $\alpha_M = 1.21$ and $U_c = 4.0$ m/s).

Vertical objects and side wall structures

Two models based on expert judgement are discussed for predicting the load factor at vertical objects and at side-wall structures. One relation characterizes the load increase just upstream of the object and the other relation represents the relative load increase of the near-bed forces along the obstacle. To determine the erosion at the obstacles the cumulative overload method is recommended to use (see also Chapter 2). As the load factor varies from 1.0 to 1.7 it is recommended to deduce theoretical models for the load increase at vertical objects and side wall structures.

In Nijmegen, a side-wall structure was tested on the horizontal berm. In the stagnation zone the grass revetment was reinforced with a concrete protection so at that location no erosion occurred. However, in the acceleration zone severe erosion was observed. The characteristic times of erosion (multiple open spots and failure of the grass cover) are adequately simulated with the model relations. However, it is recommended to validate the approaches by using more observations as the theoretical backgrounds now lack.

Following Pijpers (2013) the load factor is related to the wave volume and ranges from 1 (for the smallest waves) to 2.4 (for the largest waves). Although there are differences between his approach and the proposed modelling, this is here not further analysed. Moreover, it is recommended to investigate the erosion process near the tree at the Vechtdijk and compare that with the erosion results obtained at the side-wall structure.

As the erodibility of grass near side-wall structures was tested in Nijmegen the dimensions of these structures were relatively small compared to the width of houses. Hence, additional research is needed to extrapolate the experimental results to prototype situations. At present there are still knowledge gaps, e.g. close to stairs the erosion is still not fully understood.

5 Hydraulic load on the seaward slope

5.1 Introduction and objective

The cumulative overload method applied to wave run-up is discussed in Chapter 4 of SBW (2012) where a description of run-up levels and run-up velocities is given. The cumulative overload method, which originally was developed for wave overtopping (see also Chapter 2), can also be used for wave run-up.

For both sea dikes and lake dikes the wave heights in the Netherlands that may attack the seaward slope are relatively high (2 m or more). Therefore, most of the slope below and at the expected storm surge level is protected by e.g. block revetments or asphalt. In other words, the zone of wave impacts has been strengthened and the upper seaward slope, which often consists of clay with a grass cover, will only be attacked by wave run-up. However, as the wave heights may be high, also the wave run-up velocities may be high. Hence, for these situations tests with a modified wave run-up simulator have been planned.

However, river dikes with a lower wave regime do not have artificial protection and the clay with grass cover should withstand the wave impacts. Kruse (2010) performed an extensive study, leading to guidelines on use of clay on river dikes. He analyzed existing information on resistance of grass covers to wave impacts and deduced resistance durations, depending on the type of sod cover (closed or open vegetation) and the type of clay (fat or poor (= sandy clay)). Figure 5.1 demonstrates that grass covers can at least withstand one or two hours a significant wave height of 2 m (Kruse 2010). A wave height of 1 m can last for about 8 hours (open sod) or even 24 hours (closed sod). With an open sod a wave height of 0.5 m can be withstood for duration of 24 hours. It is anticipated that the erosion depth by wave impacts will be up to 0.3 m.

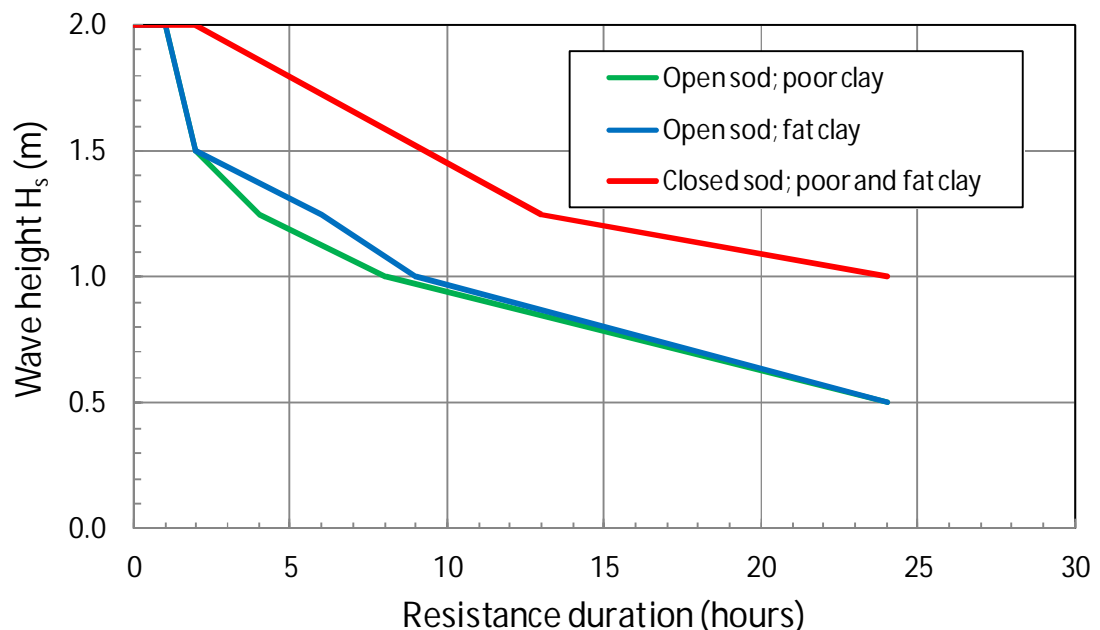


Figure 5.1. Resistance duration for grass covers on clay against wave impacts (re-plot from Kruse (2010) for erosion depths up to 0.3 m).

Based on Fig. 5.1, a guideline with safety as shown in Fig. 5.2 was developed (RWS 2012). In this graph no wave heights on grass covers are allowed higher than 1 m. It is expected that a closed sod can withstand a significant wave height of 1 m for at least 8 hours. For an open sod only a significant wave height of 0.7 m is allowed, which also will resist the wave attack for 8 hours. For longer resistance durations lower wave heights are allowed.

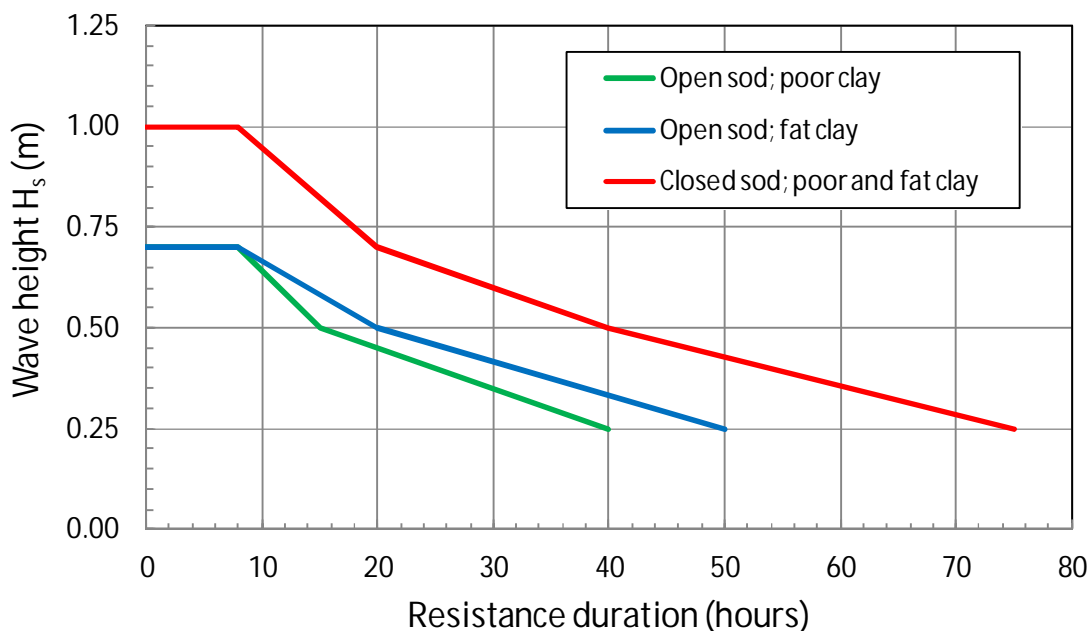


Figure 5.2. Guideline for resistance duration for grass covers on clay against wave impacts (re-plot from RWS (2012-Figure 6.7) for erosion depths up to 0.3 m).

The proposition of wave attack on grass covers is that wave impacts will always be the governing mechanism to cause damage and failure and not wave run-up only. Tests with the wave impact generator have shown that initial damage may be generated by impacts and that wave run-up may increase the damage significantly. But first damage should always occur for wave impacts.

The overload method mentioned above has been applied to wave run-up (SBW 2012)). This method assumes that damage will occur also for wave run-up only, if the velocities of wave run-up are high enough. This is the situation for sea dikes where the impact zone is protected and large wave run-up may be expected above the impact zone. The expectation that wave impacts are governing for stability (Figs. 5.1 and/or 5.2) should match with the overload method for wave run-up in the sense that the latter method may not give earlier damage than expected for impacts. That leads to the following objective of this chapter:

- Validate that the cumulative overload method for wave run-up gives indeed damage to a grass cover on clay at a later stage than with the same wave height for wave impacts.

First hydraulic loads will be determined from Fig. 5.1 and 5.2 and compared with cumulative overloads for wave run-up. Secondly, a few investigations in the Delta flume on grass covers on clay will be evaluated with the cumulative overload method for wave run-up.

5.2 Overload method for run-up versus guidelines for wave impacts

Figure 5.1 gives the following significant wave heights where changes in the curves for resistance durations are observed: $H_s = 2$ m; 1.5 m; 1.0 m and 0.5 m. Figure 5.2 gives also a maximum for $H_s = 0.7$ m and a limiting wave height of only 0.25 m. For the time being this latter wave height will be ignored as being too small to initiate damage by wave run-up.

The next step is to calculate the hydraulic overload for each of these wave heights. Of course some assumptions have to be made to enable these calculations. For run-up calculations a seaward slope has to be assumed. Here a slope of 1V:3H is taken, without a berm. This can be considered as being more or less an upper bound. Only river dikes with small wave attack may have accidentally steeper slopes. Furthermore, a wave steepness has to be assumed. As in a lot of cases the waves will not be depth limited, at least not for river dikes with high discharge and water level, a relatively large wave steepness is chosen with $s_{op} = 0.04$. This steepness is calculated for deep water and with the peak period of the wave spectrum. This assumption was also made for most of the tests with the overtopping simulator, as well as the pilot test with the wave run-up simulator.

With these assumptions of slope angle and wave steepness, wave run-up calculations can be made, as described in Chapter 4 of SBW (2012). All five wave heights give straight lines on a "Rayleigh"-graph, see Fig. 5.3. The 2% wave run-up levels for wave heights of $H_s = 0.5$ m; 0.7 m; 1.0 m; 1.5 m and 2.0 m are respectively $Ru_{2\%} = 1.33$ m; 1.86 m; 2.65 m; 3.98 m and 5.34 m. The levels are shown in Fig. 5.3 at the vertical red line at the 2%-value.

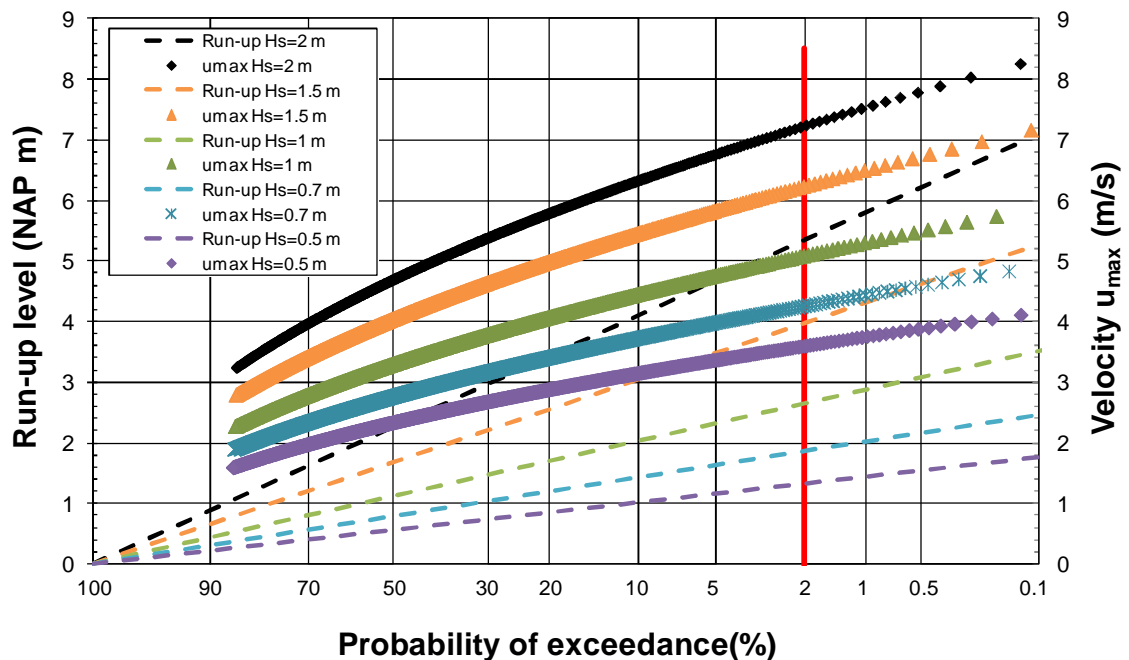


Figure 5.3 Calculated wave run-up levels and front velocities on a 1:3 slope for various wave heights, all with a wave steepness of $s_{op} = 0.04$.

Run-up velocities along a slope remain more or less constant (within 90%-100% of the maximum) between roughly 15% and 75% of the actual maximum run-up level for that wave (see also SBW (2012) and Van der Meer (2011)). It is also clear from Fig. 5.3 that locations higher on the slope will receive fewer waves. The main difference between wave run-up and

wave overtopping is that the hydraulic load decreases significantly by increasing location on the seaward slope, where it remains similar or even increases for the landward slope for wave overtopping. It means that the governing location for wave run-up is the lowest point on the slope where run-up is present, or at the location where a transition is present (from protected slope to grass cover, or from berm to upper slope). With wave run-up a distinct point should be considered.

Some run-up events start above the still water line, which probably gave the observation that maximum run-up velocities start around 15% of their maximum run-up level. Furthermore, if (small) run-up levels just exceed the point of interest (the last part between 75% and 100% of the maximum run-up level), the velocity drops significantly and should not be taken into account. For this reason the point of interest, where the maximum cumulative overload is considered for the slope, is taken at 0.15 $Ru_{2\%}$. For the given five wave heights this is at levels of 0.20 m; 0.28 m; 0.40 m; 0.60 m and 0.80 m above the still water level.

Formulae to calculate the maximum run-up velocity from given wave run-up level have been described in SBW (2012). For all wave run-up levels that should be taken into account the maximum wave velocity was calculated and given in Fig. 5.3 with similar colours as the lines for the wave run-up. The majority of the maximum wave run-up velocities are between 2 m/s and 6 m/s with maxima for the five given wave heights of roughly 4 m/s; 5 m/s; 6 m/s; 7 m/s and 8 m/s.

If the velocity of each wave run-up is known, the cumulative overload can be calculated for each assumed critical velocity U_c . The minimum critical velocity for an open or closed sod is set at 4 m/s (RWS 2012). This critical velocity was observed at the Vechtdike for wave overtopping, where a good grass sod was present, but on a 100% sand layer (no clay). Wave overtopping tests have also shown that hardly any strength is available if the grass sod is fragmentary (large open spaces without grass, etc.). In such cases the critical velocity is close to 0 m/s. But as soon the grass cover is not too open, then there will be a minimum strength with a critical velocity of 4 m/s. This value has been taken as the minimum value. Then cumulative overloads have been calculated for $u_c = 5$ m/s; 6 m/s and 7 m/s as well.

Table 5.1 gives the results for duration of wave attack of 1 hour. If no value is present in the table the critical velocity has not been exceeded by the wave run-up.

Table 5.1 Cumulative overload for wave run-up at the most critical point on a 1:3 slope, with a steepness of $s_{op} = 0.04$ and a duration of 1 hour.

H_s (m)	$u_c=4$ m/s	$u_c=5$ m/s	$u_c=6$ m/s	$u_c=7$ m/s
0.5	3			
0.7	141			
1.0	1062	83		
1.5	3855	1111	141	2
2.0	6965	3213	952	144

For wave overtopping three damage definitions were determined, see also ENW (2012):

- Start of damage (first open spot): $\Sigma(u^2 - u_c^2) = 500 \text{ m}^2/\text{s}^2$ (large scatter)
- Various open spots: $\Sigma(u^2 - u_c^2) = 1000 \text{ m}^2/\text{s}^2$ (significant scatter)

- Failure of the top layer $\Sigma(u^2 - u_c^2) = 3500 \text{ m}^2/\text{s}^2$ (less, but still scatter)

Table 5.1 shows that for the minimum critical velocity of 4 m/s it is well possible to have damage or even failure if the wave height is 1 m or higher. But for good grass covers with critical velocities of 6 m/s or higher only significant damage can be observed if the wave height is at least 2 m.

A better comparison with Fig. 5.1 and 5.2 can be made if specific points in the graphs are compared with calculated cumulative overloads. This has been done in Table 5.2 for specific points in Figure 5.1. For various wave heights the resistance duration was taken from Figure 5.1 and then the corresponding cumulative overload was calculated for that wave height and duration. For a closed sod on poor or fat clay it was assumed that the critical velocity is always 6 m/s or larger. For an open sod it was assumed that the critical velocity was not lower than 5 m/s, but also not larger than 6 m/s.

Table 5.2 Cumulative overload calculated for various wave heights and corresponding resistance durations as established from Figure 5.1 for wave impacts

Description	Wave height H_s (m)	Resistance duration (h)	Cumulative overload (m^2/s^2)		
			$u_c=5 \text{ m/s}$	$u_c=6 \text{ m/s}$	$u_c=7 \text{ m/s}$
Closed sod; poor and flat clay	2	2		1904	288
Closed sod; poor and flat clay	1.25	13		-	-
Closed sod; poor and flat clay	1	24		-	-
Open sod; fat clay	2	1	3213	952	
Open sod; fat clay	1.5	2	2222	282	
Open sod; fat clay	1.25	6	-	-	
Open sod; fat clay	1	9	747	-	
Open sod; fat clay	0.5	24	-	-	
Open sod; poor clay	2	1	3213	952	
Open sod; poor clay	1.5	2	2222	282	
Open sod; poor clay	1.25	4	-	-	
Open sod; poor clay	1	8	664	-	
Open sod; poor clay	0.5	24	-	-	

The damage for wave impacts was defined as erosion depth of 0.2 m, which can be considered more or less as a failed top layer. For wave overtopping this would mean a cumulative overload of around $3500 \text{ m}^2/\text{s}^2$. Table 5.2 shows that this value is almost reached for a 2 m wave height on an open sod with poor or fat clay if a critical velocity of 5 m/s is assumed. For all other conditions the cumulative overload remains well below the critical level of $3500 \text{ m}^2/\text{s}^2$. This all validates the proposition or hypothesis that wave impacts should lead to failure of the grass cover and not wave run-up. Only for a wave height of 2 m and the lowest critical velocity the two methods become close.

Figure 5.2 was given as a safe guideline for application of grass in the wave impact zone. There only a wave height of 1 m was given as a maximum with a closed sod. Table 5.2 gives an unlimited resistance duration for this situation. Also for a maximum wave height around 0.7 m and 0.5 m and an open sod with poor or fat clay Table 5.2 gives unlimited resistance durations. It can be concluded that for conditions that are acceptable in Figure 5.2 the wave run-up will never lead to damage or failure of the grass cover.

Only the condition of a wave height of 2 m should be considered more in depth. First of all this condition cannot and has not been tested in the Delta flume as the limiting significant wave height in that facility is around 1.7 m. It means that in this case Figure 5.2 is based on an extrapolation of existing results, not on measured results.

But another point has come up during the last year of analysis of wave overtopping results. It is only since 2010 (tests at the Vechtdike) that velocities during wave overtopping on landward slopes were measured successfully at various locations along the slope (see also the Delta flume experiments carried out by Deltares (H1565). At the Vechtdike measured velocities remained more or less constant along the 1V:5H slope and therefore the focus was directed to the maximum front velocities that were simulated by the wave overtopping simulator at the horizontal crest of the dike. These velocities have been used to calculate the cumulative overload along the landward slopes of all tested locations since 2007, see the Table B1 in RWS (2012). The three damage definitions for wave overtopping as described above were based on the overtopping velocities at the crest of the dike.

Overtopping velocities along the landward slope have later been measured more recently at Tholen and at Millingen for much steeper slopes than the 1V:5H slope at the Vechtdike. In SBW (2012) it was predicted with the theory of constant overflow that velocities could increase significantly if the friction factor was low enough. The tests at Tholen with a slope of 1V:2.4H showed indeed that velocities increased significantly over the first 10 m from the crest and that a friction factor of $f = 0.01$ should be used in the theoretical approach. The recent test at Millingen with a landward slope of 1V:3H validated the choice for this friction factor. The tests and theory show that velocities may increase along a 1V:3H slope from the crest from 4 m/s to 6 m/s; from 5 m/s to 7 m/s; from 6 m/s to 8 m/s and from 7 m/s to almost 10 m/s. These increases in velocity have a drastic effect on the calculated cumulative overload, not only by the increase of the velocity itself of a certain overtopping wave, but also by many more waves that will exceed the critical velocity further down the slope.

These very recent analysis validates the observation that hardly damage or failure was initiated in the first few meters behind the crest. The far majority of damages and failures were observed further down the slope as the velocities and cumulative overloads were much larger further down the slope. This effect has never been considered (as it was not noticed or understood at that time of analysis) when the critical velocities and according damage definitions were established. This leads for instance to two observations or recommendations.

The first is that one should also consider the location on the landward slope when analyzing results from wave overtopping simulations. The velocities at the location of damage should be considered and cumulative overloads should be recalculated with the correct velocities. This might lead to larger values of cumulative overload as given now for the three damage definitions.

Another observation is that wave run-up velocities do not increase along the seaward slope. The maximum velocity is around $0.4 Ru_{max}$, but the velocity remains within 90% of this maximum between $0.15 Ru_{max}$ and $0.75 Ru_{max}$. It never increases and the cumulative overloads as presented in Tables 5.1 and 5.2 are correct. Most likely the definition of failure of the slope (i.e. $D = 3500 \text{ m}^2/\text{s}^2$) is not correct. The actual value may well be much higher than this value. And then the distance for the 2 m significant height between wave impacts and wave run-up may become much larger than suggested in Table 5.2.

5.3 Overload method for run-up against Delta flume tests

In 1992 large scale model tests have been performed in the Delta flume on a 1V:4H slope consisting of good clay with a grass cover. The tests have been described in H1565 (1994). More analysis on results are given in H1991 (1996) and Q1584 (1998). A summary of results with guidance to practice has been given in Q1954 (1997), which eventually was the basis for TAW (1998).

Two tests from this investigation are relevant for further analysis between the cumulative overload method for run-up against erosion by wave impacts. These are test SP006 with $H_s = 1.35$ m and $T_p = 4.70$ s and test SP007 with $H_s = 0.76$ m and $T_p = 3.40$ s. The seaward slope was 1:4. The tests were performed in July 1992, where the grass cover was growing and in a good condition. The grass sod was described as fully closed. It should be noted that this grass cover and certainly the roots are stronger in summer than in winter.

Test SP006 showed a hole by impacts after 9 hours of testing, which had a depth of 0.15 m after 17 hours when the test was terminated. At that time there were also a few other holes. There was no damage in the run-up zone else than very slight surface erosion.

Test SP007 was performed with a lower water level on an undisturbed part of the slope. There was neither damage by impact nor by wave run-up after testing of 20 hours.

The wave run-up distribution can be calculated as well as the distribution of run-up velocities at a point $0.15 Ru_{2\%}$ above the still water level. From this the cumulative overload can be calculated for various critical velocities. Given the summer conditions of the fully closed grass cover, a critical velocity will probably close to 7 m/s or even larger. The cumulative overload for test SP006 becomes $0 \text{ m}^2/\text{s}^2$ for critical velocities of 6 m/s or larger. For $u_c = 5$ m/s the cumulative overload per hour is $87 \text{ m}^2/\text{s}^2$, which gives for the total test duration of 17 a cumulative overload of $1479 \text{ m}^2/\text{s}^2$. According to the definitions this would mean several open spots.

For the test conditions of SP007 with $u_c = 5$ m/s the cumulative overload becomes $0 \text{ m}^2/\text{s}^2$. This means that even for this low critical velocity no damage is expected.

Given a critical velocity of at least 6 m/s for this good grass cover in summer, no damage should be expected from run-up, not for the lower wave height at SP007 nor for the fairly high wave height at SP006. This validates the objective and hypothesis described in Section 5.1.

Also velocity measurements were performed on the seaward slope, although most of them were below the water level around the impact area. There were two measurement above water, but in all cases it was very difficult to get reliable measurements. This was also the experience with the overtopping tests with the wave overtopping simulator and that gave the development of the surfboard with paddle wheels. The following formula for run-up velocity was more or less validated with the tests:

$$\frac{Vu_{2\%}}{\sqrt{gH_s}} = \frac{1.43 \tan \alpha}{\sqrt{s_{op}}} \sqrt{1 - \frac{z}{Ru_{2\%}}}$$

with:

$Vu_{2\%}$ = 2%-value of the run-up velocity (m/s)

g = acceleration of gravity (m/s^2)

- H_s = significant wave height (m)
- $\tan\alpha$ = slope angle (-)
- S_{op} = wave steepness with the peak period (-)
- z = vertical distance from the water level to a location on the slope (m)
- $Ru_{2\%}$ = 2% run-up level

With a wave height of 1.35 m and a wave period of 4.7 s the 2%-run-up velocity becomes with the formula above 6.1 m/s at a location 0.15 $Ru_{2\%}$ above the water level (the point considered with the largest attack from up-rushing waves). The calculations for cumulative overload give a 2%-run-up velocity of 5.2 m/s, which is fairly close.

5.4 Conclusions

The overall conclusion is that indeed wave impacts are governing for damage at a grass cover, not wave run-up. For a significant wave height of 2 m the two methods come close, which should not be expected. On one side the predictions for wave impacts at a significant wave height of 2 m are extrapolated, on the other hand the cumulative overload for failure may well be on the safe side. This is due to the fact that till very recently the increase of velocity along a landward slope with wave overtopping has never been included in the development of a value of cumulative overload for various damage definitions.

It is therefore recommended to re-analyze all results with the wave overtopping simulator again, but now with corrected velocities at the location where the damage has occurred. This analysis will certainly influence the limiting values for damage.

6 Erodibility of turf

6.1 Introduction

Turf (or a grass sod) consists of soil and roots where the roots can be considered as a reinforcement mesh in the soil. Turf is proven to be an elastic-plastic material. As roots are not straight but grow subdivided in the sub-soil, turf can deform centimetres without tearing. Wave overtopping tests show that turf failure can be modelled by taking into account fatigue effects. During wave overtopping tests failure of turf did not occur during one large wave overtopping volume, but due to several large volumes where the volume at failure was not necessarily the largest.

In the winter of 2013 several turf-tensile tests were carried out in Nijmegen and Millingen aan de Rijn, see also Appendix F where the experimental results are summarised. To predict the critical (depth-averaged) flow velocity (U_c) of the tested grass revetments, clay and grass investigations were used. These predictions yielded for Nijmegen and Millingen aan de Rijn $U_c = 6$ m/s and $U_c = 7$ m/s respectively (see also Chapter 3).

Under pressures acting on a piece of turf can stretch and break the weakest roots and/or the roots orientated in such a way that they react the stiffest and take the largest load. Breaking a few roots will weaken the turf (element), but redistribution of forces to other roots can still be possible. However, the redistribution stops, if the displacements reach critical values.

Here a brief summary of the strength of grass including the effects of suction pressures is presented. First estimations are given and expert judgement is used to model the force transmission, deformation and the fatigue strength of grass. Therefore, this Chapter must be considered as the state of the art, a first step in modelling the erodibility of turf.

6.2 Grass strength

Grass can easily resist flow velocities of 2 m/s. Higher velocities can also be withstood. However, the critical value depends strongly on the root qualities and the changes in the suction pressures. The mean grass strength is a function of the root area ratio, the mean root diameter, the critical mean root tensile strength, the surface roughness (expressed by the friction factor or bed turbulence) and the open spots.

Figure 6.1 shows the total strength of the soil as function of the depth (Valk 2009). The right profile shows a sketch of a badly rooted soil and the left shows a well rooted soil. The strength obtained by the effective soil cohesion is assumed constant. The frictional strength determined by the roots is not constant over the depth but decreases. Near the surface the root system dominates, whereas with increasing depth the submerged weight and the internal friction of the clay (by the effective soil cohesion) dominate.

Clay shrinks and expands as a result of drying and wetting, and these changes are directly connected to changes in the water content of the clay. Above the water table the pore water pressure in clay is usually negative in relation to the atmospheric pressure. This under (or negative) pore water pressure is usually referred to as suction pressure because clay can 'suck up' water from the water table. The suction pressure holds the water films around the aggregates. As more water drains, the films of water around the aggregates become thinner and the air-water interface becomes sharply curved, leading to increased suction.

The pore water pressure in the larger pores only becomes positive when water percolates directly through these open spaces due to precipitation or infiltration by outside water. However, in the smaller pores of the aggregates into which water cannot easily infiltrate there are still under pressures. As a result of the water over pressures the water in the larger pores is attracted to the water in the smaller aggregates. Consequently, the aggregates gradually swell. This time-dependent process of volume change is slow because of the low permeability of the aggregates.

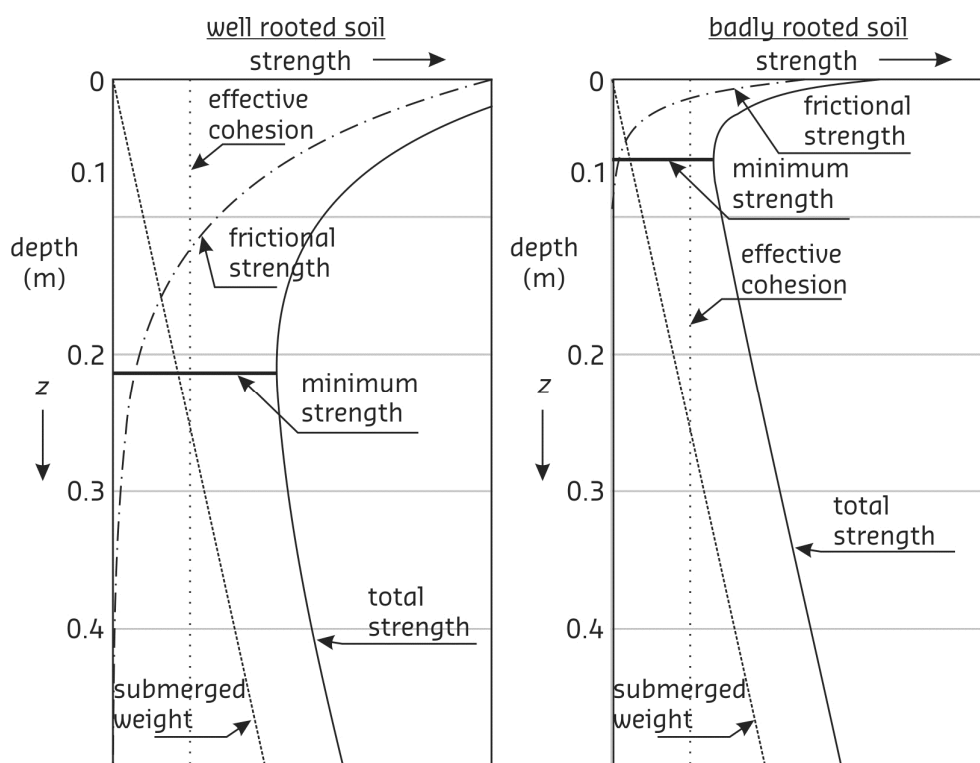


Figure 6.1 Strength function as function of the depth (Valk 2009)

Evaporation into the atmosphere also plays an important role in the suction pressure, and this can take place directly from the soil into the atmosphere or via the vegetation. Among other factors, the rate of evaporation is dependent on the relative humidity of the air. Close to the surface of a dike, the suction pressure can be often higher than 1000 kN/m^2 (or a 100 m head of water) in the summer, mainly as a result of the relatively high temperature and the suction power of the vegetation. Precipitation and temperature changes can allow this suction pressure to vary greatly and when it rains, it is often less than 50 kN/m^2 .

In winter conditions, in wet periods, on average the suction pressure in the clay cover of a dike is usually less than 10 kN/m^2 . The suction pressure can be considerably higher only in dry freezing air, especially in south facing banks. The greatest changes in suction pressure take place in the turf layer due to changes in precipitation, water extraction by roots, and very large temperature differences. Variations in the suction pressure in the core of the dike are caused by changes in the position of the water table, and by atmospheric effects. The effects of changes in atmospheric conditions are very slight and the variations in suction pressure in the dike core are usually slow and of limited size.

The suction pressure in the core of a dike can vary from 0 kN/m² to rarely more than 50 kN/m². The suction pressure is inversely proportional to the particle diameter or to the dimensions of the capillaries, thus the suction pressure increases with a decreasing hydraulic conductivity. The suction pressure also depends on how much water is in the soil. If the soil is completely saturated the suction pressure is nil. Figure 6.2 shows the suction pressure (through the pF curve) as function of the water content.

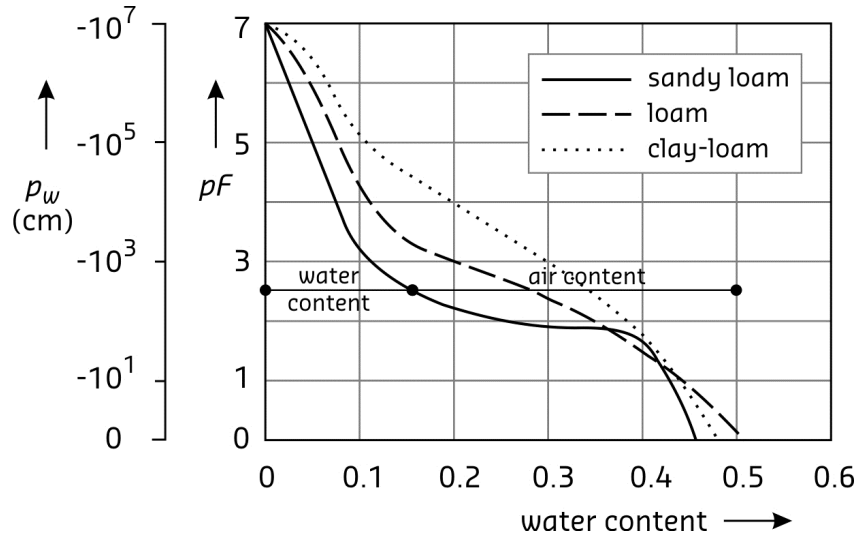


Figure 6.2 Suction pressure as function of water content

The turf element model describes the forces acting on a turf cube with a length scale of 10 cm. Working out the vertical force balance and by using both the equation of Chézy and the definition of the bed shear stress the critical flow velocity can be estimated by (see also Chapter 2 where indicative values of U_c are presented)

$$U_c = 2r_0^{-1} \sqrt{\Psi_c (\sigma_{grass,c}(0) - p_w) / \rho} \quad (6.1)$$

where r_0 is the relative (depth-averaged) turbulence intensity, ρ is the water density, $\sigma_{grass,c}(0)$ is the critical mean grass normal stress at the ground level and $\Psi_c (= 0.03)$ is the critical Shields parameter. The pore water pressure (p_w), which has a negative sign, represents the suction pressure in the sub soil.

6.3 Turf-tensile tests

Turf-tensile tests were carried out on the river dike near Millingen aan de Rijn on Tuesday March 5th in 2013 (Deltares 2013, Figs. 6.3 and 6.4). The weather conditions were sunny and the temperature varied from 12 to 18 degrees. In April 2013 Infram also conducted turf-tensile experiments (Appendix F) which are here partly analysed (Sections 6.4 and 6.5). All these tests aim to model the strength of the grass.

Before starting the tensile experiment a U-frame with dimensions of 5 cm x 15 cm x 15 cm was gradually pushed in the sub soil. Next, the soil was carefully removed with a small spade either on four sides (Condition A) or on two sides (Condition B). Finally, when the soil sample was anchored by horizontal pins at about 3 cm below the ground surface (see also Fig. 6.3) the test could begin.

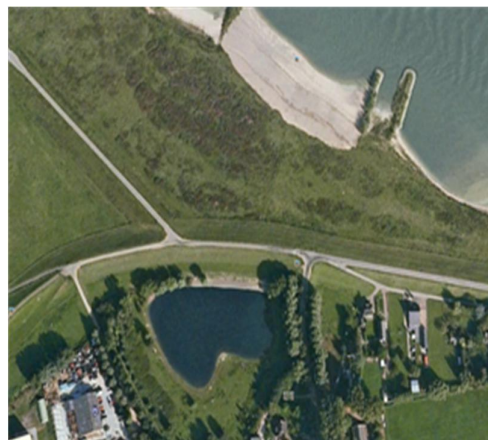
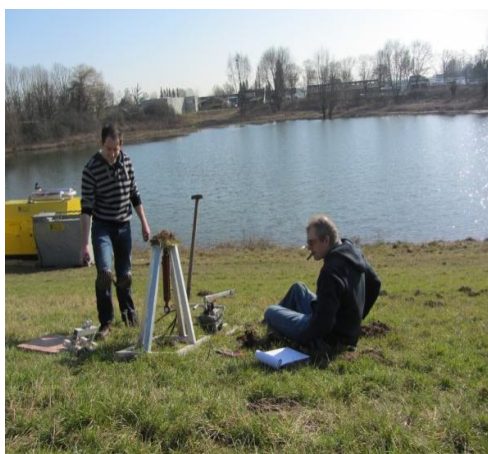


Figure 6.3 Turf-tensile apparatus

Figure 6.4 Test location Millingen aan de Rijn

In the first experiments the turf was tested on both the north and the south (or sunny) side of the dike. Distinction was made in the way of testing (Condition A or B). The turf was not watered artificially, thus the soil sample was tested under unsaturated conditions. Not only turf was tested but also moss and weak spots of digging moles. After the tests the maximum and mean turf thickness were measured including the cross-sectional area (see also Deltares 2013).

In these experiments oil pressures were measured manually with a pressure gauge. The pressures represent the tensile forces acting on the grass sods. As the relation between measured pressures and measured tensile forces is still being examined these tests are here not used.

In April 2013 Infram carried out 24 turf-tensile tests at the dike in Millingen aan de Rijn and 24 tests in Nijmegen at different locations for unsaturated soil conditions. In these tests the tensile force as function of the deformation was measured at different locations on the dike. The forces and deformations were measured with a force transducer and a displacement meter. The force-deformation curve is analysed in relation to the strength of the grass revetment. Also the influence of fatigue on the strength of grass is investigated (Section 6.6).

6.4 Deformations

The maximum deformation of turf is extremely high, i.e. approximately 6 cm. However, the tensile force reaches its maximum value after 5 mm to 10 mm. Figure 6.5 shows an example of the deformation as function of the force, see also Appendix F where more experimental results are presented. The grass sod was deformed gradually until the grass sod failed completely. In these tests the grass sod was pulled up with a constant speed of order 1.5 cm/s (Fig. 6.5). During the experiments you could continuous hear the tearing of roots. Hence, short roots break in the beginning of the tests and longer ones later.

Also fatigue tests were performed to analyse the elastic and plastic behaviour of turf (Fig. 6.6). In these experiments, repeatedly a deformation step of 0.5 cm was applied until failure of the grass sod occurred. After each deformation step the load was reduced. The loading and unloading were repeated continuously. After a series of 5 deformation steps the deformation increased with 0.5 cm (from 0.5 cm to 1.0 cm and so on). The total number of load repetitions measured approximately 60 as the maximum deformation was about 6 cm as can be seen in Fig. 6.6b.

The fatigue tests showed that after a deformation of 20 mm (or after 20 load repetitions) the maximum tensile force was reached. This deformation is about two times larger than the deformation when the maximum tensile force occurred in the gradual deformation tests. This relation is not examined here in greater detail. Moreover, it is recommended to investigate the elastic and plastic behaviour of turf (is not yet investigated).

In the prototype situation when the grass revetment is loaded by the overtopping waves on the landward slope, the deformations are most likely less than 10 mm because of the high-frequency pressure fluctuations. As the eddies with the highest energy have a period of about 0.03 s (or a frequency of 30 Hz) the maximum values of the measured tensile forces are representative for determining the critical flow velocity (see also the next Sections).

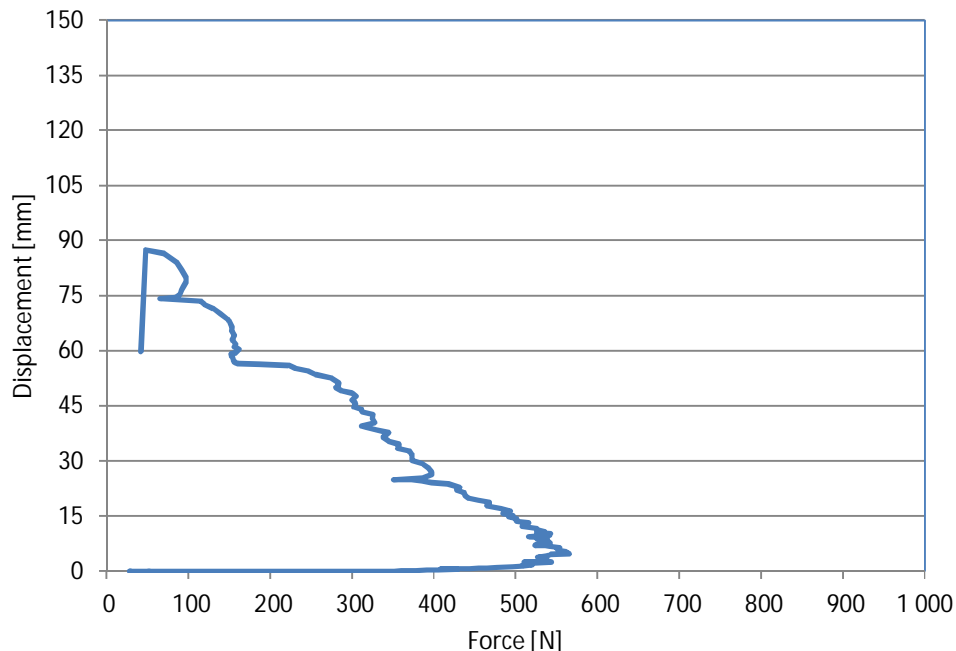


Fig. 6.5 Deformation versus force (Millingen, Section 8, Number 23)

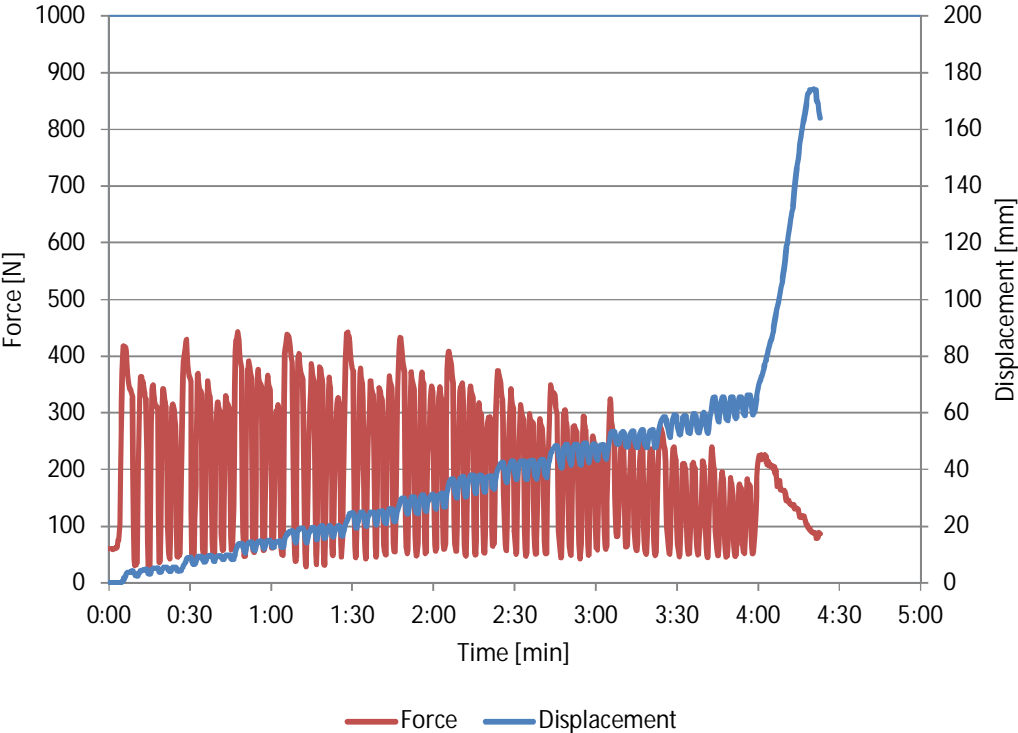


Fig. 6.6a Force as function of time and deformation as function of time (Millingen, Section 6, Number 18)

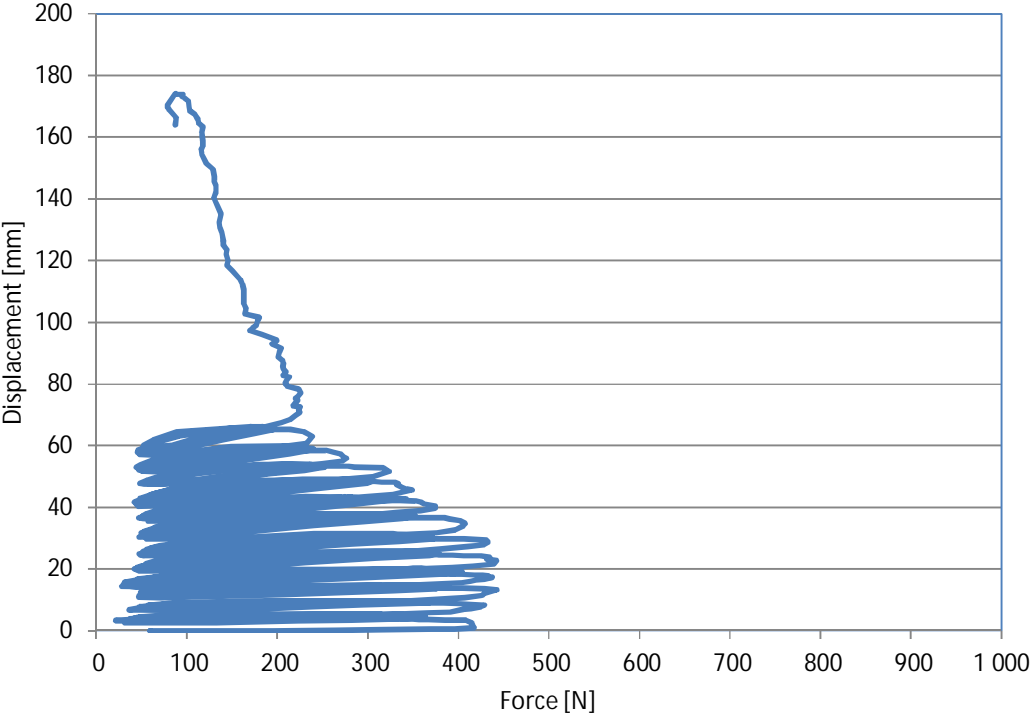


Fig. 6.6b Deformation as function of force (Millingen, Section 6, Number 18)

6.5 Force transmission

Two different force transmissions were tested as discussed above (Condition A or B). The cross-sectional area of the grass sod was about $15 \text{ cm} \times 15 \text{ cm} = 225 \text{ cm}^2$. The turf thickness varied from 3 cm to 7 cm with a mean value of 5 cm. Condition A represents the force transmission through the underside of the grass sod only (thus there are no side walls; see also SBW 2012-2 where more details are given)

$$\sigma_{grass,c} = \frac{F_{m,A}}{0.6A_b} \quad (6.2)$$

Condition B reflects the force transmission through the underside and two sidewalls

$$\sigma_{grass,c} = \frac{F_{m,B}}{0.6A_b + 2 \cdot 0.8A_s} \quad (6.3)$$

where $A_b (= 15 \text{ cm} \times 15 \text{ cm} = 225 \text{ cm}^2)$ is the cross sectional area at the bottom, $A_s (= 5 \text{ cm} \times 15 \text{ cm} = 75 \text{ cm}^2)$ is the cross sectional area of one side wall, F_m is the maximum force obtained from the turf-tensile apparatus (subscripts A and B denote the conditions A and B) and $\sigma_{grass,c}$ is the critical mean grass normal stress at the ground level (not at 5 cm below the ground level, so the coefficients 0.6 and 0.8 in Eqs. 6.2 and 6.3 represent the decrease of the strength, see also Fig. 6.1).

When the bottom of the grass sod contributes in the force transmission only, experiments at Millingen showed (Table 6.1) that the maximum tensile force varied from 0.21 kN to 0.55 kN. When the two side walls also contributed the maximum tensile force increased and ranged from 0.41 kN to 0.95 kN. For the tests in Nijmegen similar results were obtained (Table 6.2). These forces are relatively large as they can easily lift stones with dimensions of 15 cm x 15 cm x 50 cm. However, this comparison cannot be made as the influence of the fatigue strength of grass is not yet included (see also Section 6.6).

The strength factor (α_s , see also Chapter 2) is a factor to model the reduction of the grass strength at revetment transitions. Since the maximum tensile forces are measured for two test conditions α_s can be determined by using the following equation (see also Tables 6.1 and 6.2 and Box A)

$$\alpha_s = \frac{1.5F_{m,B} - 0.5F_{m,A}}{2F_{m,B} - F_{m,A}} \quad (6.4)$$

in which $F_{m,A}$ is the maximum force for condition A (4 side walls are loose) and $F_{m,B}$ represents the maximum force for condition B (2 side walls are loose). Based on about 20 experiments the strength factor ranges from 0.81 to 0.97 with a mean value of $\alpha_s = 0.9$.

6.6 Fatigue strength

Fatigue is the progressive and localized structural damage that occurs when a material is subjected to cyclic loading. Fatigue strength is an expression used to describe a property of a material: the amplitude (or range) of cyclic stress that can be applied to the material without causing fatigue failure. Typically, the fatigue strength is defined as the value of stress at which failure occurs after N_f cycles. Figure 6.6 shows an example of the results of a fatigue

test, i.e. force as function of time, deformation as function of time and deformation as function of force (see also Appendix F).

The number of cycles that grass can endure before it fails is a complex function of the static and cyclic stress values, the root properties, the soil heterogeneity or the root area ratio, effective soil cohesion and several other factors. Although various turf-tensile tests were conducted during the winter period 2013 the fatigue properties of turf are still not fully understood. Measurements show that the tensile force with the number of loads decreases (see also Fig. 6.6b). However, at present no fatigue curve of turf is available.

Table 6.1 Test-tensile measurements (Millingen) and computed U_c with Eq. 6.1 ($p_w = 0$, $r_0 = 0.2$, $\Psi_c = 0.03$)

Series	Location	Condition	F_m (kN)	$\sigma_{grass,c}$ (kN/m ²)	⁽³⁾ $\sigma_{grass,c}(0)$ (kN/m ²)	⁽⁴⁾ U_c (m/s)	⁽⁵⁾ α_s (-)
M.1.1	North	A	0.55	⁽¹⁾ 40.7	12.2	6.06	
M.1.2	North	B	0.59	⁽²⁾ 23.1	6.94	4.56	0.97
M.1.3	North	B (fatigue)	0.64	⁽²⁾ 25.1	7.53	4.75	0.94
M.2.4	North	A	0.40	⁽¹⁾ 29.6	8.89	5.16	
M.2.5	North	B	0.65	⁽²⁾ 25.5	7.65	4.79	0.86
M.2.6	North	B (fatigue)	0.65	⁽²⁾ 25.5	7.65	4.79	0.86
M.3.7	North	A	0.45	⁽¹⁾ 33.3	10.0	5.48	
M.3.8	North	B	0.75	⁽²⁾ 29.4	8.82	5.14	0.86
M.3.9	North	B (fatigue)	0.65	⁽²⁾ 25.5	7.65	4.79	0.88
M.4.10	North	A	0.41	⁽¹⁾ 30.4	9.11	5.23	
M.4.11	North	B	0.75	⁽²⁾ 29.4	8.82	5.14	0.84
M.4.12	North	B (fatigue)	0.70	⁽²⁾ 27.5	8.24	4.97	0.85
M.5.13	North	A	0.42	⁽¹⁾ 31.1	9.33	5.29	
M.5.14	North	B	0.72	⁽²⁾ 28.2	8.47	5.04	0.85
M.5.15	North	B (fatigue)	0.95	⁽²⁾ 37.3	11.2	5.79	0.82
M.6.16	North	A	0.30	⁽¹⁾ 22.2	6.67	4.47	
M.6.17	North	B	0.57	⁽²⁾ 22.4	6.71	4.49	0.84
M.6.18	North	B (fatigue)	0.45	⁽²⁾ 17.6	5.29	3.99	0.88
M.7.19	North	A	0.21	⁽¹⁾ 15.6	4.67	3.74	
M.7.20	North	B	0.43	⁽²⁾ 16.9	5.06	3.90	0.83
M.7.21	North	B (fatigue)	0.41	⁽²⁾ 16.1	4.82	3.80	0.84
M.8.22	North	A	0.31	⁽¹⁾ 23.0	6.89	4.55	
M.8.23	North	B	0.55	⁽²⁾ 21.6	6.47	4.41	0.85
M.8.24	North	B (fatigue)	0.60	⁽²⁾ 23.5	7.06	4.60	0.84
Mean values				25.9	7.76	4.79	0.86

⁽¹⁾ calculated by using Eq. 6.2; ⁽²⁾ calculated by using Eq. 6.3; ⁽³⁾ calculated by using Eq. 6.5;

⁽⁴⁾ calculated by using Eq. 6.1; ⁽⁵⁾ calculated by using Eq. 6.4;

In this study the following assumptions are made

- Time duration of overtopping wave is 10 s;
- Turbulence period of the largest eddies with the highest energy is $T = 0.03$ s (see also Chapter 4);
- For conventional tests the number of waves per storm lies in the range of 3000 to 4000;
- For short tests the number of waves per storm is 450.

Table 6.2 Test-tensile measurements (Nijmegen) and computed U_c with Eq. 6.1 ($p_w = 0$, $r_0 = 0.2$, $\Psi_c = 0.03$)

Series	Location	Condition	F_m (kN)	$\sigma_{grass,c}$ (kN/m ²)	⁽³⁾ $\sigma_{grass,c}(0)$ (kN/m ²)	⁽⁴⁾ U_c (m/s)	⁽⁵⁾ α_s (-)
N.4.10	South East	A	0.34	⁽¹⁾ 25.2	7.56	4.76	
N.4.11	South East	B	0.75	⁽²⁾ 29.4	8.82	5.14	0.82
N.4.12	South East	B (fatigue)	0.79	⁽²⁾ 31.0	9.29	5.28	0.82
N.5.13	South East	A	0.62	⁽¹⁾ 45.9	13.8	6.43	
N.5.14	South East	B	0.50	⁽²⁾ 19.6	5.88	4.20	
N.6.16	South East	A	0.40	⁽¹⁾ 29.6	8.89	5.16	
N.6.17	South East	B	1.10	⁽²⁾ 43.1	12.9	6.23	0.81
N.6.18	South East	B (fatigue)	0.73	⁽²⁾ 28.8	8.59	5.08	0.84
N.7.20	South East	B	0.53	⁽²⁾ 20.8	6.24	4.33	
N.7.21	South East	B (fatigue)	0.45	⁽²⁾ 17.6	5.29	3.99	
Mean values				29.1	8.73	5.06	0.82

⁽¹⁾ calculated by using Eq. 6.2; ⁽²⁾ calculated by using Eq. 6.3; ⁽³⁾ calculated by using Eq. 6.5;

⁽⁴⁾ calculated by using Eq. 6.1; ⁽⁵⁾ calculated by using Eq. 6.4;

Box A Mathematical working out of the strength factor (see also Eq. 6.4)

Two conditions of testing are distinguished. Condition A represents the testing in which the soil at all side walls is removed, thus there is only grass at the bottom of the sample. Also experiments were conducted in which the strength of both the bottom and two side walls was tested (Condition B). Hence, the experimental results yield two forces, namely force $F_{m,A}$ and force $F_{m,B}$. The force acting on one side wall can be written as

$$F_{side-wall} = \frac{1}{2}(F_{m,B} - F_{m,A}) \quad (A1)$$

When the forces at all side walls are active including at the bottom the total force is

$$F_{total} = F_{m,A} + 4 \cdot \frac{1}{2}(F_{m,B} - F_{m,A}) = 2F_{m,B} - F_{m,A}$$

or

$$F_{total} = F_{m,B} + 2 \cdot \frac{1}{2}(F_{m,B} - F_{m,A}) = 2F_{m,B} - F_{m,A} \quad (A2)$$

If the friction force at one side wall is not working the remaining force becomes

$$F_{total} - F_{side-wall} = 2F_{m,B} - F_{m,A} - \frac{1}{2}(F_{m,B} - F_{m,A}) = 1.5F_{m,B} - 0.5F_{m,A} \quad (A3)$$

Consequently, the strength factor can be given by (see also Eq. 6.4)

$$\alpha_s = \frac{F_{total} - F_{side-wall}}{F_{total}} = \frac{1.5F_{m,B} - 0.5F_{m,A}}{2F_{m,B} - F_{m,A}}$$

Hence, the number of pressure fluctuations per wave is $10/0.03 = 300$. In Nijmegen and Millingen two different tests were carried out, the conventional tests (about 5 storms with 3000 to 4000 waves) and the short tests with approximately 450 waves. For the conventional tests the number of load repetitions is $N_f = 300 \times 3500 \approx 10^6$ and for the short test holds $N_f = 300 \times 450 \approx 10^5$.

De Looft et al (2011) examined the strength of several asphalt concrete dike revetments. They found an experimental relation between the strength of asphalt after one load repetition (or flexural strength) and the fatigue strength (or applied bending stress) as function of the number of loads. Figure 6.7 shows the fatigue strength of pine heartwood which is a material comparable with roots of grass.

Considering this material the stress reduction, expressed as $C_{red-fat}$, is about 0.3 if the number of loads is 10^6 . If $N_f \approx 10^5$ then $C_{red-fat}$ is about 0.4. These values of stress reduction are here used to predict the fatigue strength of turf on dikes, see also Table 6.3 where an overview of the reduction factors is given.

$$C_{red-fat} = \frac{\sigma_{grass,c}(0)}{\sigma_{grass,c}} \quad (6.5)$$

where $\sigma_{grass,c}(0)$ is the mean grass normal stress at the ground surface after N_f load repetitions (i.e., during winter conditions when the critical stage is achieved).

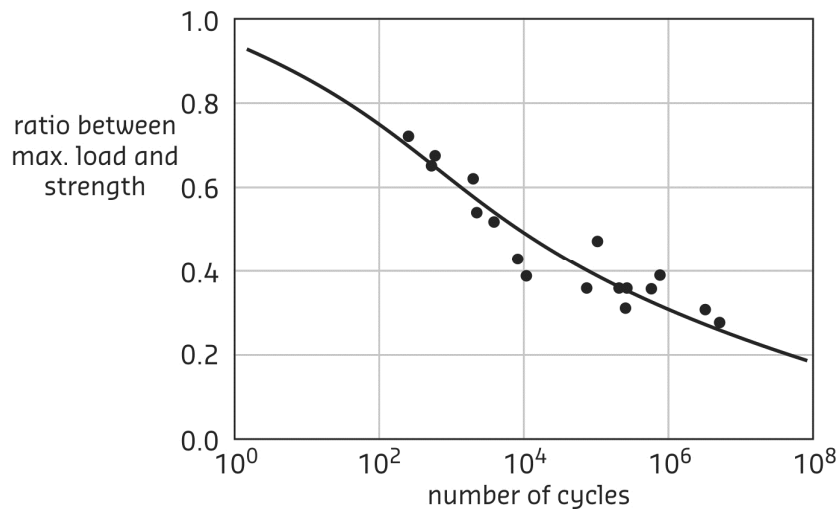


Figure 6.7 Stress reduction versus number of loads for pine heartwood (Kollman and Côté 1968)

Table 6.3 Characteristic values of reduction

Type of test	Number of waves	N_f	$C_{red-fat}$
Conventional tests	3500	10^6	0.3
Short tests	450	10^5	0.4

At present it is unknown whether the suction pressures are included in the maximum tensile force. Further research on this subject is needed. By using Eqs. 6.1, 6.2, 6.3 and 6.5 with p_w

= 0 kN/m², $r_0 = 0.2$ and $\Psi_c = 0.03$ yields for Millingen $U_c = 4.8$ m/s (based on 24 experiments). For Nijmegen the critical flow velocity measures 5.1 m/s (basis is 10 tests).

Table 6.4 presents an overview of the critical flow velocities on the crest of the dike and halfway the dike for both conventional and short tests. As the turbulence decreases from the crest of the dike to the toe, the critical flow velocities increase with the streamwise direction. Although the range 3.5 m/s < U_c < 5 m/s was 'measured' by using the cumulative overload method (see also Chapter 3) it is recommended to investigate the fatigue of the grass strength in greater detail.

Table 6.4 Predictions of U_c with respect to the location for different experiments in Rivierenland

Location	r_0	Millingen conventional U_c (m/s)	Nijmegen conventional U_c (m/s)	Millingen short test U_c (m/s)	Nijmegen short test U_c (m/s)
Crest of dike	0.20	4.8	5.1	5.6	5.9
Halfway the slope	0.15	6.4	6.7		

Summarising, the local critical flow velocity is here determined as follows

- Measure the maximum value of the tensile force (F_m) by using the turf-tensile apparatus;
- Determine the critical mean grass normal stress at the ground level ($\sigma_{grass,c}$) (see Eqs. 6.2 or 6.3).
- Determine the number of load repetitions. For conventional tests holds $N_f = 10^6$ yielding $C_{red-fat} = 0.3$, for the short tests the reduction factor is $C_{red-fat} = 0.4$ (see Fig. 6.7);
- Compute the critical mean grass normal stress at the ground level $\sigma_{grass,c}(0)$ after N_f loadings by using Eq. 6.5;
- Estimate the suction pressure by expert judgement; default value is $p_w = 0$ kPa;
- Determine the turbulence intensity (r_0); at the crest of the dike $r_0 = 0.2$;
- Calculate U_c by applying Eq. 6.1 with $\rho = 1000$ kg/m³ and $\Psi_c = 0.03$.

6.7 Conclusion

The critical flow velocity represents the strength of the grass revetment and depends on the root properties (root diameter, root tensile strength and root area ratio or root intensity), the suction pressures in the sub soil and the roughness of the surface (expressed by the bed turbulence). Note that the damage number (in the cumulative overload method as discussed in chapter 2) expresses the measure of erosion. If the damage number increases then the erosion/damage becomes larger.

The maximum tensile force obtained from the turf tensile apparatus measures about 0.5 kN (or 50 kgf) at a grass sod surface of 15 cm to 15 cm. The maximum tensile force is reached after a deformation of 5 mm to 10 mm which is assumed to be representative in the prototype situations.

The strength factor as used in the cumulative overload model (see also Chapter 2) depends on the soil heterogeneity and varies from 0.8 to 1.0 with a mean value of $\alpha_s = 0.9$. This value agrees with the research findings of Pijpers (2013). He found $\alpha_s = 0.95$.

The difference between U_c for the conventional (3000 to 4000 waves) and short tests (450 waves) can probably be ascribed to the number of pressure fluctuations. For conventional tests the total number of load repetitions is here estimated by $N_f = 10^6$ yielding a stress

reduction of $C_{red-fat} = 0.3$. For the short tests of 4 hours holds $C_{red-fat} = 0.4$. Although the stress reduction factors are based on the fatigue curve of pine heartwood so there is indirectly a relation with roots it is strongly recommended to analyse the fatigue of roots in greater detail.

At the crest of the dike the turbulence intensity is about $r_0 = 0.2$. By using $r_0 = 0.2$ and $C_{red-fat} = 0.3$ the mean value of U_c for Nijmegen and Millingen measures $U_c = 5.1$ m/s and $U_c = 4.8$ m/s respectively (see also Table 6.4). By using $C_{red-fat} = 0.4$ the critical flow velocities are $U_c = 5.6$ m/s (Millingen) and $U_c = 5.9$ m/s (Nijmegen). These predictions of U_c are approximately in agreement with the 'measured' U_c (see also Chapter 3).

If the flow velocities on the landward slope increase then the turbulence intensities decrease. Hence, the critical flow velocities should also increase. However, this conclusion is doubtful and should be further investigated. Therefore, it is recommended to investigate the flow on the landward slope in greater detail, for example, by using the CFD model Open Foam.

So far, a 'quick and dirty' analysis is carried out for modelling the erodibility of turf. The assumption of a fatigue reduction should be examined in greater detail as there is still no fatigue curve for grass revetments. As the influence of suction pressures on the critical flow velocity is significantly it is also recommended to analyse these effects in the next studies of WTI-2017.

7 Conclusions and recommendations

Chapter 2

The overload method is discussed including the extensions to predict the load increase or the load decrease at transitions and obstacles. In this study these effects are expressed by a load factor. When a down-flow occurs the load factor is greater than 1. The load decreases provided there is an up-flow resulting in a load factor that lies in the range of 0 to 1. The reduction of the strength is here modelled by a strength factor which reduces the critical depth-averaged flow velocity.

To include the effects of transitions and obstacles on dikes the cumulative overload model is

$$\sum_{i=1}^N (\alpha_M U_{i,crest}^2 - \alpha_s U_c^2) = D \quad \text{for } U_i > U_c$$

in which D is the damage number, U_i is the representative flow velocity of the overtopping wave, U_c is the critical (depth-averaged) flow velocity, N is the number of the waves in which $U_i > U_c$, α_M is the load factor and α_s is the strength factor. The first term on the left side is a measure for the load and the second term represents the measure for strength.

The damage number is determined by considering the number of waves and the flow velocities of the largest wave volumes as well as from observations after the hydraulic measurements.

Chapter 3

The overall conclusion is that there seems to be a difference between the short tests and the conventional tests. For the conventional tests the critical flow velocity for sections N1 and N2 were 3.5 m/s and 5 m/s, respectively, and for section M1 this was 4.5 m/s. The critical flow velocity from the short tests (sections N3 and M2) was 6.3 m/s or even higher. A reason for the low critical flow velocity of 3.5 m/s at section N1 might be that the damage occurred at a very steep slope of about 1V:2H, which means that the velocity must have increased enormously compared to the velocity at the crest. But even then the conventionally tested slopes showed critical velocities of about 5 m/s or lower, compared to 6.3 m/s or higher for the short tests.

Consequently, one may not conclude that the short tests gave similar results as the longer conventional tests. This conclusion will not change if the damage number would be calculated by the actual velocities at the location of the damage. The reason is that the test sections were more or less similar and the damage occurred more or less at the same location for most cases. This might be different for the first test at N1, where a very steep slope was tested.

Owing to the steep slope at the location N1 the computed flow velocities (obtained from Eq. 3.6) are most likely too low. Hence, by using the cumulative overload model including the definitions of damage and failure the critical flow velocity is probably also too low. Therefore, the 'measured' critical flow velocity should be higher than 3.5 m/s. It is recommended to modify Eq. 3.6 for steep slopes (steeper than 1V:3H).

Table 7.1 presents the predicted and ‘measured’ critical flow velocities for the test locations Nijmegen and Millingen aan de Rijn. To predict the critical flow velocity 5 parameters have to be known (see also Section 2.4). The ‘measured’ U_c is based on measurements/observations and determined by using the cumulative overload method (so it cannot be considered as a 100% measurement). Below the evaluation is given between the predictions and ‘measurements’.

Table 7.1 demonstrates that the predicted and ‘measured’ U_c have approximately the same values for the short tests. However, for the conventional tests the ‘measured’ critical flow velocities are significantly lower, which could be ascribed to the more wetted soil (suction pressures are lower), to the lower fatigue strength (more load repetitions) and to the bed roughness (acceleration effects on the landward slope).

Table 7.1 Overview of predicted and ‘measured’ critical flow velocities for the test sections in Rivierenland

Test location	Type of test	Predictions (conditions halfway slope)		‘Measurements’ (crest conditions)	
		U_c (m/s)	α_a (-)	U_c (m/s)	α_a (-)
Nijmegen N1	conventional	6	1.25	3.5?	1.00
Nijmegen N2	conventional	6	1.25	5.0	1.00
Nijmegen N3	short	6	1.25	6.3	1.00
Millingen M1	conventional	7	1.25	4.5	1.00
Millingen M2	short	7	1.25	> 6.3	1.00

? Most likely U_c is higher than 3.5 m/s due to the steepness of the slope (1V:2H)

The total test duration for the conventional tests was approximately 18 hours. The test duration for the total short tests was only 4 hours. When the soil becomes wetter the suction pressure decreases so the critical flow velocities for the tests N1, N2 and M1 may be smaller than the critical flow velocities for the short tests (N3 and M2).

Also the fatigue strength (see also Chapter 6) influences the magnitude of U_c . The longer the tests the smaller the critical flow velocity becomes. Therefore, U_c for the conventional tests is smaller as there were more load repetitions (see also Chapter 6).

Heterogeneity refers to the fact that turf consists of clay, roots and many different things. As they are not mixed evenly throughout the soil (humus, sand particles, clay particles, root structure) the standard deviation of the grass strength can be large, see also Chapter 6 where experimental results of the turf-tensile apparatus are discussed. Hence, the minimum value of the strength determines the magnitude of U_c as well.

There is more to evaluate. Measurements showed that the flow velocities increased on the landward slope (see also SBW 2012-2 and Chapter 4). For large wave volumes the maximum value of the acceleration factor is approximately 1.5, thus the maximum flow velocity at the lower part of the landward slope, is 1.5 times the flow velocity at the crest of the dike. Before the experiments started, the prediction for the acceleration factor was carried out with expert judgement resulting in $\alpha_a = 1.25$. If the predictions $U_c = 6$ m/s and $\alpha_a = 1.25$ are used then more open spots occur at 6.0 h - 100 ℓ /s/m and the grass cover fails at 2.0 h - 200 ℓ /s/m for the test location Nijmegen N2. These two predicted times are about in agreement with the measured times (Table 7.2). Hence, if α_a increases (or if the turbulence decreases) then U_c also increases. As this hypothesis is not examined thoroughly for all the tests it is recommended to study this more in detail in 2014.

At present the effects of the fatigue strength, heterogeneity and turbulence on erosion are processes which are still not fully understood, see also Chapters 4 and 6. The evaluation of the load and strength factors for different transitions and obstacles are discussed in relation to the measured U_c (see Chapter 4) as less information was available about the modelling.

Table 7.2 Predicted and measured times regarding two characteristic events

Nijmegen N2	Predictions (about halfway the landward slope: $r_0 \approx 0.15$)			'Measurements' (crest conditions: $r_0 \approx 0.2$)		
	U_c (m/s)	α_a (-)	predicted time	U_c (m/s)	α_a (-)	'measured' time
Definition	(see Table 7.1)	(see Table 7.1)	(see Table 3.1)	(see Table 7.1)	(see Table 7.1)	(see Table 3.1)
more open spots	6.0	1.25	6.0 h - 100 l/s/m	5.0	1.0	6.0 h - 100 l/s/m
failure grass cover	6.0	1.25	2.0 h - 200 l/s/m	5.0	1.0	1.5 h - 200 l/s/m

Chapter 4

Flow velocities and flow depths

The theory of steady state overtopping as developed by Schüttrumpf and Oumeraci (2005) is used for predicting the flow velocities and flow thicknesses. All hydraulic measurements from 2008 to 2012 were re-analysed, giving (new) relations between overtopping wave volume and flow velocity as well as overtopping wave volume and flow thickness at the crest of the dike. Also the development of the flow velocity and the flow thickness along the landward slope is analysed and compared with the theory.

In general one may conclude that a friction factor of $f = 0.01$ leads to the correct trends for both flow velocity and flow thickness. The actual values for the flow velocity are well predicted by the theory of steady state. It is more difficult to predict the correct flow thickness. But the flow velocities are governing in the cumulative overload, which makes the prediction of flow thicknesses less relevant.

Schüttrumpf and Oumeraci (2005) found a friction factor which most likely is too low given the corresponding values for the turbulence. However, measured flow velocities can be predicted well with a value of $f = 0.01$. Probably the German model predicts relative small values of f as the influence of air is not taken into account. It is recommended to investigate the relation between air content and friction factor in greater detail.

Load penetration in subsoil

At about 10 cm below the ground surface, the measured pore pressures varied from 0 kPa to -7.5 kPa. When the experiments in Millingen aan de Rijn started the measurements showed that the pore pressures were about -7.5 kPa with a small response. Most likely, the suction pressures were active when the soil was not wet enough. Later, when the soil was more saturated the suction pressures reduced to zero.

The pressure measurements at the test location Millingen aan de Rijn show that the load penetration in turf decreases very fast. This observation is also confirmed by the one-dimensional consolidation theory. Hence, the relevant load for causing erosion/damage occurs mainly on top of the sample/ground surface.

As the load at a reference level of about 10 cm below is mainly determined by the suction pressures and not by the turbulence near the ground surface the assumption made in the turf-

element model is adequate, i.e. the load acts on the top of the turf element and not on the side walls.

Laboratory tests and Pluto calculations demonstrate that the load penetration as a result of over pressures decreases slowly. Therefore, these results may not be compared with the measured load penetration obtained from the test location in Millingen. Most likely the differences can be ascribed to the different pressure periods. Therefore, it is recommended to make new Pluto calculations with a measured pressure period ($T = 0.03$ s).

Revetment transitions

A conceptual model is discussed for predicting the load factor at revetment transitions. The load factor represents the relative increase (or decrease) of the load. To determine the erosion/damage the cumulative overload method is used.

The load factor for an asphalt road to a grass revetment varies from 1.5 to 2.0 with a best guess value of $\alpha_M = 1.75$. The reduction of the strength, expressed by α_s is about 0.9. This value is approximately in agreement with the research results of Pijpers (2013).

Although the computational results are in the range of expectations it is recommended to validate the theoretical modelling by applying more (prototype) tests. Therefore, it is needed to select experiments where damage at transitions is/was observed. In addition, guidelines are needed for predicting the strength of different materials.

Furthermore, it is recommended to examine the literature on revetment transitions, e.g., Antonia and Luxton (1971) and Benson (2005). Here, a limited literature review is carried out. Moreover, it is recommended to make computations with mathematical flow models to investigate the effects of supercritical flow on the load factor (i.e., when the Froude number is greater than 1).

Geometrical transition

A conceptual model is discussed for predicting the load factor at geometrical transitions. The load factor represents the relative increase (or decrease) of the load. To determine the erosion/damage the cumulative overload method is used.

The load factor depends on the steepness of the dike. If there is no geometrical transition or if $\theta = 0^\circ$ then $\alpha_M = 1$. If $\theta = 20^\circ$ (steepness is 1V:2.7H) then $\alpha_M = 1.17$. The predictions of the load factor were based on a scour approach and therefore they are less reliable.

By using both the experimental data and the cumulative overload method the load factor varies from 1.25 to 1.35 for Nijmegen (N1 and N2). For the steepest slope (N1) the load factor is 1.35. In Millingen the multiple open spots at both the slope and at the transition of the slope-berm were observed at the same time as the water could not flow away. Most likely the pool at the berm reduced the erosion process. Therefore, the load factor is $\alpha_M \approx 1$.

By using the proposed conceptual model the predicted load factor lies in the range of 1.16 (Nijmegen N2) to 1.23 (Nijmegen N1). Although there are differences between the measured and calculated load factors the relative error is less than 10%. The range of the load factor obtained from the conceptual model is in agreement with other prototype measurements. The load factor varied from 1.05 to 1.21 (Boonweg: $\alpha_M = 1.05$ and $U_c = 6.3$ m/s; St. Philipsland: $\alpha_M = 1.09$ and $U_c = 5.0$ m/s; Tholen: $\alpha_M = 1.21$ and $U_c = 4.0$ m/s).

Vertical objects and side wall structures

Two models based on expert judgement are discussed for predicting the load factor at vertical objects and at side-wall structures. One relation characterizes the load increase just upstream of the object and the other relation represents the relative load increase of the near-bed forces along the obstacle. To determine the erosion at the obstacles the cumulative overload method is used (see also Chapter 2). As the load factor varies from 1.0 to 1.7 it is recommended to deduce theoretical models for the load increase at vertical objects and side wall structures.

In Nijmegen, a side-wall structure was tested on the horizontal berm. In the stagnation zone the grass revetment was reinforced with a concrete protection so at that location no erosion occurred. However, in the acceleration zone severe erosion was observed. The characteristic times of erosion (multiple open spots and failure of the grass cover) are adequately simulated with the model relations. However, it is recommended to validate the approaches by using more observations as the theoretical backgrounds now lack.

Following Pijpers (2013) the load factor is related to the wave volume and ranges from 1 (for the smallest waves) to 2.4 (for the largest waves). Although there are differences between his approach and the proposed modelling, this is here not further analysed. Moreover, it is recommended to investigate the erosion process near the tree at the Vechtdijk and compare that with the erosion results obtained at the side-wall structure.

As the erodibility of grass near side-wall structures was tested in Nijmegen the dimensions of these structures were relatively small compared to the width of houses. Hence, additional research is needed to extrapolate the experimental results to prototype situations. At present there are still knowledge gaps, e.g. close to stairs the erosion is still not fully understood.

Chapter 5

The overall conclusion is that indeed wave impacts are governing for damage at a grass cover, not wave run-up. For a significant wave height of 2 m the two methods come close, which should not be expected. On one side the predictions for wave impacts at a significant wave height of 2 m are extrapolated, on the other hand the cumulative overload for failure may well be on the safe side. This is due to the fact that till very recently the increase of velocity along a landward slope with wave overtopping has never been included in the development of a value of cumulative overload for various damage definitions.

It is therefore recommended to re-analyze all results with the wave overtopping simulator again, but now with corrected velocities at the location where the damage has occurred. This analysis will certainly influence the limiting values for damage.

Chapter 6

The critical flow velocity represents the strength of the grass revetment and depends on the root properties (root diameter, root tensile strength and root area ratio or root intensity), the suction pressures in the sub soil and the roughness of the surface (expressed by the bed turbulence). Note that the damage number (in the cumulative overload method as discussed in chapter 2) expresses the measure of erosion. If the damage number increases then the erosion/damage becomes larger.

The maximum tensile force obtained from the turf tensile apparatus measures about 0.5 kN (or 50 kgf) at a grass sod surface of 15 cm to 15 cm. The maximum tensile force is reached

after a deformation of 5 mm to 10 mm which is assumed to be representative in the prototype situations.

The strength factor as used in the cumulative overload model (see also Chapter 2) depends on the soil heterogeneity and varies from 0.8 to 1.0 with a mean value of $\alpha_s = 0.9$. This value agrees with the research findings of Pijpers (2013). He found $\alpha_s = 0.95$.

The difference between U_c for the conventional (3000 to 4000 waves) and short tests (450 waves) can probably be ascribed to the number of pressure fluctuations. For conventional tests the total number of load repetitions is here estimated by $N_f = 10^6$ yielding a stress reduction of $C_{red-fat} = 0.3$. For the short tests of 4 hours holds $C_{red-fat} = 0.4$. Although the stress reduction factors are based on the fatigue curve of pine heartwood so there is indirectly a relation with roots it is strongly recommended to analyse the fatigue of roots in greater detail.

At the crest of the dike the turbulence intensity is about $r_0 = 0.2$. By using $r_0 = 0.2$ and $C_{red-fat} = 0.3$ the mean value of U_c for Nijmegen and Millingen measures $U_c = 5.1$ m/s and $U_c = 4.8$ m/s respectively (see also Table 7.3). By using $C_{red-fat} = 0.4$ the critical flow velocities are $U_c = 5.6$ m/s (Millingen) and $U_c = 5.9$ m/s (Nijmegen). These predictions of U_c are approximately in agreement with the 'measured' U_c (see also Chapter 3), except for the test location Nijmegen N1. Most likely the flow velocities obtained from Eq. 2.3 are not correct because of the very steep slope (1V:2H). Therefore, it is recommended to extend Eq. 2.3 (or Eq. 3.6) with the steepness of the dike.

If the flow velocities on the landward slope increase then the turbulence intensities decrease. Hence, the critical flow velocities should also increase. However, this conclusion is doubtful and should be further investigated. Therefore, it is recommended to investigate the flow on the landward slope in greater detail, for example, by using the CFD model Open Foam.

So far, a 'quick and dirty' analysis is carried out for modelling the erodibility of turf. The assumption of a fatigue reduction should be examined in greater detail as there is still no fatigue curve for grass revetments. As the influence of suction pressures on the critical flow velocity is significantly it is also recommended to analyse these effects in the next studies of WTI-2017.

Table 7.3 Overview of computed and 'measured' critical flow velocities for the test sections in Rivierenland

Test location	Computations (crest conditions) obtained by turf-element model		'Measurements' (crest conditions) (see also Table 7.1)	
	U_c (m/s)	α_a (-)	U_c (m/s)	α_a (-)
Nijmegen N1	5.1	1.0	3.5?	1.0
Nijmegen N2	5.1	1.0	5.0	1.0
Nijmegen N3	5.9	1.0	6.3	1.0
Millingen M1	4.8	1.0	4.5	1.0
Millingen M2	5.6	1.0	> 6.3	1.0

? Most likely U_c is higher than 3.5 m/s due to the steepness of the slope (1V:2H)

8 Relevant symbols

c_e	effective soil cohesion (N/m ²)
c_v	consolidation coefficient (m ² /s)
C_D	drag coefficient (-)
d_{f50}	mean grain size (m)
D	damage number (m ² /s ²)
F_n	mean normal force (related to the weight of the water) (N)
F_s	mean shear force (related to the mean bed shear stress) (N)
F_n	maximum dynamic normal force (related to p_m) (N)
F_s	maximum dynamic shear force (related to p_m) (N)
F_i	Force (N)
g	acceleration of gravity (m/s ²)
h	flow depth (m)
k	turbulence energy (m ² /s ²)
k_b	turbulence energy near the bed (m ² /s ²)
k_f	turbulence energy in the filter layer (m ² /s ²)
k_N	Nikuradse roughness (m)
K	hydraulic conductivity (m/s)
L	length scale (m)
M	one-dimensional stiffness parameter (N/m ²)
n	porosity (-)
n_M	Manning coefficient (s/m ^{1/3})
N	number of the waves in which $U > U_c$ (-)
p_m	maximum pressure fluctuation (N/m ²)
p_{top}	sample pressure on top (N/m ²)
p_w	pore pressure (N/m ²)
q	wave overtopping discharge (m ² /s)
r_0	relative depth-averaged turbulence intensity (-)
T	period (related to the turbulence scale) (s)
u_*	bed shear velocity (m/s)
U	flow velocity of the overtopping wave (m/s)
U_c	critical depth-averaged flow velocity (m/s)
z	vertical coordinate (m)
α_a	acceleration factor (-)
α_i	dimensional coefficient
α_M	load factor (for load) (-)
α_s	reduction factor (for strength) (-)
β	compressibility of grass (m/N ²)
θ	angle of inner dike slope (°)
ϕ_e	effective internal friction angle (°)
ρ	density of water (kg/m ³)
ρ_n	bulk density of soil (kg/m ³)
$\sigma_{grass,c}$	critical mean grass normal stress after one load repetition (N/m ²)
$\sigma_{grass,c}(0)$	critical mean grass normal stress at the surface (N/m ²)
ν	Poisson ratio (-) or kinematic viscosity (m ² /s)
Ψ_c	critical Shields parameter (-)

Subscripts

<i>b</i>	represents bottom
<i>m</i>	maximum
<i>r</i>	represents rough bed
<i>s</i>	represents smooth bed

9 References

- Antonia, R. A. and Luxton, R. E., 1971. The response of a turbulent boundary layer to a step change in surface roughness. Part 1. Smooth to Rough. *Journal of Fluid Mechanics*, 48, 721-761.
- Barends, F.B.J., 1992. Personal communications, Delft University of Technology, Delft.
- Benson, J., 2005. Boundary-layer response to a change in surface roughness, MSc-thesis, University of Reading Department of Meteorology, UK.
- Dean, R.G., Rosati, J.D., Walton, T.L., Edge, B.L., 2010. Erosional equivalences of levees: Steady and intermittent wave overtopping, *Ocean Engineering*, 37, 104-113.
- De Groot, M.B., Andersen, K.H., Burcharth, H.F., Ibsen, L.B., Kortenhaus, A., Lundgren, H., Magda, W., Oumeraci, H., Richwien, W., 1996. Foundation design of caisson breakwaters, Publication 198, Norwegian Geotechnical Institute, Oslo, Norway.
- De Looff, A.K., Van de Ven, M.F.C., 't Hart, R., 2011. Resistance of aged asphalt concrete to wave attack, Coastal Structures, Paper No. 0172.
- Deltares, 2013. Turf-tensile experiments, location Millingen (factual report). Project number 1207811-001 (author: G. Hoffmans).
- Emmerling, A., 1973. Die momentane Struktur des Wanddruckes einer turbulenten Grenzschichtströmung, Max-Planck-Institut für Strömungsforschung, Bericht 9.
- Graf, W.H., 1998. *Fluvial Hydraulics*, Flow and transport processes in channels of simple geometry, Wiley & Sons, New York.
- Grass, A.J., 1970. Initial instability of fine sand, Hydraulic Division, *Proc. of the ASCE*, Vol. 96, No. HY3, 619-632.
- Greeuw, G., 2013. Dynamic load tests on two sods from Millingen, (project number 1206016-008), Deltares, Delft.
- Infram, 2013. Factual Report. Overslagproeven Rivierenland. Report 12i071, 19-06-2013.
- Hoffmans, G., G.J. Akkerman, H. Verheij, A. van Hoven and J.W. van der Meer. 2008. The erodibility of grassed inner dike slopes against wave overtopping. *ASCE, Proc. ICCE 2008*, Hamburg, 3224- 3236.
- Hoffmans, G.J.C.M., Van Hoven, A., Verheij, H.J., 2010. Instability of grass caused by wave overtopping, *Proc. of ICSE-6*, San Francisco, 1023-1033.
- Hoffmans, G.J.C.M., 2012. *The influence of turbulence on soil erosion*, Eburon, Delft.
- Hoffmans, G.J.C.M. and Verheij H.J., Scour Manual, Balkema, Rotterdam, The Netherlands. H1565 (1994). Grasdijken. Graserosie, reststerkte en golfoverslag. Report Waterloopkundig Laboratorium, author G.M. Smith.
- H1991 (1996). Grasdijken. Aanvullende analyse van de waterbeweging op het binnentalud. Report Waterloopkundig Laboratorium, authors M. Klein Breteler and G.M. Smith.
- Klar, M., 2005. Design of an endoscopic 3-D particle-tracking velocimetry system and its application in flow measurements within a gravel layer, Doctoral Thesis, University of Heidelberg, Germany.
- Kollman, F.F.P., Wilfred A. Côté, W.A., 1968. Principles of wood science and technology: Solid wood, Springer-Verlag, 592 pages.
- Kruse (2010). Studie voor richtlijnen klei op dijktaaluds in het rivierengebied. Deltares report 1202512-000.
- Lambe, T.W., Whitman, R.V., 1969. *Soil Mechanics*, John Wiley, New York.
- Nezu, I., 1977. Turbulent structure in open-channel flows, (*Translation of Doctoral Dissertation in Japanese*), Kyoto University, Kyoto, Japan.
- Nezu, I, Nakagawa, H., 1993. *Turbulence in open channel flow*, IAHR Monograph, Balkema, Rotterdam, The Netherlands.

- Pijpers, R., 2013. Vulnerability of structural transitions in flood defences: erosion of grass covers due to wave overtopping", MSc-thesis, Delft University of Technology, Delft.
- RWS 2012. Handreiking Toetsen Grasbekledingen op Dijken t.b.v. het opstellen van het beheerdersoordeel (BO) in de verlengde derde toetsronde, Rijkswaterstaat.
- Q1584 (1998). Grasdijken. Analyse meetresultaten grootschalig onderzoek. Report Waterloopkundig Laboratorium, authors D.G. Meijer and H.J. Verheij.
- Q1954 (1997). Erosiebestendigheid van grasland als dijkbekleding. Samenvattend rapport van vijf jaar onderzoek. Report Waterloopkundig Laboratorium, author H.J. Verheij.
- SBW, 2012-1. SBW Wave overtopping and grass cover strength. Model development. Deltares report 120616-007, June 2012. Authors: Gosse Jan Steendam, Gijs Hoffmans, Jan Bakker, Jentsje van der Meer, Joep Frissel, Maurice Paulissen and Henk Verheij.
- SBW, 2012-2. SBW Wave overtopping and grass cover strength. Predictions of Prototype Tests. Deltares report 120616-007, November 2012.
- Schüttrumpf, H.; Oumeraci, H., 2005. Layer thicknesses and velocities of wave overtopping flow at seadikes. Amsterdam, The Netherlands: *Elsevier, Coastal Engineering*, Vol. 52, No. 6, 473-495 (PIANC award for PhD thesis 2004).
- TAW (1998). Technisch Rapport Erosiebestendigheid van grasland als dijkbekleding.
- Teunissen, H., 2010. PLUTO 4.3 (Version 3) Manual, Deltares, Delft (E:\pluto\manuals\pluto-manual-new-1.doc).
- Valk, A., 2009. Wave overtopping: impact of water jets on grassed inner slope transitions, MSc-thesis, Delft University of Technology, Delft, The Netherlands.
- Van der Meer, J.W., Hardeman, B., Steendam, G.J., Schüttrumpf, H., Verheij, H.J., 2010. Flow depths and velocities at crest and inner slope of a dike, in theory and with the wave overtopping simulator. *ASCE Proc. ICCE*, Shanghai, China.
- Van der Meer, J.W. (2011). The Wave Run-up Simulator. Idea, necessity, theoretical background and design. Report Van der Meer Consulting vdm11355, version 1.1. Available at www.vandermeerconsulting.nl.
- Van Ooijen, D.C., (chairman), 1996. *Technical Report Clay for dikes*, Technical Advisory Committee on Water Defences, Ministry of Transport, Public Works and Water Management, Rijkswaterstaat, Delft.

A Load parameters on the dike

Predictions of flow thickness and flow velocity

The theory of steady state overtopping with a friction coefficient of $f = 0.01$ was used in SBW, 2012-2 to predict the flow velocity and the flow thickness at a 1V:3H landward slope as present in Millingen. The predictions for wave overtopping velocities at the crest of 4, 5, 6 and 7 m/s respectively, are given in Figs. A1 to A4. The fast increase in velocity over the first 5 m of the slope can be noticed as well as a slower increase further down the slope.

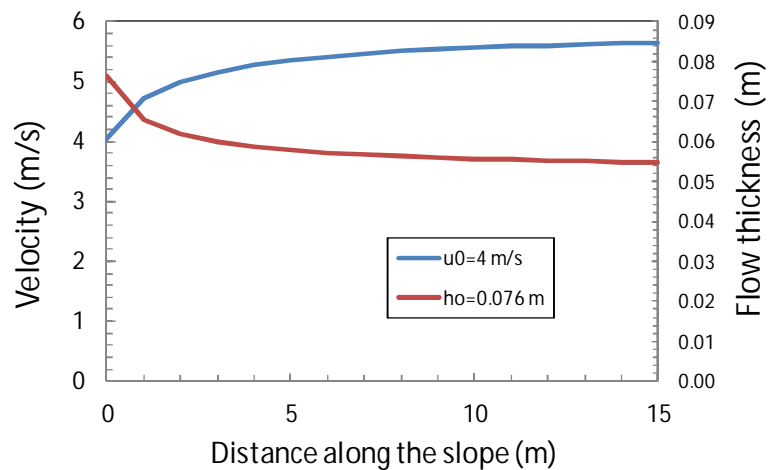


Figure A1 Flow velocities and thicknesses along a 1:3 slope, starting with a velocity of $u_0 = 4 \text{ m/s}$ at the crest (SBW, 2012-2)

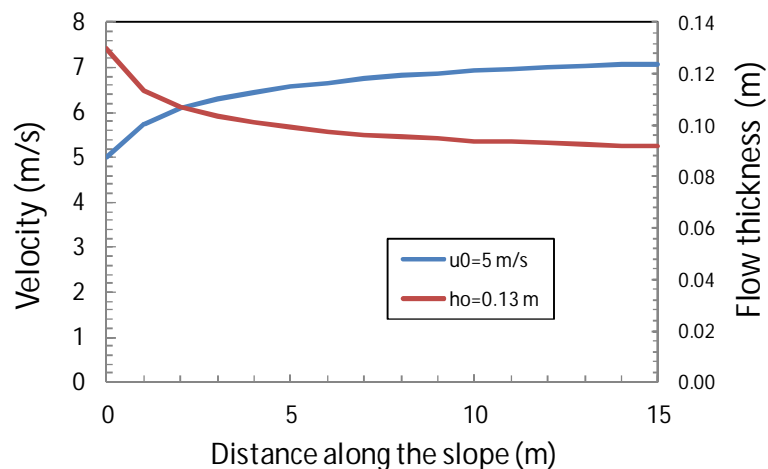


Figure A2 Flow velocities and thicknesses along a 1:3 slope, starting with a velocity of $u_0 = 5 \text{ m/s}$ at the crest (SBW, 2012-2)

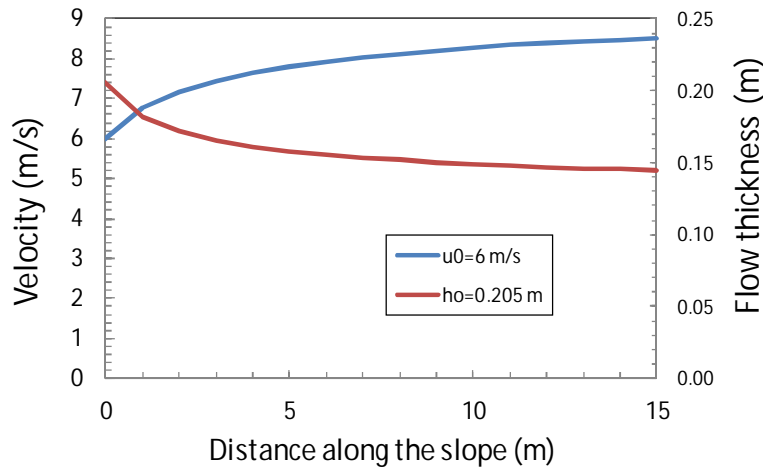


Figure A3 Flow velocities and thicknesses along a 1:3 slope, starting with a velocity of $u_0 = 6$ m/s at the crest (SBW, 2012-2)

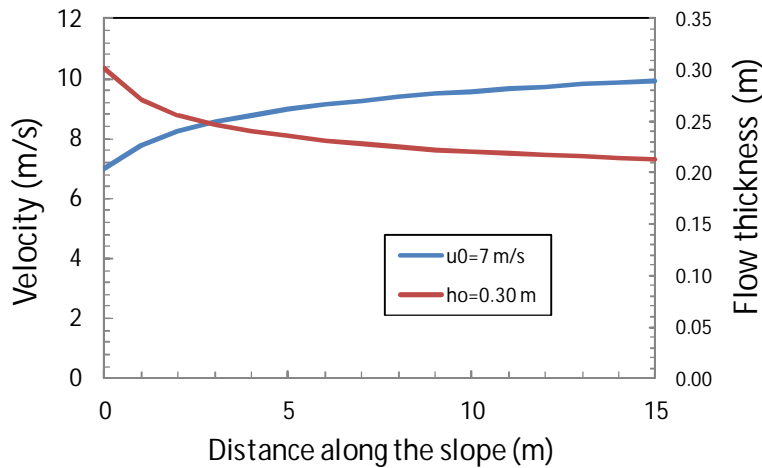


Figure A4 Flow velocities and thicknesses along a 1:3 slope, starting with a velocity of $u_0 = 7$ m/s at the crest (SBW, 2012-2)

Measurements and data processing

Predefined overtopping volumes were released from the wave overtopping simulator in ascending order. Each released volume was in principle repeated once. The smallest released volume was $0.4 \text{ m}^3/\text{m}$ and the largest was $5.5 \text{ m}^3/\text{m}$. Measurements of flow velocity and thickness were performed in Volts.

It was noticed during earlier hydraulic measurements that it is better to split the series from 0.4 to $5.5 \text{ m}^3/\text{m}$ in two series and to adjust the level of the axis of the surfboard a little upwards when going to larger overtopping volumes. In that way the paddle wheel remains better on top of the flow and will not be pushed out of the water by a too low axis point. The first series was taken from $0.4 \text{ m}^3/\text{m}$ up to $2.5 \text{ m}^3/\text{m}$ and the second series from $3.0 \text{ m}^3/\text{m}$ to $5.5 \text{ m}^3/\text{m}$. After the second series it was noticed that the hinges of the surfboards were not

fully positioned in the correct way, although this would probably not cause an effect on the measurements. In order to be sure about this, series 2 was repeated, which resulted in series 3.

Table A1. Locations of paddle wheels and surfboards at Millingen

	Distance from outer crest line (= zero line)		
	Axis level above surface		
	(m)	(m)	(m)
		Series 1	Series 2/3
Surfboard 1 + PW1	-2.0	0.680	0.825
Surfboard 2 + PW2	0.0	0.635	0.780
PW3	1.0		
Surfboard 4 + PW4	2.0	0.735	0.870
PW5	3.0		
Surfboard 6 + PW6	4.0	0.635	0.785
PW7	5.0		
Surfboard 8 + PW8	14.0	0.690	0.690

The hydraulic measurements took place on a fresh section of the dike. After the hydraulic measurements the so-called u_c -tests had to be performed and for a good calculation of the cumulative overload each overtopping volume is important and had to be recorded. The u_c -tests would then start with a pre-loading due to the hydraulic measurements. Between series 2 and 3 five times an overtopping volume of $1,5 \text{ m}^3/\text{m}$ was released for demonstration purposes. No measurements took place, but these waves have to be added to the cumulative overload. Table 2 gives the overtopping wave volumes that have been released.

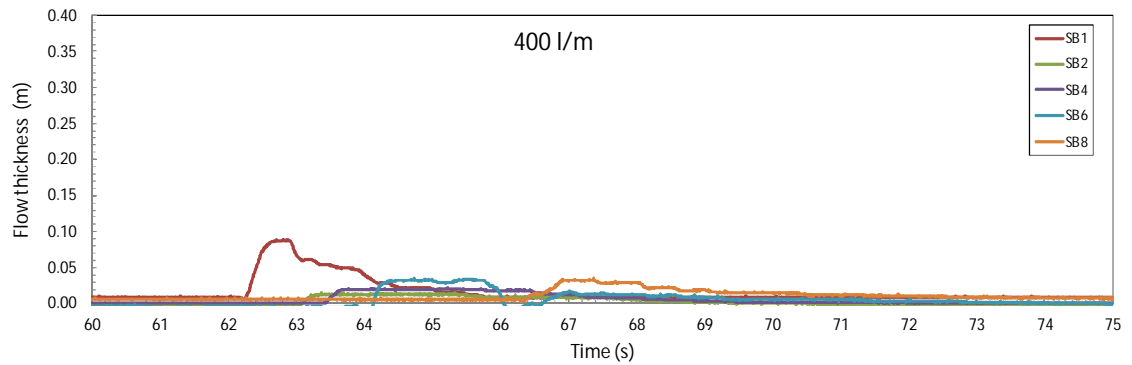
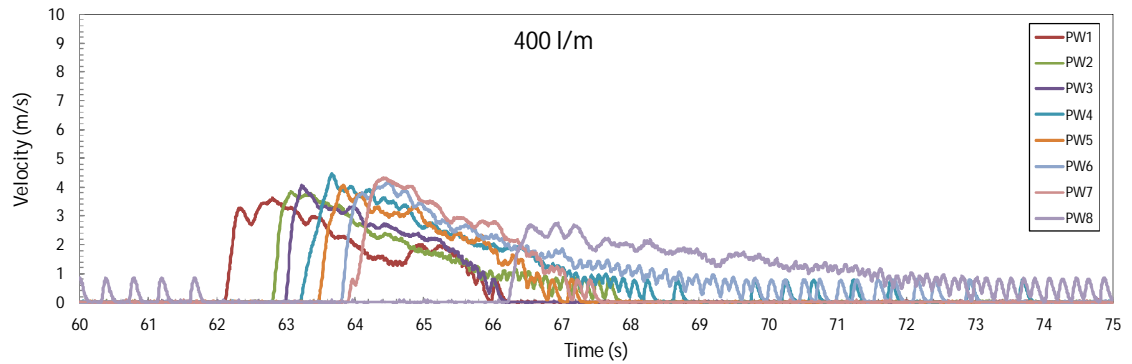
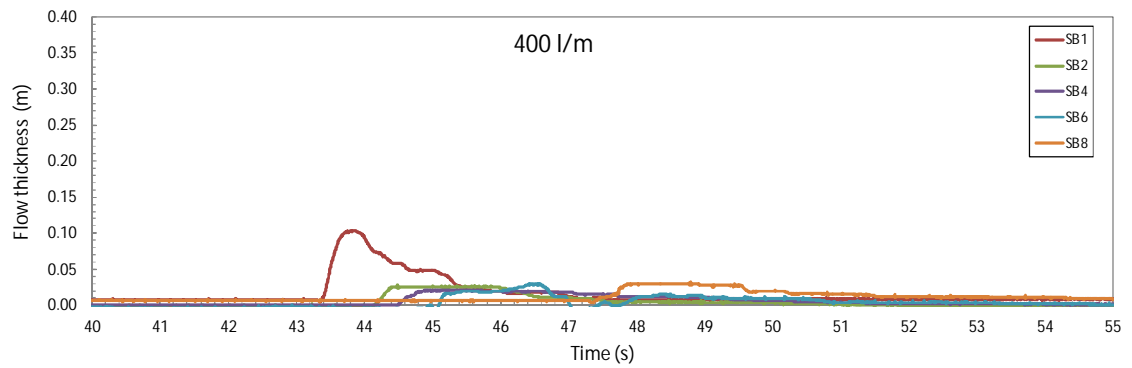
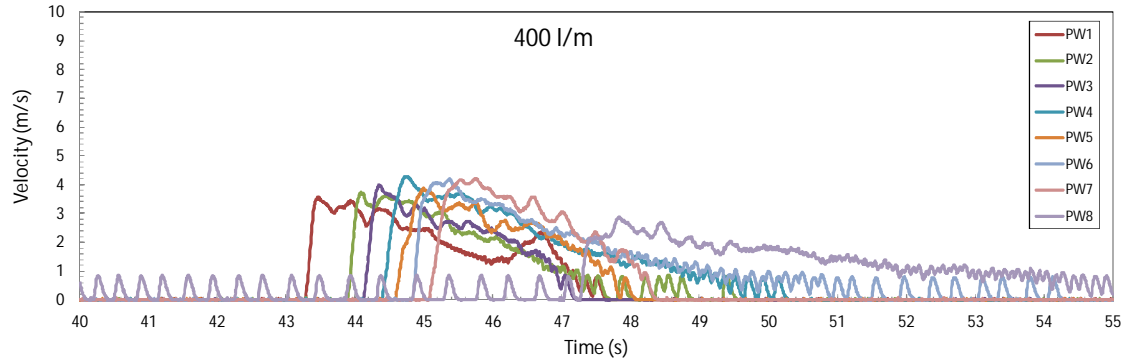
Table A2. Released overtopping volumes in l/m.

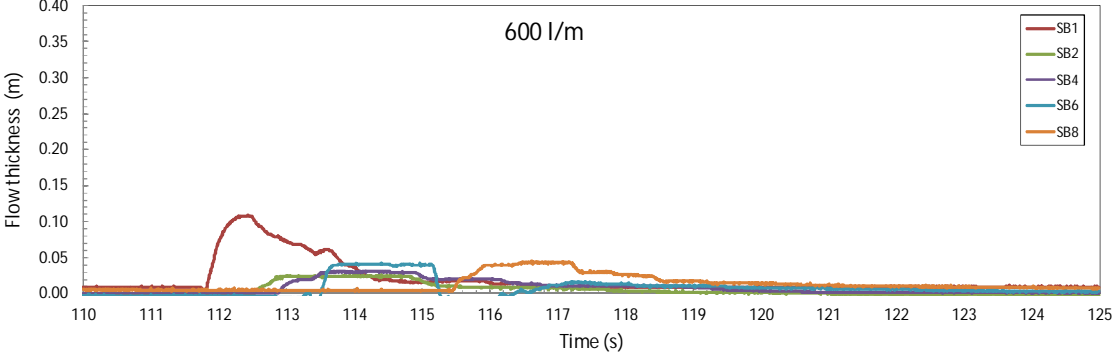
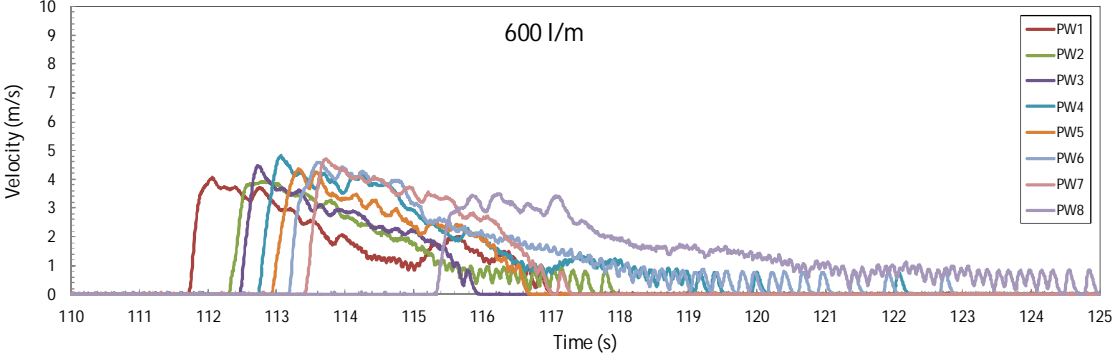
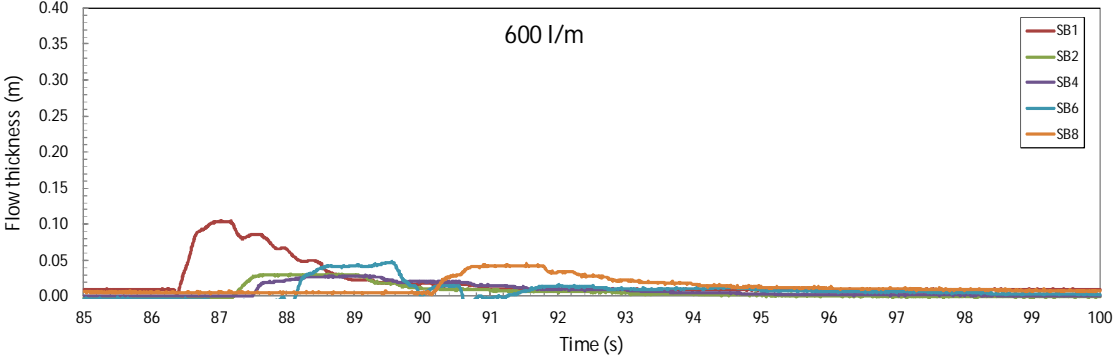
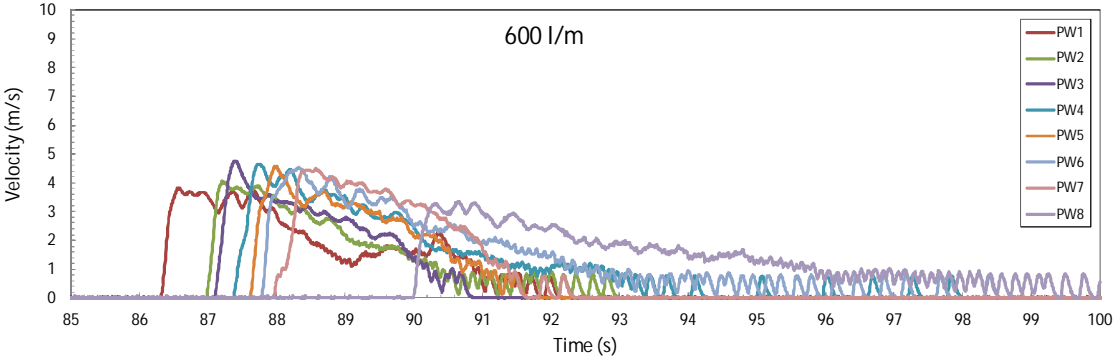
Series 1	Series 2	Series 3	
400	3000	3000	
400	3000	3000	
600	4000	4000	
600	4000	4000	
800	5000	5000	
800	5000	5500	
1000	5500		
1000	5500		
1500			
1500	1500	not recorded	
2000	1500	not recorded	
2000	1500	not recorded	
2500	1500	not recorded	
2500	1500	not recorded	

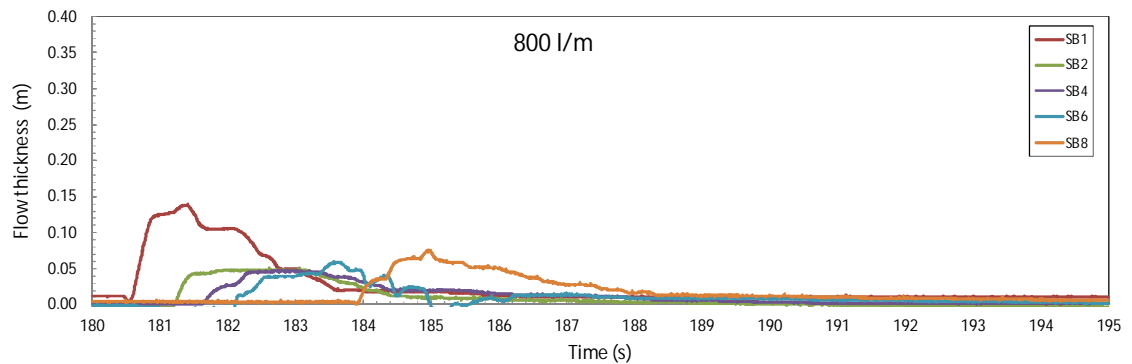
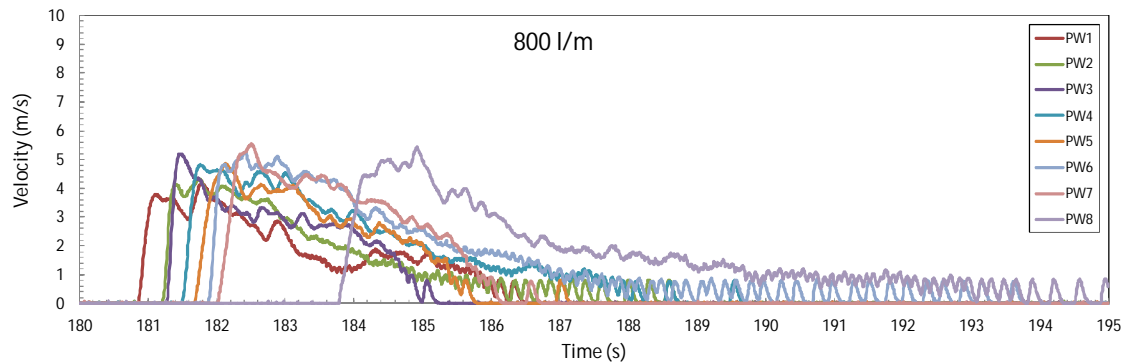
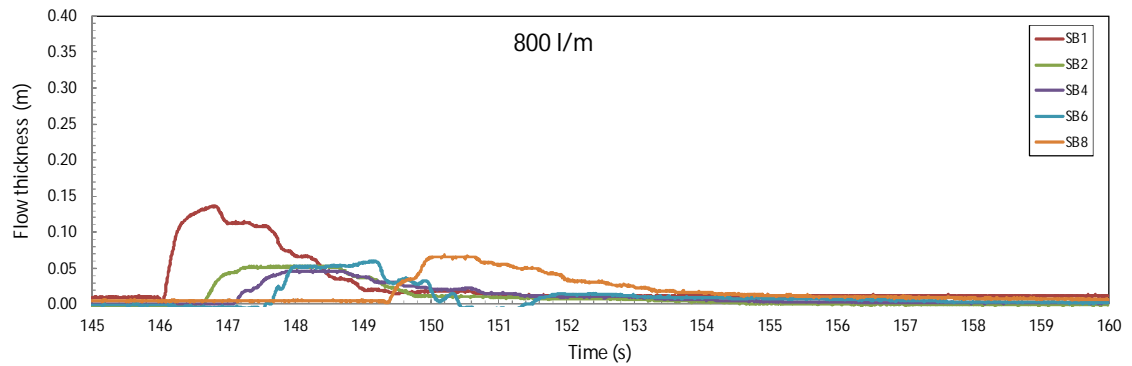
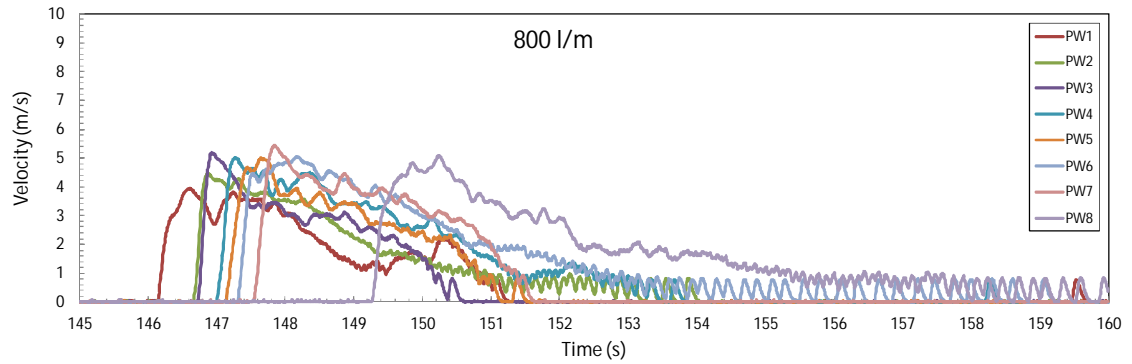
As the recorded signals were in Volts, the first data processing was to change them to records in SI-units. The paddle wheels have a default calibration function of $u = \text{Volt} * 8.57 \text{ (m/s)}$. The surfboards have to be individually calibrated at each location. The calibration functions for the surfboards are given in Table A3.

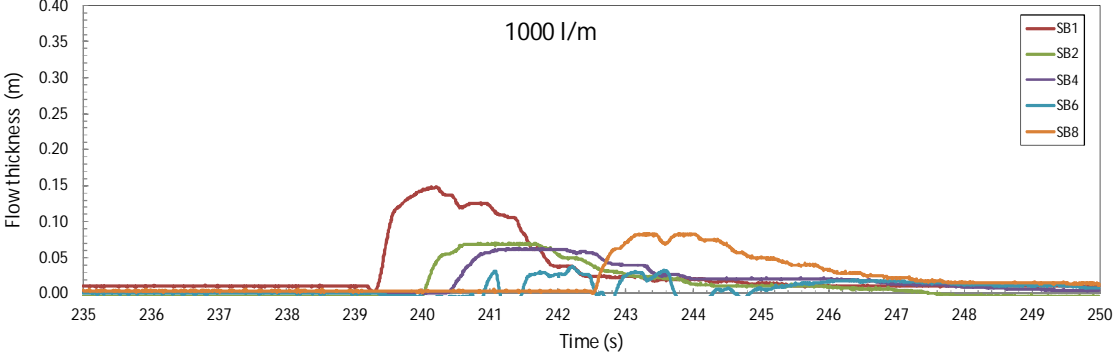
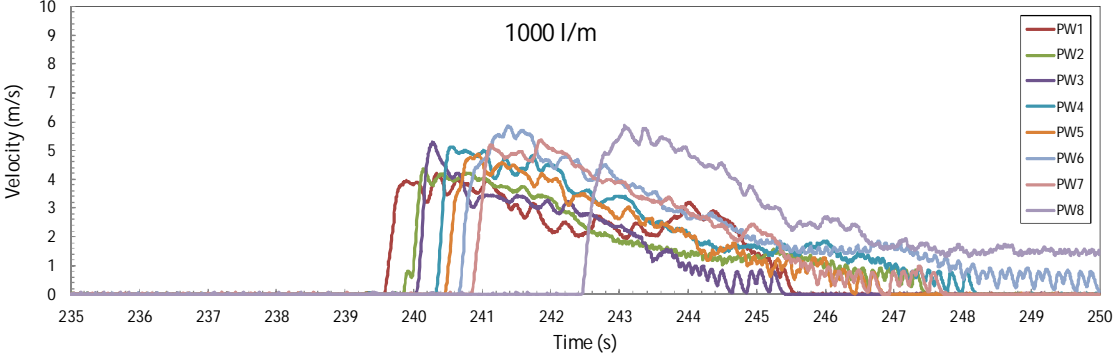
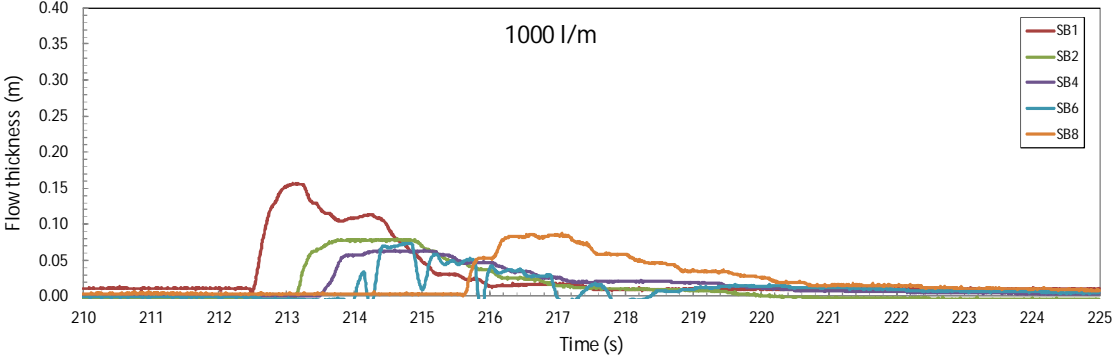
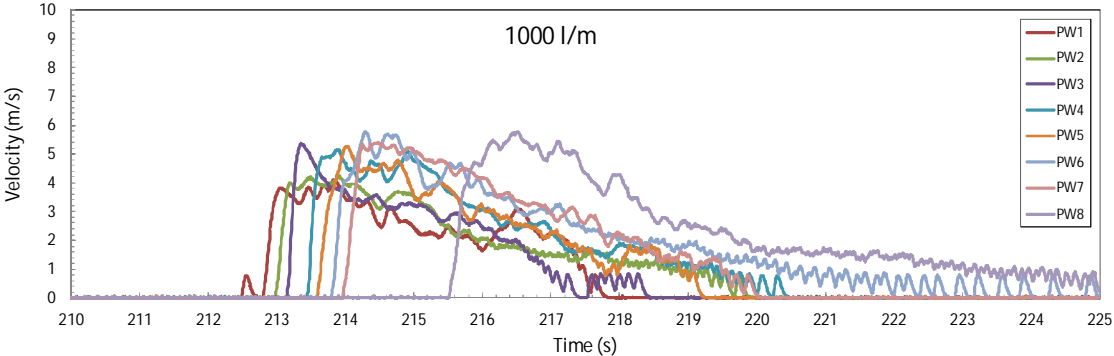
The first data processing of the measurements, after calibration to SI-units, is to plot the measurements in order to be able to visually analyze the behaviour of the records. Appendix A gives two graphs for each released volume with all the measured records. The upper graph shows the measured flow velocities and the lower graph the flow thicknesses.

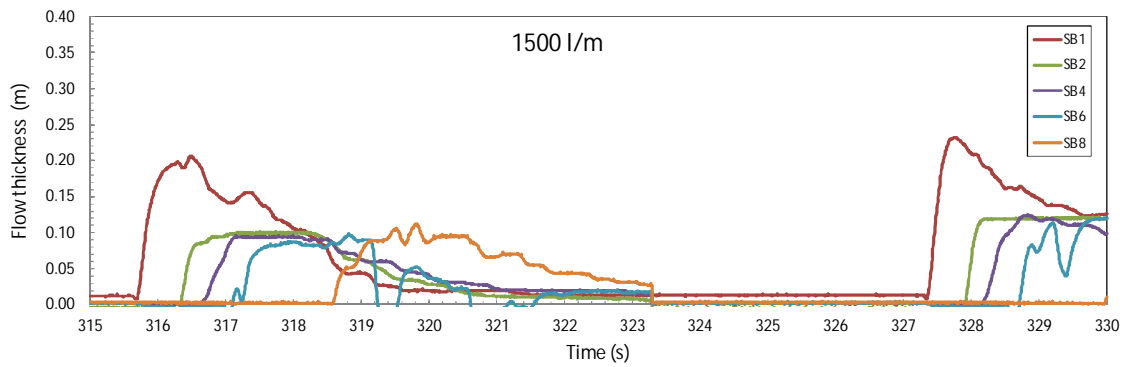
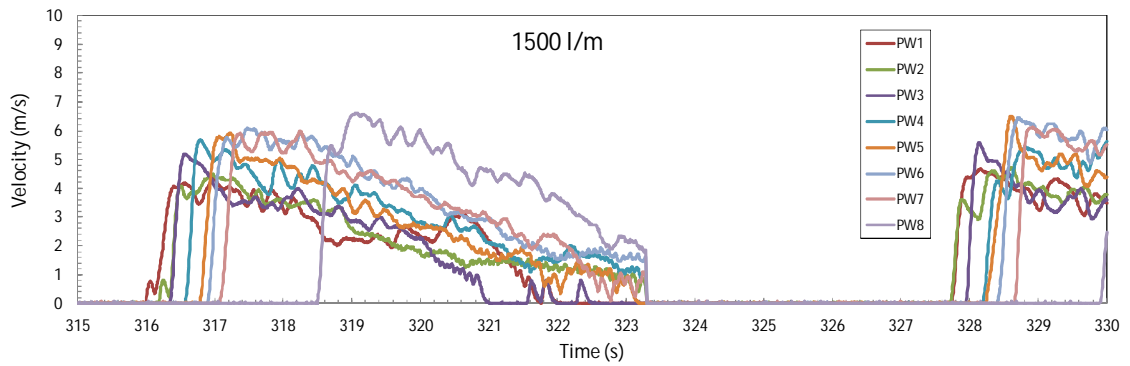
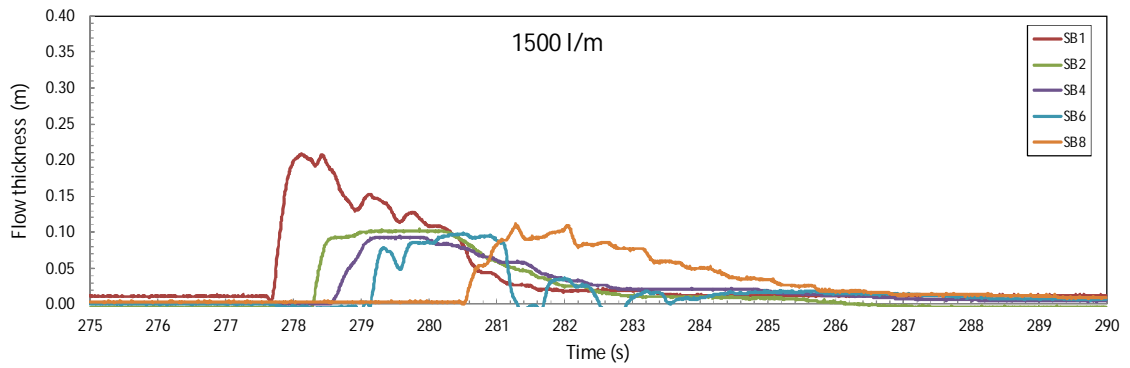
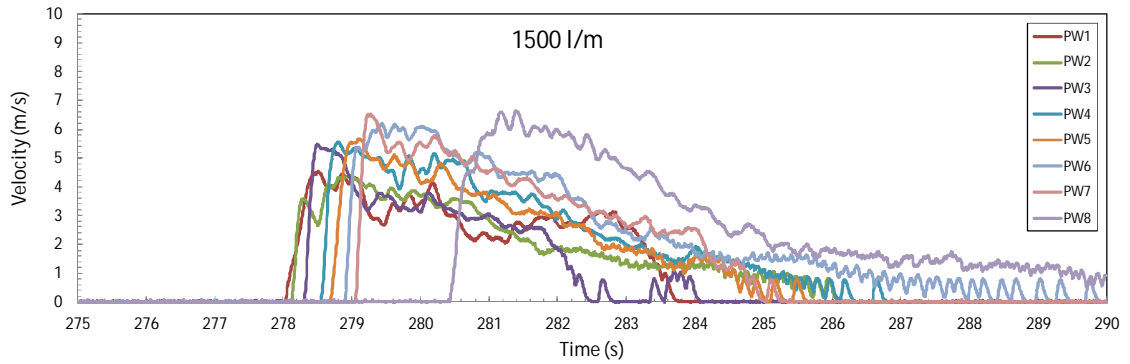
Experimental results of flow velocities and thicknesses (Millingen)

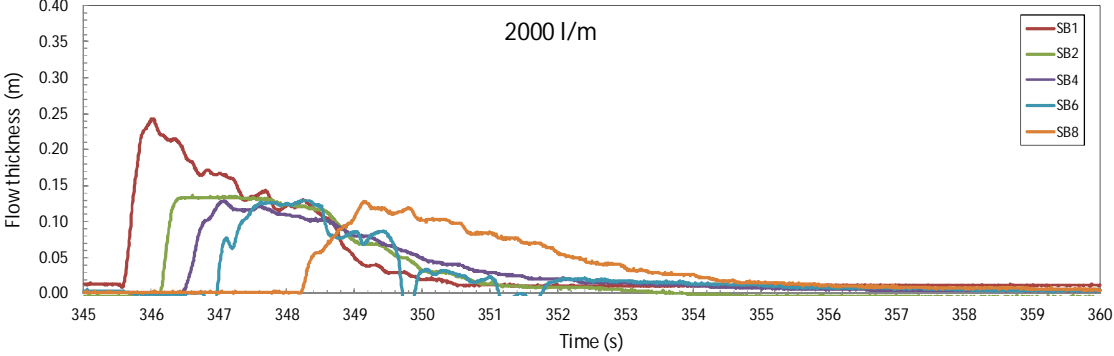
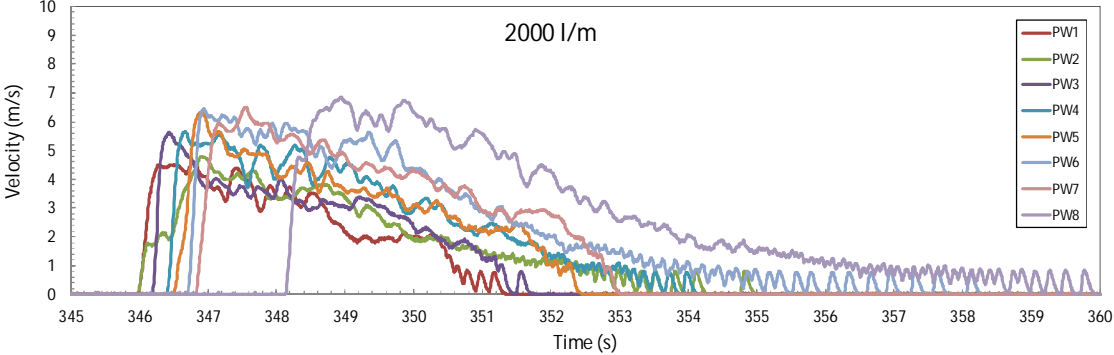
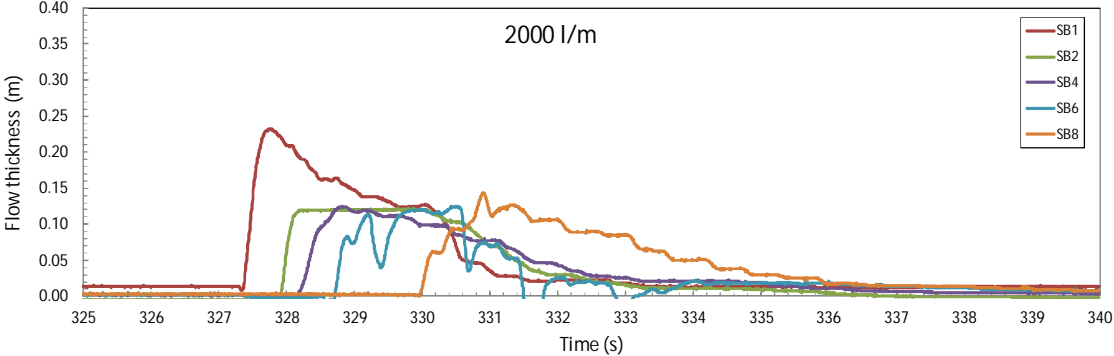
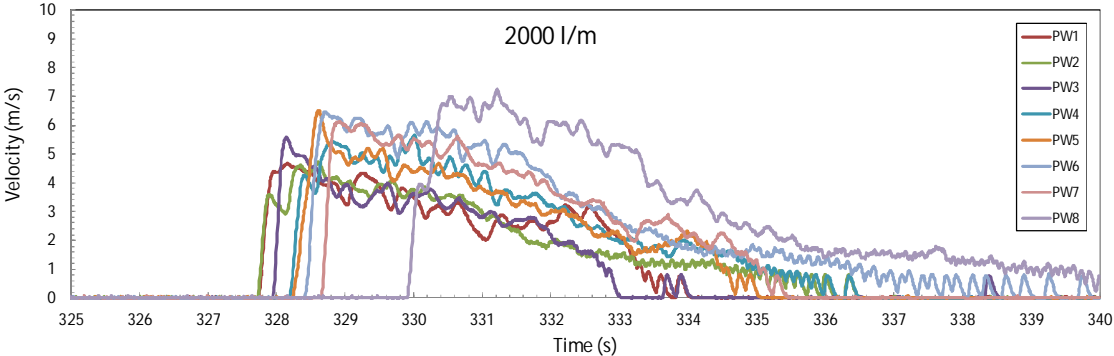


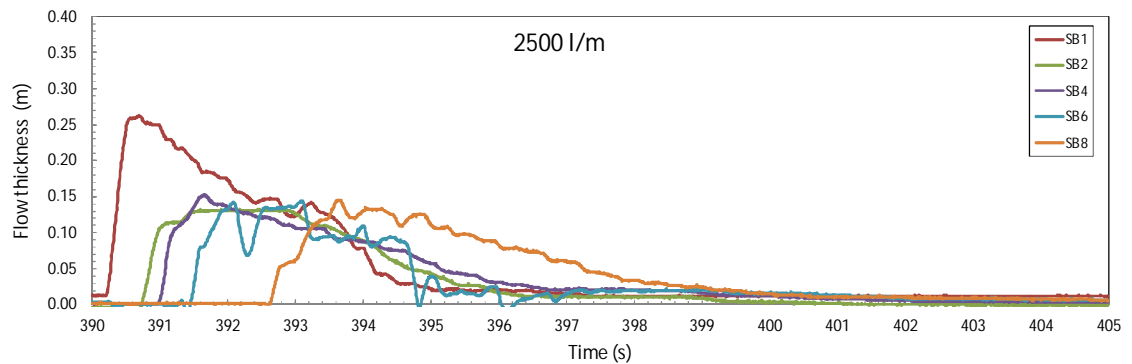
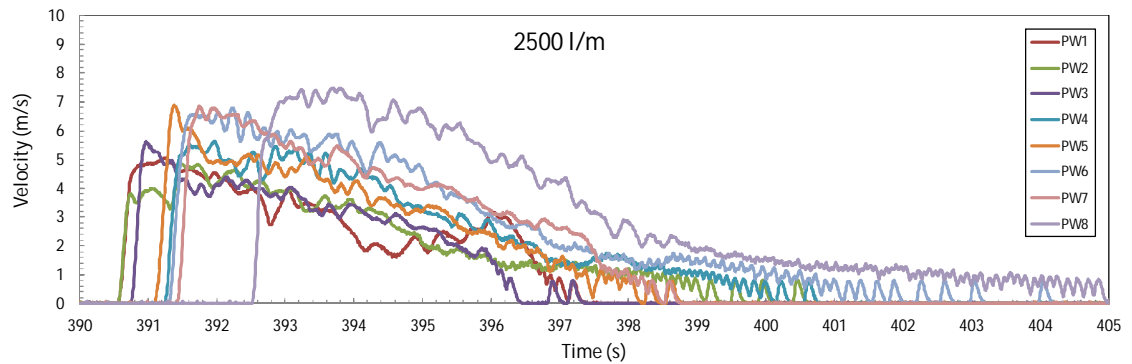
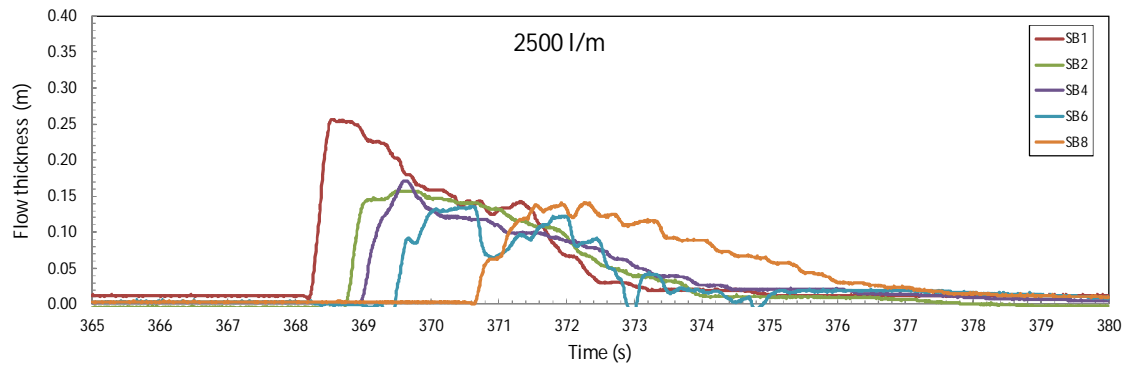
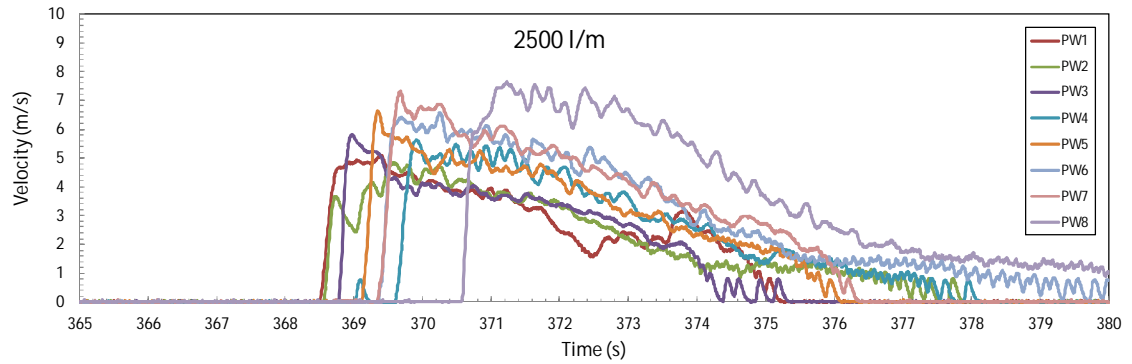


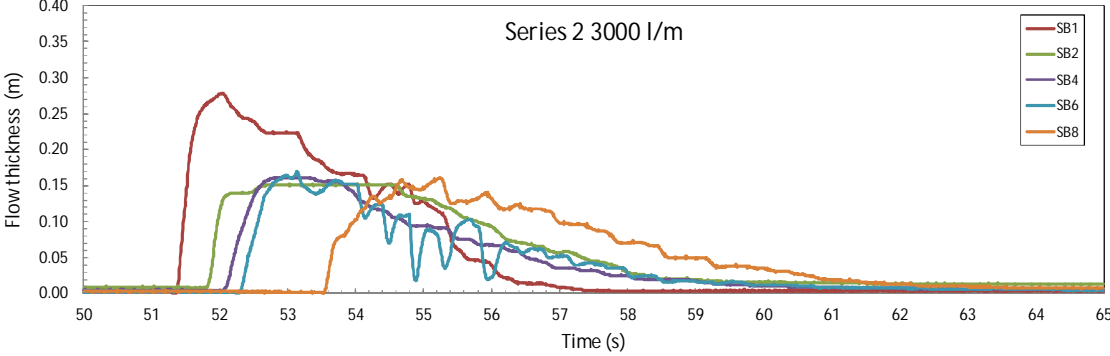
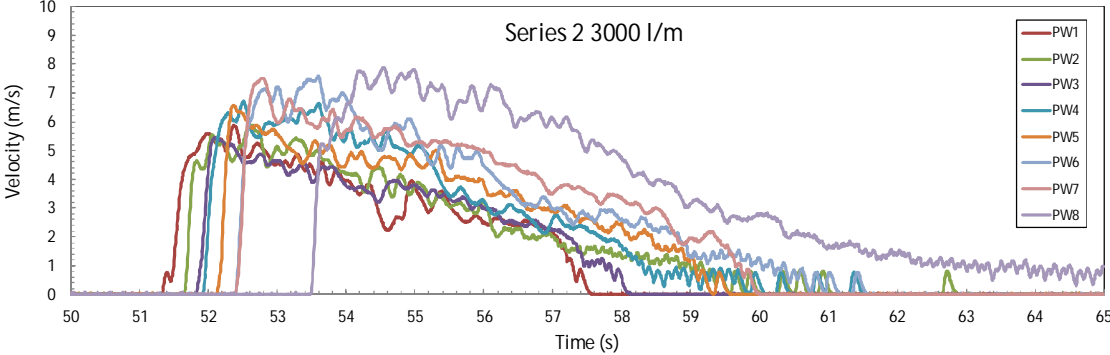
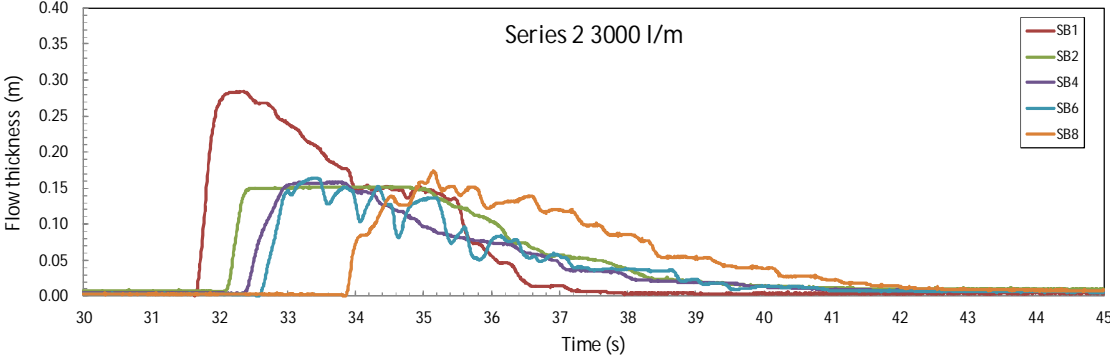
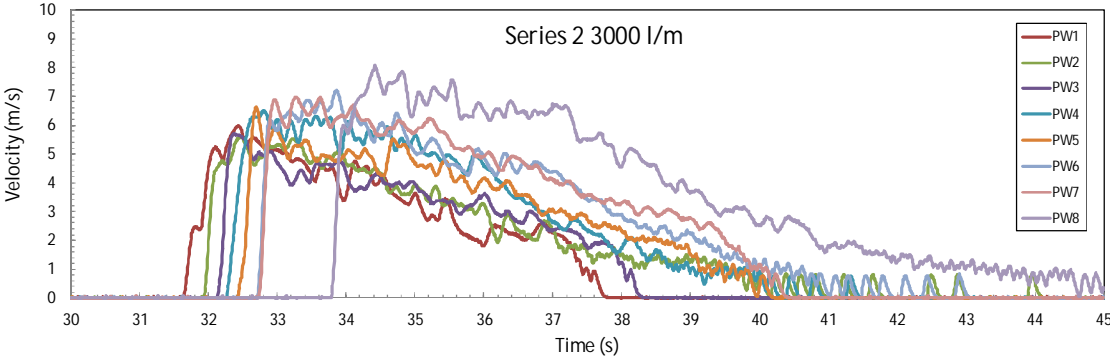


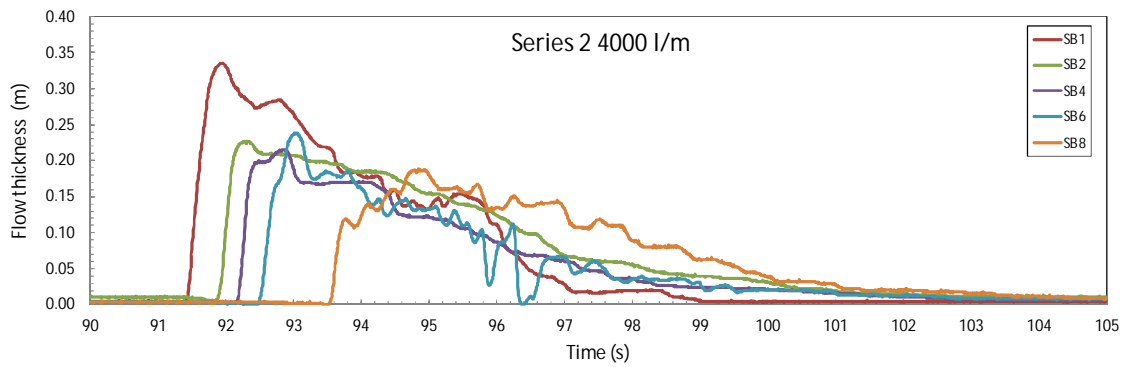
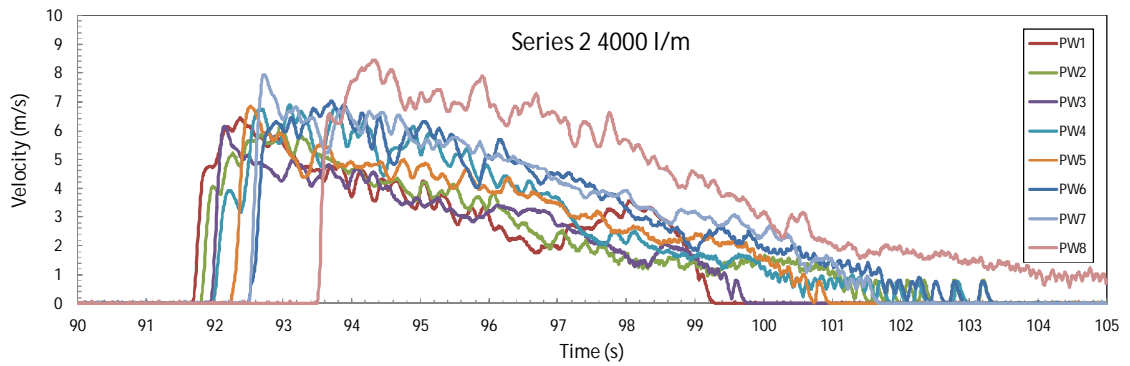
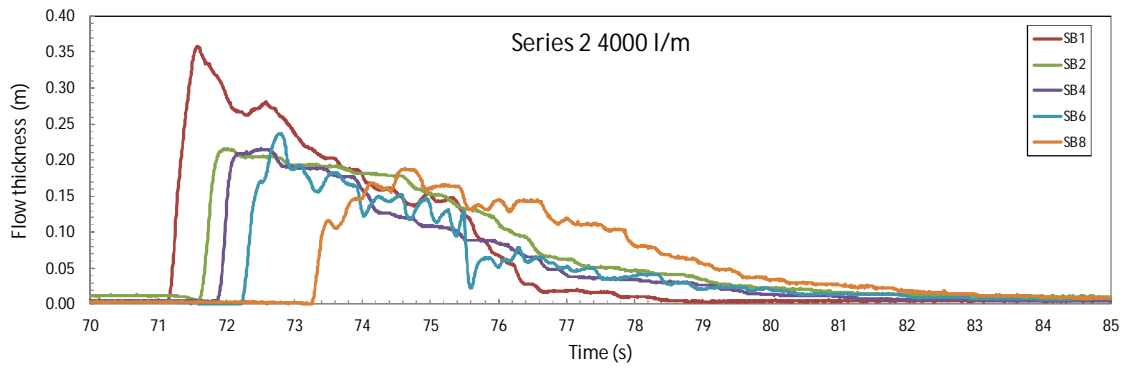
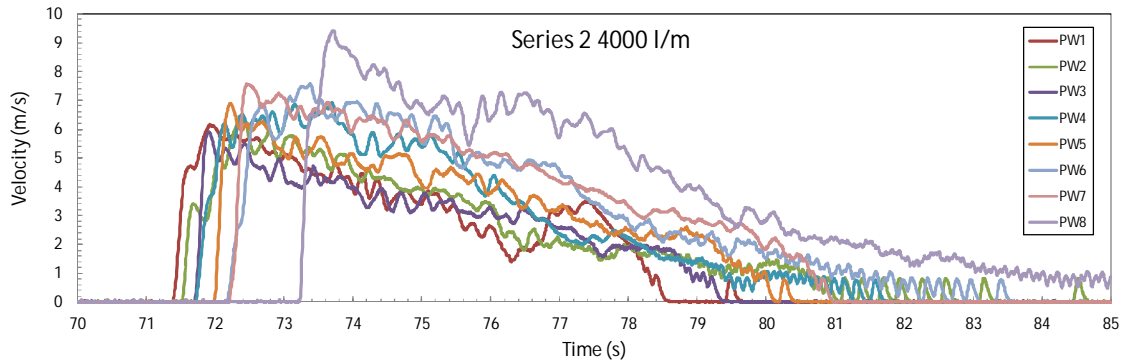


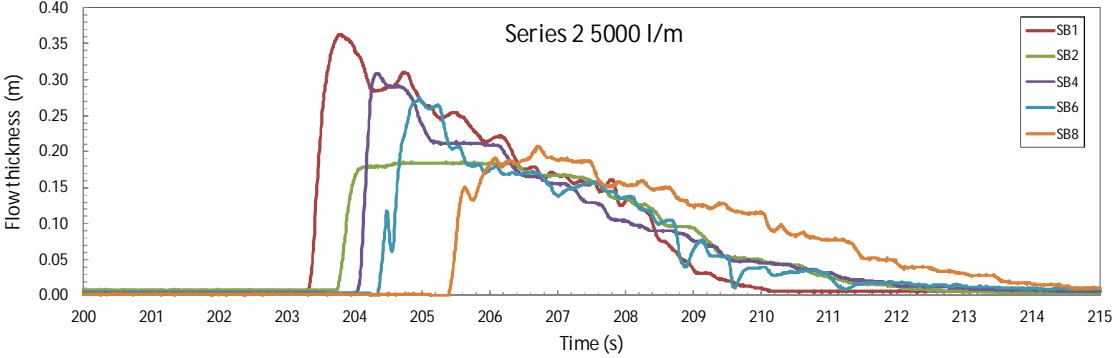
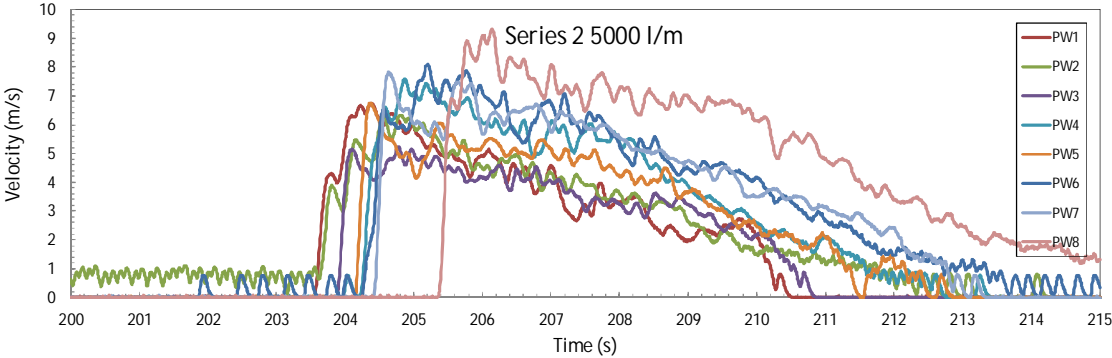
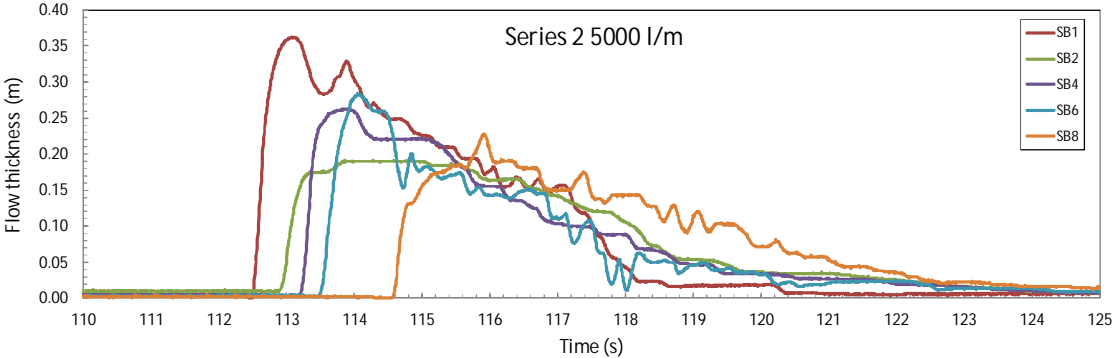
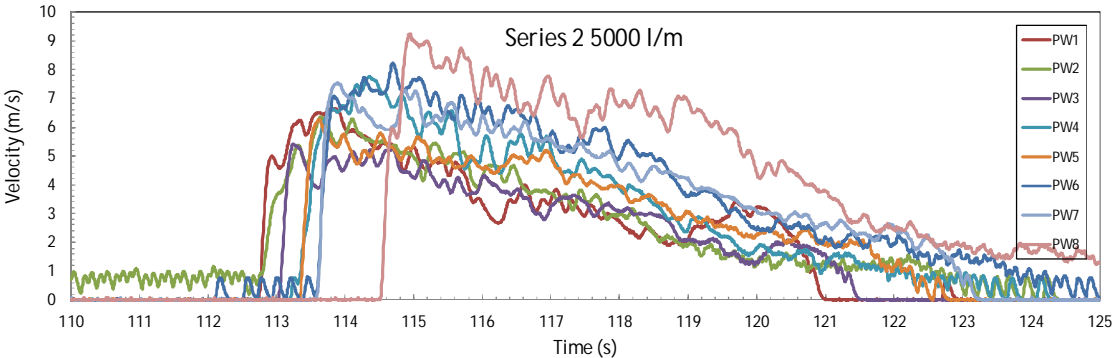


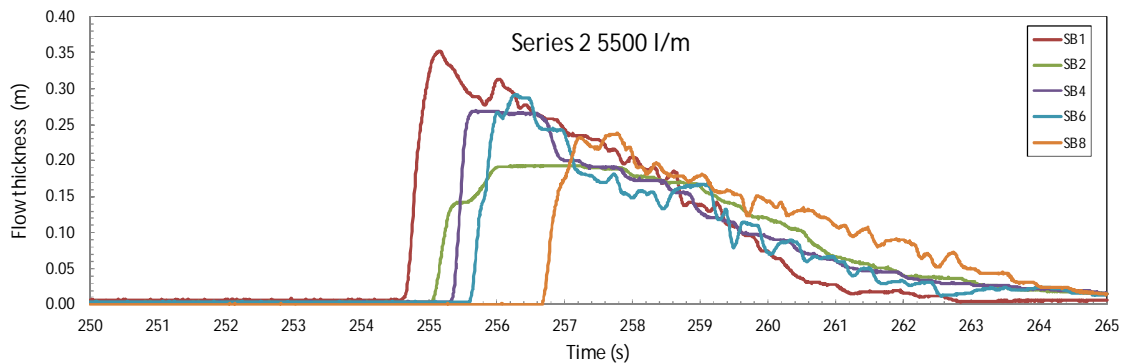
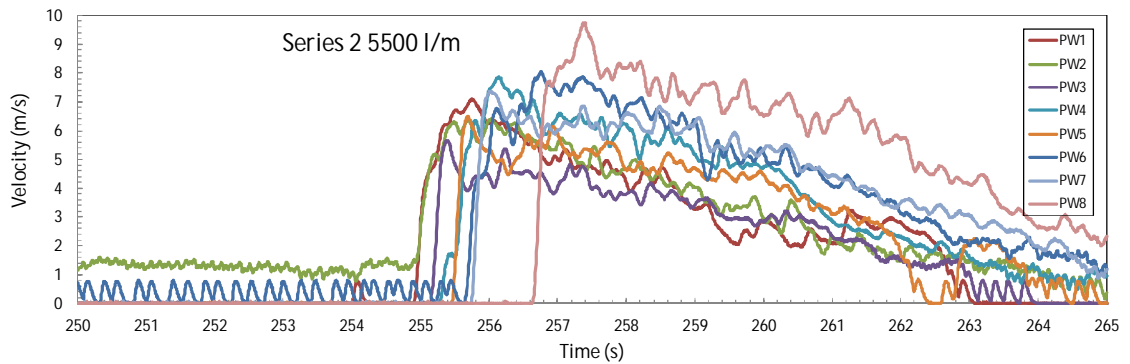
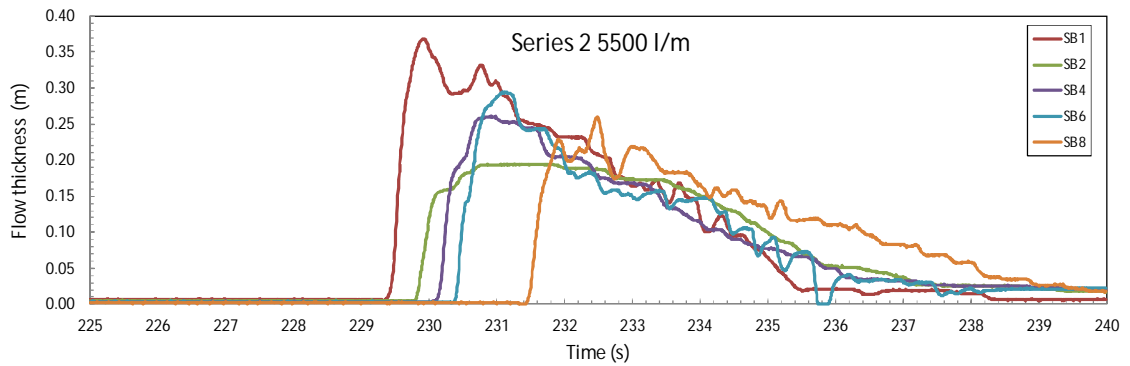
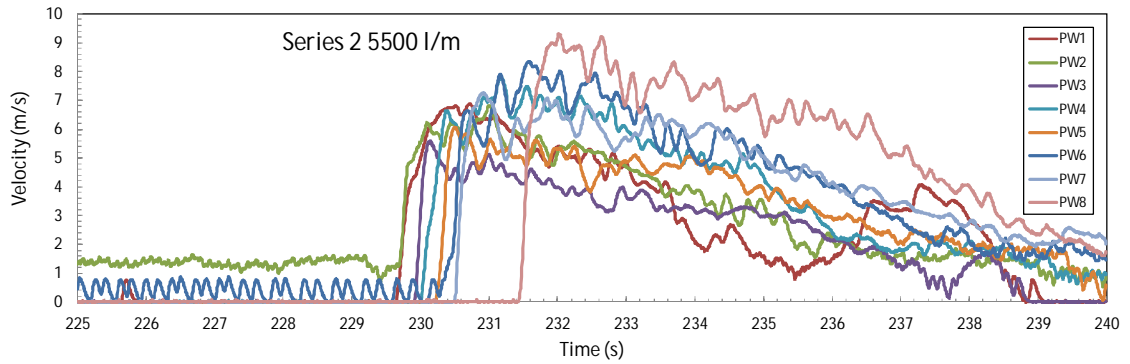


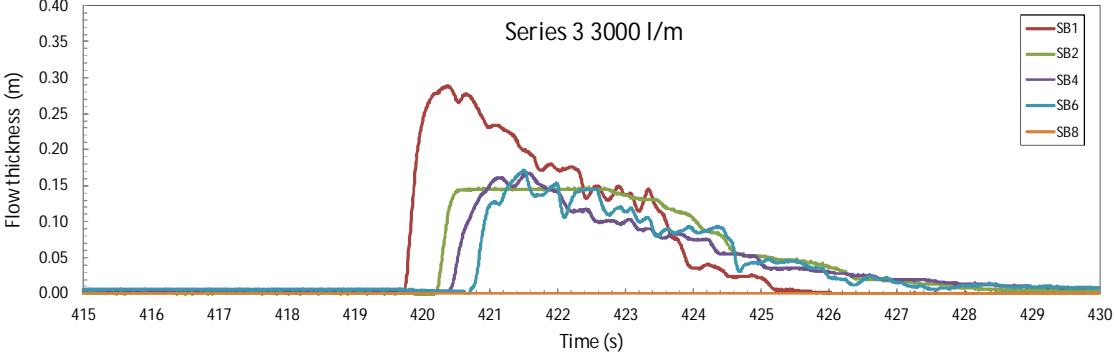
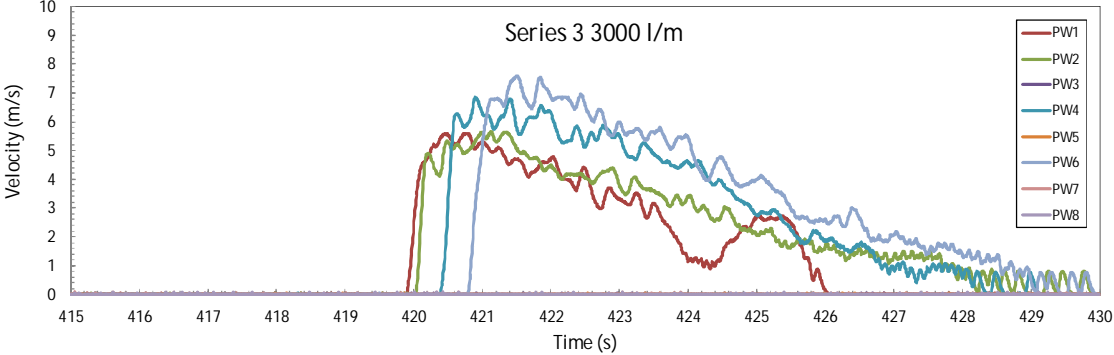
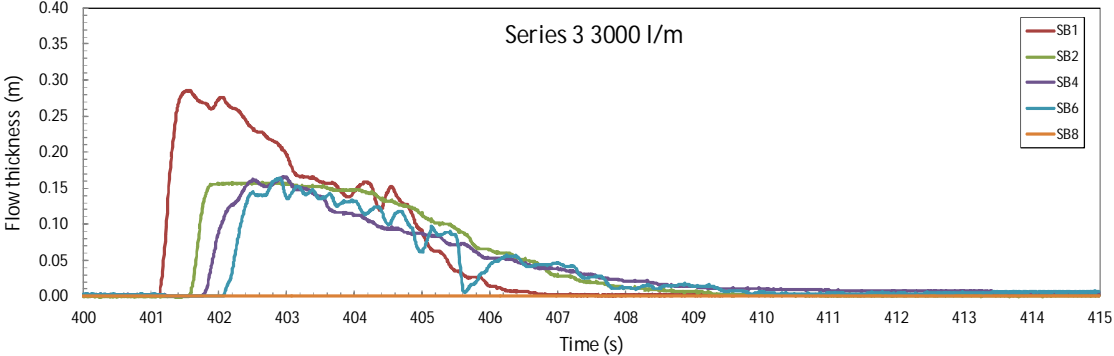
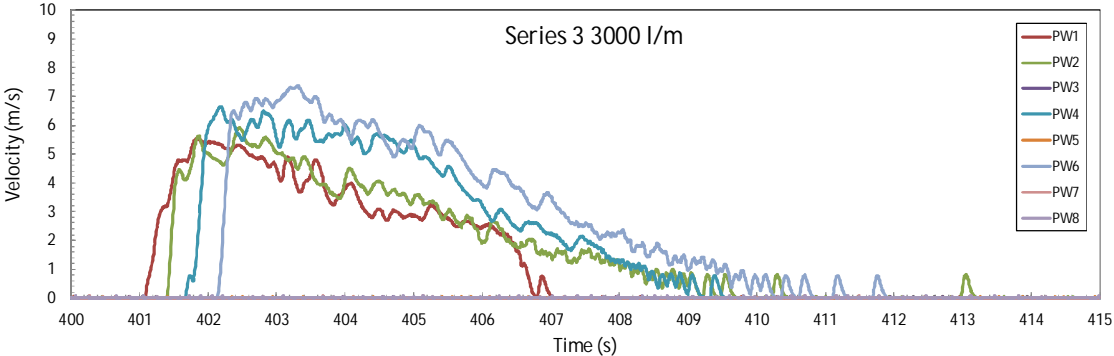


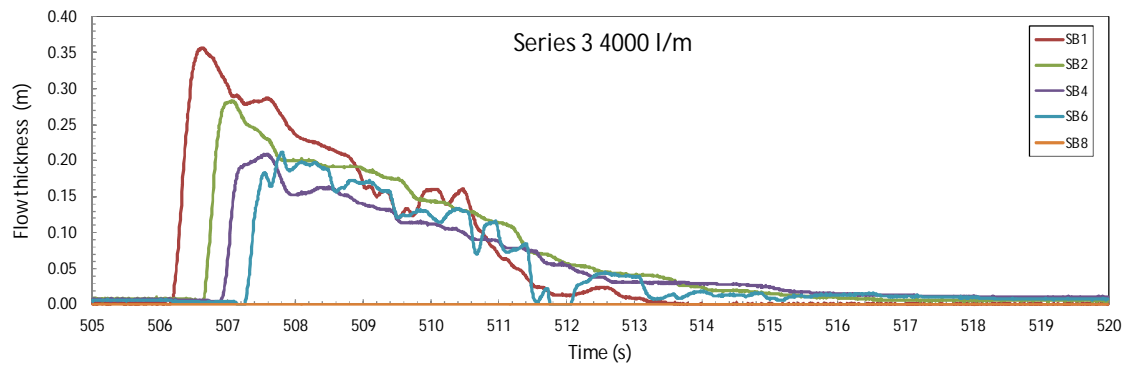
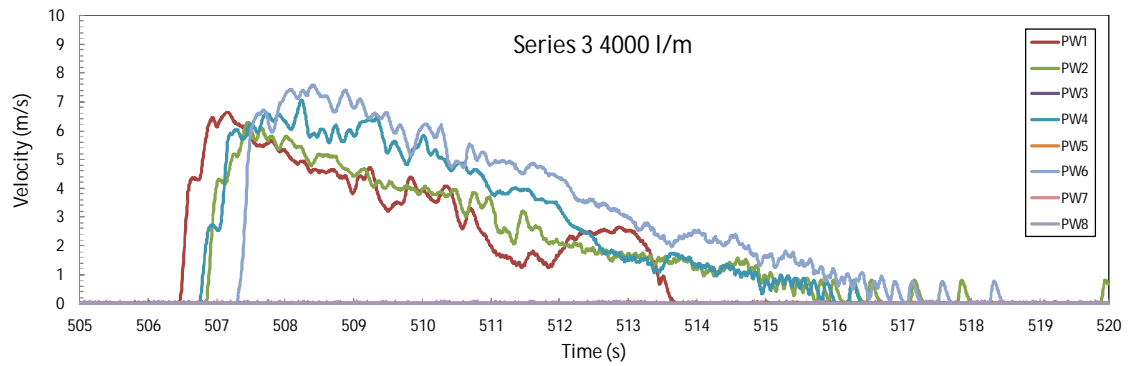
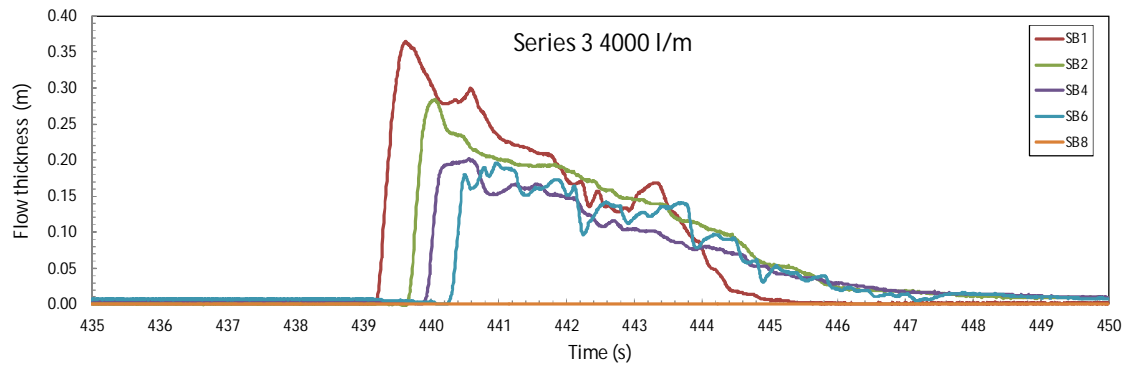
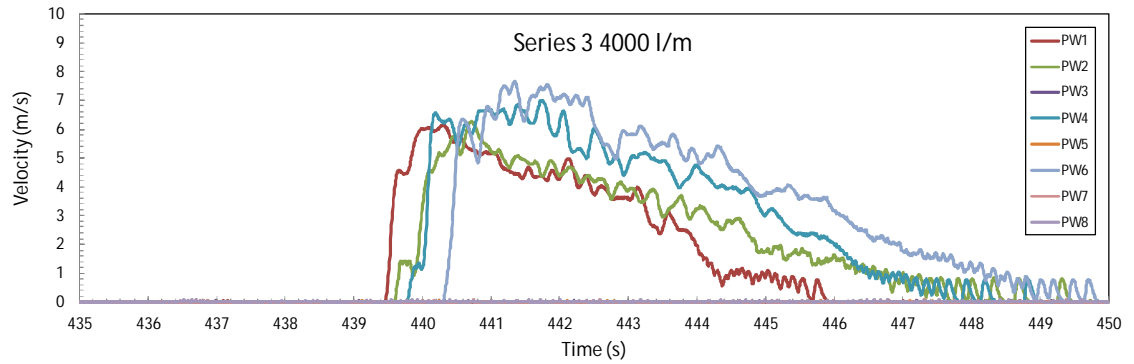


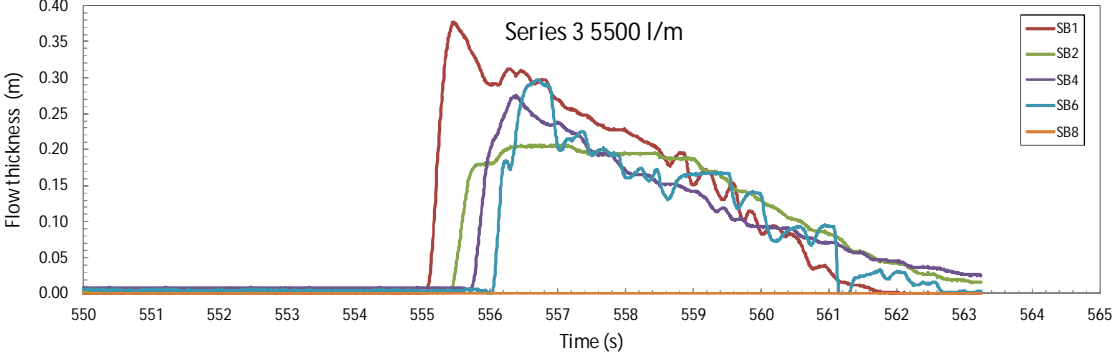
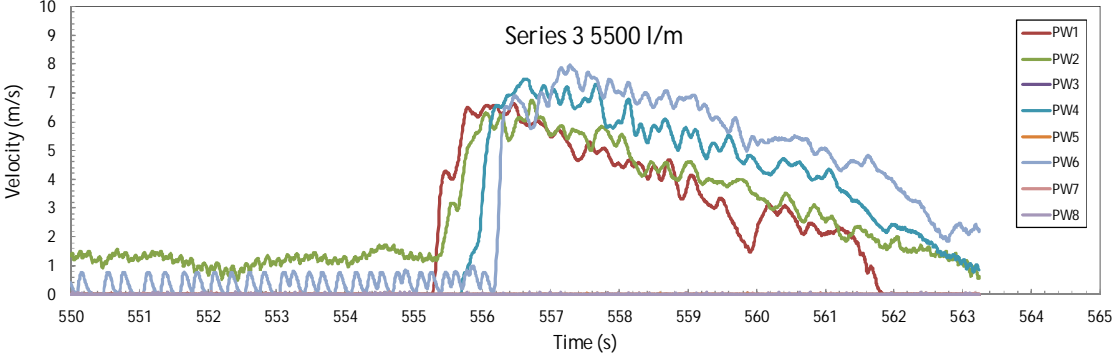
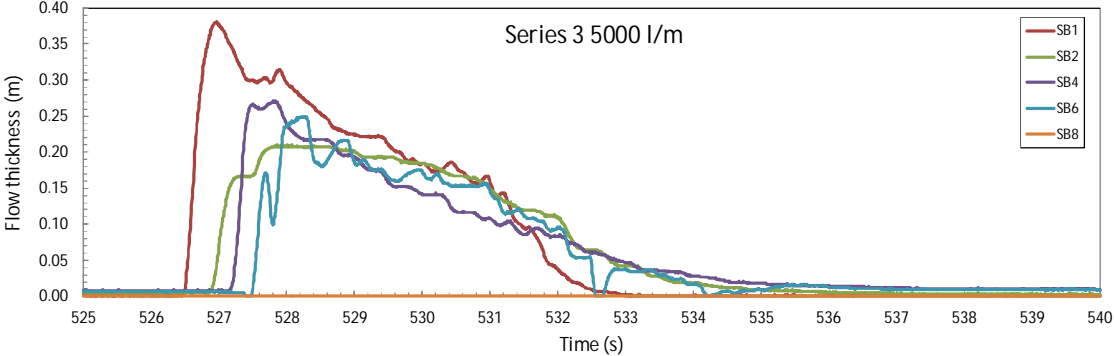
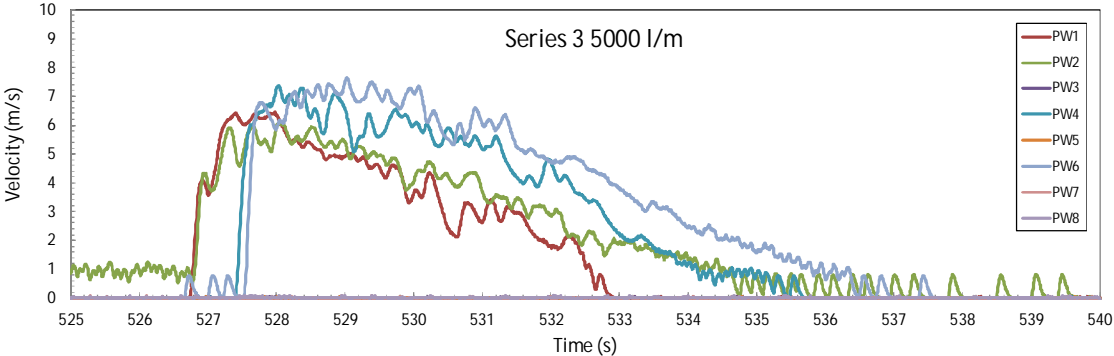












B Grass properties

Introduction

To determine the properties of grass (dynamic) load tests and (falling head) permeability tests were performed at Deltares in December 2012 at room temperature. Two grass sods were dug out on a revetment near Millingen and stored in a cold room for about one month. Subsequently, the grass sods were subjected to a load test for approximately 30 minutes, followed by a series of 3 permeability tests. As both grass sods are from the same location the variation of the results may be considered as natural variation of the investigated soil properties.

Sample preparation

Although the samples 'Millingen' and 'Millingen1' were not fully saturated before each load phase about 0.2 litre of water was gushed on the top. Some air is expected to be trapped in the top layer of the sample, similar to the case of wave overtopping conditions. Before testing, the grass sods were trimmed on the top side to remove the grass plants. Next, a steel tube with 23 cm diameter and 9 cm high ($\ell = 9$ cm) was pushed around the grass sod. After the tests the volumetric weight was determined in saturated condition. Special precaution was taken on the preparation of the samples to prevent smearing of the top and bottom side which would reduce the permeability by an unknown factor.

On the bottom side a layer of about 1 cm gravel was installed to make the surface flat and to allow drainage. The water pressure at the bottom of the sample, inside the gravel layer was kept at zero. To decrease friction forces on the sides, the tube wall was smeared with a layer of Molykote grease. Hence, also possible water paths along the sides were blocked. In the second sample (Millingen1) a large fracture was observed (Fig. B2). To close the fracture a tie wrap around the sample was applied. The samples were loaded by a 20 cm diameter plate, leaving a small gap between the piston and the sample containment tube. Between the top of the sample and the plate a drainage layer of metal wire was applied. The schematized cross section of the test set up is given in Fig. B3. At the bottom of the sample, inside the clay, a pore pressure transducer was placed at 1 cm above the bottom to measure the pore pressure during the dynamic load tests.

Dynamic load tests

Tables B1 and B2 show the series of loading steps (phases) in terms of displacement amplitude (mm) that have been applied to the samples. In the first test on sample 'Millingen' 5 cycles were applied in each phase. In the second test on sample 'Millingen1' 25 cycles were applied in most of the phases to study the time development of the stress amplitude signals. The displacement controlled movement of the piston results in a periodic vertical stress and a periodic pore pressure near the bottom of the sample (Figs. B4 to B10). The ratio of the average sample pressure (p_{top}) and the vertical strain (ε_v) can be interpreted as a (dynamic) stiffness parameter (M).

$$M = \frac{P_{top}}{\varepsilon_v} \quad (B1)$$

with

$$\varepsilon_v = \frac{d\ell}{\ell} \quad (B2)$$



Figure B2 Sod for test 2 with a large fracture on top and the right side

The stiffness parameter represents the combined stiffness of both the soil skeleton and the pore water, with air intrusions (if present). The saturation degree of the soil was not determined. However, it is most likely that the soil was far from full saturation.

Table B1 Experimental results of the dynamic load test (Millingen) and derived stiffness M

phase	d_l (mm)	p_{top} (kPa)	ϵ_v (-)	M (kPa)
1	2	3.5	0.022	158
2	2	3.3	0.022	149
3	2	3.5	0.022	158
4	3	6.2	0.033	186
5	3	5.8	0.033	174
6	3	5.3	0.033	159
7	3	4.8	0.033	144
8	4	9	0.044	203

Table B2 Experimental results of the dynamic load test (Millingen1) and derived stiffness M

phase	d_l (mm)	p_{top} (kPa)	ϵ_v (-)	M (kPa)
3	2	2.4	0.022	108
4	2	2.3	0.022	104
5	2	3.2	0.022	144
6	3	6	0.033	180
7	3	6	0.033	180
8	4	10	0.044	225

Permeability tests

Directly after the dynamic load tests, the samples were subjected to a permeability test. The bottom of the sample tube was positioned in a bath with constant water level. The top of the tube was completely filled with tap water (Fig. B11). The decreasing water level was measured in time passing three levels, marked in the tube. During the test, the water head decreased from about 22 cm to about 7 cm. Table B3 shows the measured hydraulic conductivity. Note that the test was repeated three times. During the first run the sample was probably not fully saturated.

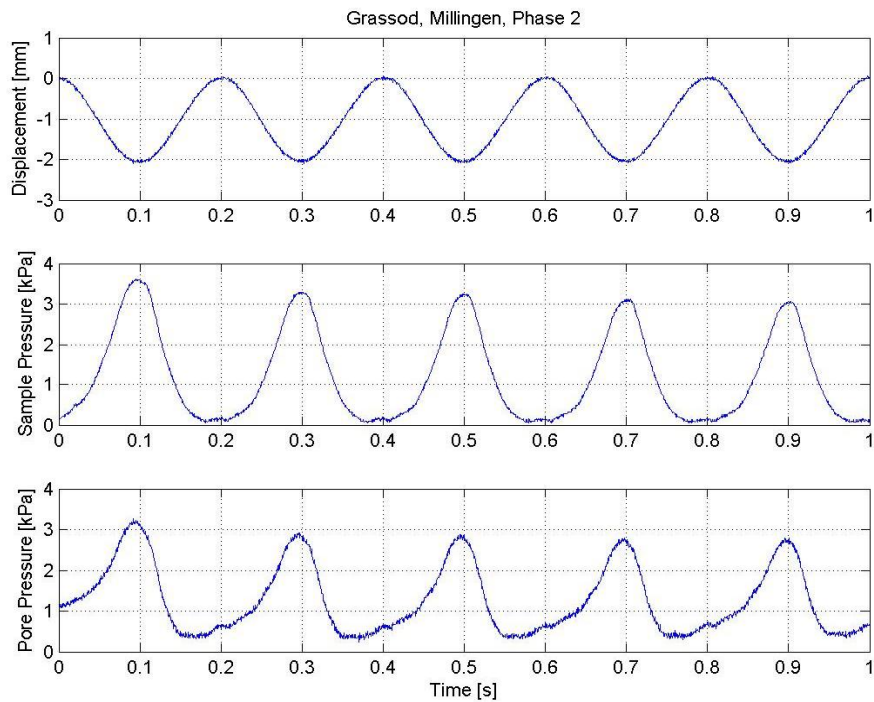


Figure B4 Pore pressure (at bottom of sample), sample pressure (on top) and displacement as function of time (Phase 2)

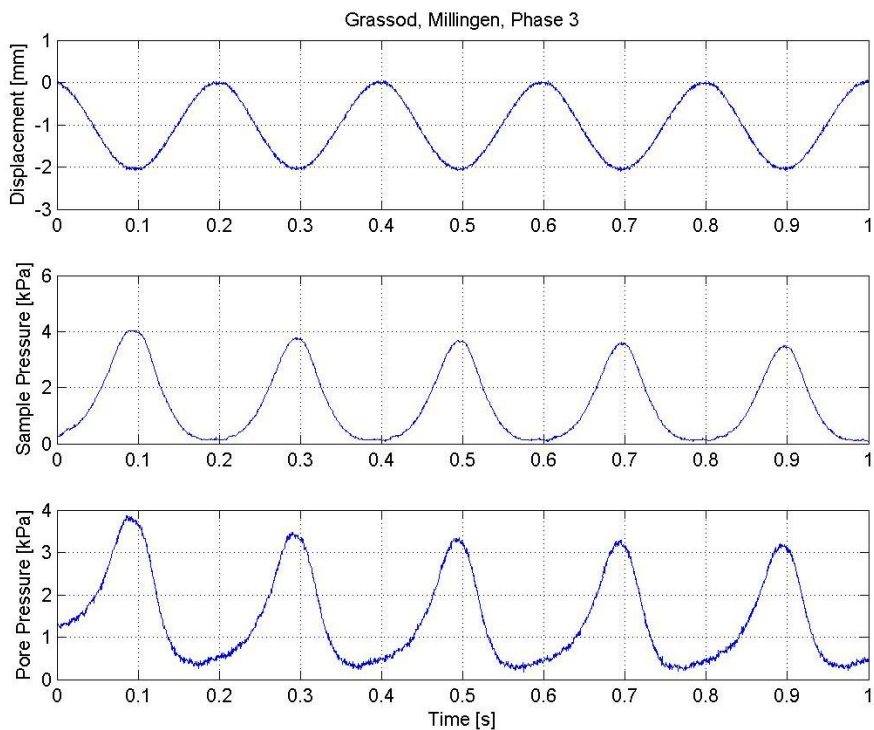


Figure B5 Pore pressure, sample pressure and displacement as function of time (Phase 3)

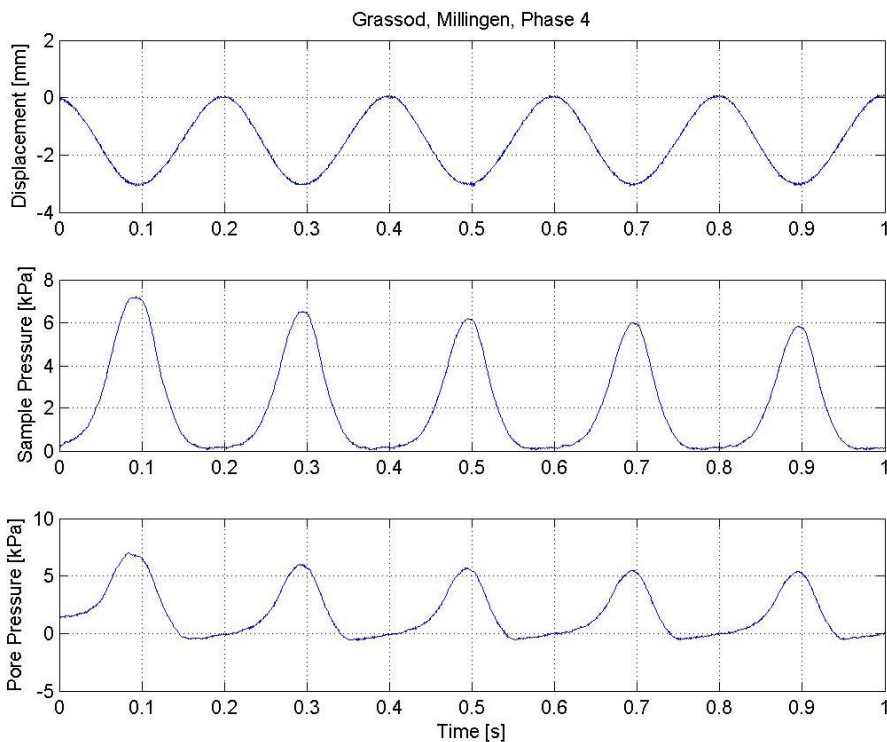


Figure B6 Pore pressure, sample pressure and displacement as function of time (Phase 4)

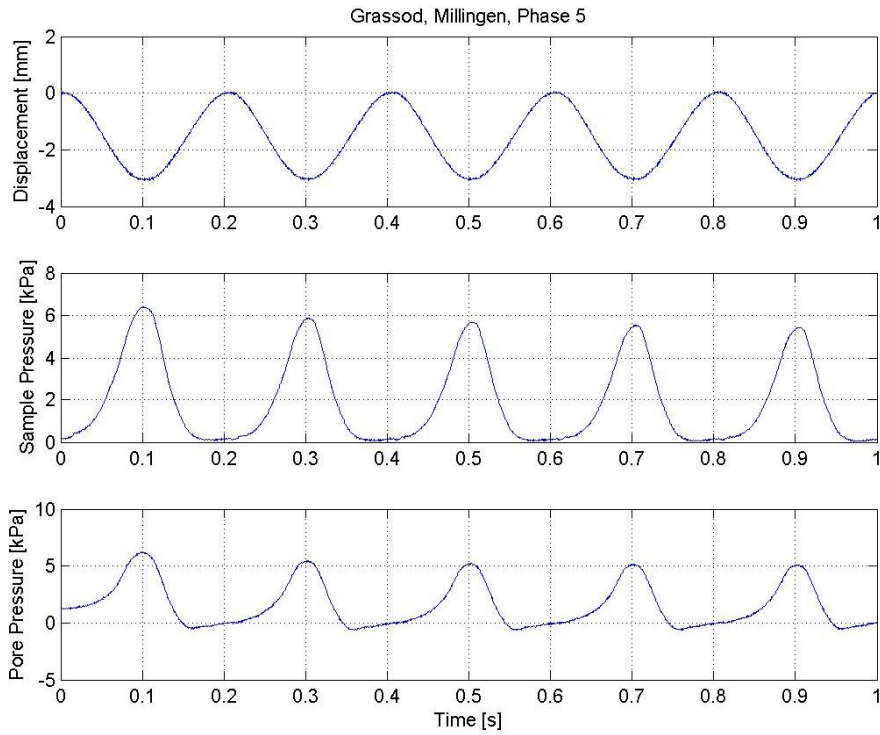


Figure B7 Pore pressure, sample pressure and displacement as function of time (Phase 5)

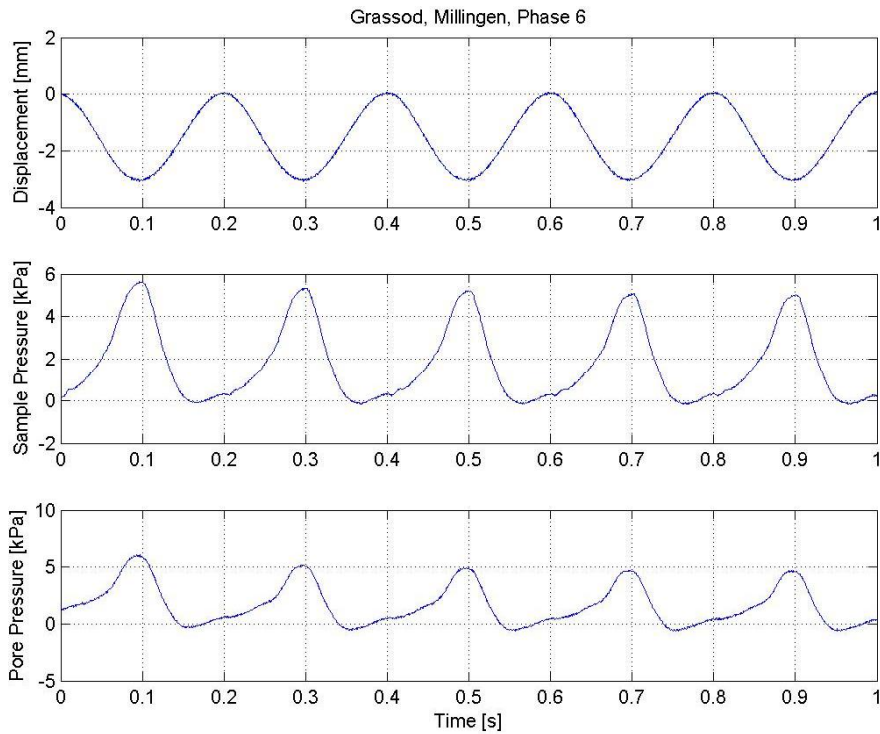


Figure B8 Pore pressure, sample pressure and displacement as function of time (Phase 6)

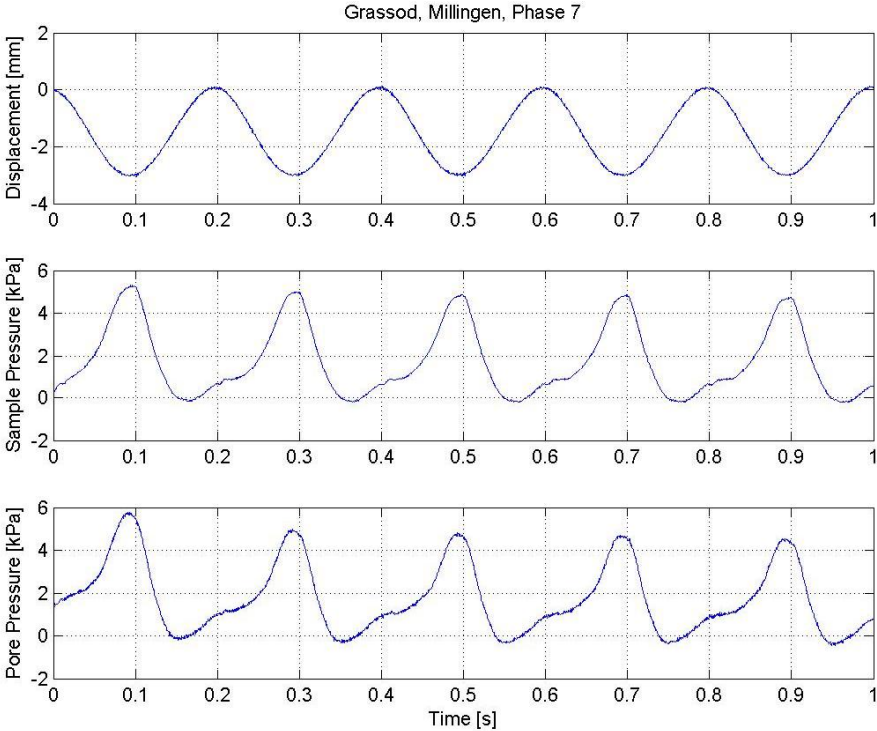


Figure B9 Pore pressure, sample pressure and displacement as function of time (Phase 7)

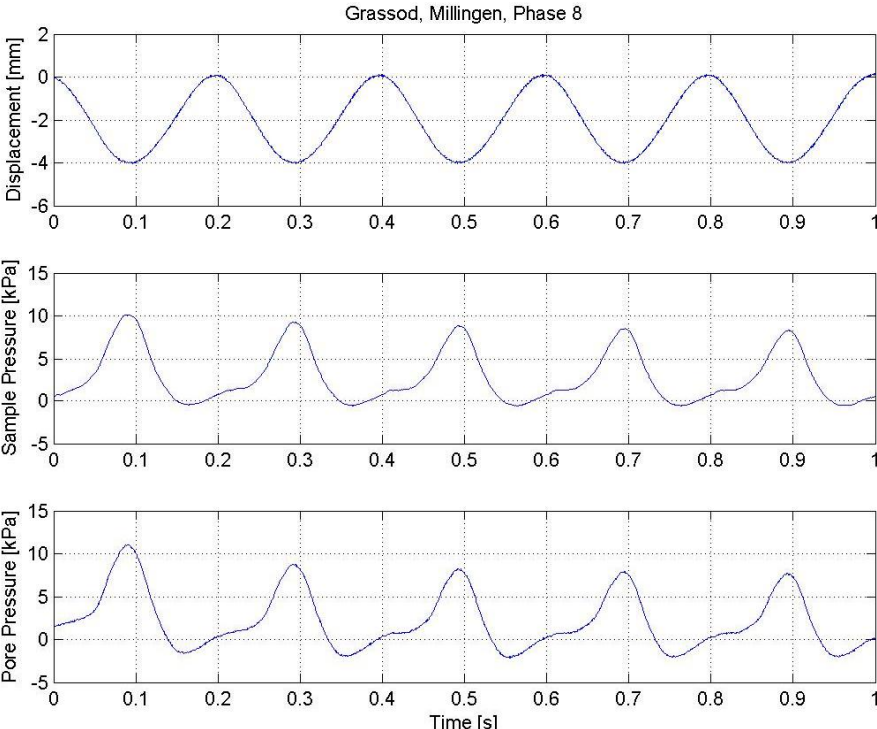


Figure B10 Pore pressure, sample pressure and displacement as function of time (Phase 8)



Figure B11 Running falling head test on the first sample

Table B3 Falling head results for first sample

head (mm)	K_1 (m/s)	K_2 (m/s)	K_3 (m/s)
171	0.00026	0.00023	0.00020
119	0.00027	0.00023	0.00021
68	0.00029	0.00025	0.00022

The second sample was tested in the same manner and showed somewhat lower K -values, (Table B4).

Table B4 Falling head results for second sample

head (mm)	K_1 (m/s)	K_2 (m/s)	K_3 (m/s)
169	0.00016	0.00016	0.00016
117	0.00017	0.00016	0.00017
66	0.00019	0.00018	0.00018

Pore pressure response

The pore pressure sensor is located on the axis of the sample, about 1 cm above the bottom drainage layer. Despite of this short distance a relatively large response was observed in both tests (Figs. B4 to B10).

In the first test 80% to 100% of the applied vertical stress is transferred to the pore pressure. Figure B12 shows the relation between both stresses for the last phase (nr.8). The mean

slope of the fitting line is 1.1. These data can be used to validate a consolidation model for the top layer of the revetment.

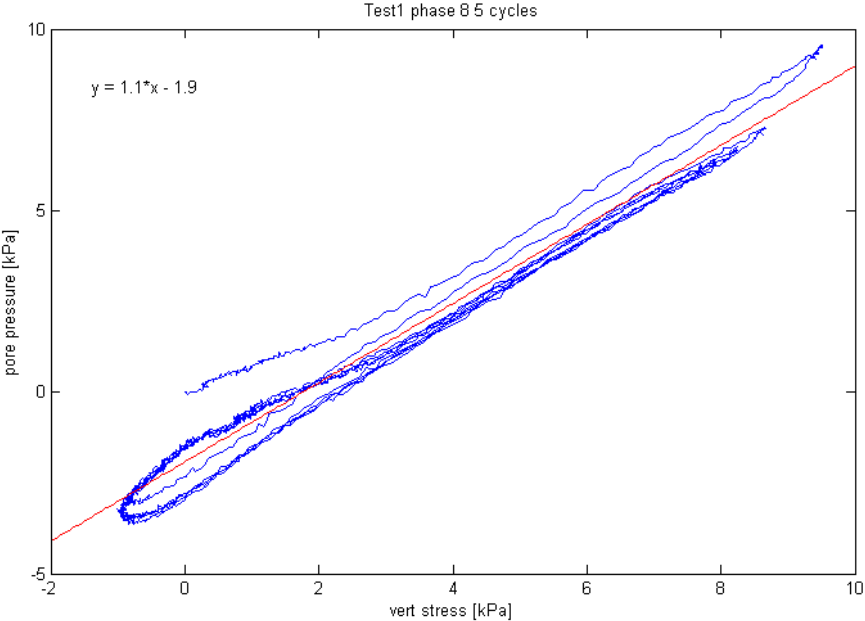


Fig. B12 Pore pressure vs. total vertical stress for the last phase of test 1

The second test shows a different behaviour, but the response is also 80% to 100%. In this case, more cycles were obtained (Greeuw 2013). A stress plot of the last phase is given in Fig. B13. The pore pressure response shows more hysteresis than with the first test.

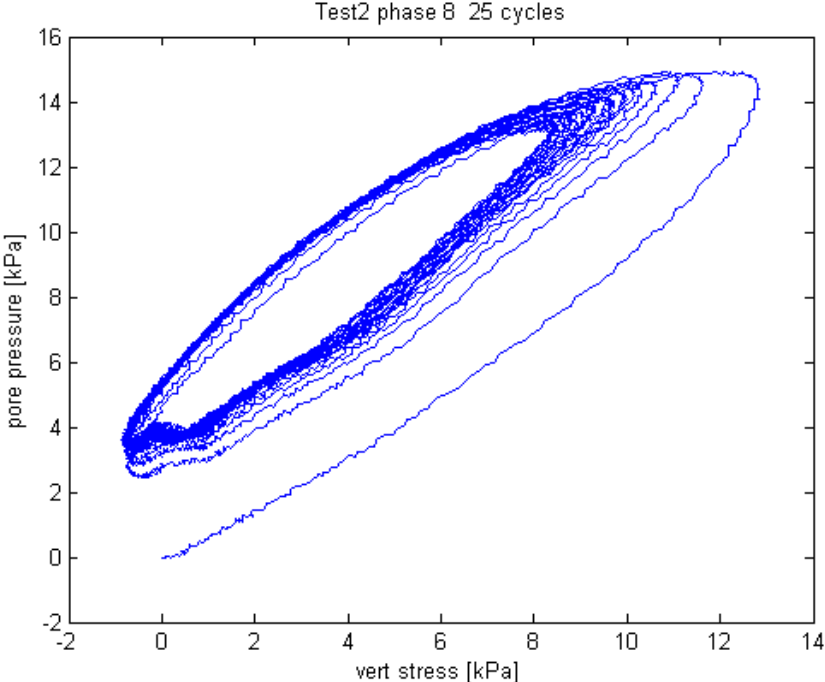


Fig. B13 Pore pressure vs. total vertical stress for the last phase of test 2

Symbols

$d\ell$	deformation/displacement (m)
K	hydraulic conductivity (m/s)
ℓ	height of sample (m)
M	dynamic stiffness parameter (N/m ²)
ρ_{top}	vertical stress or sample pressure (N/m ²)
ν	Poisson ratio
ε_v	vertical strain (-)

References

Greeuw, G., 2013. Dynamic load tests on two sods from Millingen, (project number 1206016-008), Deltares, Delft.

C Load factor at revetment transitions

Introduction

Erosion by wave overtopping at dike transitions is a major cause of dike damage or failure during severe overtopping events. When the flow of the waves is directed from a smooth to a rough bed the load increases. In the direction from rough to smooth the load decreases. These effects are here expressed by a load factor. The damage at transitions can be predicted by the overload method as proposed by Van der Meer et al (2010) in which the load is corrected by the load factor. This Appendix provides insight in the load modelling at (dike) transitions between protections with different roughness, perpendicular to the general flow direction.

Current over smooth and rough strip beds

Hinze and Nezu (Nezu and Nakagawa 1993) found experimentally that up-flows occurred over smooth-bed strips, whereas down-flows occurred over rough-bed strips for air and water flows (Fig. C1) In the down-flow region over the rough bed the production of the turbulence kinetic energy (P) is greater than the turbulent dissipation (ε). Consequently, the bed shear stress on the rough bed is about twice as large as the mean bed shear stress (Fig. C2).

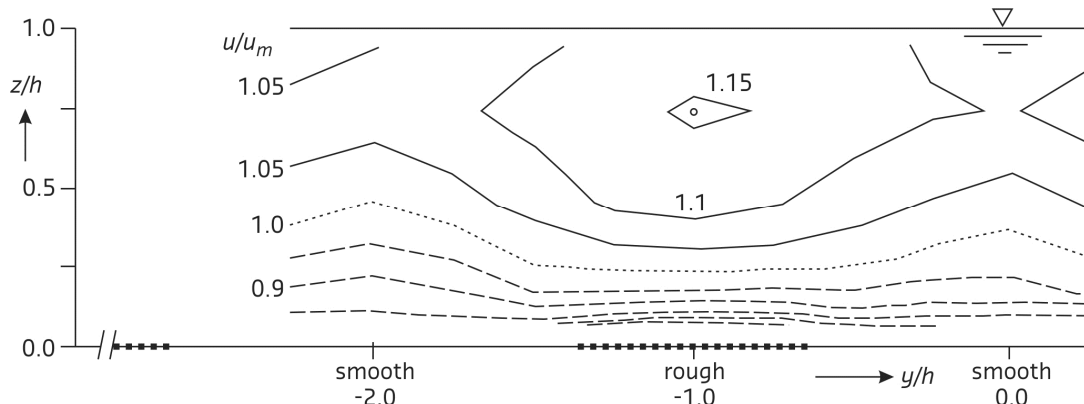


Figure C1 Velocity vector for cellular secondary currents over smooth and rough bed strips; experimental results from Studerus 1982 (Nezu and Nakagawa 1993)

When the bed condition changes abruptly an internal boundary layer develops at the transition. Nezu observed experimentally that the bed shear stress and the turbulence reach a maximum value immediately downstream from smooth to rough bed conditions. Beyond this location, the bed shear stress decreases in the streamwise direction to its equilibrium value.

When the bed changes from smooth to rough the longitudinal flow velocity decreases abruptly in the internal boundary layer, which is a direct effect of the bed roughness (Fig. C3) so the velocity gradient close to the bed becomes smaller (is not drawn in Fig. C3). However, the velocity outside the internal boundary layer increases to compensate the deceleration near the bed.

The streamwise variation of the bed shear stress and turbulence characteristics shows a sharp peak around the roughness discontinuity. A less sharp peak is observed in the measurements in the laboratory flume (Check also publication of Chen and Chiew JHE 2003; They measured a gradually increase of bed shear stresses and turbulence intensities).

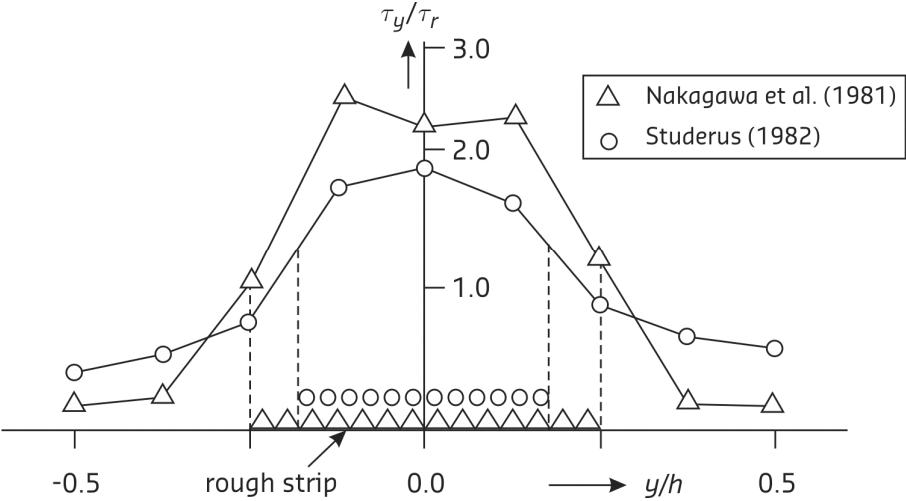


Figure C2a Spanwise distributions of bed shear stress over smooth and rough bed strips (Nezu and Nakagawa (1993))

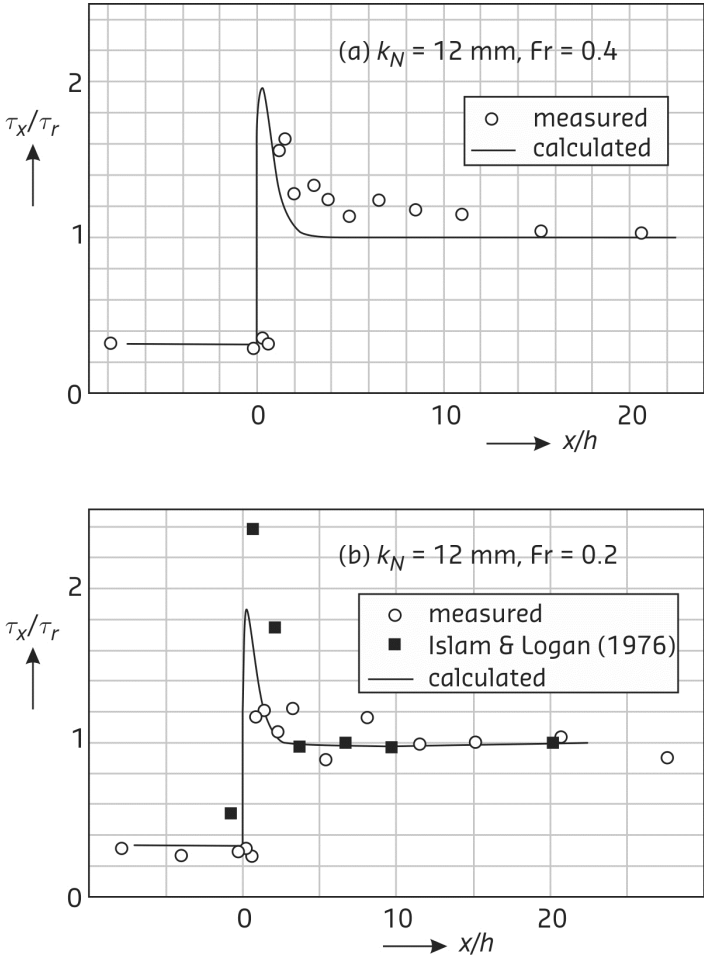


Figure C2b Overshooting property of bed shear stress in open channel flows (Nezu and Nakagawa 1993)

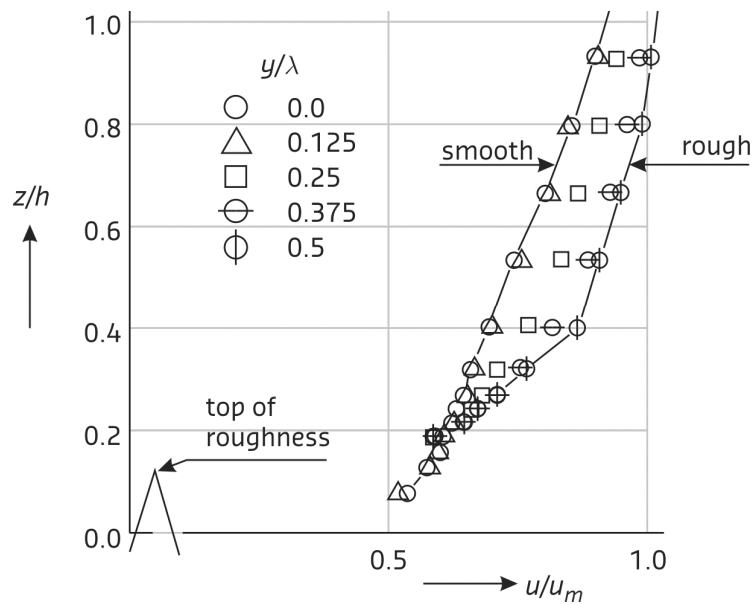


Figure C3 Measured velocities (Nezu and Nakagawa 1993)

At smooth and rough bed strips measurements show that for $z > 0.2h$ to $0.4h$

- Local time-averaged flow velocity at smooth bed is smaller than the local time-averaged flow velocity at rough bed (thus $u_s < u_r$ (Fig. C3) (subscripts s and r refer to smooth and rough);
- Local turbulent flow fluctuation at smooth bed is smaller than the local turbulent flow fluctuation at rough bed (thus $u'_s < u'_r$ (Fig. C4));
- Bed shear stress at smooth bed is smaller than the bed shear stress at rough bed (thus $u_{*,s} < u_{*,r}$ (Fig. C4))

According to Nezu and Nakagawa (1993) the overshoot effects can be ascribed by bursting events to the Reynolds stresses (see also Fig. C4). They suggest that the burst period should be scaled with the outer parameters rather than the inner parameters. Therefore, in the modelling a reference height near the transition is chosen at $z = \delta = 0.3h$.

Analysis

When a flow is considered which is directed from a smooth to a rough bed the load factor (α_M) can be given by (see also Chapter 3)

$$\alpha_M = 1 + \frac{dF_{s,r}}{F_{s,r}} \quad (C1)$$

where $dF_{s,r}$ is the increase of the mean shear force at the transition and $F_{s,r}$ is the mean shear force at the rough bed under uniform flow conditions. Assuming that (see also Fig. C2)

$$dF_{s,r} = F_{s,r} - F_{s,s} \quad (C2)$$

where $F_{s,s}$ is the mean shear force near the smooth bed, it follows that

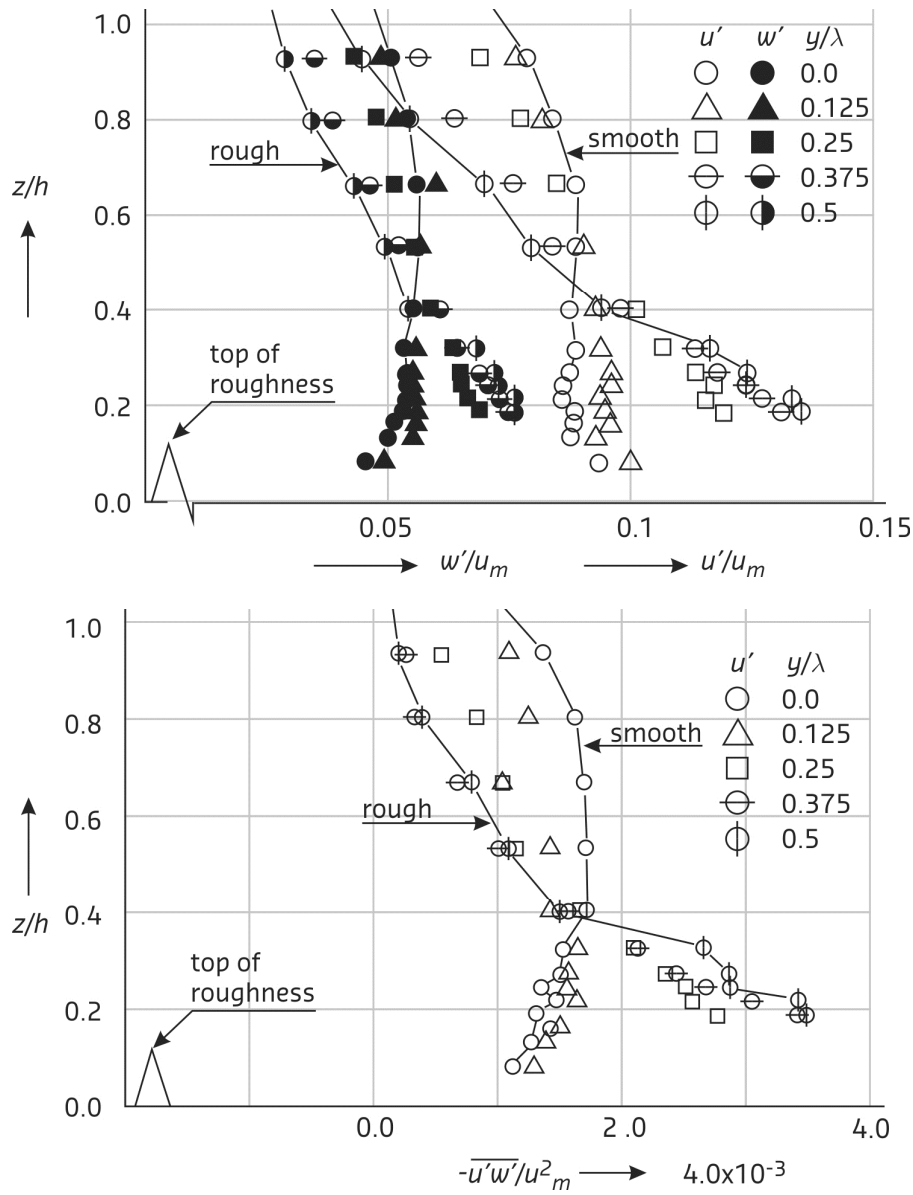


Figure C4 Turbulence measurements (Nezu and Nakagawa 1993)

$$\alpha_M = 2 - \frac{F_{s,s}}{F_{s,r}} \quad (C3)$$

or in terms of shear stresses

$$\alpha_M = 2 - \frac{\tau_s(\delta)}{\tau_r(\delta)} \quad (C4)$$

with

$$\tau_r(\delta) \propto \rho u_r^2(\delta) \quad (C5)$$

and

$$\tau_s(\delta) \propto \rho u_s^2(\delta) \quad (C6)$$

where u_r is the local time-averaged flow velocity at the rough bed, u_s is the local time-averaged flow velocity at the smooth bed, τ_r is the shear stress at a reference level δ at the rough bed, τ_s is the shear stress at a reference level δ at the smooth bed and ρ is the density of water. Hence,

$$\alpha_M = 2 - \left(\frac{u_s(\delta)}{u_r(\delta)} \right)^2 \quad (C7)$$

In the extreme situation the load factor equals $\alpha_M = 2$. If there is no transition then the load factor reduces to 1, so α_M ranges from 1 to 2.

Next, to model the load factor in terms of roughness parameters an assumption is made for the flow velocity in the streamwise direction. For nearly uniform flow conditions the time-averaged longitudinal flow velocity as function of the vertical can be approximated by

$$u(z) = \frac{u_*}{\kappa} \ln \frac{z}{z_0} \quad (C8)$$

with

$$z_0 = \frac{k_N}{33} \quad (C9)$$

where k_N is the Nikuradse roughness, u_* is the bed shear velocity, z is the vertical coordinate, z_0 is the zero velocity level and κ is the constant of von Kármán. Combining Eqs. C7, C8 and C9 yields for $z = \delta$

$$\alpha_M = 2 - \left(\frac{\left(\frac{u_*}{\kappa} \ln \frac{\delta}{z_0} \right)_s}{\left(\frac{u_*}{\kappa} \ln \frac{\delta}{z_0} \right)_r} \right)^2$$

or

$$\alpha_M = 2 - \left(\frac{\left(u_* \ln \frac{33\delta}{k_N} \right)_s}{\left(u_* \ln \frac{33\delta}{k_N} \right)_r} \right)^2 \quad (C10)$$

According to Shields the bed shear velocity is

$$u_* = \sqrt{\Delta g d \Psi} \quad (C11)$$

where d is the particle diameter, g is the acceleration of gravity and Δ is the relative density. As the Nikuradse roughness is proportional to the particle diameter it follows from Eq. C11 that

$$u_* \propto \sqrt{k_N}$$

thus

$$\alpha_M = 2 - \frac{k_{N,s}}{k_{N,r}} \left(\frac{\left(\ln \frac{33\delta}{k_N} \right)_s}{\left(\ln \frac{33\delta}{k_N} \right)_r} \right)^2 \quad (\text{C12})$$

Substituting $\delta = 0.3h$ in Eq. C12 gives

$$\alpha_M = 2 - \frac{k_{N,s}}{k_{N,r}} \left(\frac{\left(\ln \frac{10h}{k_N} \right)_s}{\left(\ln \frac{10h}{k_N} \right)_r} \right)^2 \quad (\text{C13})$$

The relation between the Nikuradse roughness and the Manning coefficient (n_M) is for uniform flow conditions

$$k_N = \left(8\sqrt{g}n_M \right)^6 \quad (\text{C14})$$

Hence, Eq. C13 can be rewritten as

$$\alpha_M = 2 - \left(\frac{n_{M,s}}{n_{M,r}} \right)^6 \left(\frac{\ln \frac{10h}{\left(8\sqrt{g}n_{M,s} \right)^6}}{\ln \frac{10h}{\left(8\sqrt{g}n_{M,r} \right)^6}} \right)^2 \quad (\text{C15})$$

When the flow is directed from a rough to a smooth bed the load factor can be written as

$$\alpha_{M,r \rightarrow s} = 1 - \frac{dF_{s,r}}{F_{s,r}} \quad (\text{C16})$$

Combining Eqs. C2 and C16 yields

$$\alpha_{M,r \rightarrow s} = \frac{dF_{s,s}}{F_{s,r}} \quad (\text{C17})$$

or with Eq. C3

$$\alpha_{M,r \rightarrow s} = 2 - \alpha_M \quad (C18)$$

Hence, in the extreme case the load on the smooth bed reduces to nil at the transition. (Check undershoot effects by using the study of Reinders (2001)).

Symbols and references

d	particle diameter (m)
F_i	mean shear force (related to the bed shear stress) (N)
Fr	Froude number (-)
g	acceleration of gravity (m/s^2)
h	flow depth (m)
k_N	Nikuradse roughness (m)
n_M	Manning coefficient ($s/m^{1/3}$)
P	production of turbulence kinetic energy (m^2/s^3)
u'	root mean square value of longitudinal flow velocity (m/s)
u_*	bed shear velocity (m/s)
u	time-averaged local longitudinal flow velocity (m/s)
U	depth-averaged flow velocity (m/s)
u_{max}	maximum time-averaged flow velocity (m/s)
w'	root mean square value of vertical flow velocity (m/s)
y	transverse coordinate (m)
z	vertical coordinate (m)
z_0	zero velocity level (m)
α_M	load factor (-)
δ	(= $0.3h$) reference height (m)
Δ	(= 1.65) relative density (-)
ε	turbulent dissipation (m^2/s^3)
κ	(= 0.4) constant of von Kármán (-)
λ	length of smooth/rough strip (m)
ρ	density of water (kg/m^3)
$-\overline{\rho u'w'}$	Reynolds shear stresses (N/m^2)
τ	shear stress (N/m^2)
Ψ	Shields parameter (-)

Subscripts

r	represents rough bed
s	represents smooth bed
x	refers to streamwise direction
y	refers to transverse direction

Chen, X., Chiew, Y-M., 2003. Response of Velocity and Turbulence to Sudden Change of Bed Roughness in Open-Channel Flow, *J. of Hydr. Engrg.*, Vol. 129, p. 35 -43.

Nezu, I., Nakagawa, H. 1993. *Turbulence in open channel flow*, IAHR Monograph, Balkema, Rotterdam, The Netherlands.

Nezu, I., Tominaga, A. 1994. Response of velocity and turbulence to abrupt changes from smooth to rough beds in open-channel flows, *Proc. of Symp., Fundamentals and Advancements in Hydraulic Measurements and Experimentation*, ASCE, Buffalo, NY, pp. 195-204.

Reinders, M., 2001. Hydrodynamic modelling of roughness discontinuities, MSc-thesis, Delft University of Technology, Delft.

D Load factor at geometrical transitions

Introduction

Typically, the equilibrium scour depth caused by jets and at piers/abutments is predicted by applying empirical relations. Hoffmans (2012) discusses a scour approach which is based on two steps. A control volume is considered on which the relevant forces are determined. Next, Newton's second law is applied, that is, the sum of forces equals zero as the scour hole is in equilibrium. To deduce the load factor at geometrical transitions here a similar approach is used. The momentum forces acting on the control volume and the steepness of the dike govern the centripetal force and thus the load factor (Fig. D1).

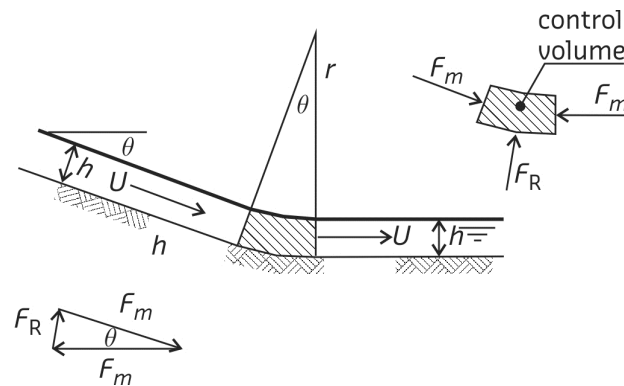


Figure D1 Control volume at transition (figuur nog aanpassen)

Analysis

If a control volume at a geometrical transition is considered, i.e. from a landward slope to a horizontal berm and if the following assumptions are made

- Hydrostatic forces are neglected (is validated below);
- Mean shear force close to the bed or friction force is marginal with respect to the momentum force (is validated below);
- Centripetal force causes a down-flow at the geometrical transition resulting in a load increase (see also Appendix C);
- Acceleration effects in the control volume are not included;
- Length of the control volume in the streamwise direction is approximately five times the flow depth (see also Chapter 4).

then the centripetal force (F_R) is

$$F_R = 2F_m \sin \frac{1}{2}\theta \quad (D1)$$

where F_m is the sum of the hydrostatic and momentum forces

$$F_m = \frac{1}{2}\rho g B h^2 + \rho B h U^2$$

or

$$F_m = \rho g B h^2 \left(\frac{1}{2} + Fr^2 \right) \approx \rho B h U^2 \quad (D2)$$

in which B is the width of the test section, Fr is the Froude number, g is the acceleration of gravity, $h_{slope} = h_{berm} = h$ is the flow depth, $U_{slope} = U_{berm} = U$ is the maximum flow velocity, θ represents the angle of the landward slope and ρ is the density of water. As the flow is supercritical (Froude number is greater than 1, thus $Fr^2 \gg \frac{1}{2}$) the hydrostatic force can be neglected with respect to the momentum force.

The mean shear force (F_s) or the friction force acting on the control volume with L as the length of the control volume can be given by

$$F_s = \tau_0 BL \quad (D3)$$

where the bed shear stress (τ_0) with r_0 as the depth-averaged relative turbulence intensity is

$$\tau_0 = 0.7 \rho (r_0 U)^2 \quad (D4)$$

The mean shear force is assumed to be negligible with respect to the momentum force. Hence, the following equation holds

$$F_s = 0.7 \rho (r_0 U)^2 BL \ll F_m = \rho B h U^2$$

or

$$0.7 (r_0)^2 L \ll h \quad (D5)$$

Measurements demonstrate that the erosion occurs in a zone which equals the length (L) of the control volume. This length is about five times the flow depth (see also Chapter 4)

$$L \approx 5h \quad (D6)$$

Consequently, Eq. D5 can be written as

$$3.5 (r_0)^2 \ll 1$$

or

$$r_0 \ll 0.5 \quad (D7)$$

On the landward slope r_0 varies from 0.1 (at the toe of the dike) to 0.2 (on the crest of the dike) (see also Chapter 4). Hence, F_s can be neglected with respect to F_m .

Analogous to the theories as discussed in Chapter 2 and Appendix C the load factor (α_M) can be given by

$$\alpha_M = \frac{F'_{s,m}}{F'_s} \quad (D8)$$

The maximum shear force ($F_{s,m}$) at the geometrical transition and the maximum shear force (F_s) under uniform flow conditions are both related to the energy grade line which represents the maximum height to which water may be delivered. In terms of normal forces, the load factor can also be written as (note that $F_{s,m} = f \cdot P_{n,m}$ and $F_s = f \cdot P_n$ with f is the friction factor)

$$\alpha_M = \frac{F'_{n,m}}{F'_n} \quad (D9)$$

with

$$F'_{n,m} = F'_n + F_R \quad (D10)$$

The maximum normal force (F_n) can be given by

$$F'_n = \rho g \left(h + \frac{U^2}{2g} \right) BL$$

or

$$F'_n = \rho gh \left(1 + \frac{1}{2} Fr^2 \right) BL \quad (D11)$$

For super critical flow Eq. D11 can be rewritten as (note that the Froude number is greater than 1, thus $Fr^2 \gg 1$)

$$F'_n = \frac{1}{2} \rho U^2 BL \quad (D12)$$

The load factor is (combine Eqs. D9 and D10)

$$\alpha_M = 1 + \frac{F_R}{F'_n}$$

or with Eqs. D1, D2 and D11

$$\alpha_M = 1 + \frac{2\rho g B h^2 \left(\frac{1}{2} + Fr^2 \right) \sin \frac{1}{2} \theta}{\rho gh BL \left(1 + \frac{1}{2} Fr^2 \right)}$$

or with $Fr^2 \gg 1$

$$\alpha_M \approx 1 + \frac{4h \sin \frac{1}{2} \theta}{L} \quad (D13)$$

or with Eq. D6

$$\alpha_M = 1 + \sin \frac{1}{2} \theta \quad (D14)$$

Summarizing, forces acting on a control volume are considered near the transition of the dike slope to the (horizontal) berm. The momentum forces determine mainly the centripetal force. If the steepness of the landward slope increases then the impact or the down-flow near the transition increases. Consequently, the friction force and load factor become larger. In this study the load factor depends on the steepness of the slope. If there is no geometrical transition or if $\theta = 0^\circ$ then $\alpha_M = 1$. If $\theta = 20^\circ$ (steepness is 1V:2.7H) then $\alpha_M = 1.17$. If the landward slope has a steepness of 1V:2H then $\alpha_M = 1.23$.

If the flow is directed from a horizontal crest to the landward slope then the load factor can be given by (note that the centripetal force is directed upwards)

$$\alpha_M = 1 - \frac{F_R}{F'_n} \quad (\text{D15})$$

or

$$\alpha_M = 1 - \sin \frac{1}{2}\theta \quad (\text{D16})$$

Symbols and references

B	width of test section (m)
f	friction factor (-)
F_m	sum of the momentum and hydrostatic forces (N)
F_R	centripetal force (N)
F_s	mean shear force (related to the bed shear stress) (N)
F'_n	mean normal force (related to the energy grade line) (N)
F'_s	mean shear force (related to the energy grade line) (N)
Fr	Froude number (-)
g	acceleration of gravity (m/s^2)
h	flow depth (m)
L	erosion length (m)
r_0	depth-averaged relative turbulence intensity (-)
U	depth-averaged flow velocity (m/s)
α_M	load factor (-)
θ	angle of the landward slope ($^\circ$)
ρ	density of water (kg/m^3)
τ_0	bed shear stress (N/m^2)

Subscripts

<i>berm</i>	refers to the horizontal berm
<i>m</i>	maximum
<i>s</i>	represents shear
<i>slope</i>	refers to the landward slope

Hoffmans, G.J.C.M., 2012. *The influence of turbulence on soil erosion*, Eburon, Delft.

E Pressure measurements

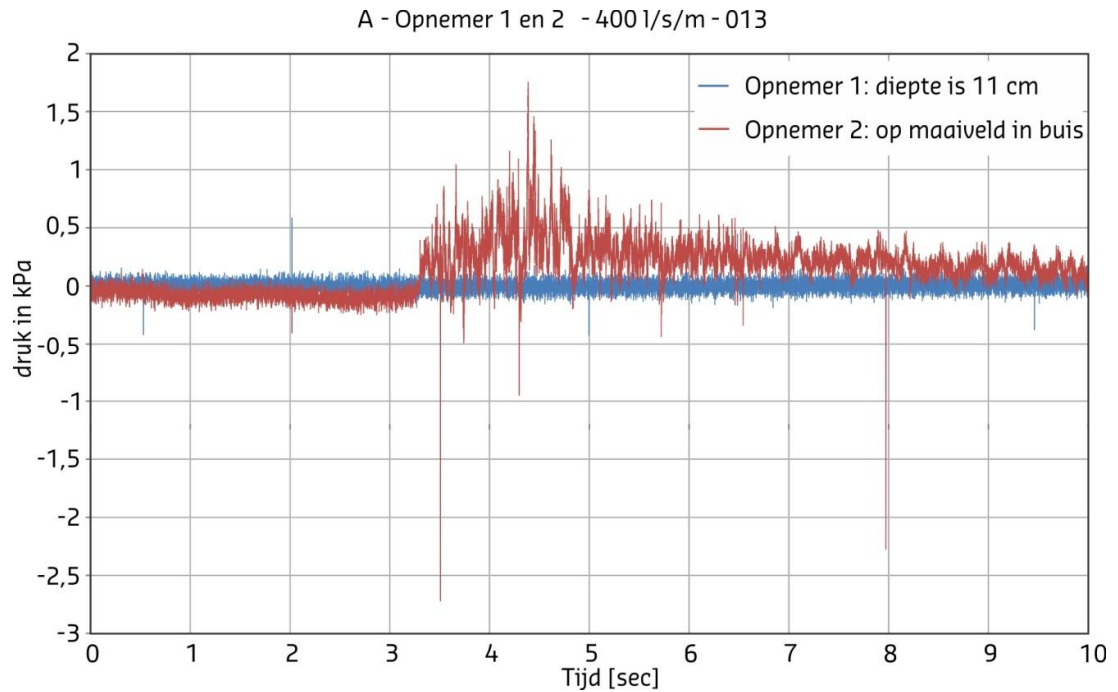


Figure F1 Pressure distributions as function of time at the surface and about 10 cm below for $V = 400 \text{ l/s per m}$ (Location A)

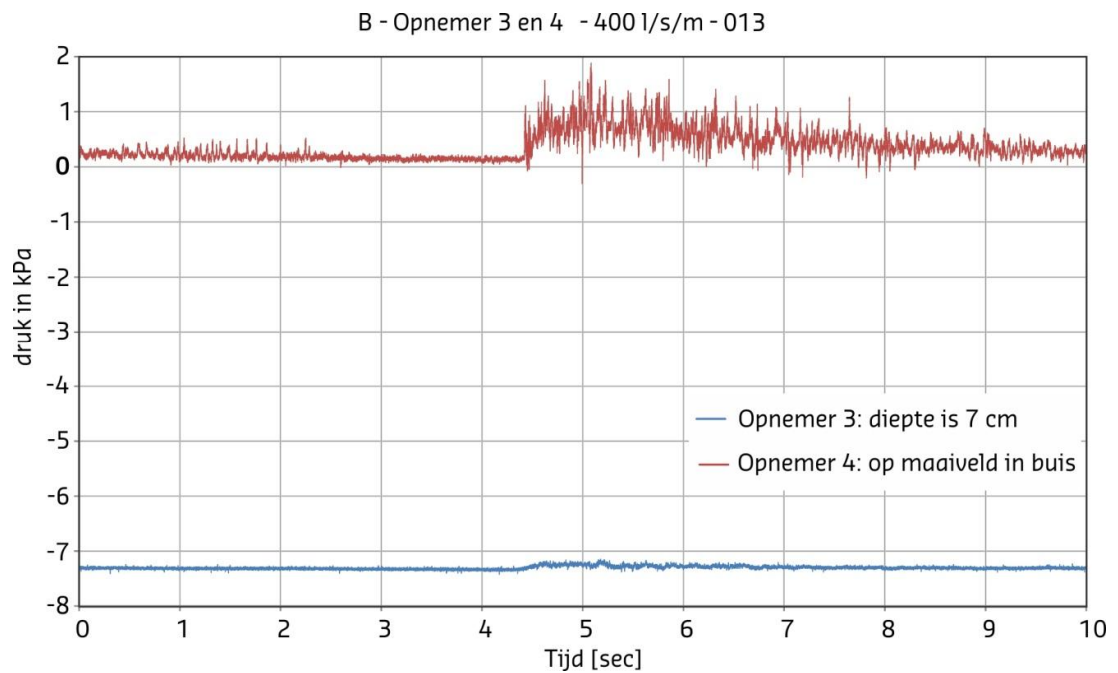


Figure F2 Pressure distributions as function of time at the surface and about 10 cm below for $V = 400 \text{ l/s per m}$ (Location B)

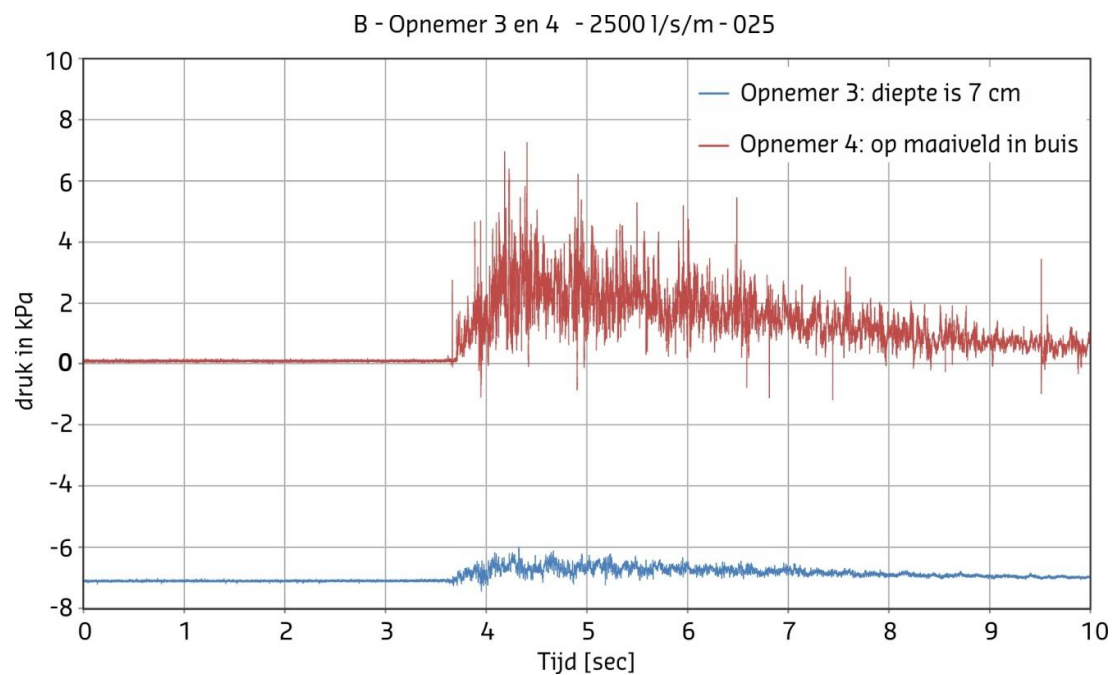


Figure F3 Pressure distributions as function of time at the surface and about 10 cm below for $V = 2500 \text{ l/s per m}$ (Location A)

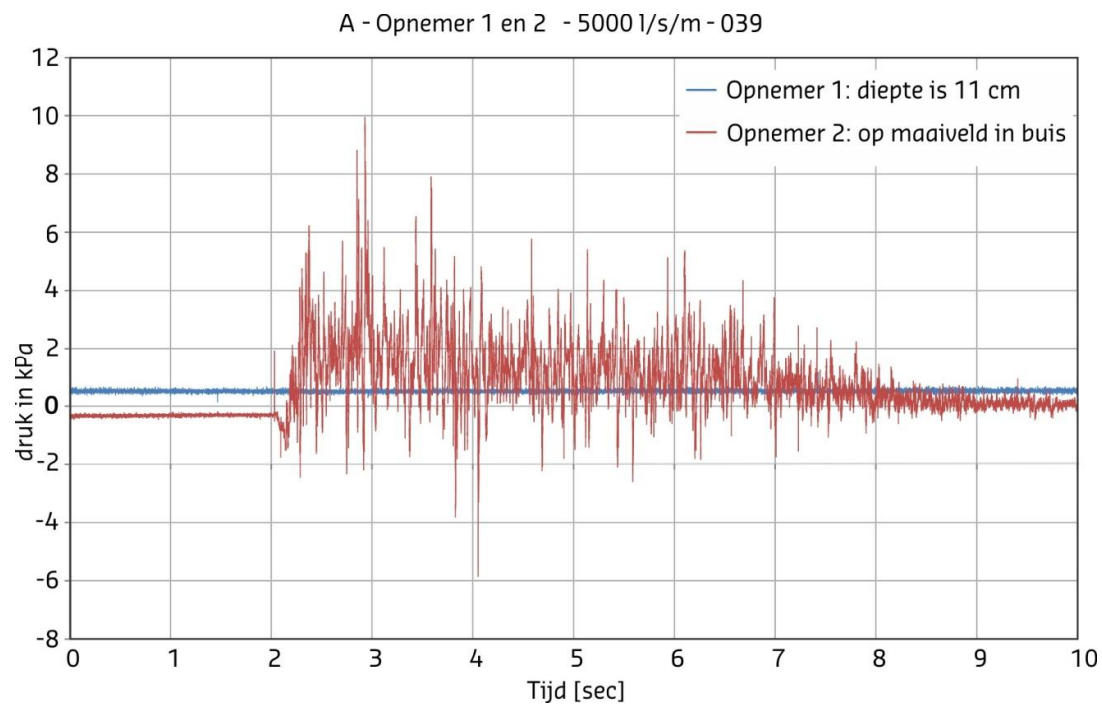


Figure F4 Pressure distributions as function of time at the surface and about 10 cm below for $V = 2500 \text{ l/s per m}$ (Location B)

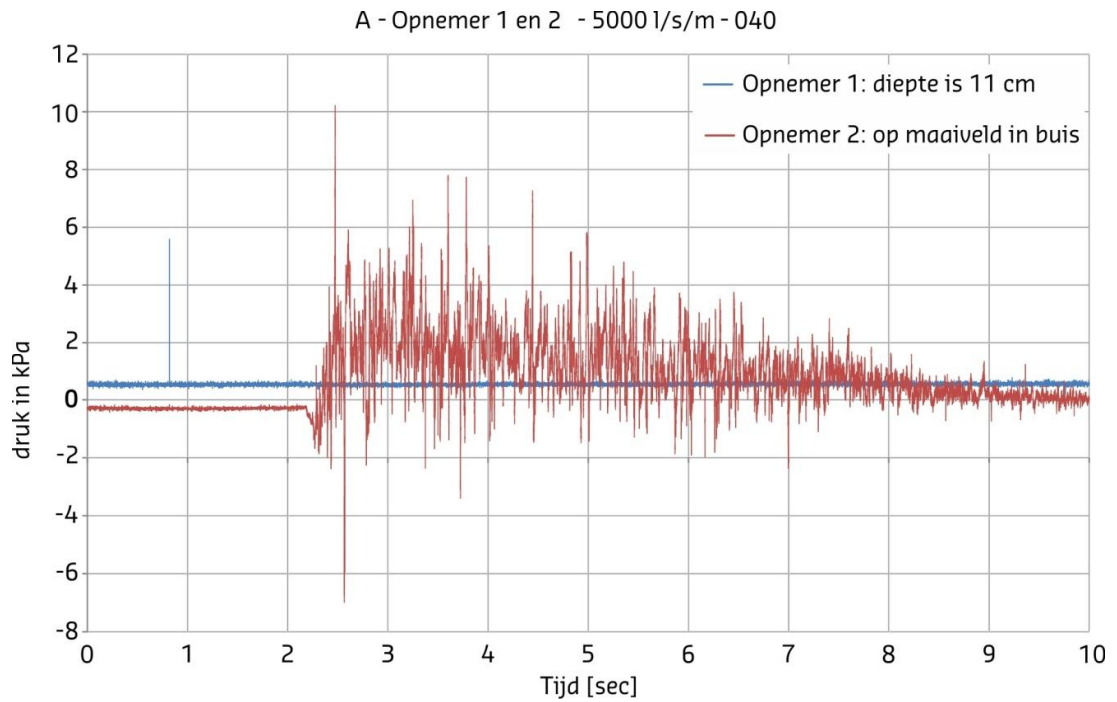


Figure F5 Pressure distributions as function of time at the surface and about 10 cm below for $V = 5000$ l/s per m (Location A; series 1)

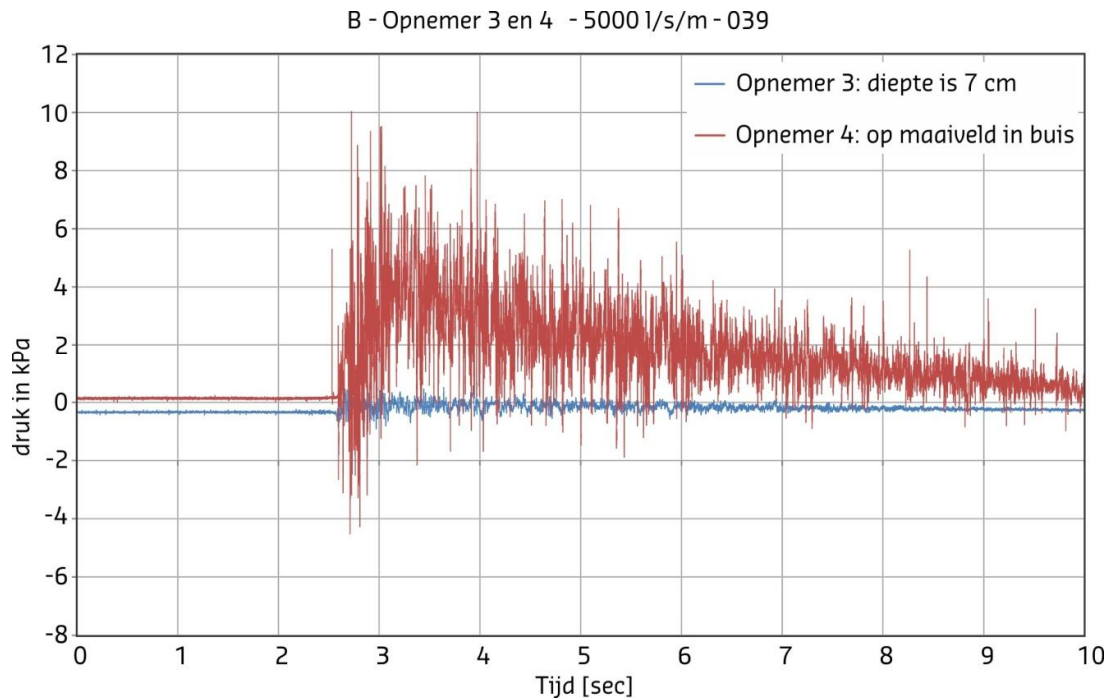


Figure F6 Pressure distributions as function of time at the surface and about 10 cm below for $V = 5000$ l/s per m (Location A; series 2)

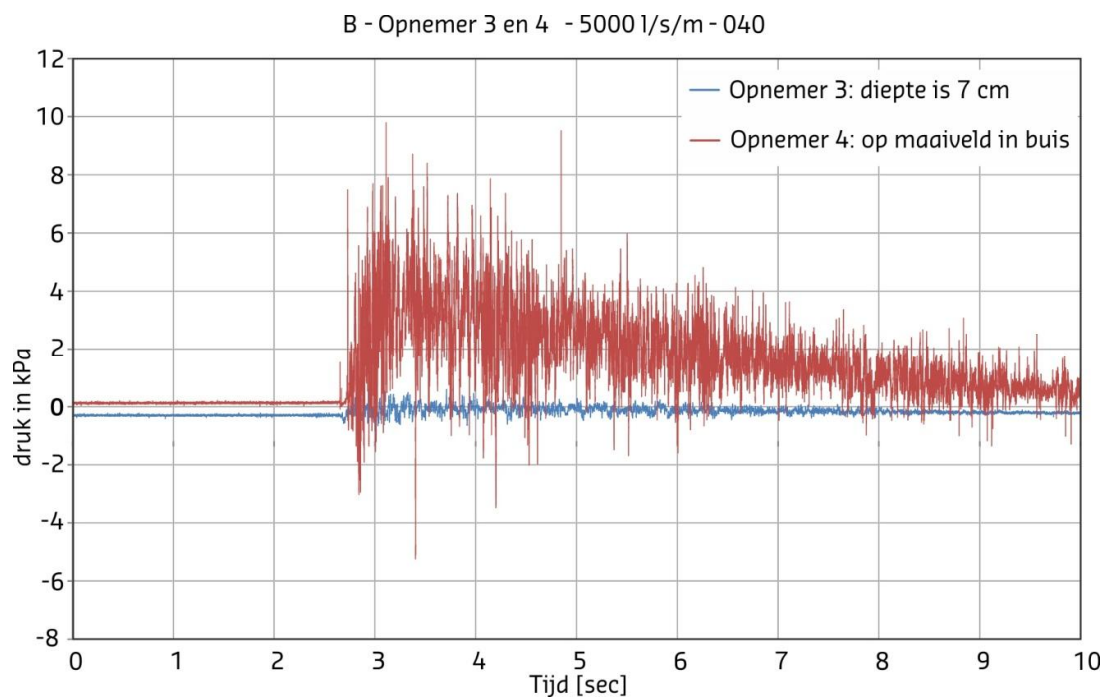
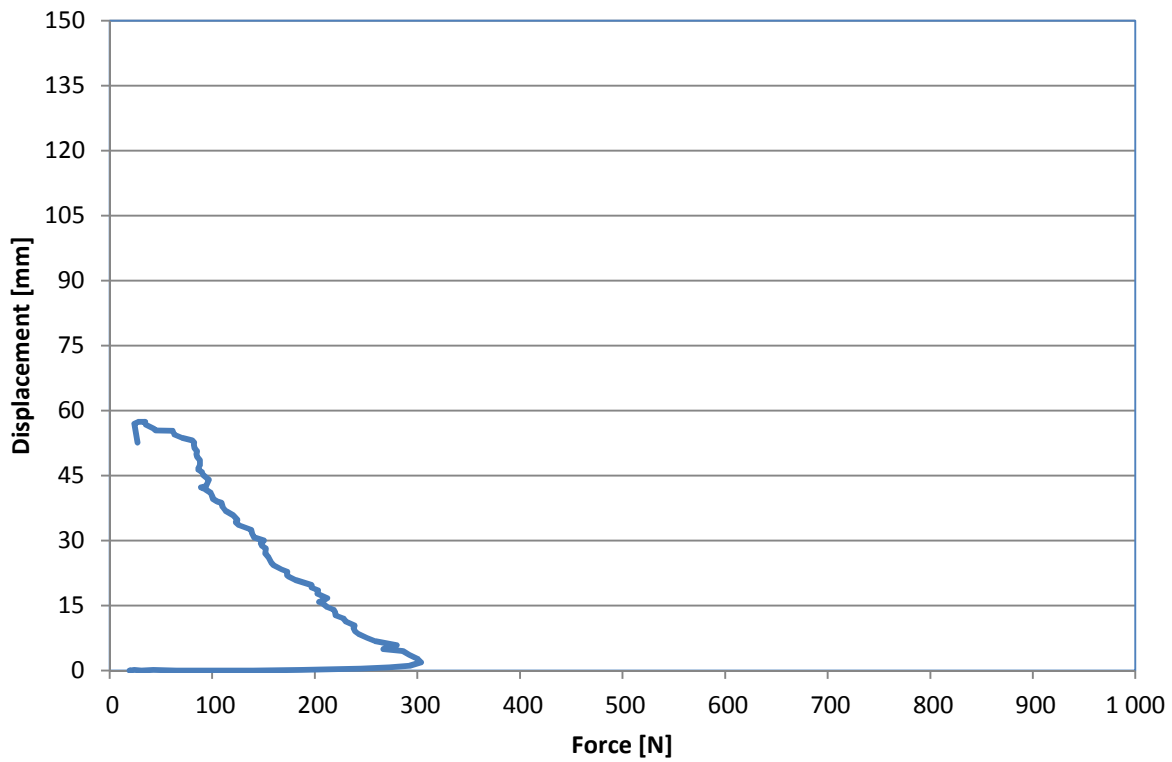
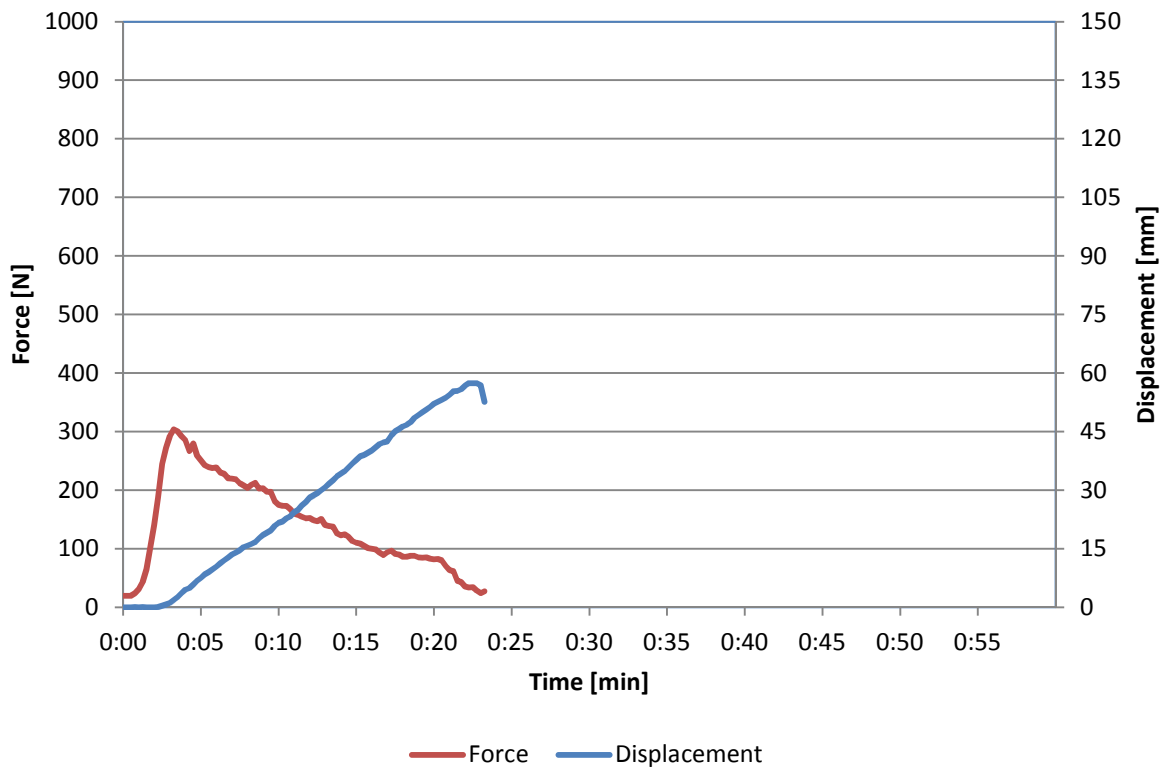


Figure F7 Pressure distributions as function of time at the surface and about 10 cm below for $V = 5000 \text{ l/s per m}$ (Location B; series 1)

Figure E8 Pressure distributions as function of time at the surface and about 10 cm below for $V = 5000 \text{ l/s per m}$ (Location B; series 2)

F Turf-tensile tests

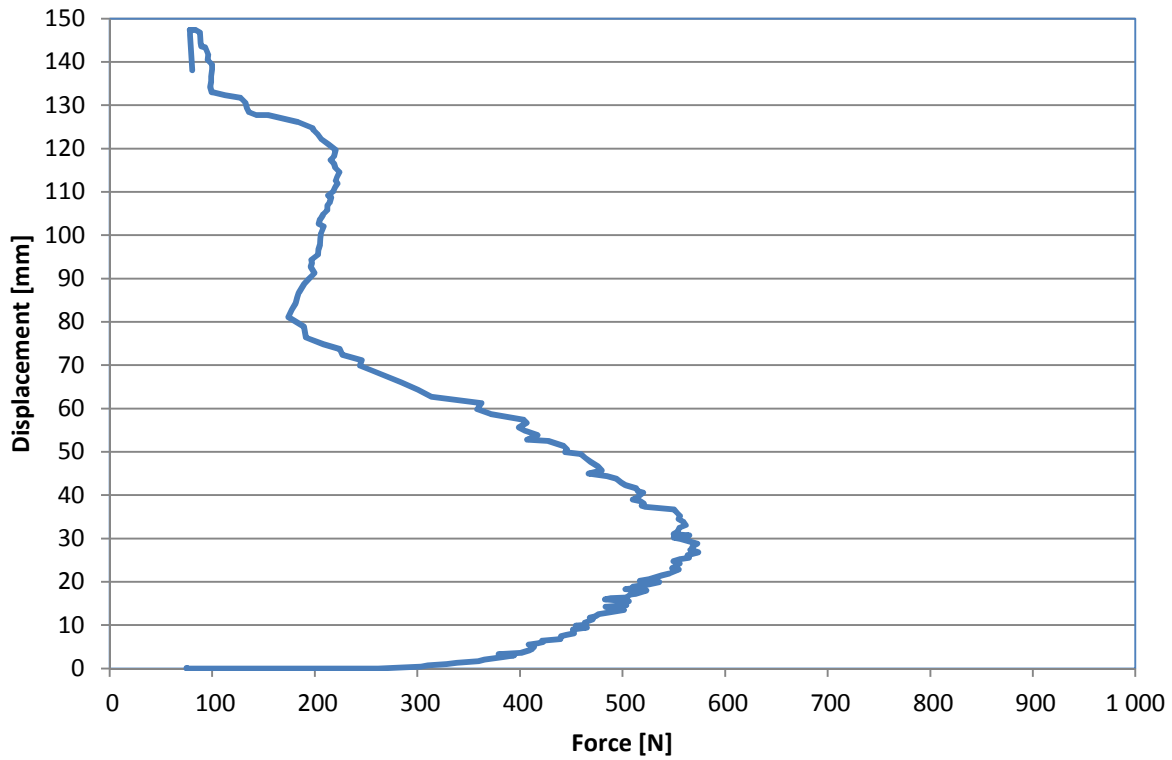
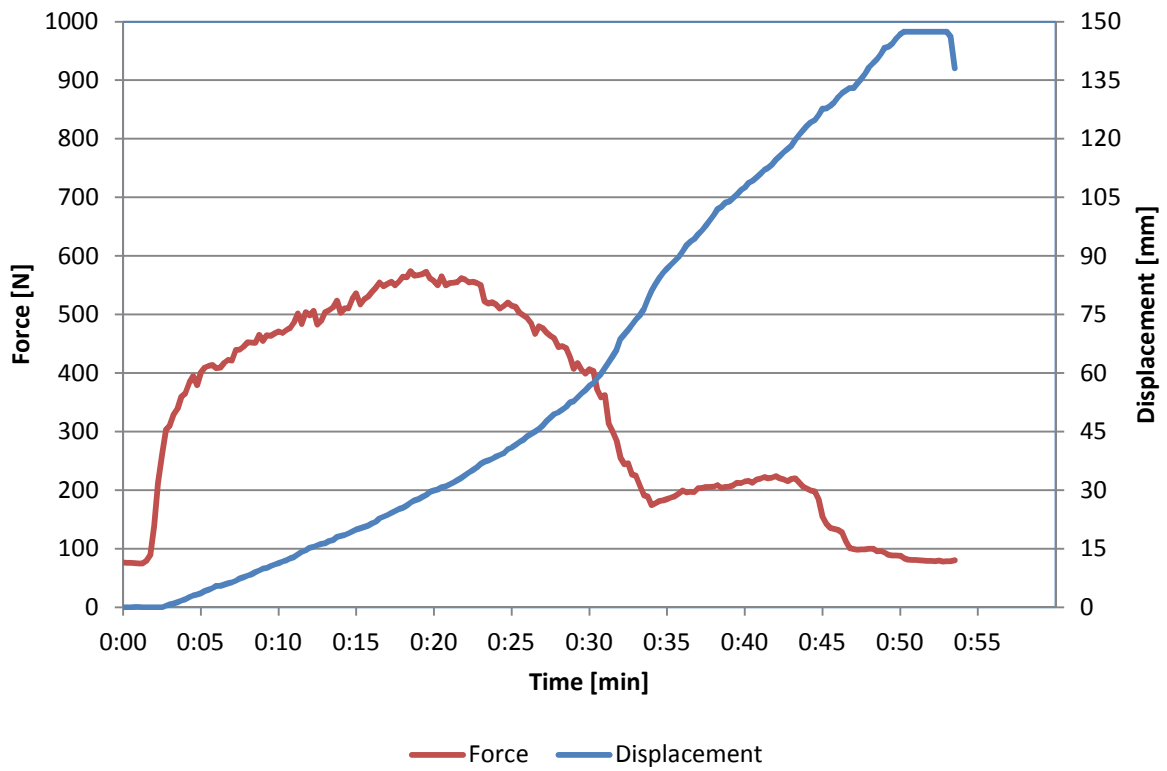
This appendix summarizes the experimental results of the turf-tensile tests. The experiments were carried out by Infram and Deltares in April 2013 at two locations Nijmegen and Millingen aan de Rijn (see also Tables 6.1 and 6.2 in Chapter 6).



1

Location: M
 Section: 6
 Number: 16

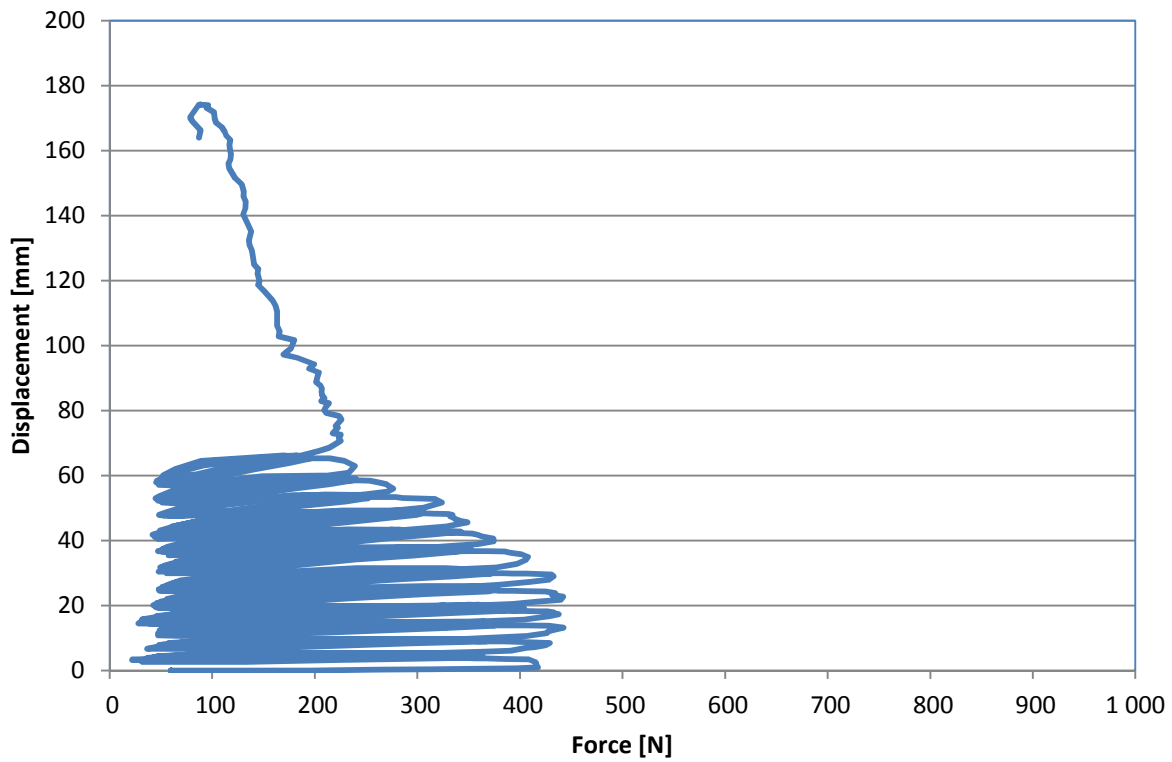
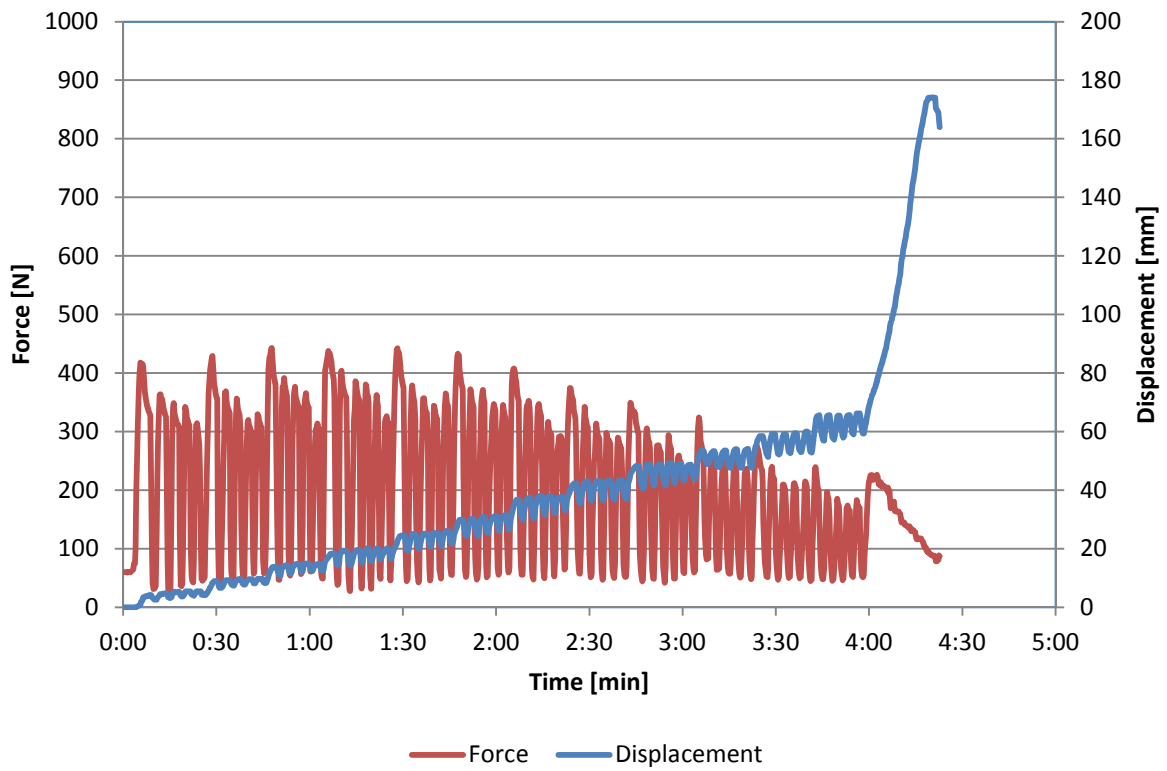
Date: 09-04-2013
 Time: 11:30



2

Location: M
 Section: 6
 Number: 17

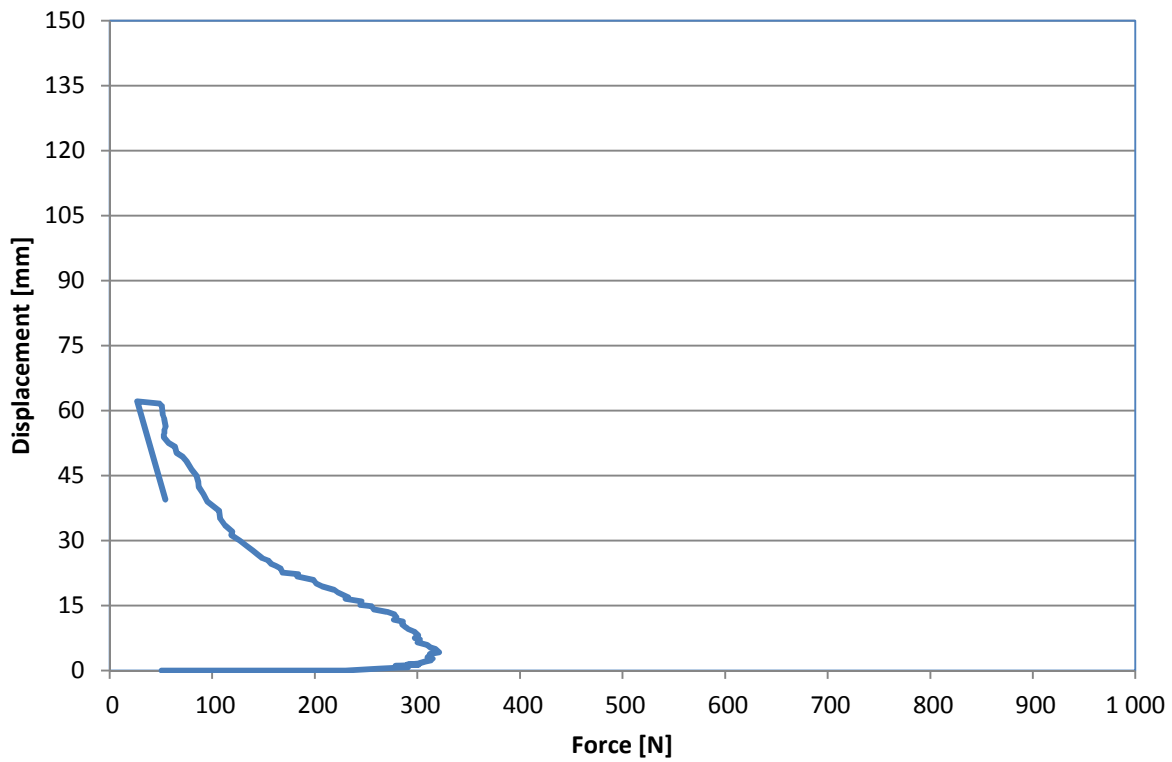
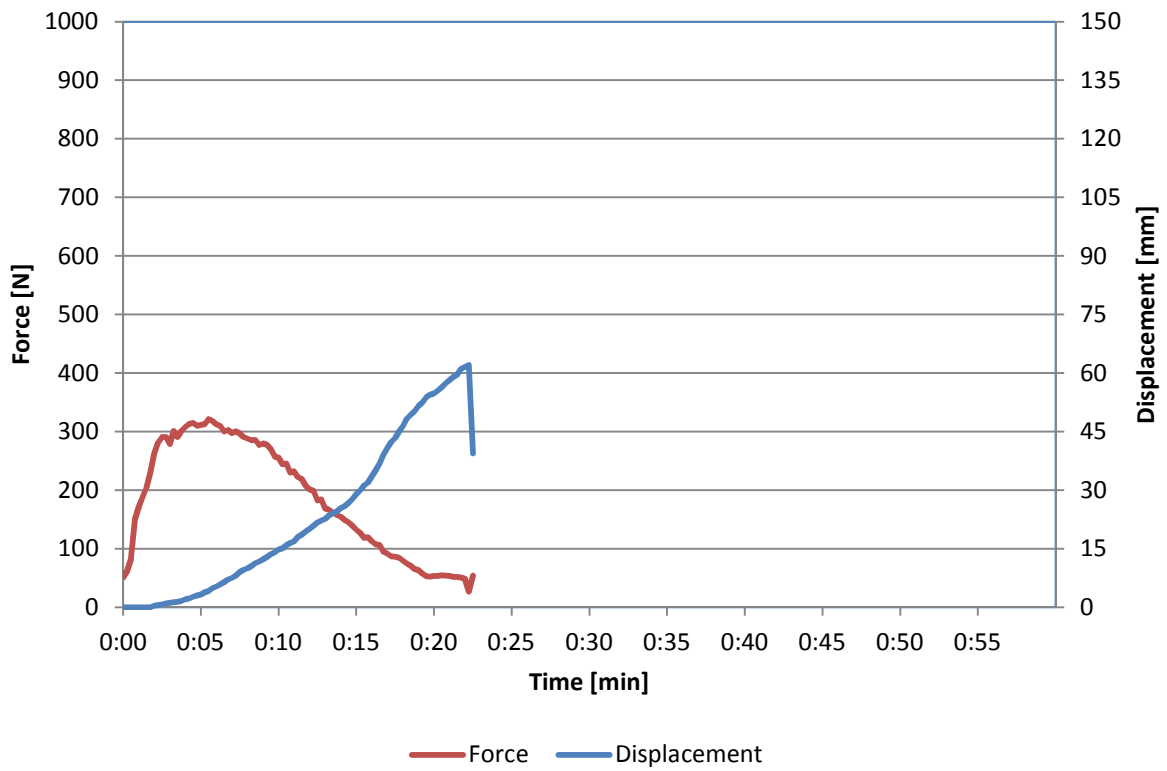
Date: 09-04-2013
 Time: 11:35



3

Location: M
 Section: 6
 Number: 18

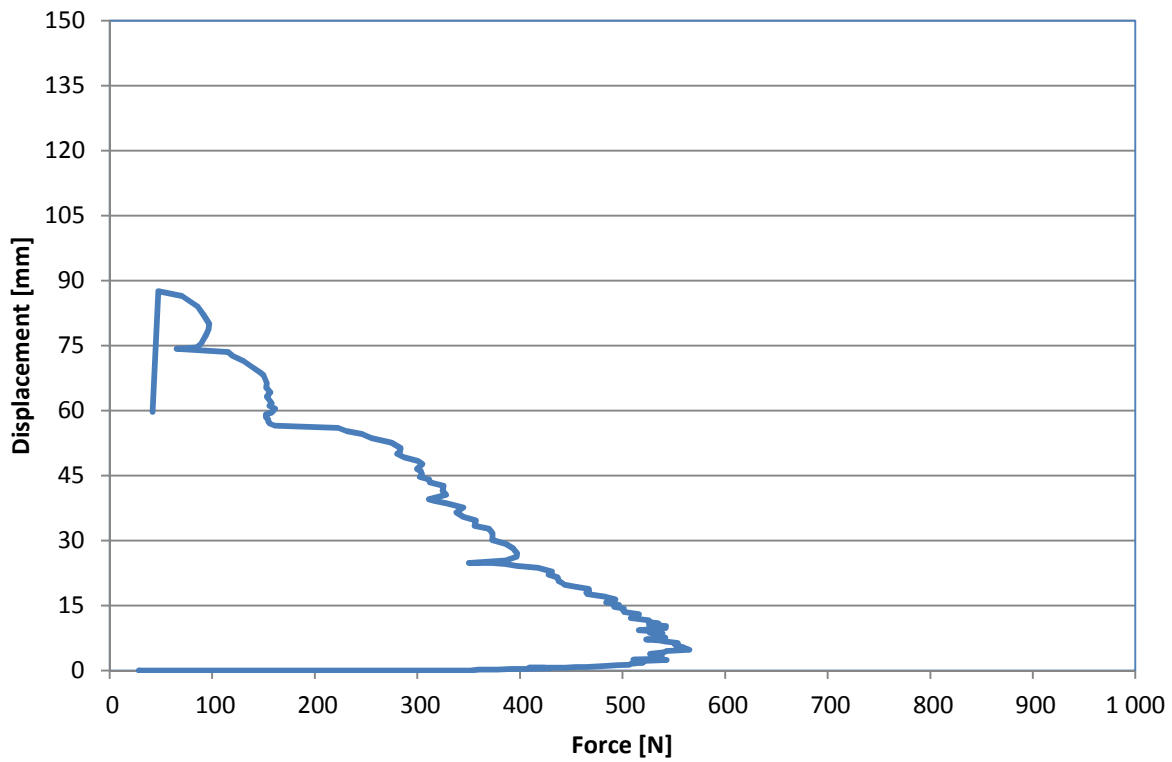
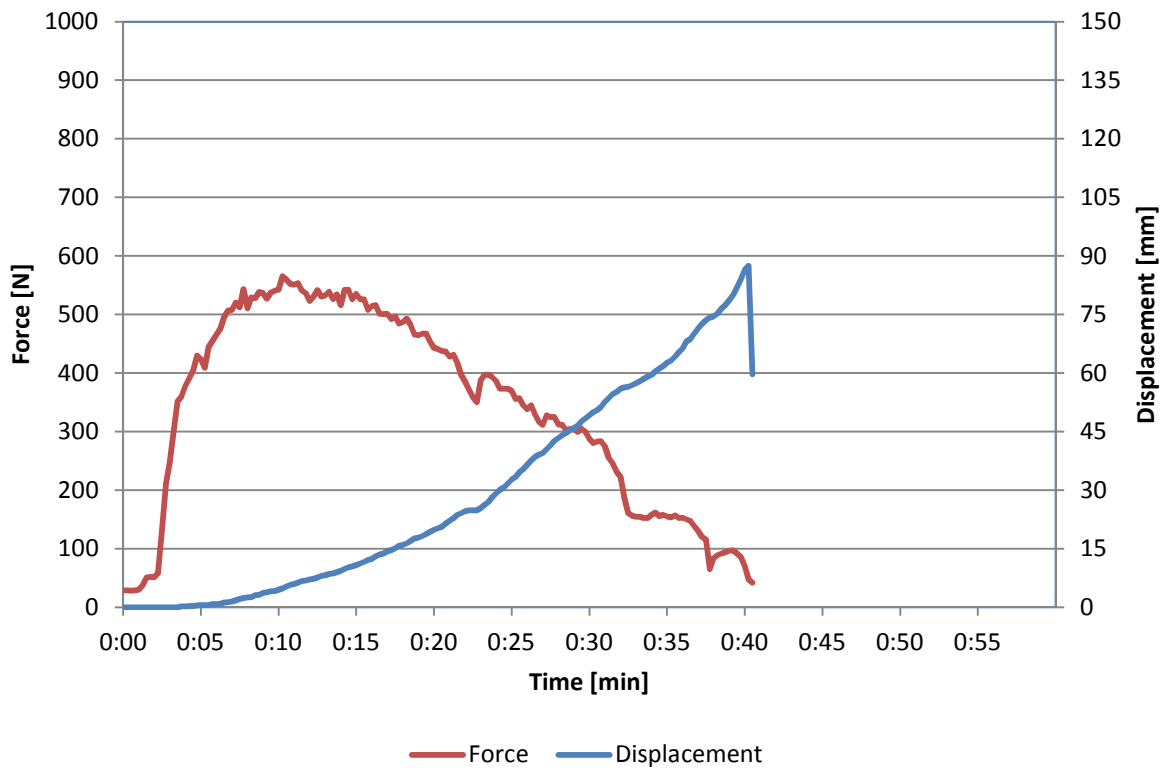
Date: 09-04-2013
 Time: 11:45



4

Location: M
 Section: 8
 Number: 22

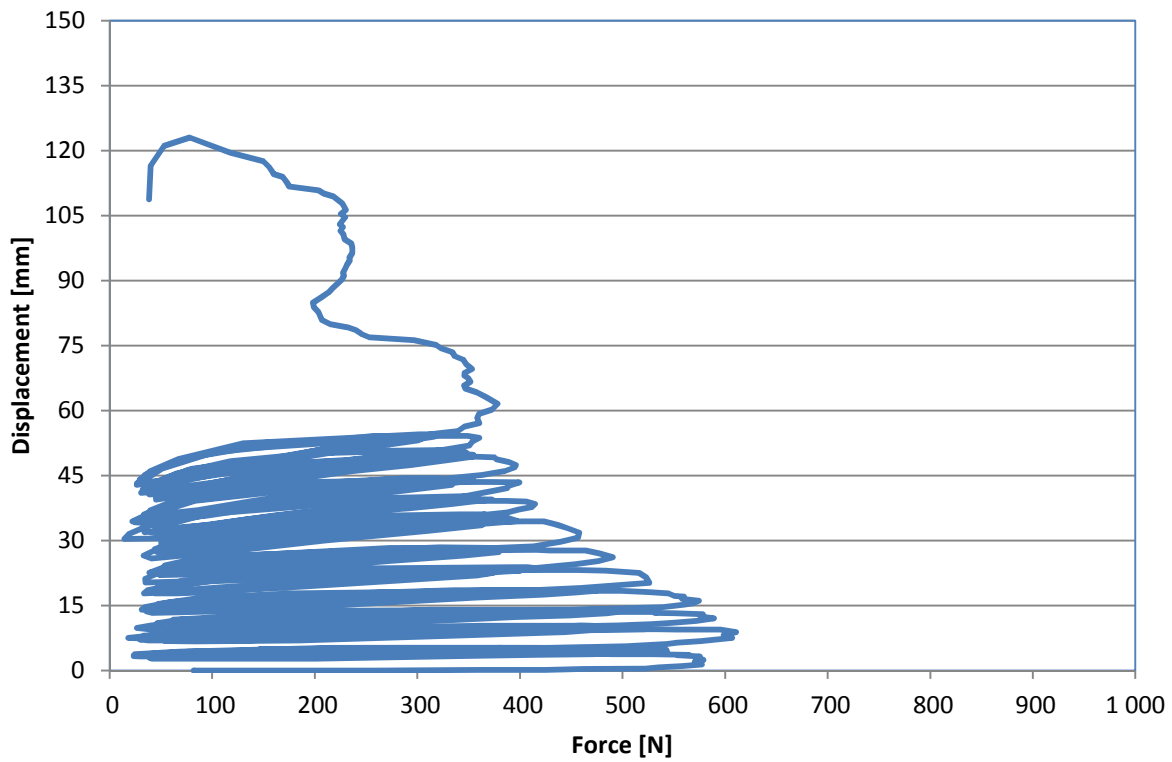
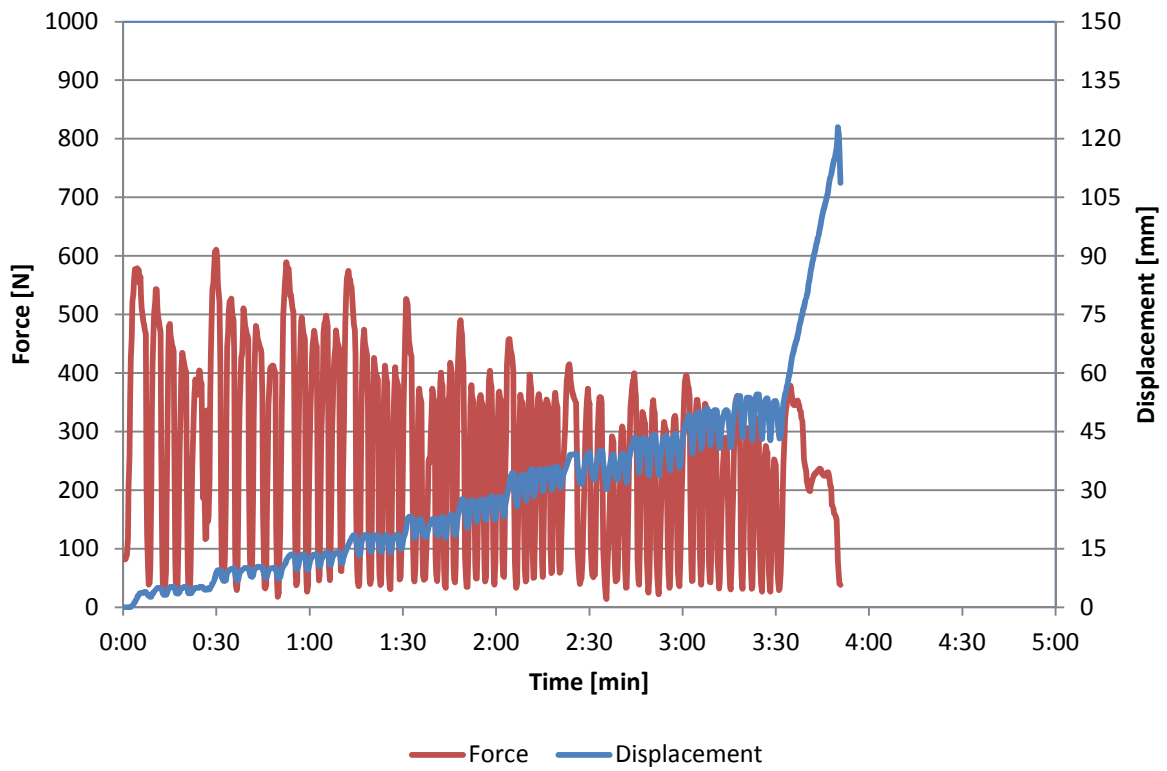
Date: 09-04-2013
 Time: 12:48



5

Location: M
 Section: 8
 Number: 23

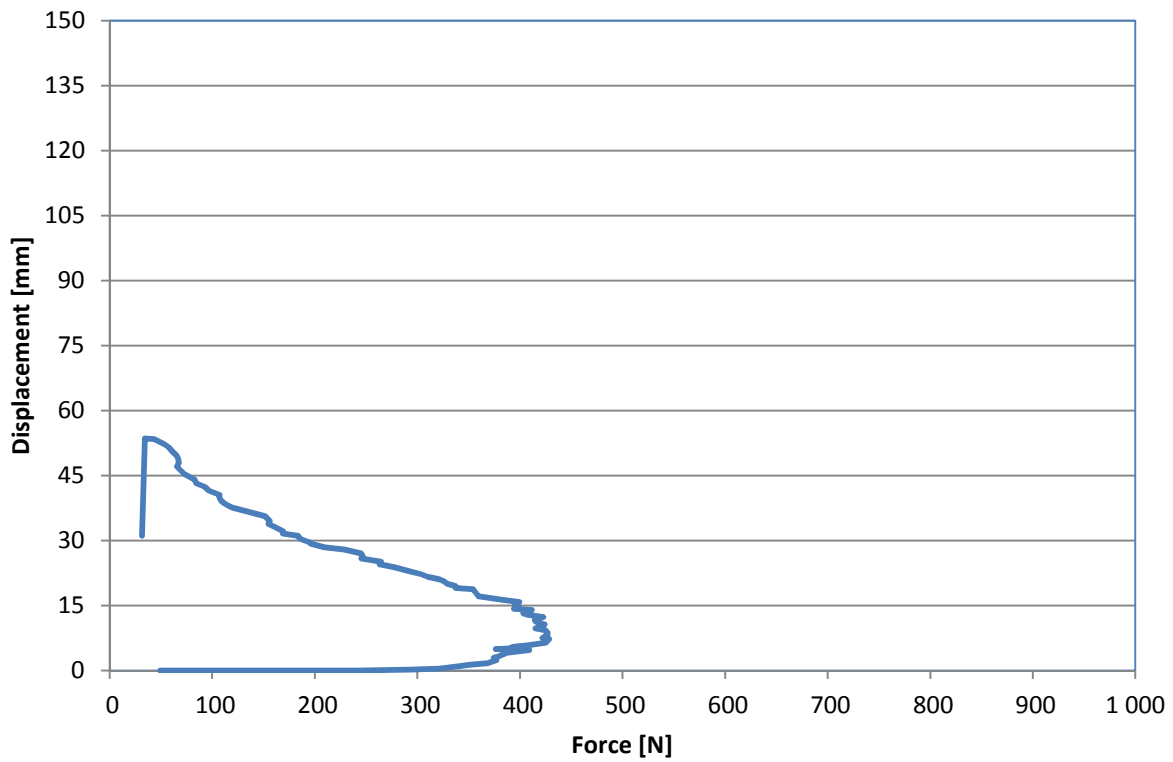
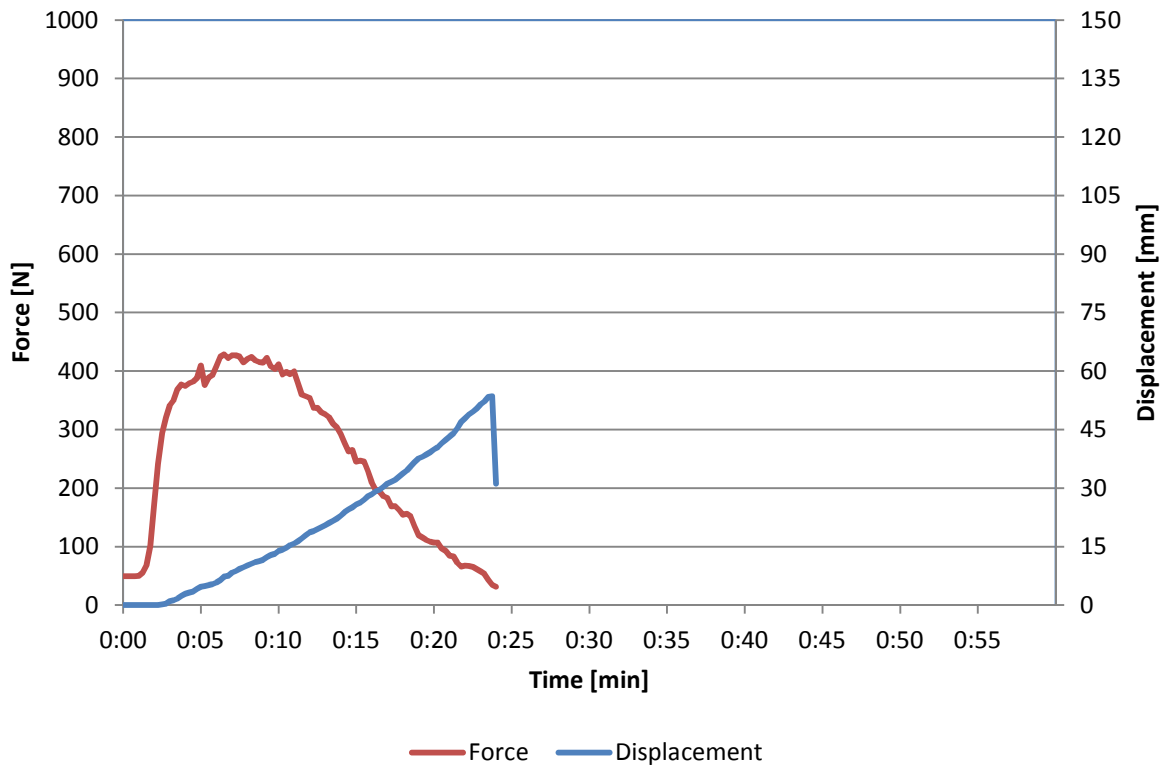
Date: 09-04-2013
 Time: 12:57



6

Location: M
 Section: 8
 Number: 24

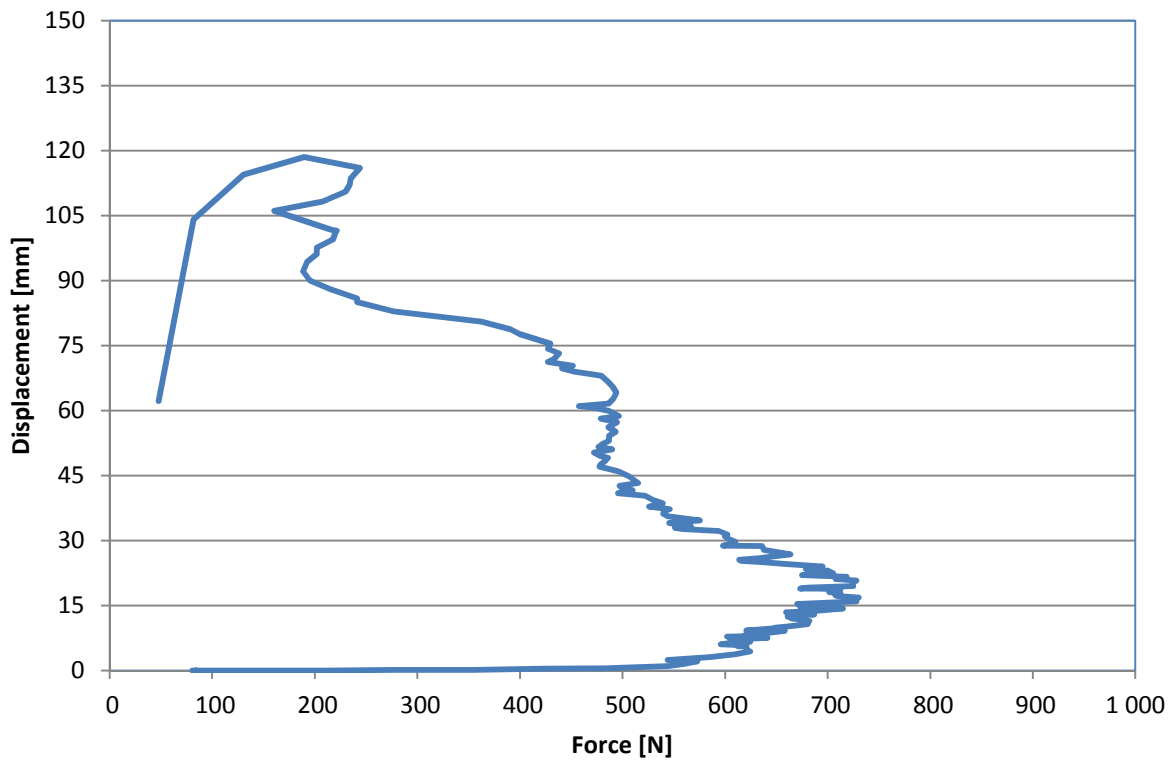
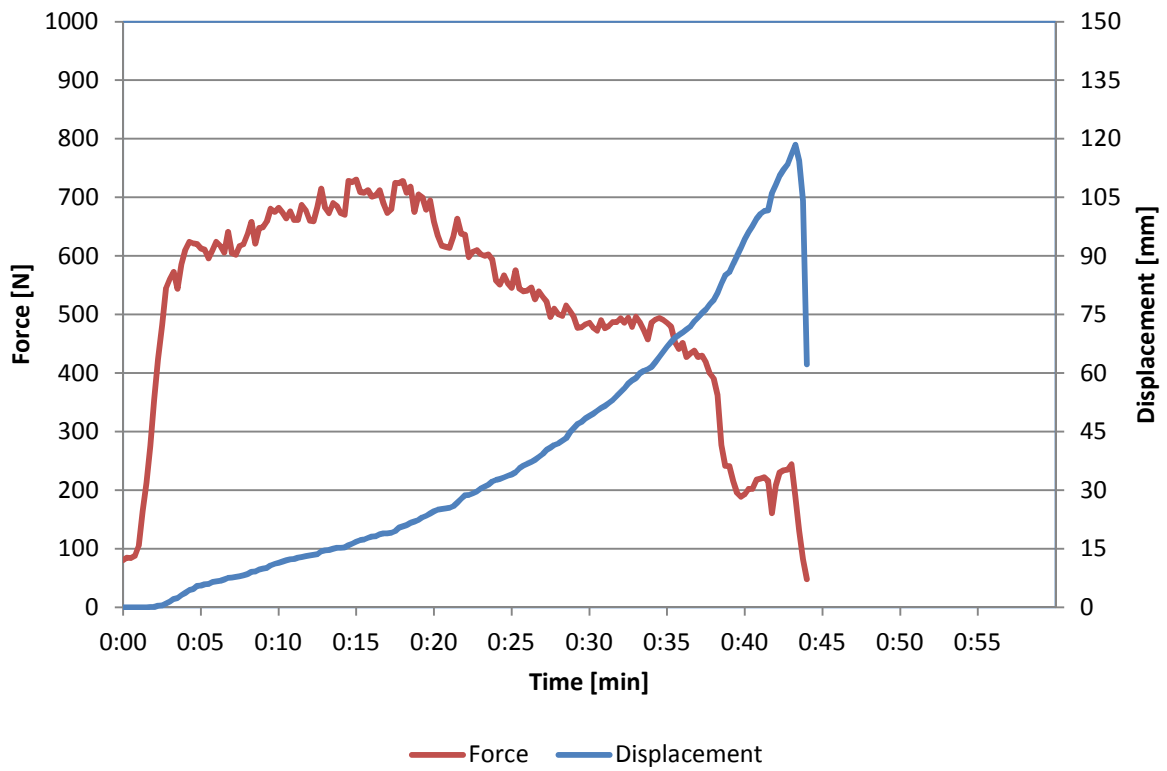
Date: 09-04-2013
 Time: 13:07



7

Location: M
 Section: 5
 Number: 13

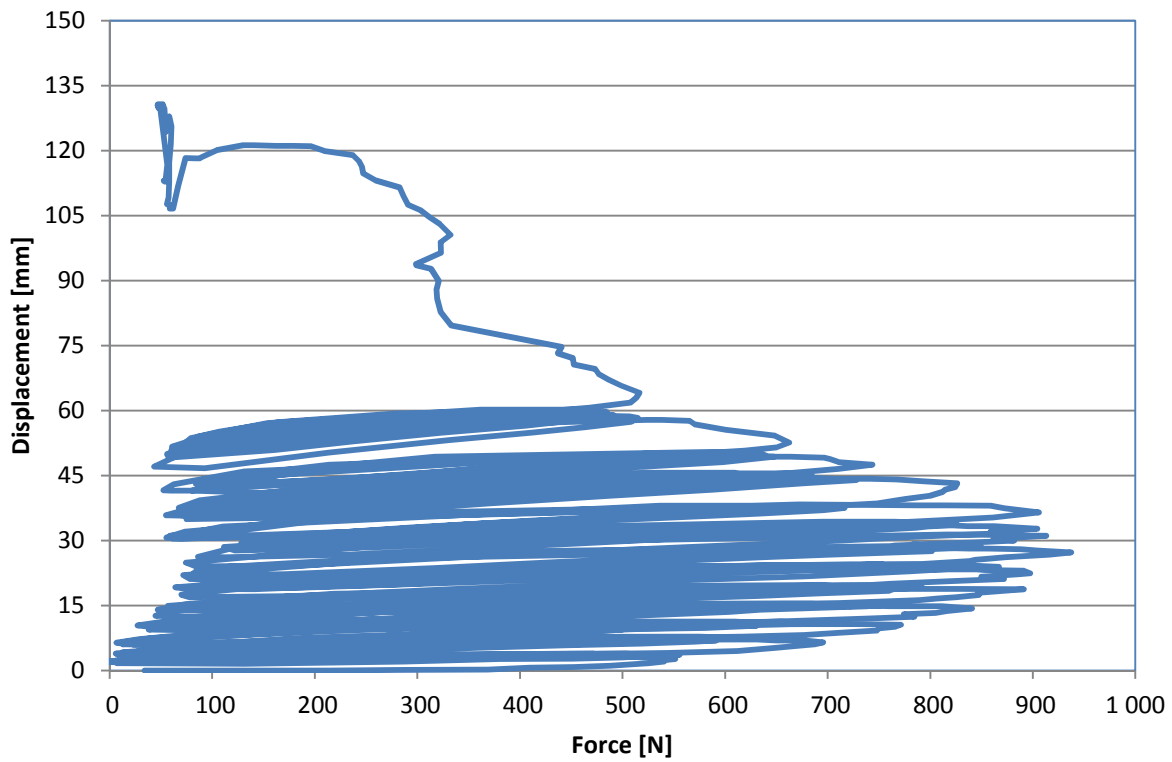
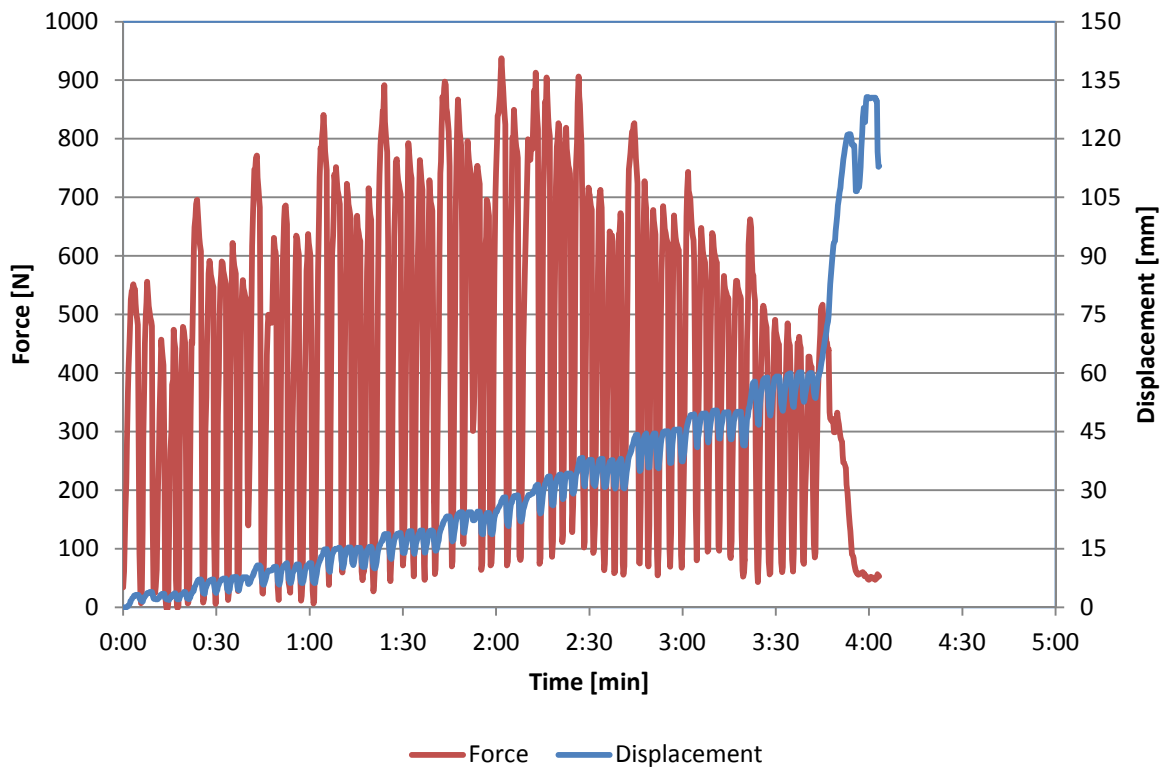
Date: 09-04-2013
 Time: 13:20



8

Location: M
 Section: 5
 Number: 14

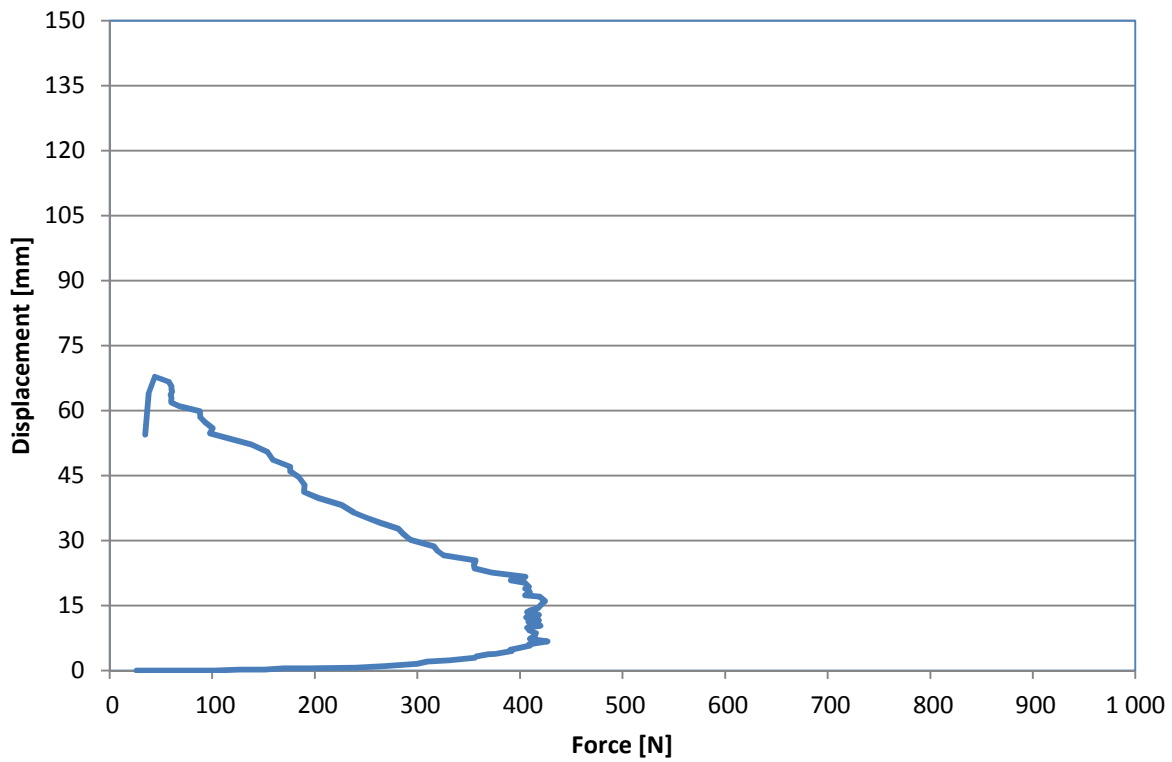
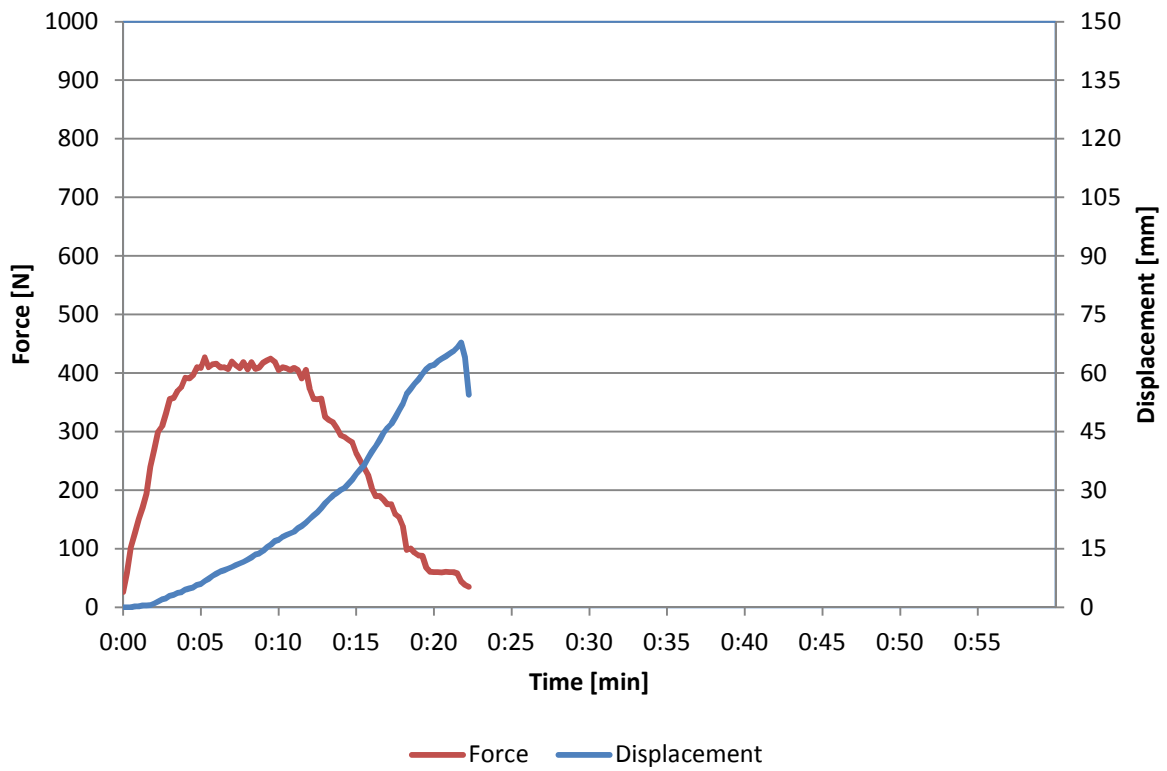
Date: 09-04-2013
 Time: 13:30



9

Location: M
 Section: 5
 Number: 15

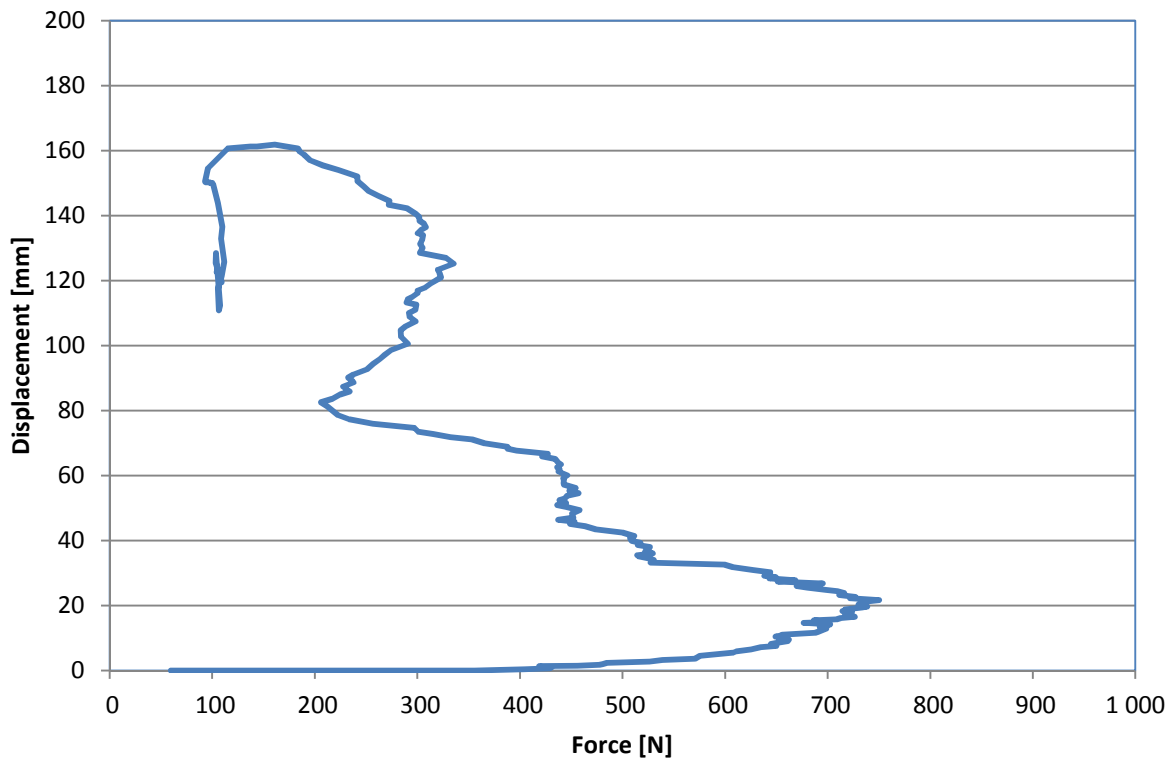
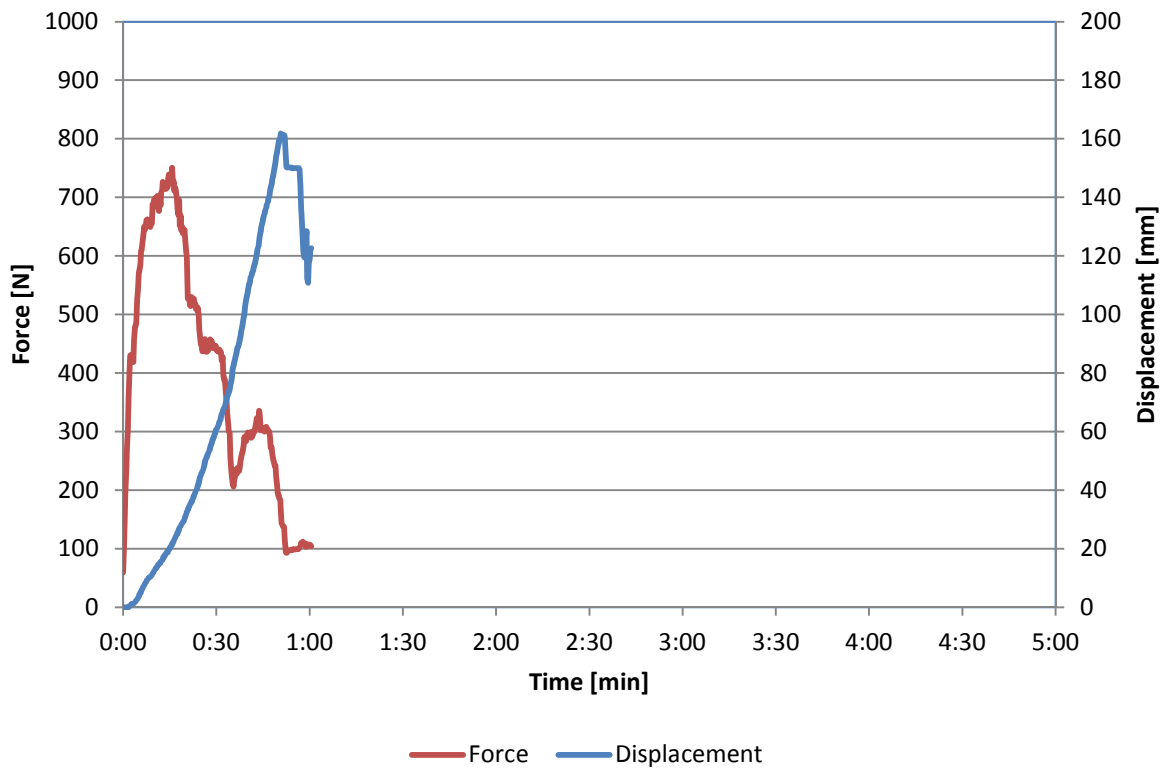
Date: 09-04-2013
 Time: 13:45



10

Location: M
 Section: 4
 Number: 10

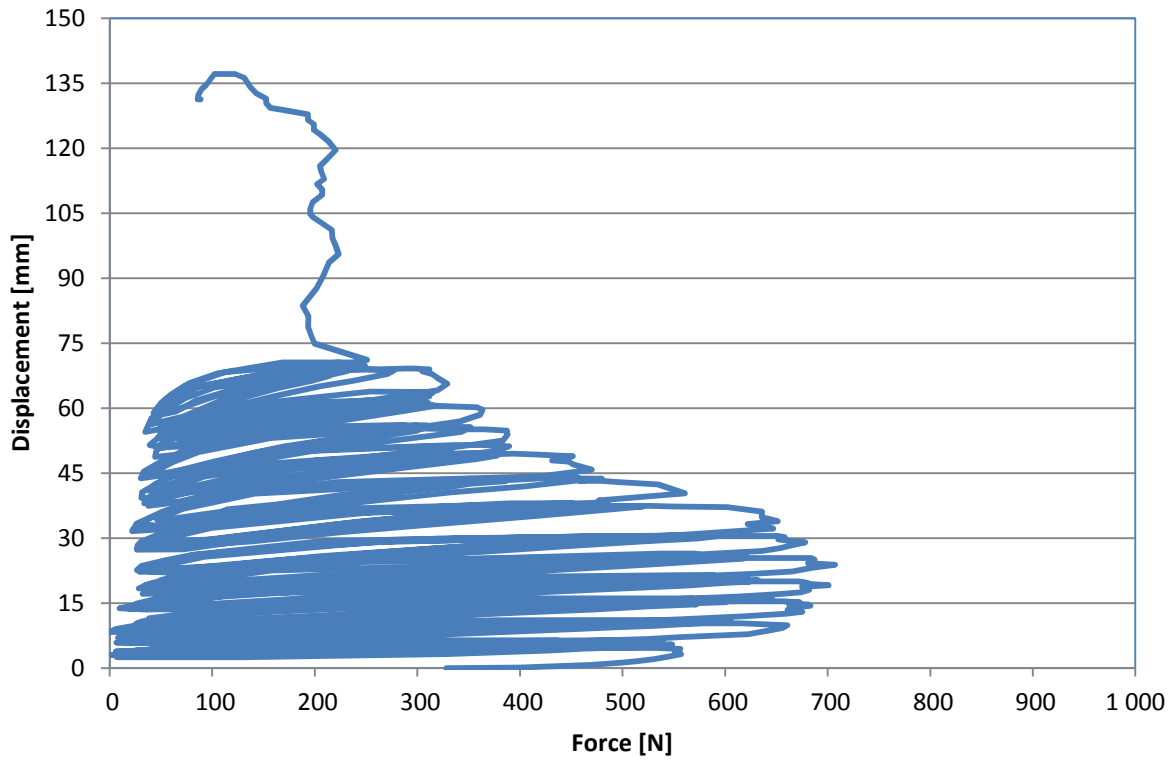
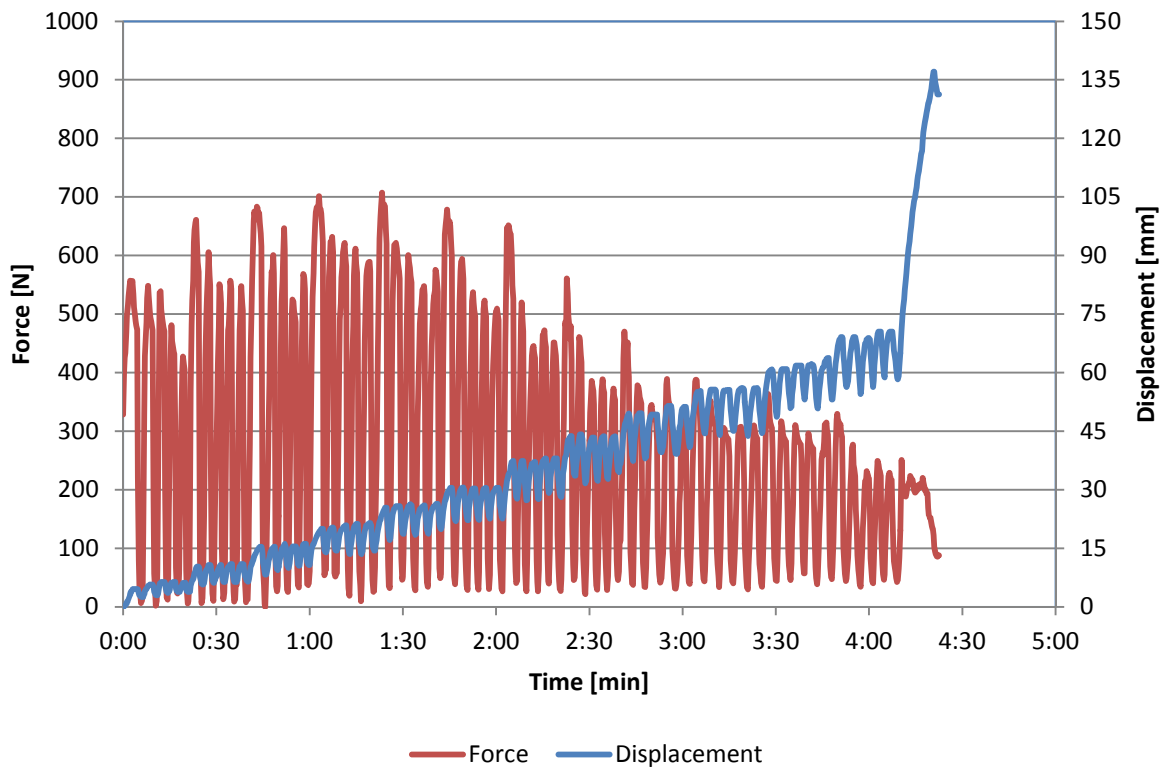
Date: 09-04-2013
 Time: 14:04



11

Location: M
 Section: 4
 Number: 11

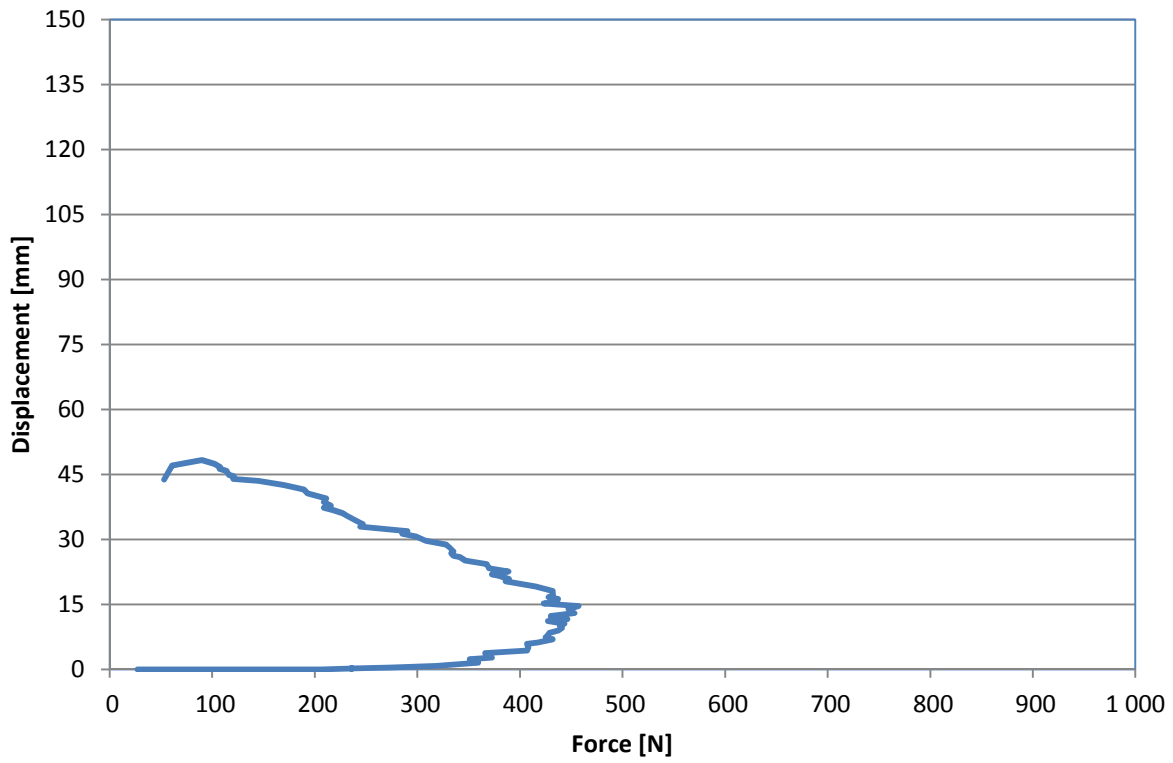
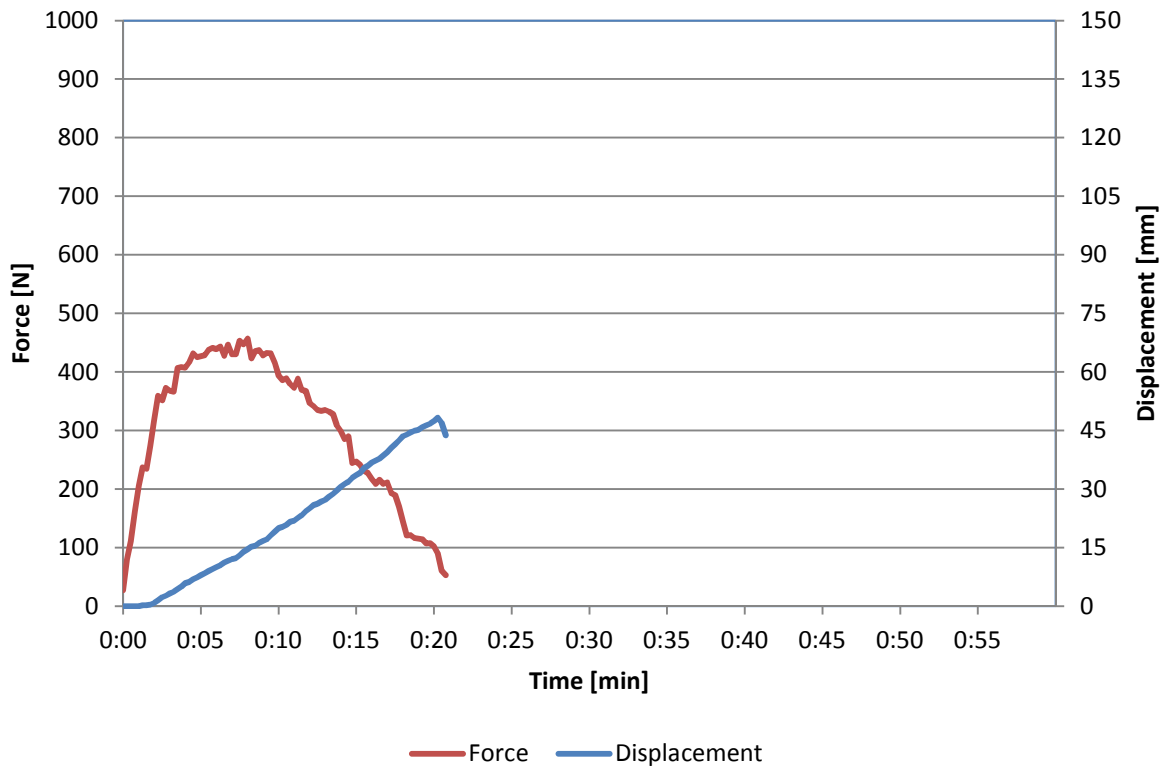
Date: 09-04-2013
 Time: 14:16



12

Location: M
 Section: 4
 Number: 12

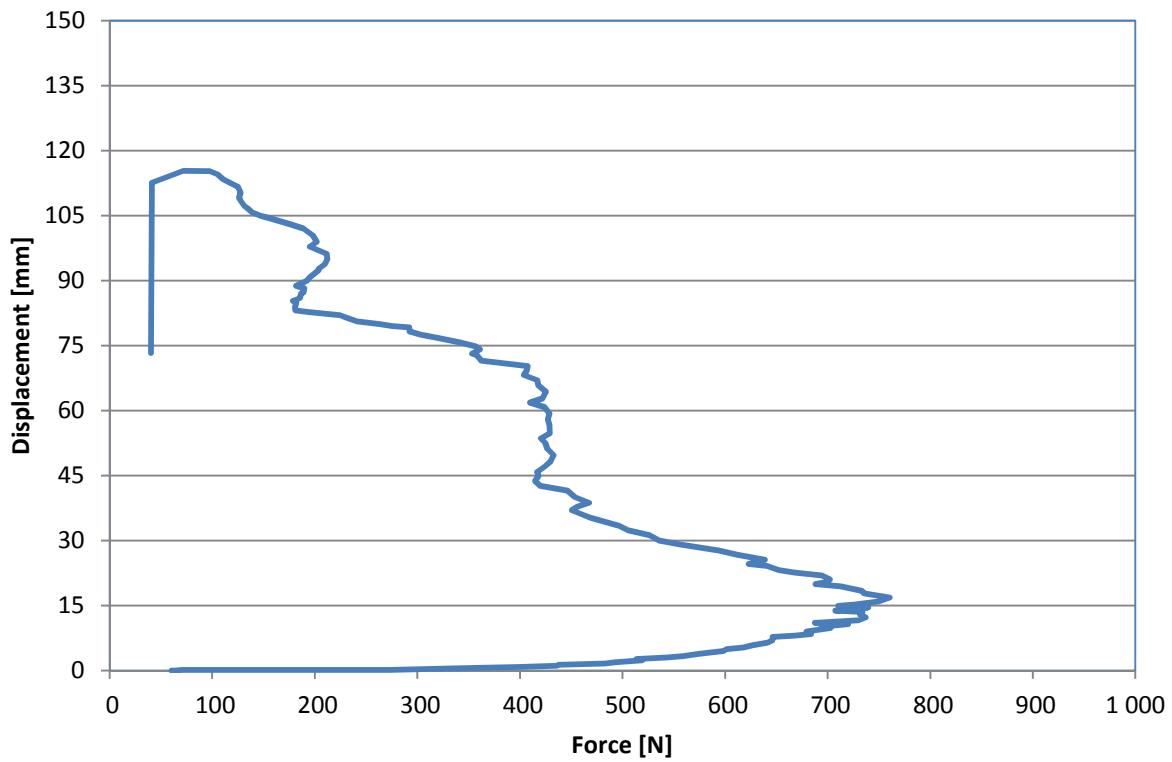
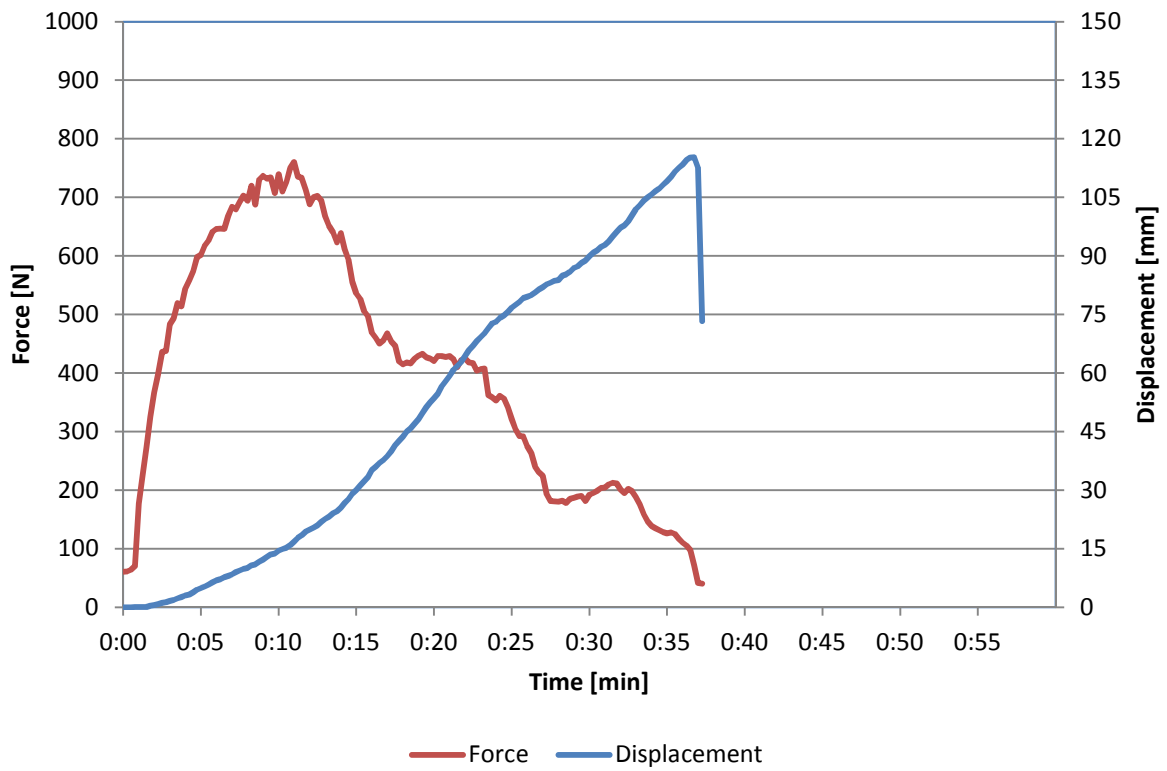
Date: 09-04-2013
 Time: 14:30



13

Location: M
 Section: 3
 Number: 7

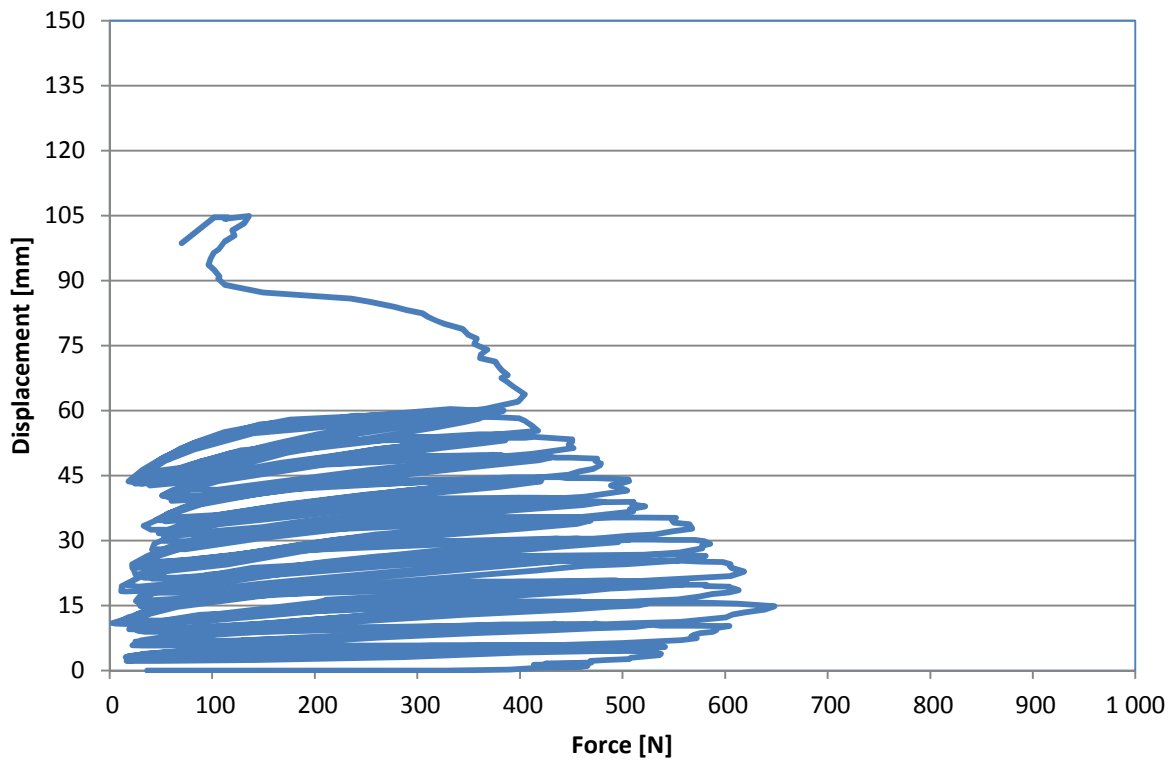
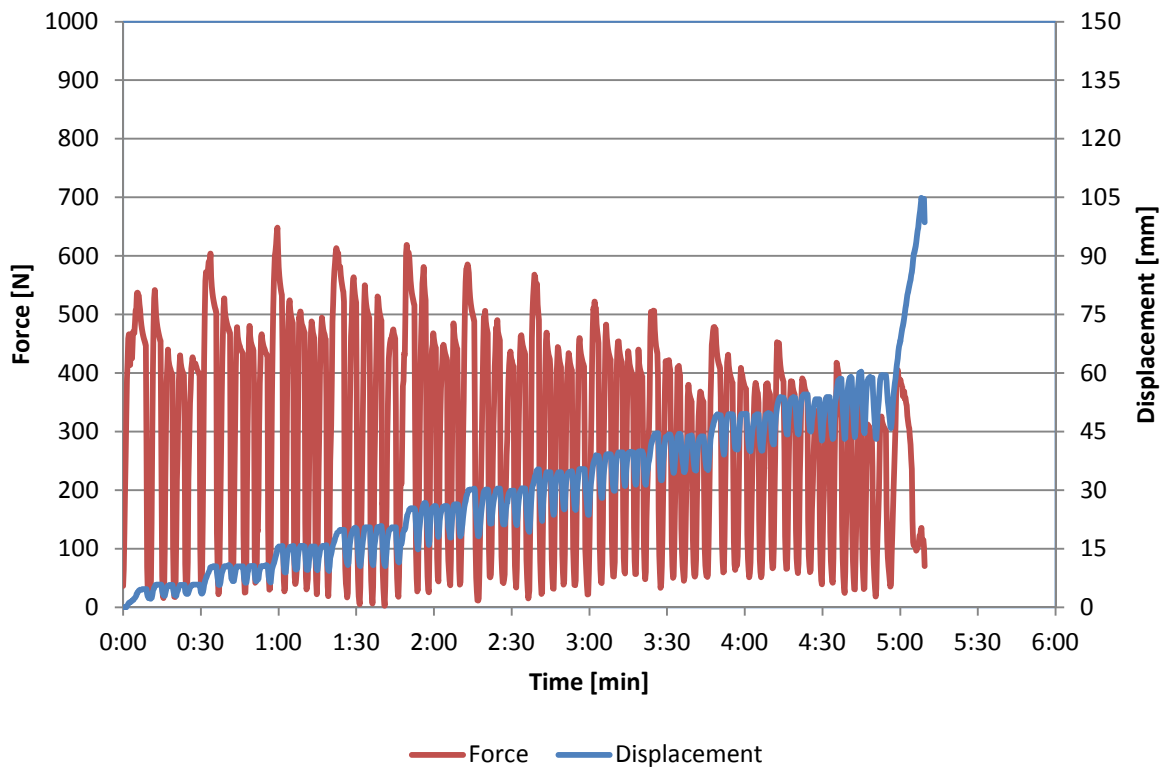
Date: 09-04-2013
 Time: 14:45



14

Location: M
 Section: 3
 Number: 8

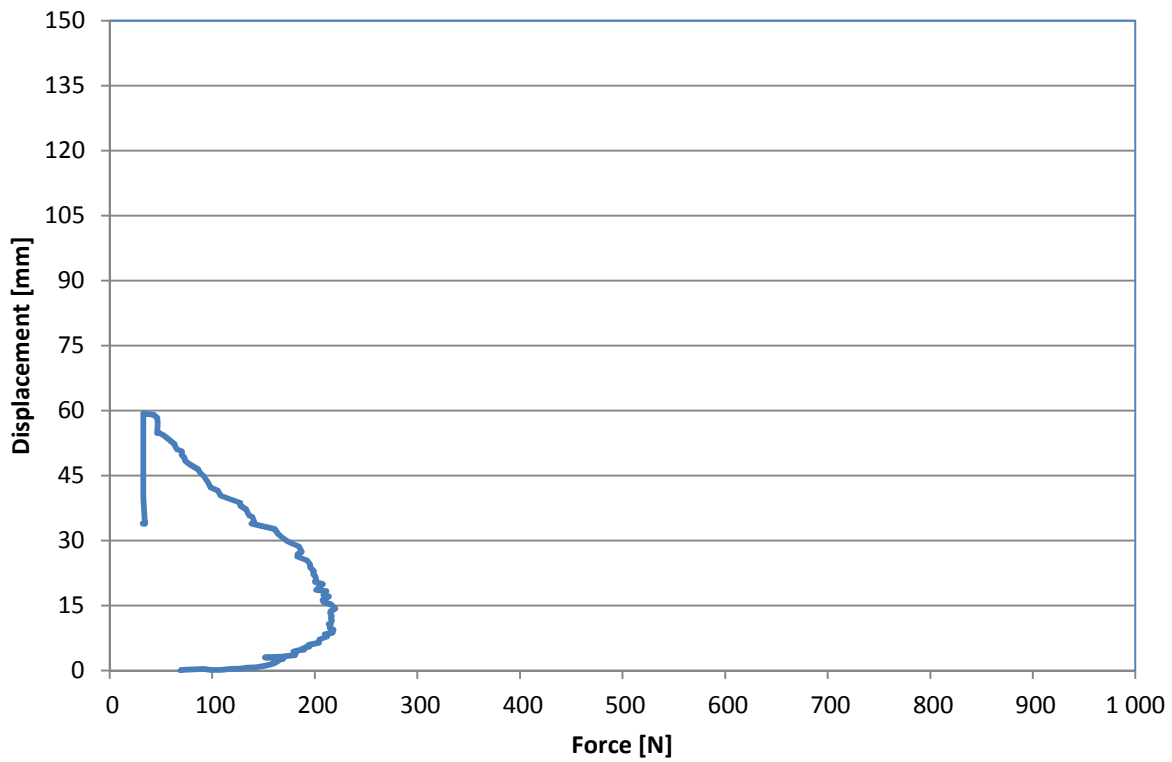
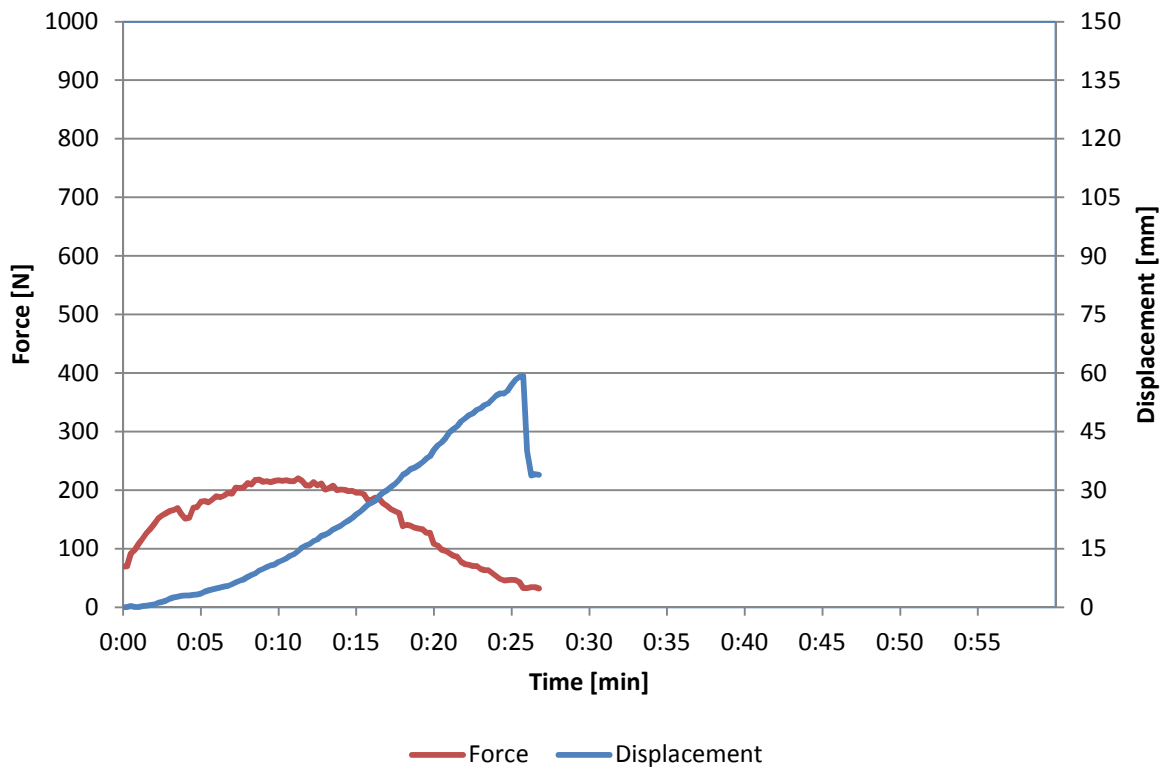
Date: 09-04-2013
 Time: 15:23



15

Location: M
 Section: 3
 Number: 9

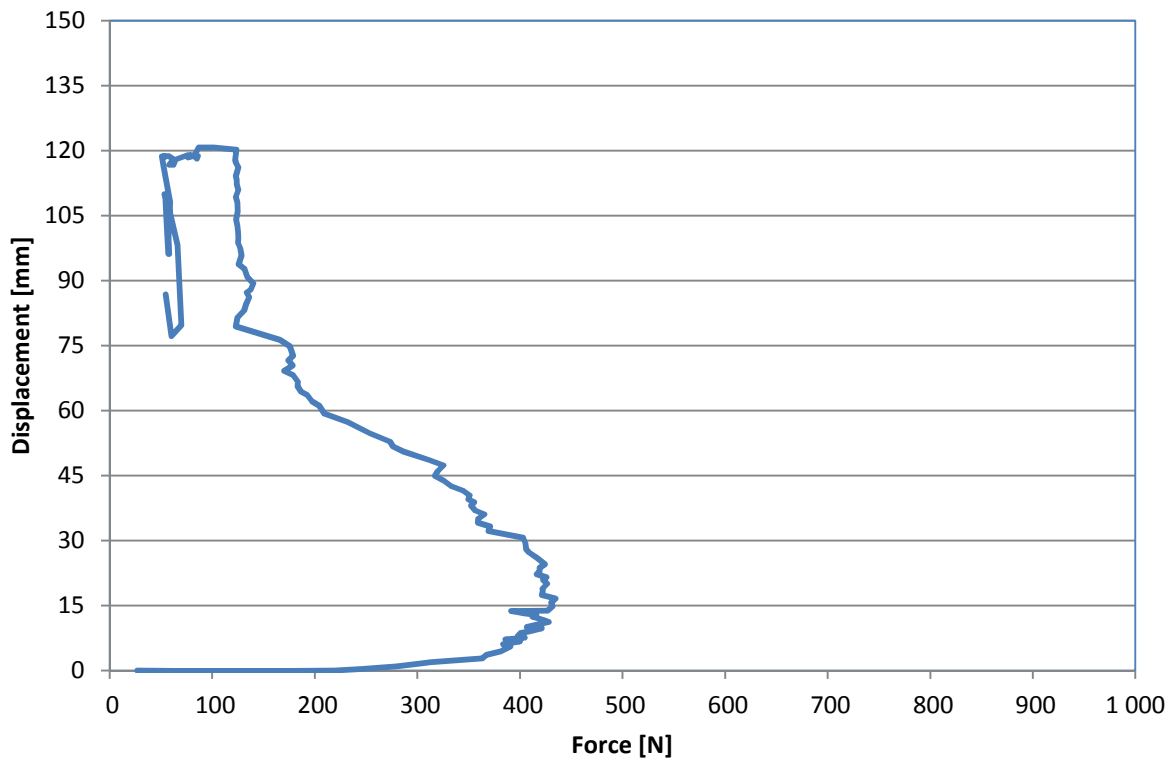
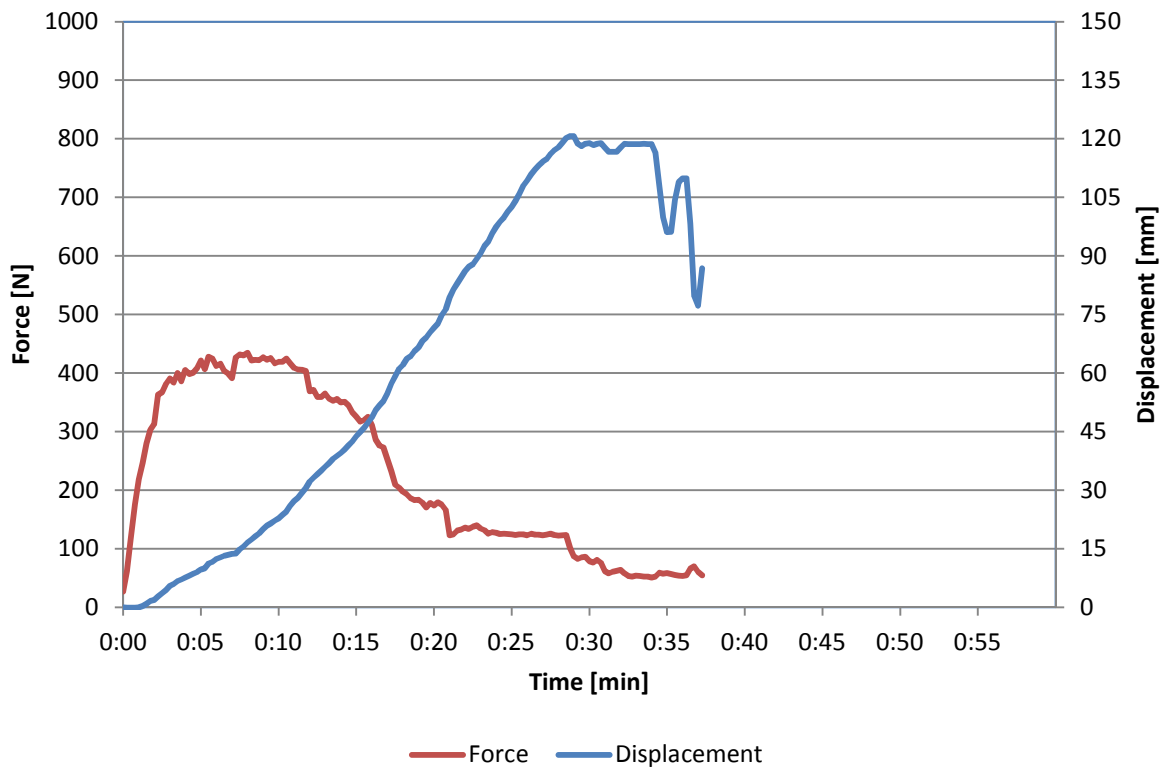
Date: 09-04-2013
 Time: 15:35



16

Location: M
 Section: 7
 Number: 19

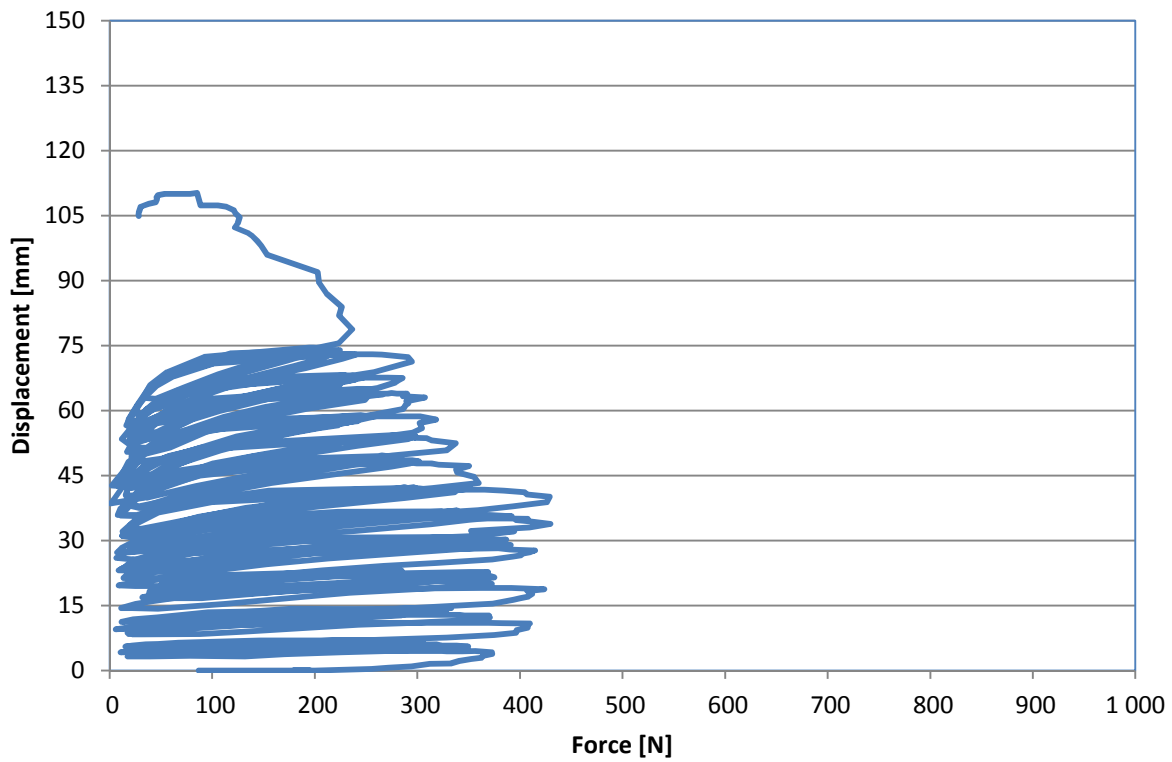
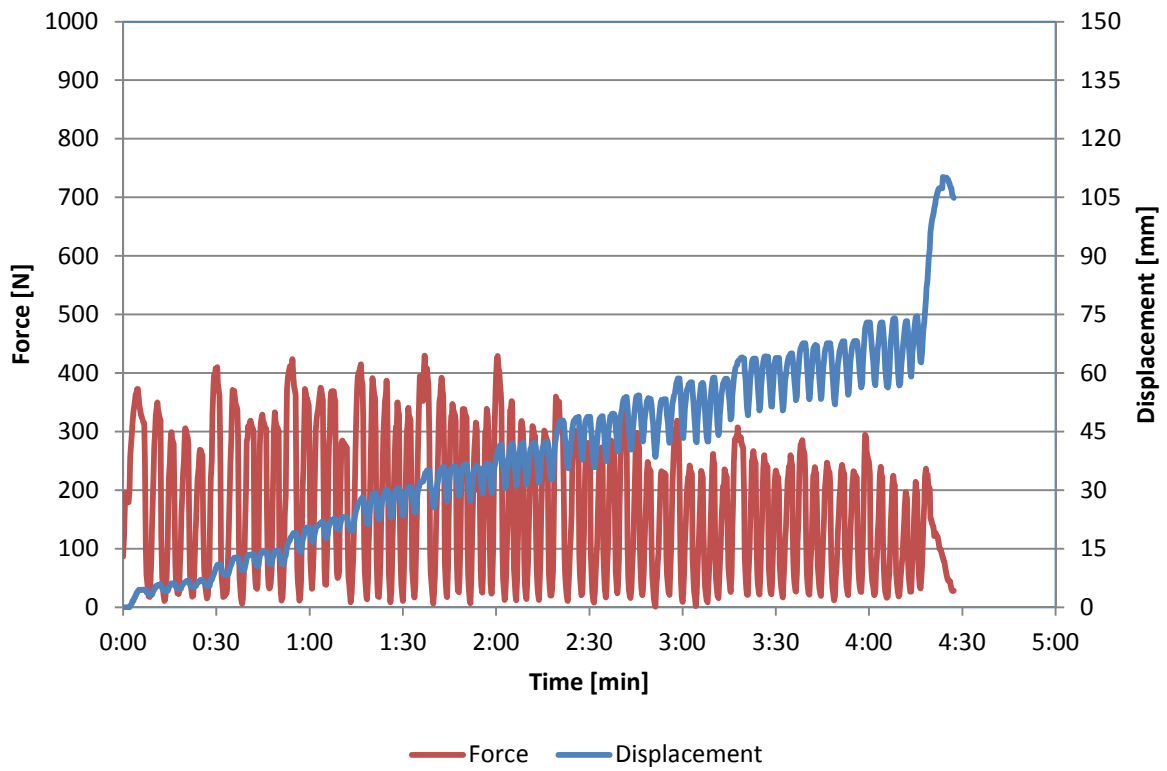
Date: 09-04-2013
 Time: 15:56



17

Location: M
 Section: 7
 Number: 20

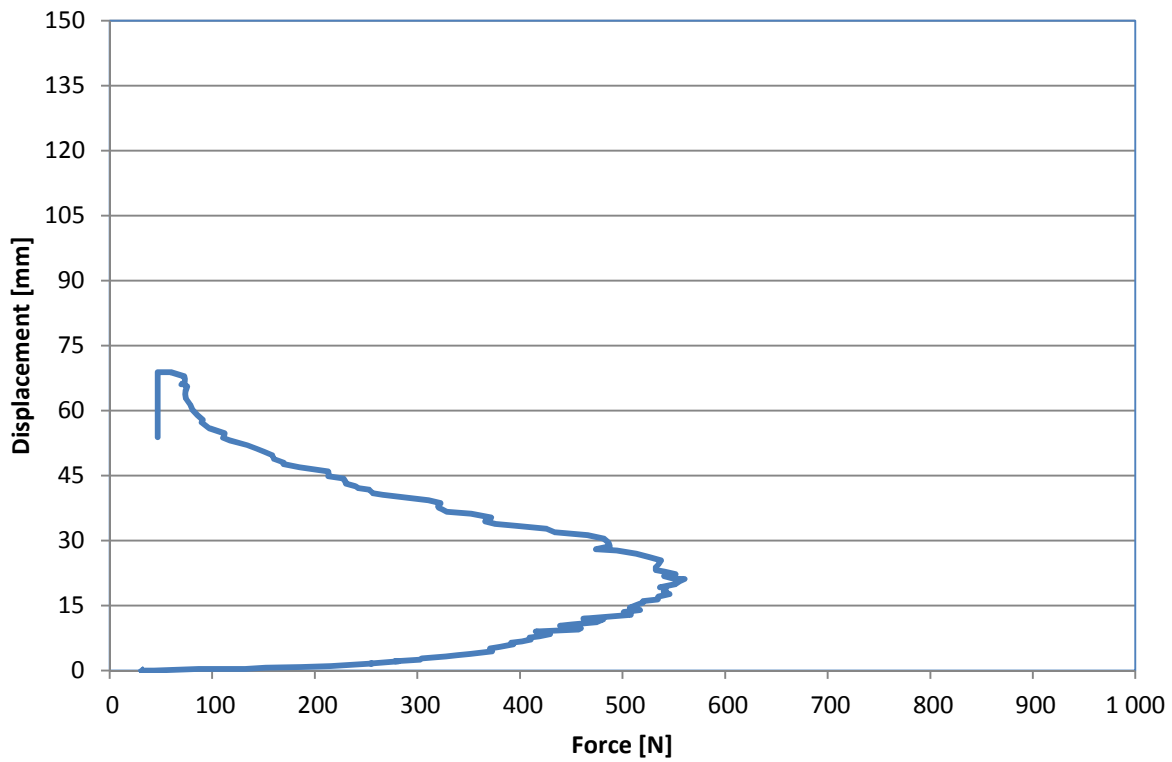
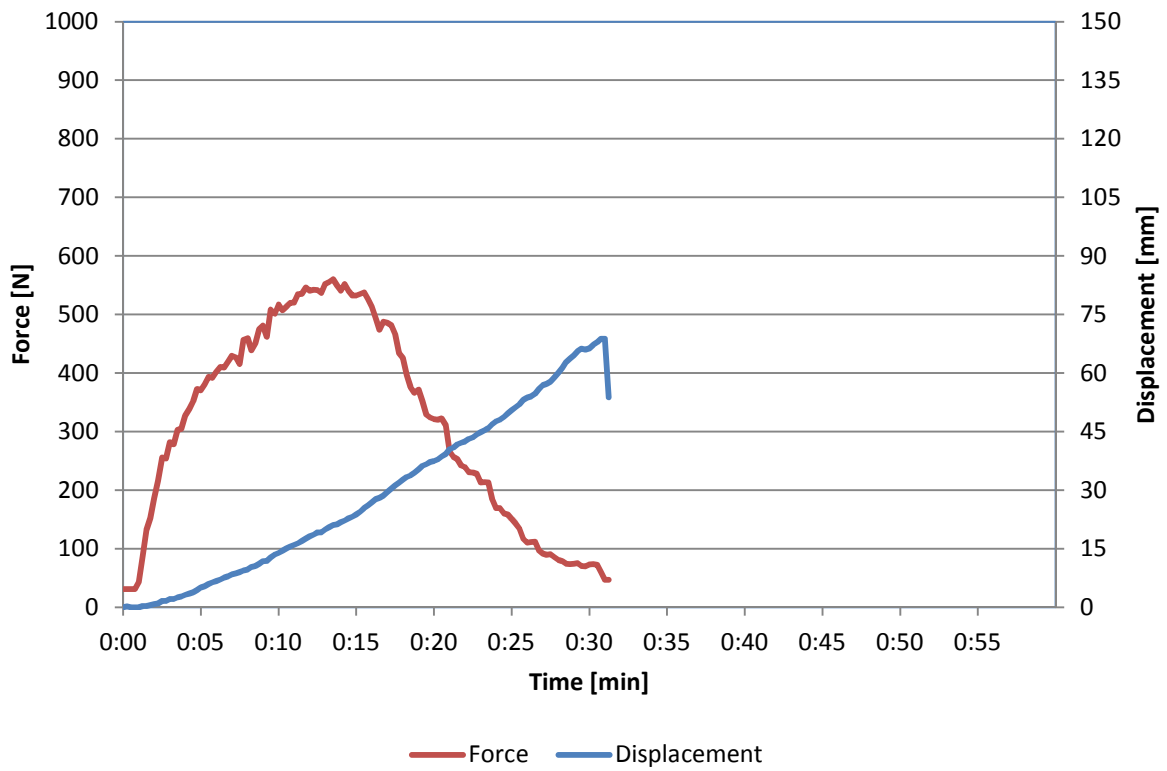
Date: 09-04-2013
 Time: 16:02



18

Location: M
 Section: 7
 Number: 21

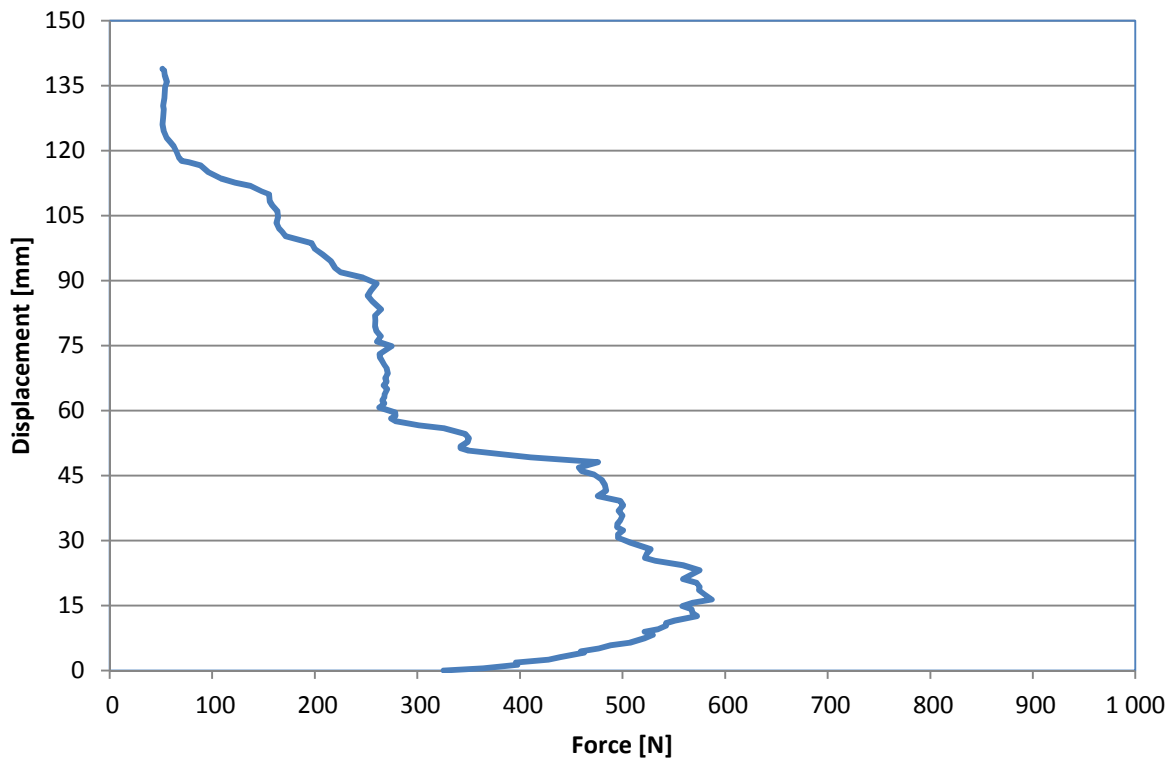
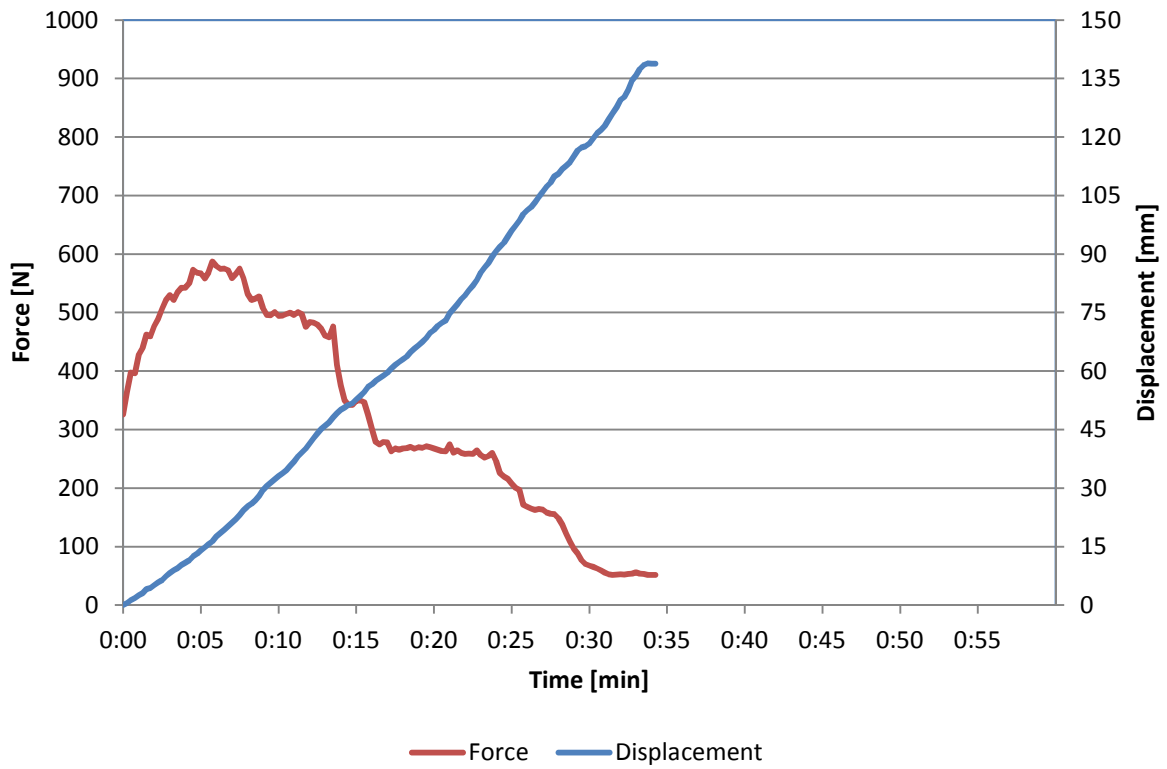
Date: 09-04-2013
 Time: 16:15



19

Location: M
 Section: 1
 Number: 1

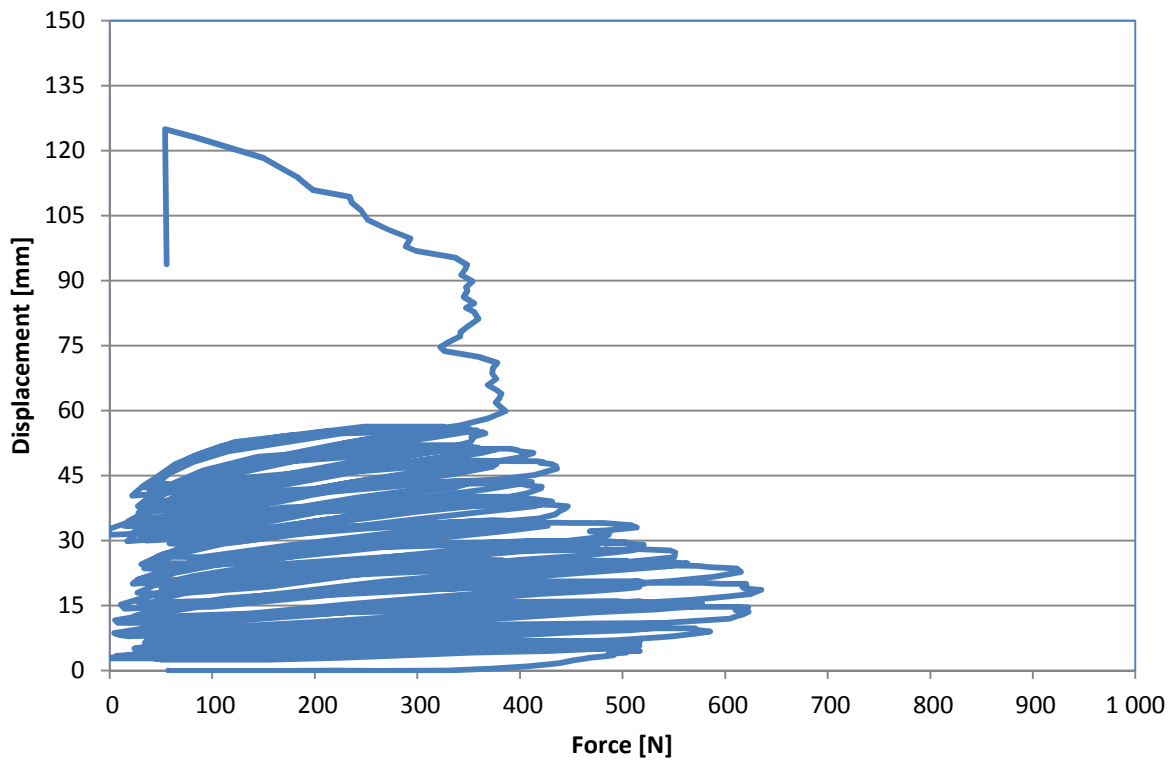
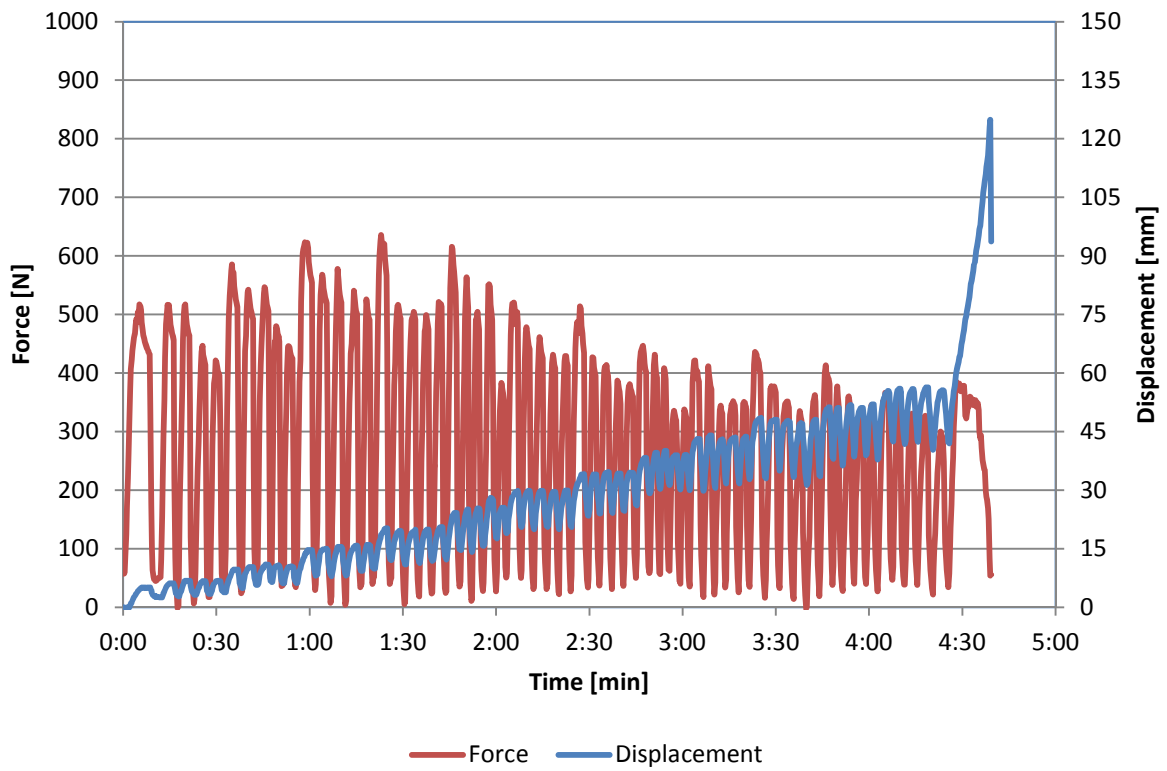
Date: 09-04-2013
 Time: 16:34



20

Location: M
 Section: 1
 Number: 2

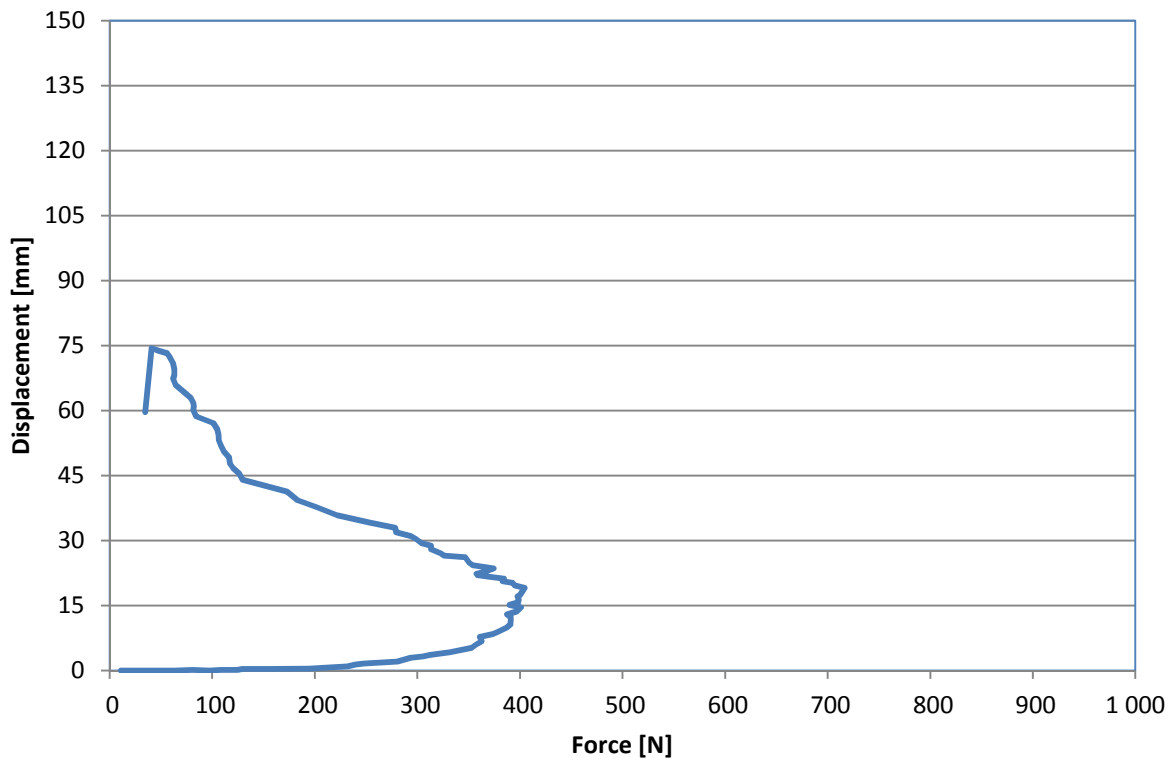
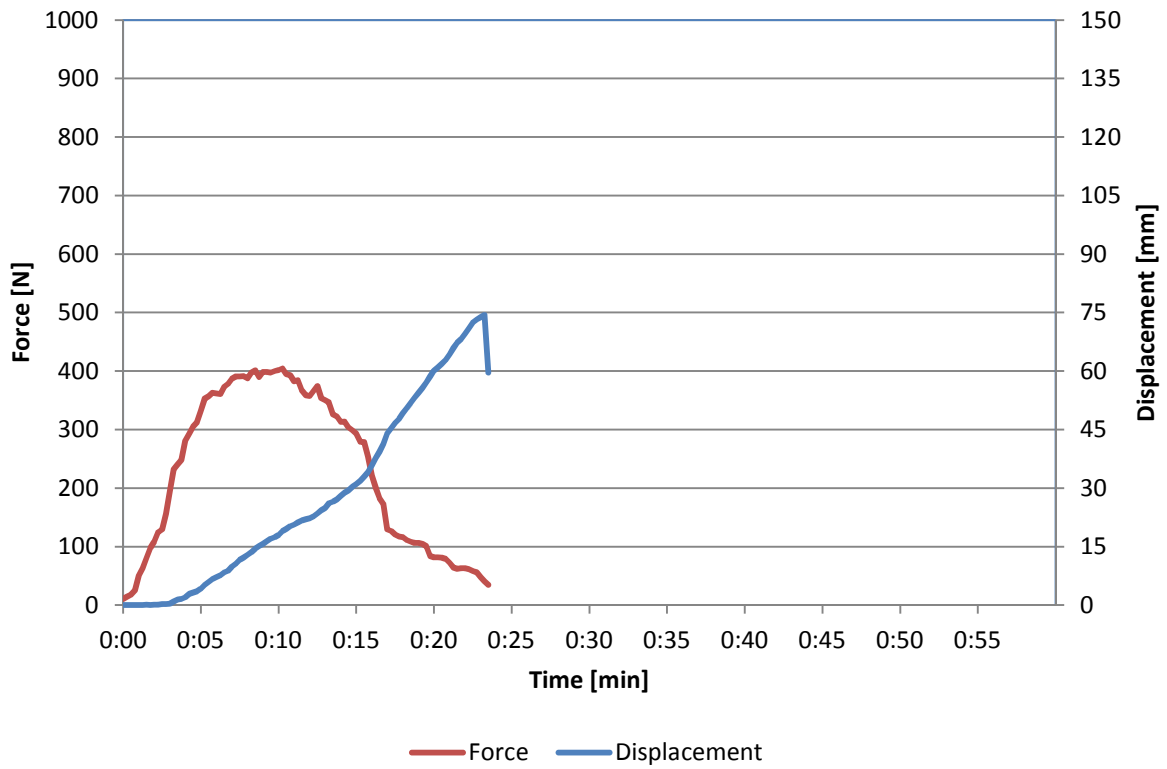
Date: 09-04-2013
 Time: 16:47



21

Location: M
 Section: 1
 Number: 3

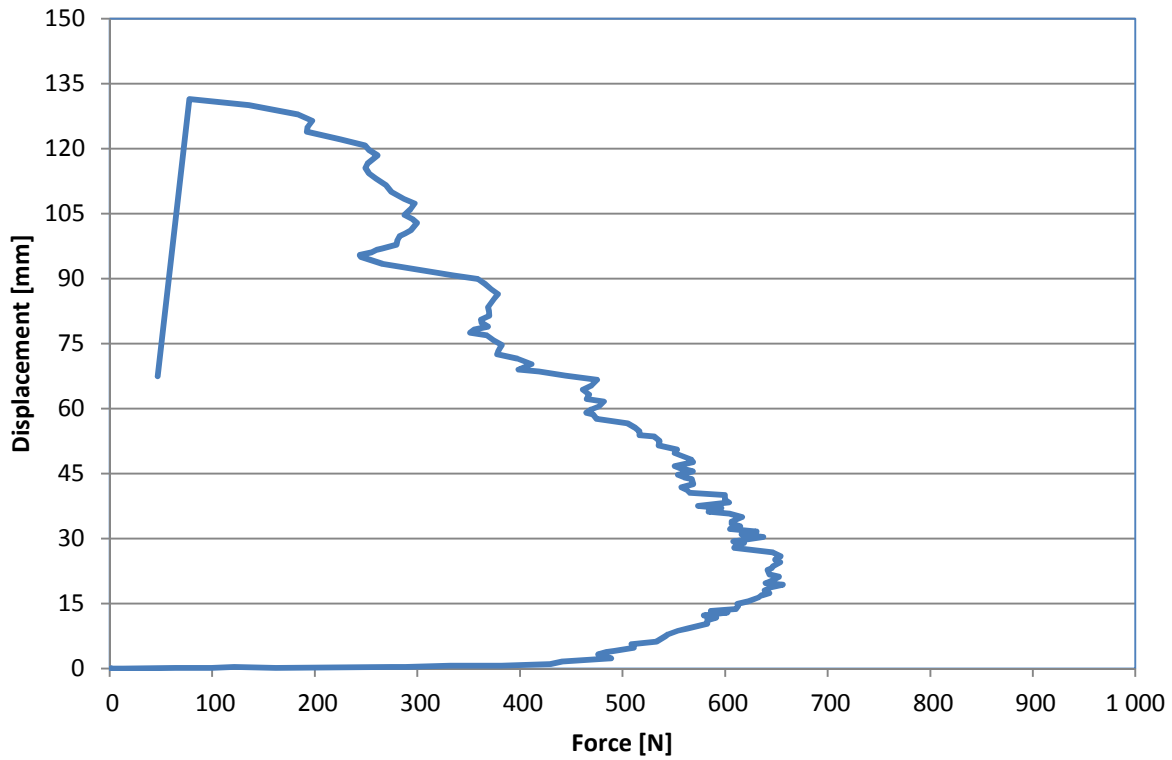
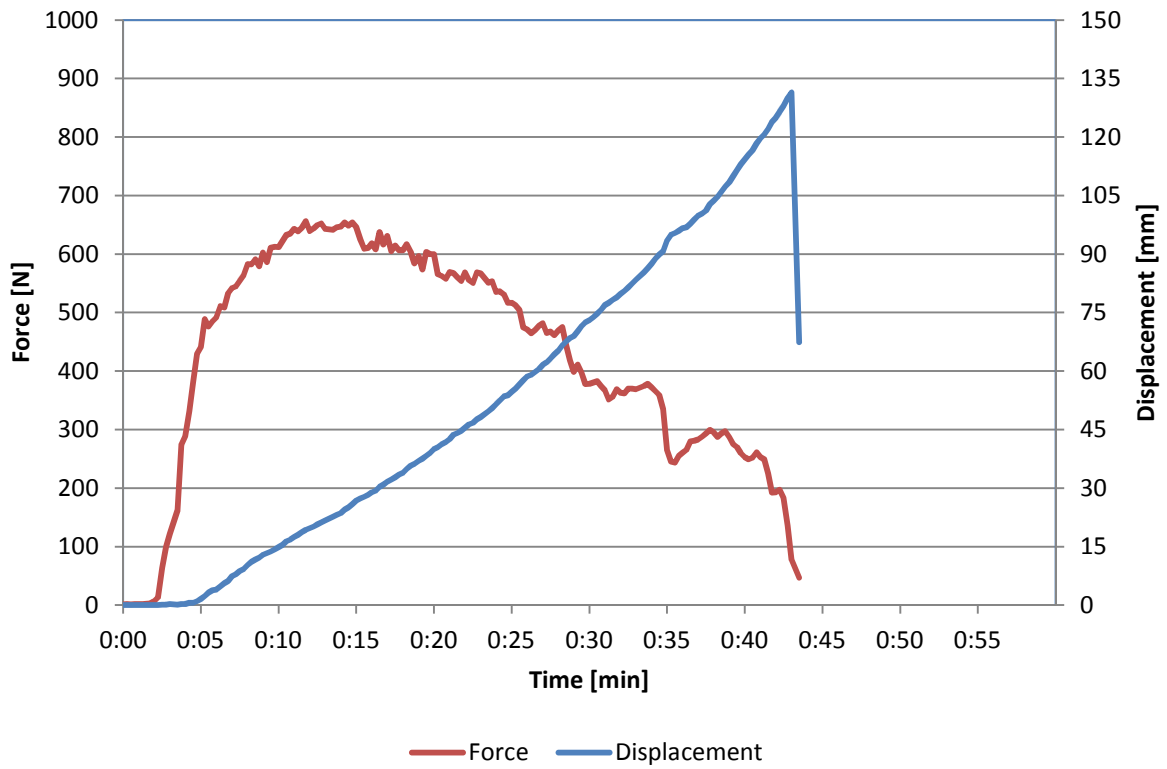
Date: 09-04-2013
 Time: 17:00



22

Location: M
 Section: 2
 Number: 4

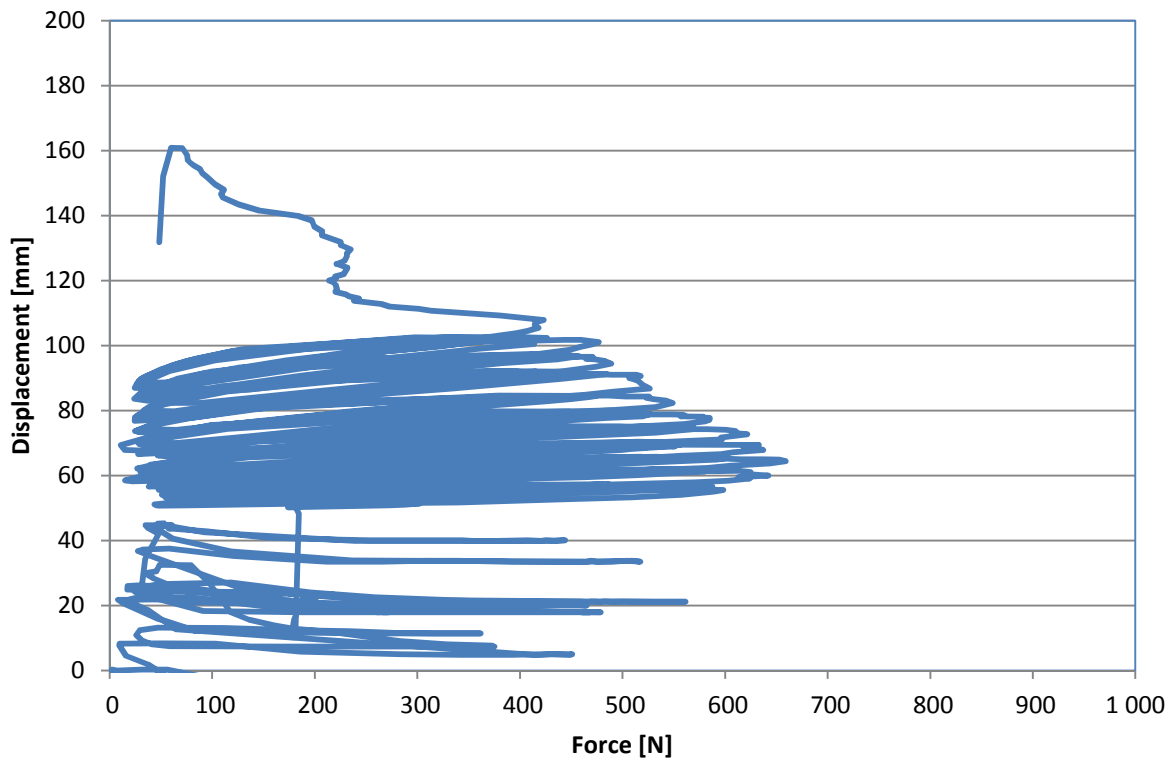
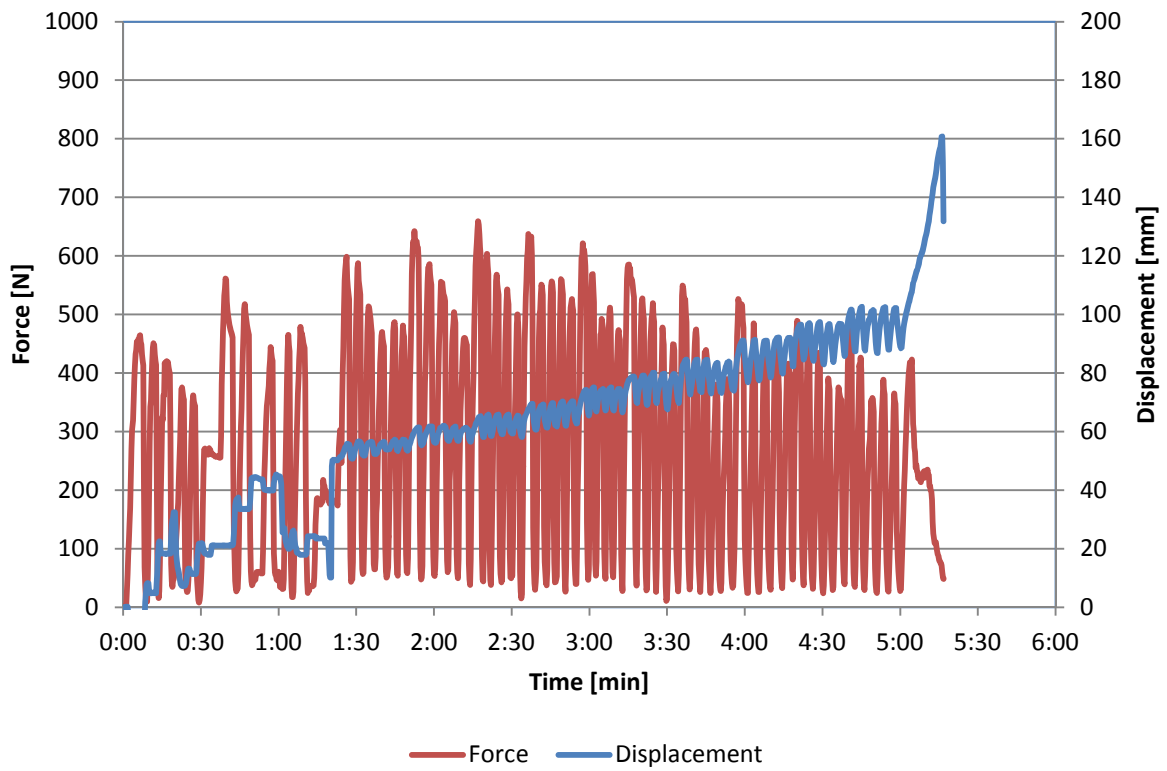
Date: 09-04-2013
 Time: 17:14



23

Location: M
 Section: 2
 Number: 5

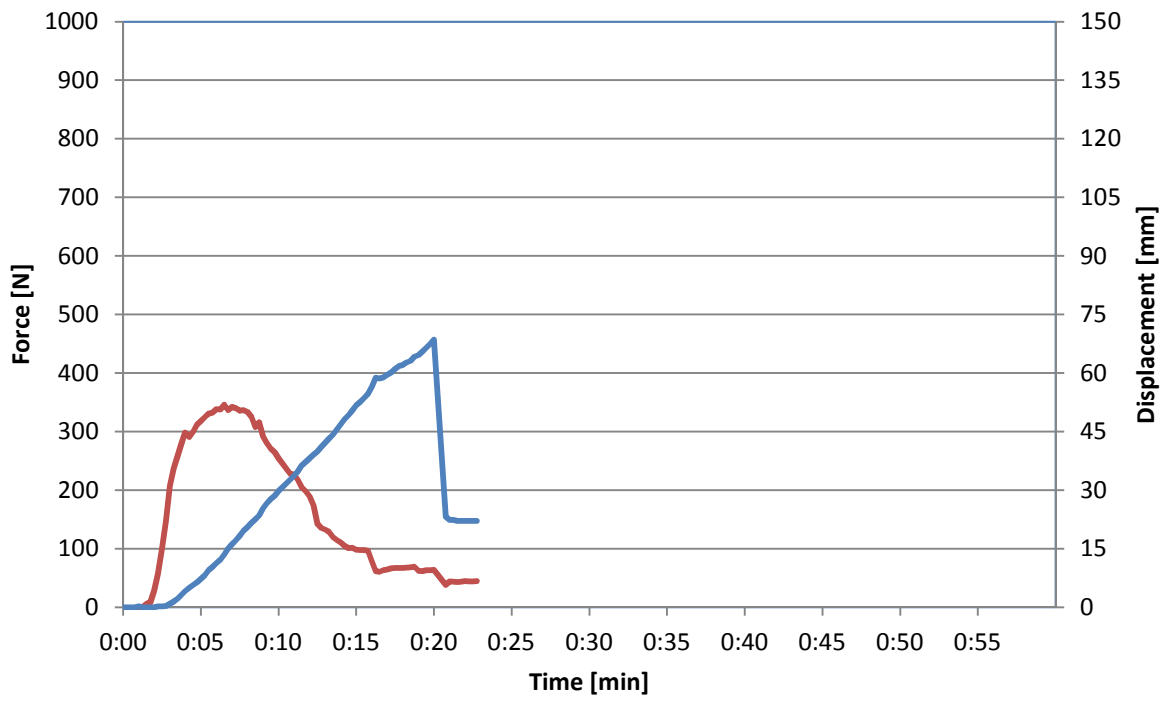
Date: 09-04-2013
 Time: 17:26



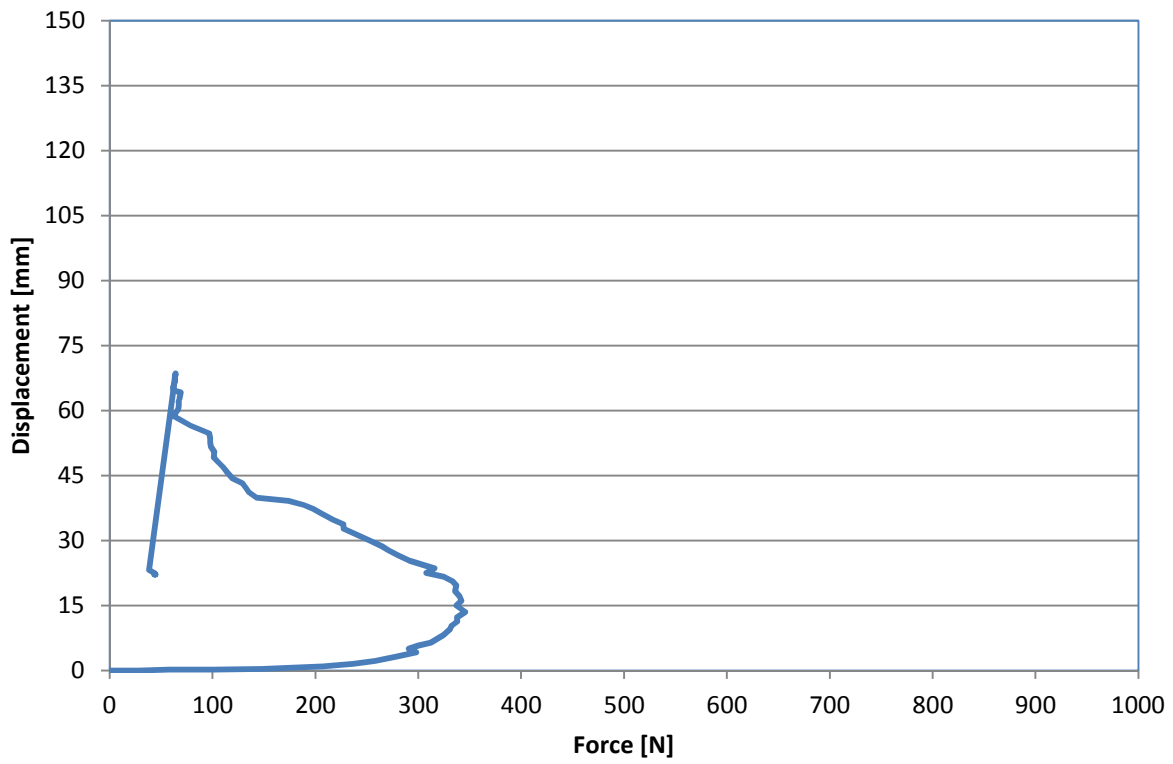
24

Location: M
 Section: 2
 Number: 6

Date: 09-04-2013
 Time: 17:37



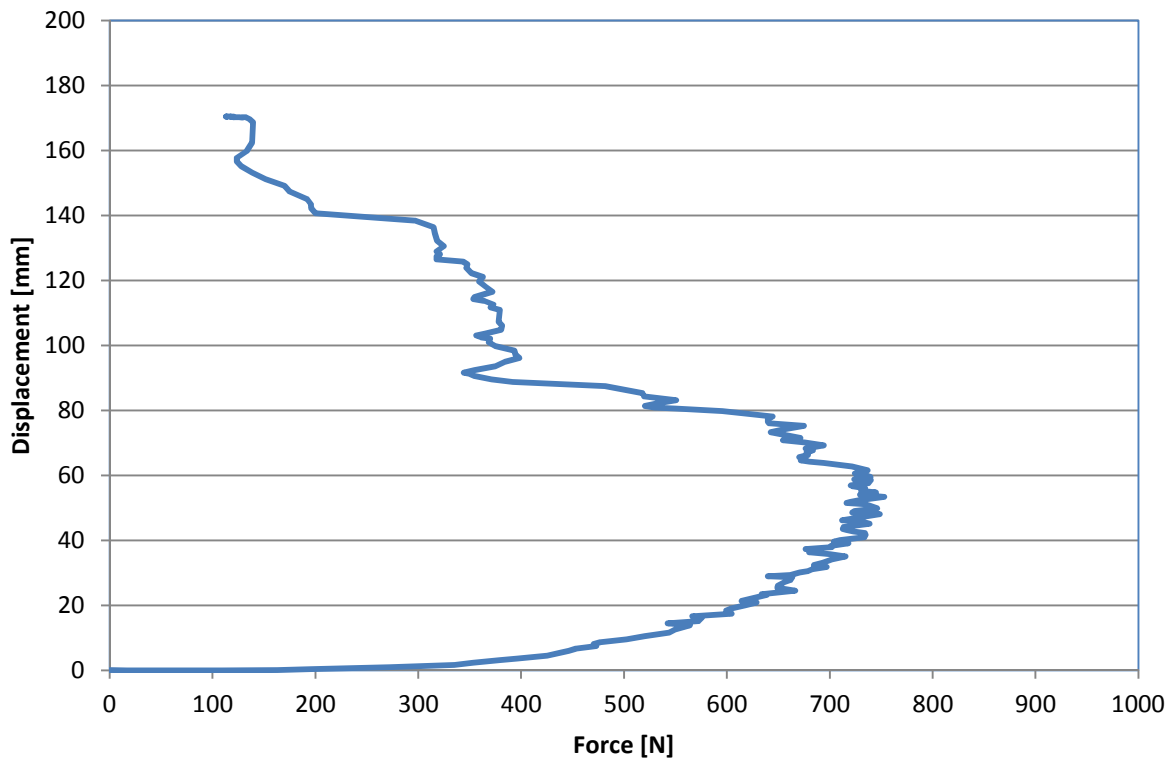
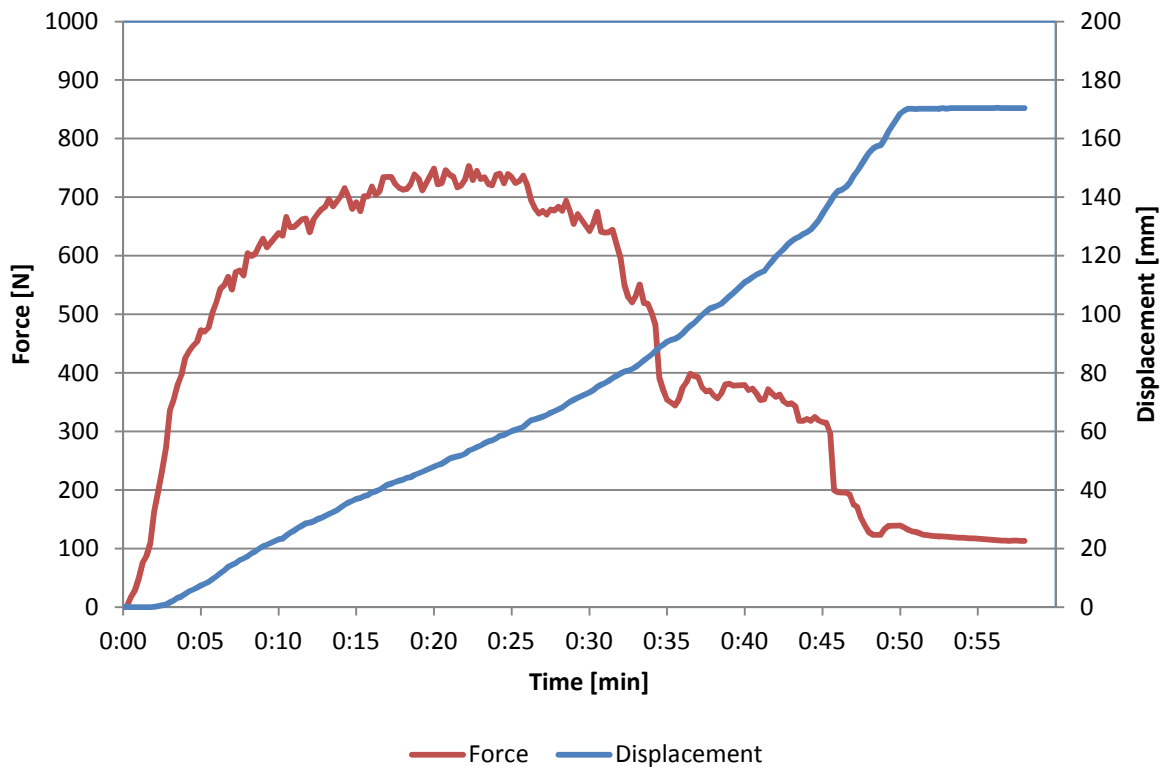
— Force — Displacement



25

Location: N
 Section: 4
 Number: 10

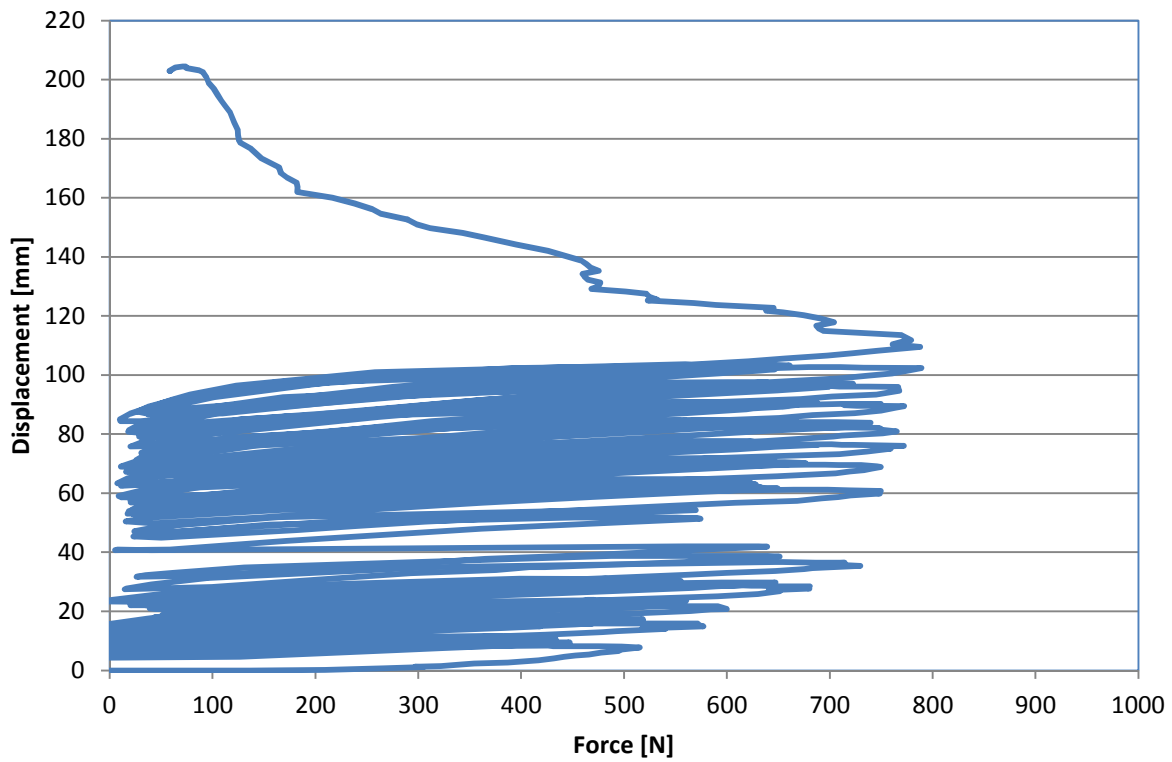
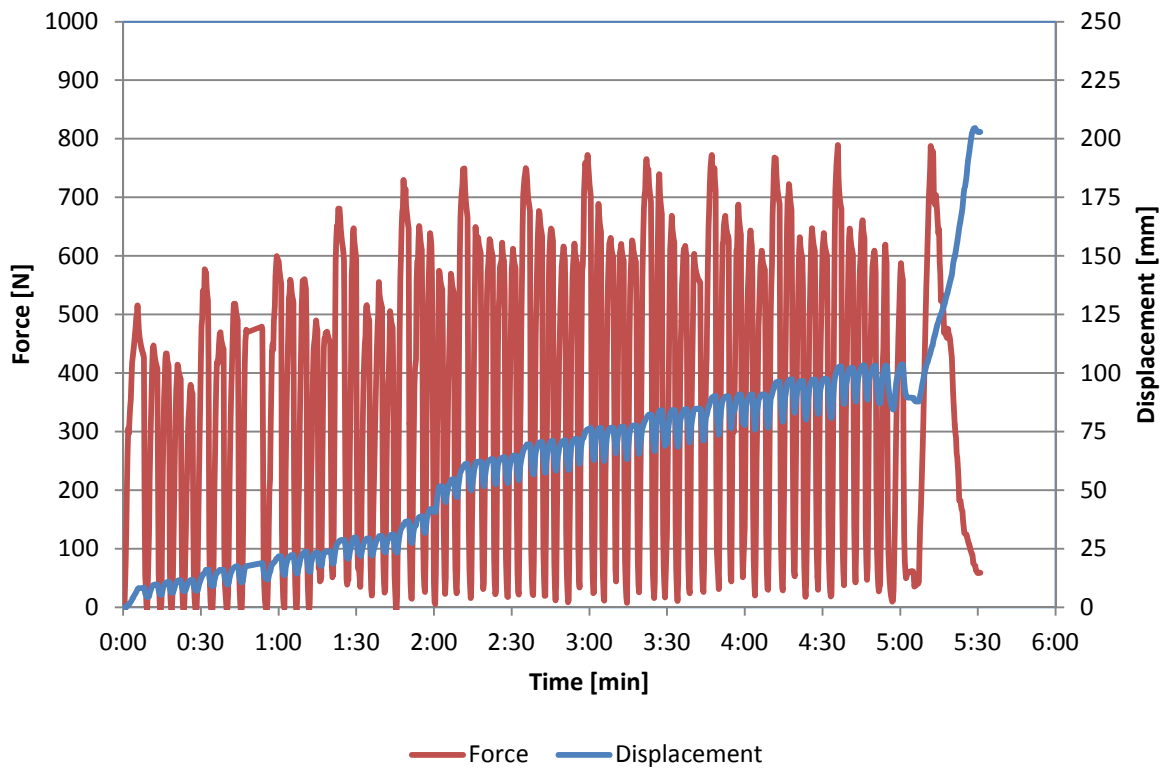
Date: 10-04-2013
 Time: 13:01



26

Location: N
 Section: 4
 Number: 11

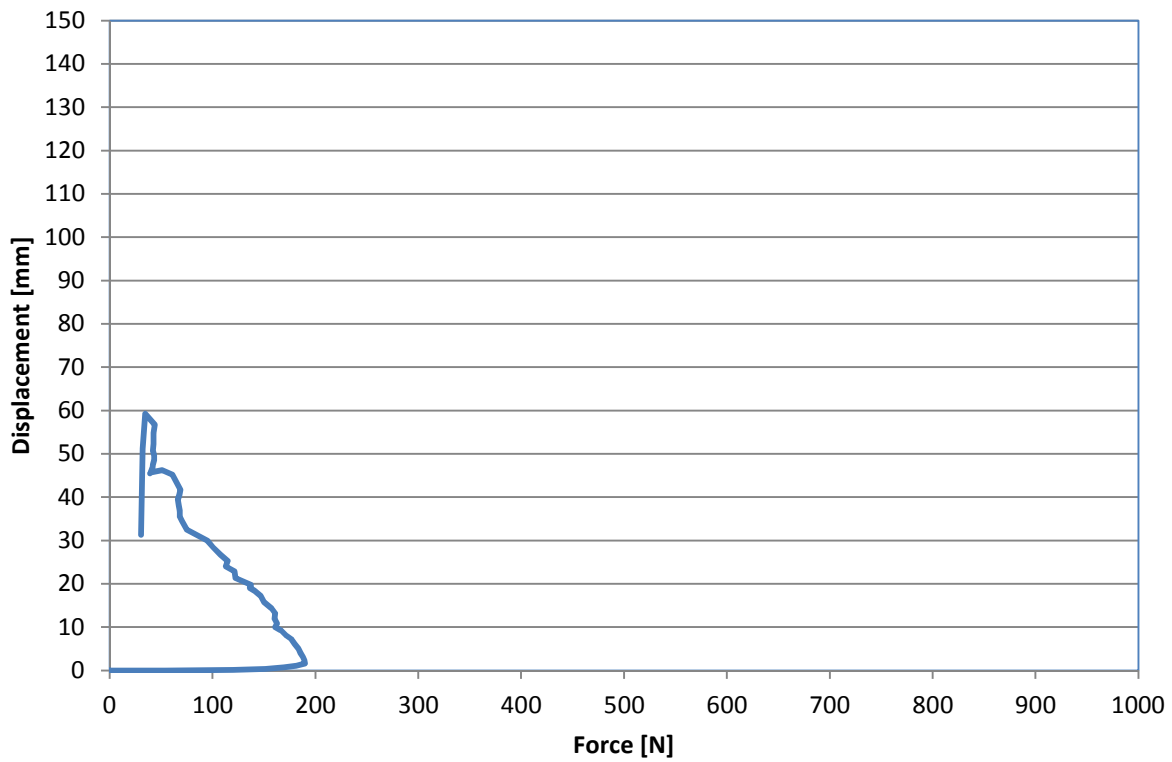
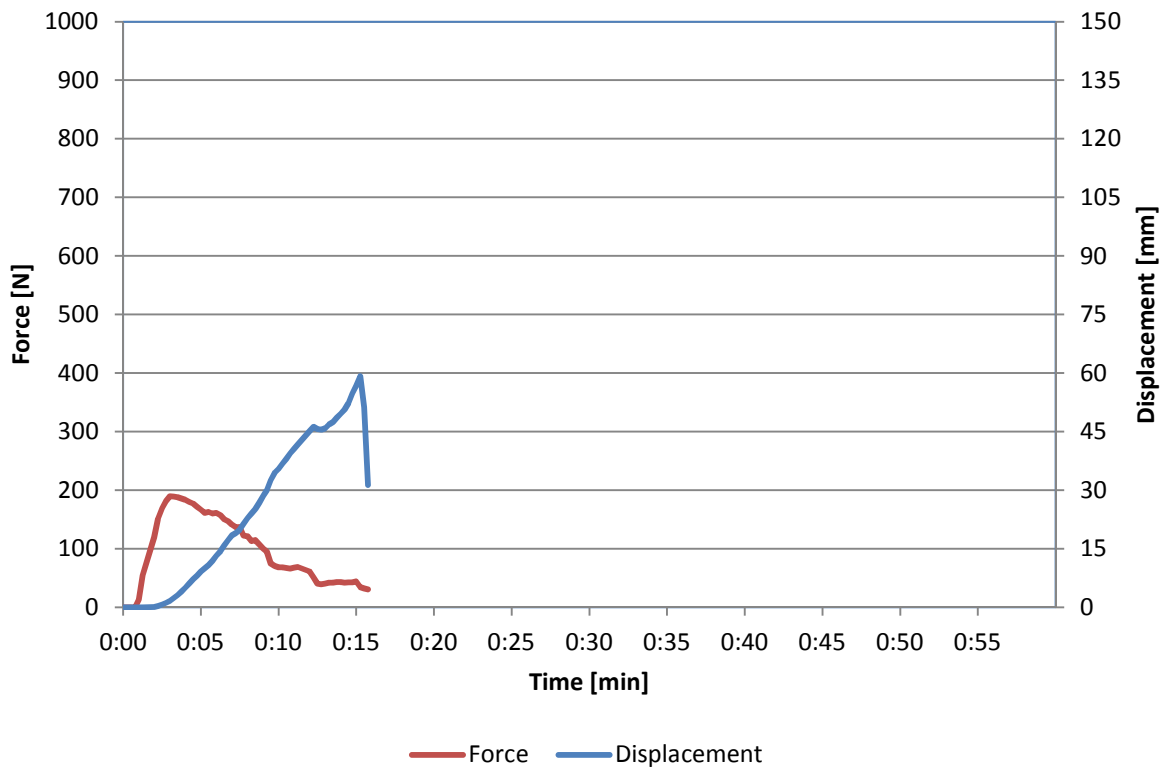
Date: 10-04-2013
 Time: 13:11

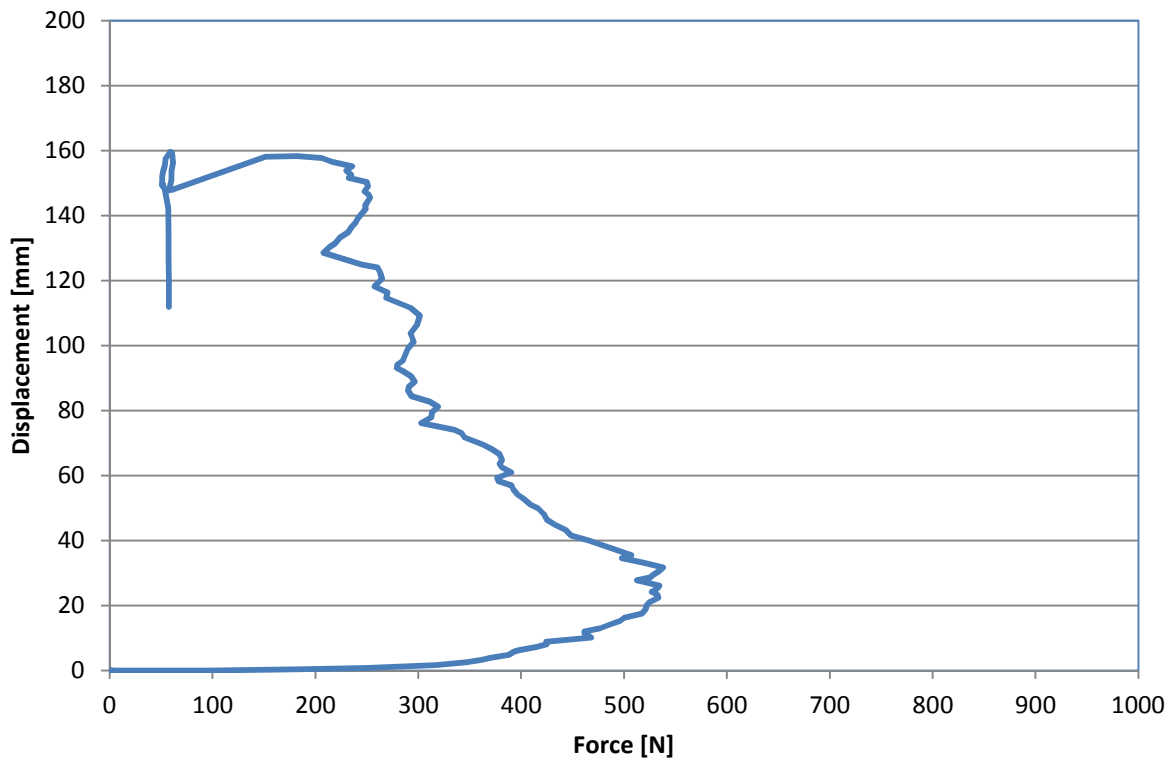
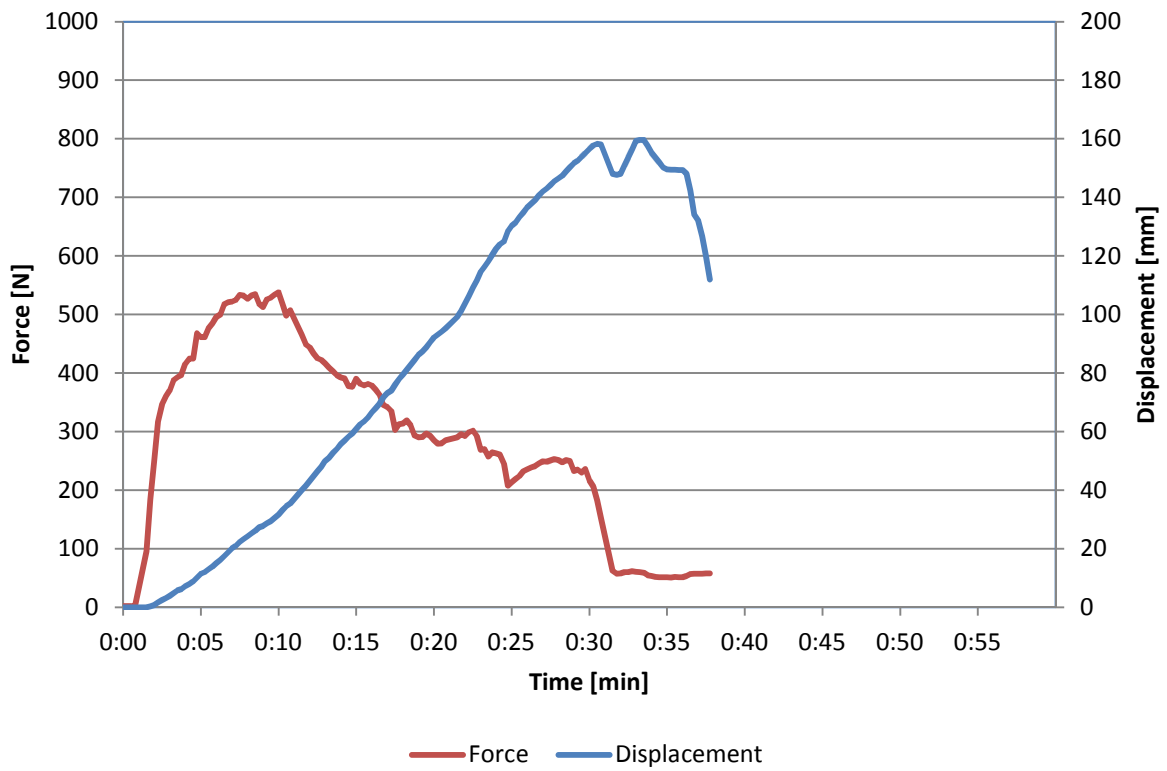


27

Location: N
 Section: 4
 Number: 12

Date: 10-04-2013
 Time: 13:19

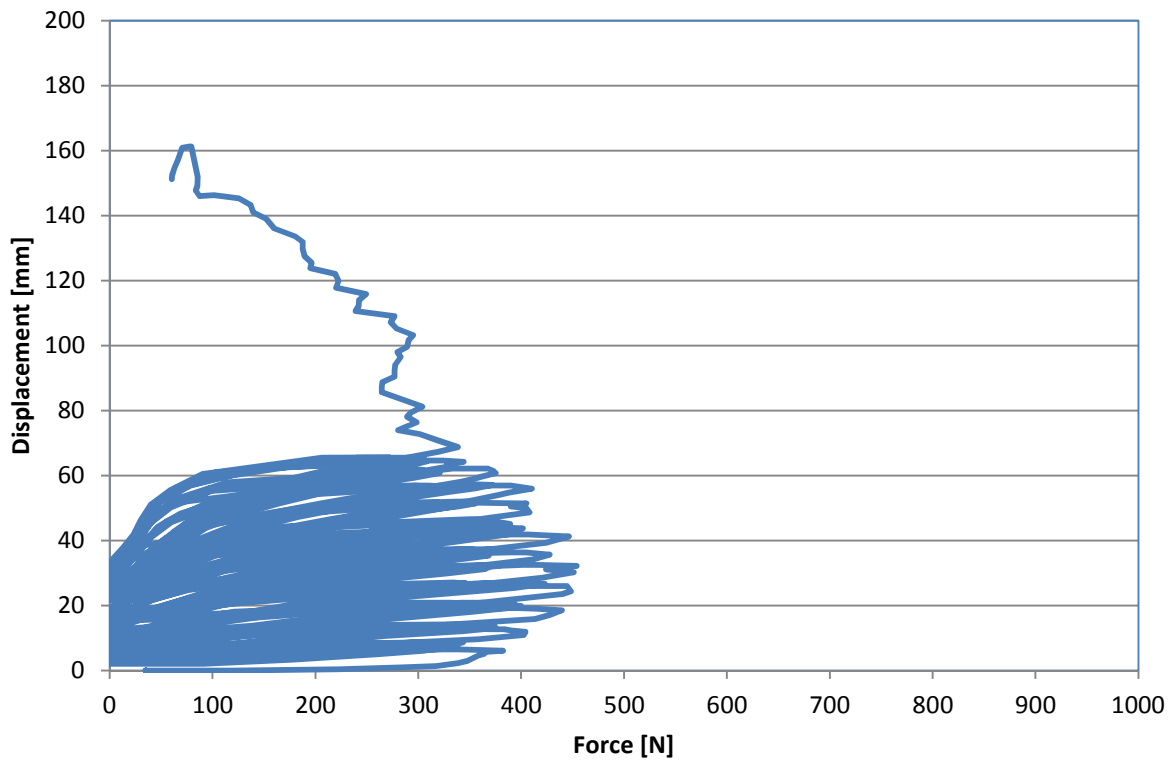
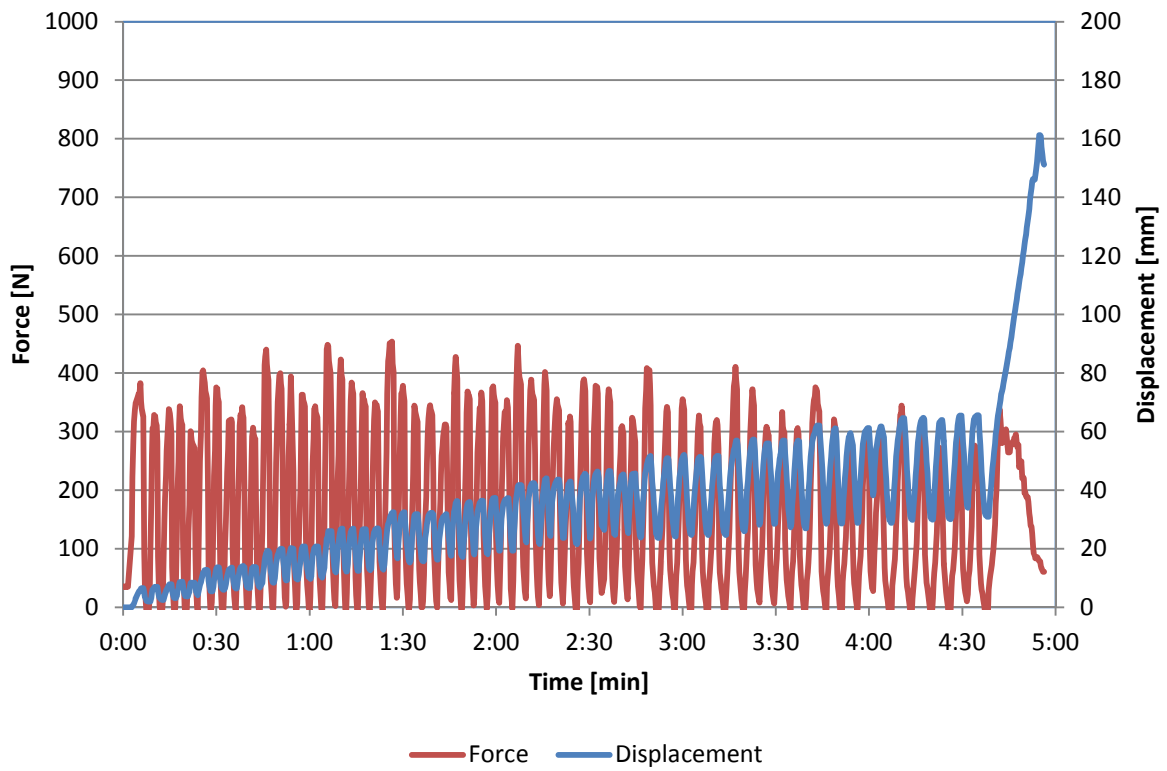




29

Location: N
 Section: 7
 Number: 20

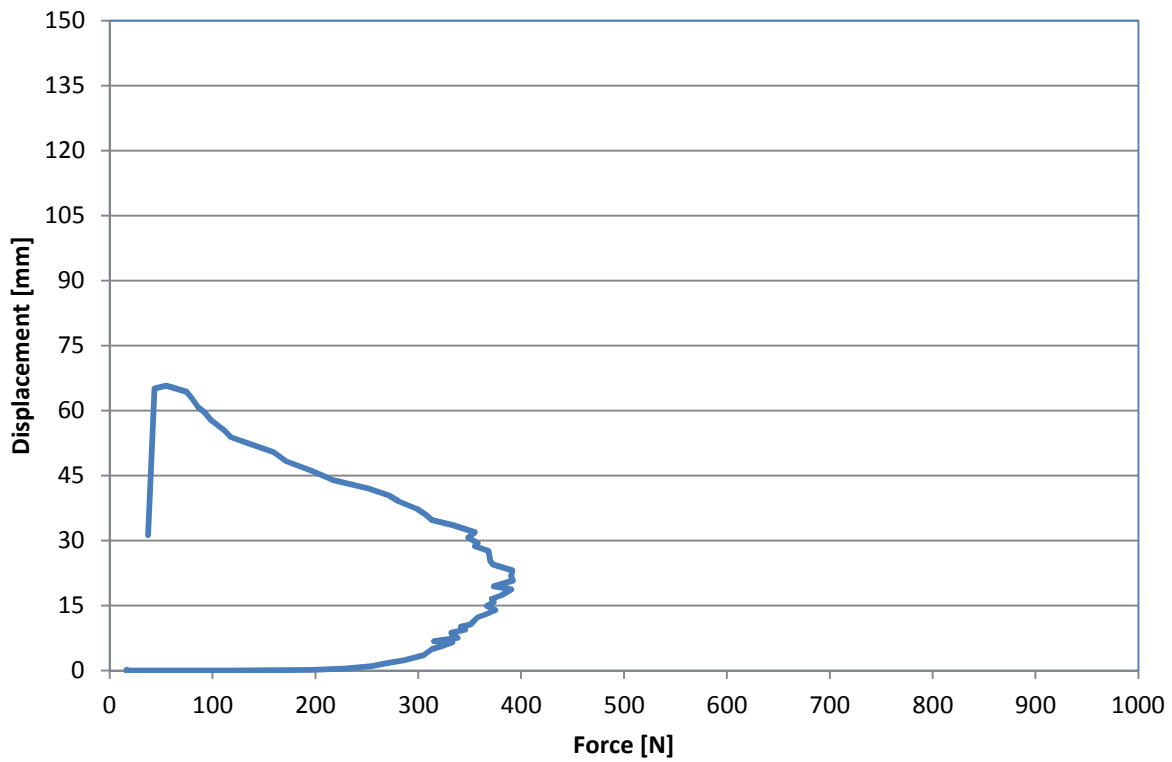
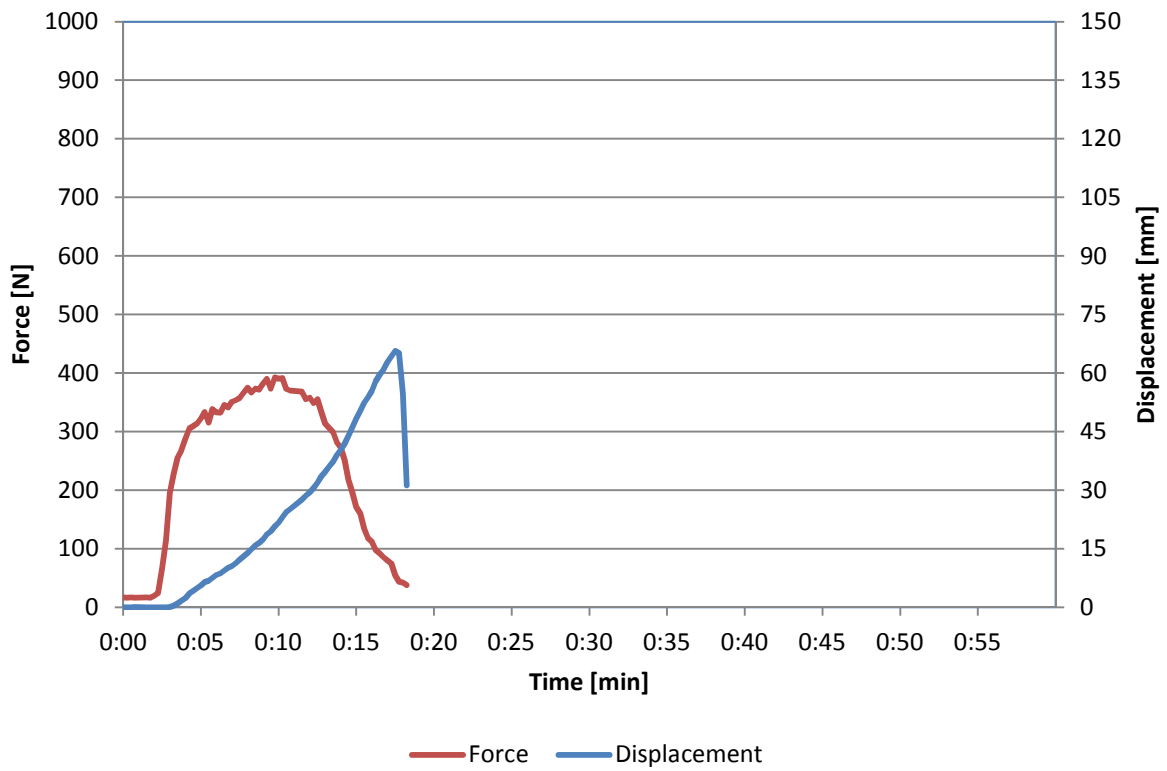
Date: 10-04-2013
 Time: 13:43

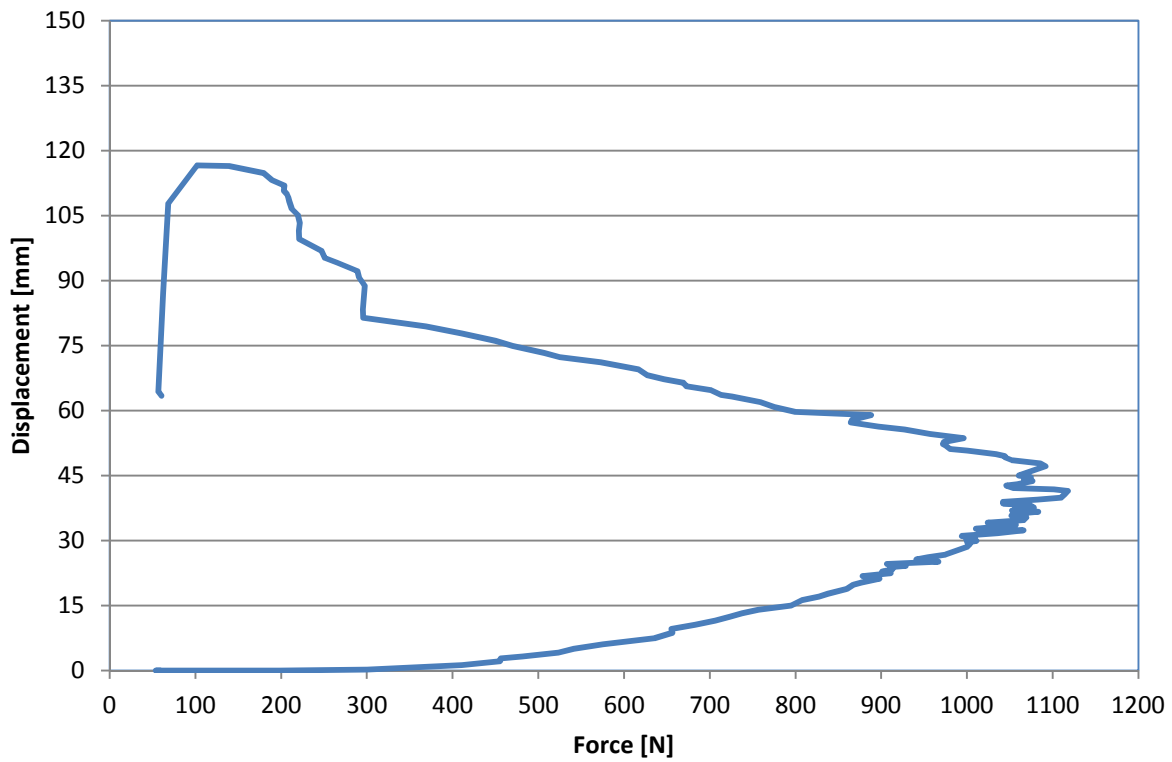
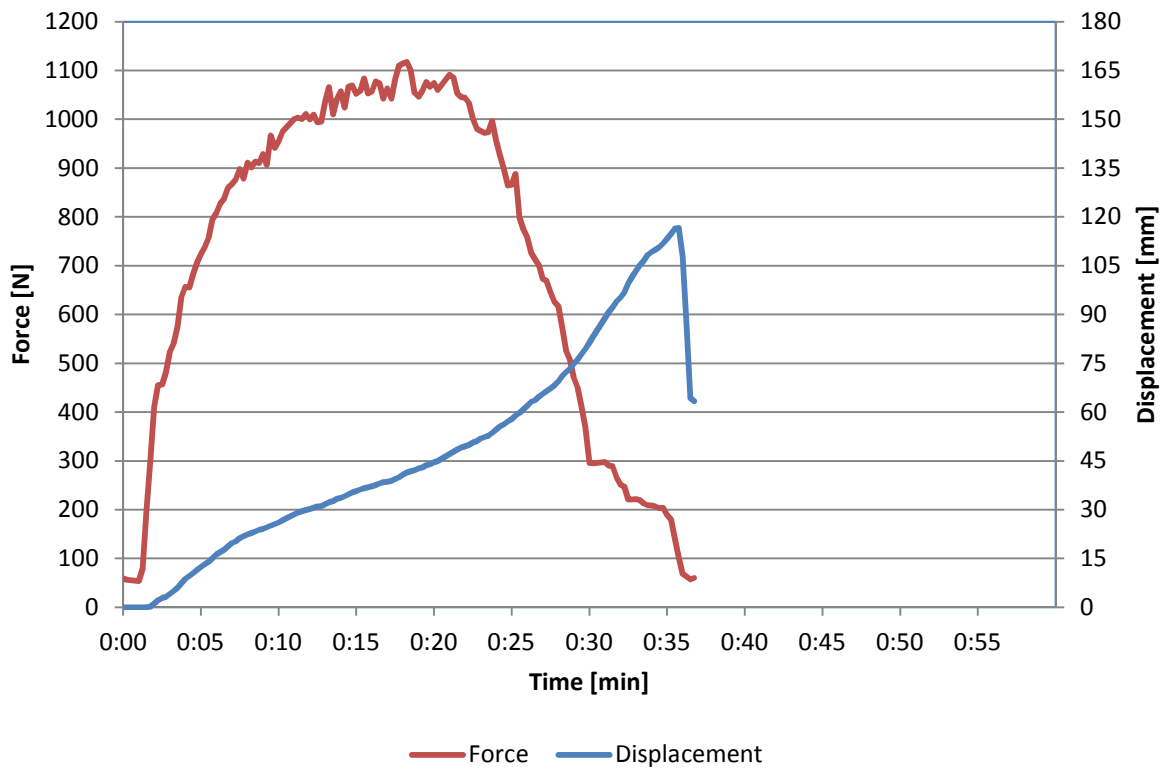


30

Location: N
 Section: 7
 Number: 21

Date: 10-04-2013
 Time: 13:50

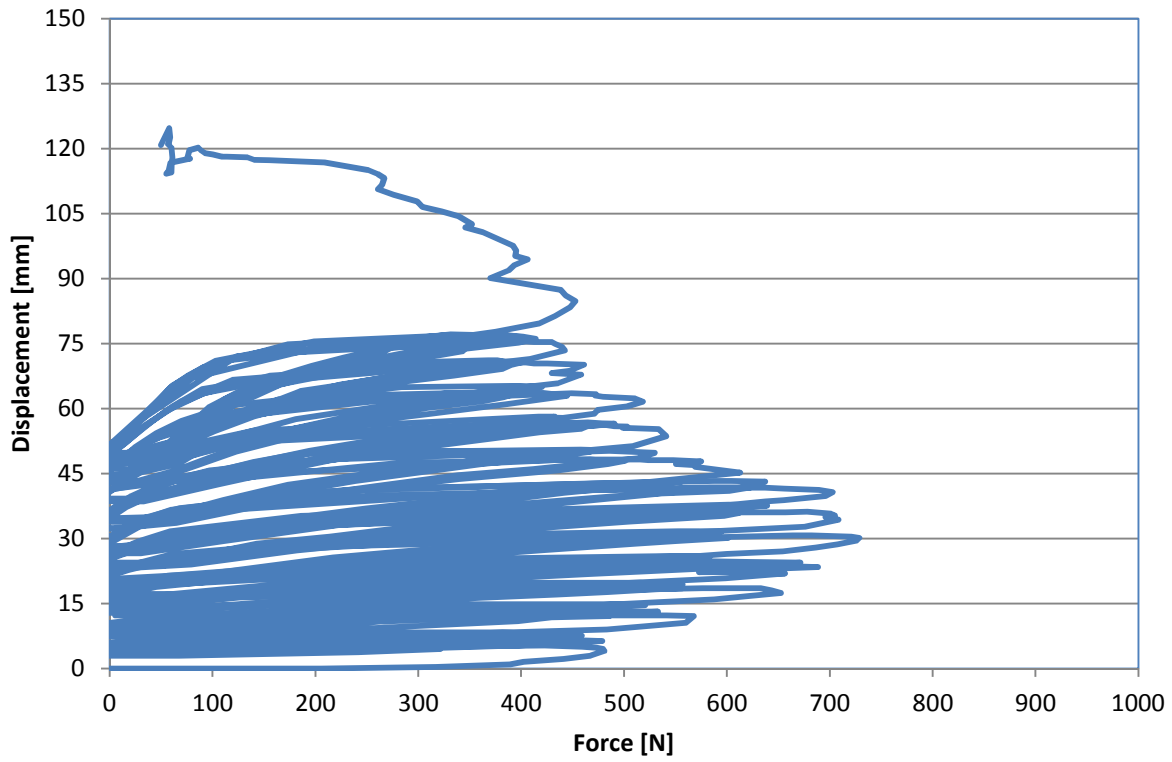
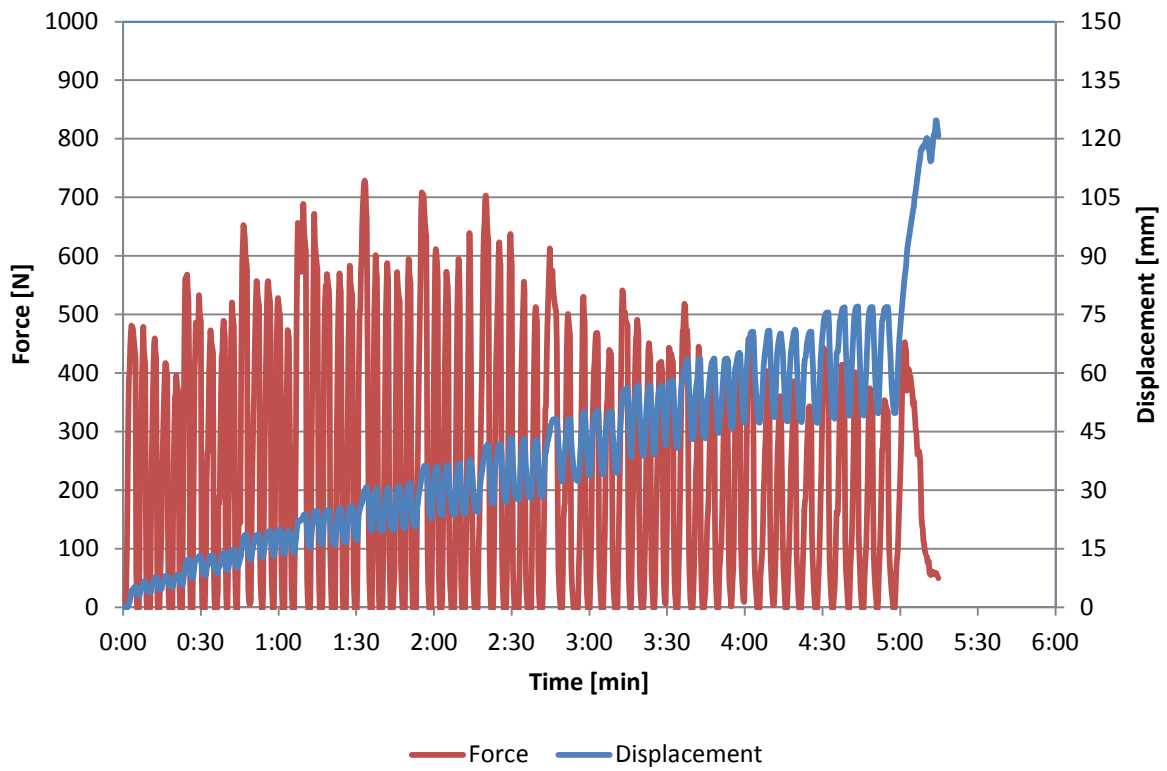




32

Location: N
 Section: 6
 Number: 17

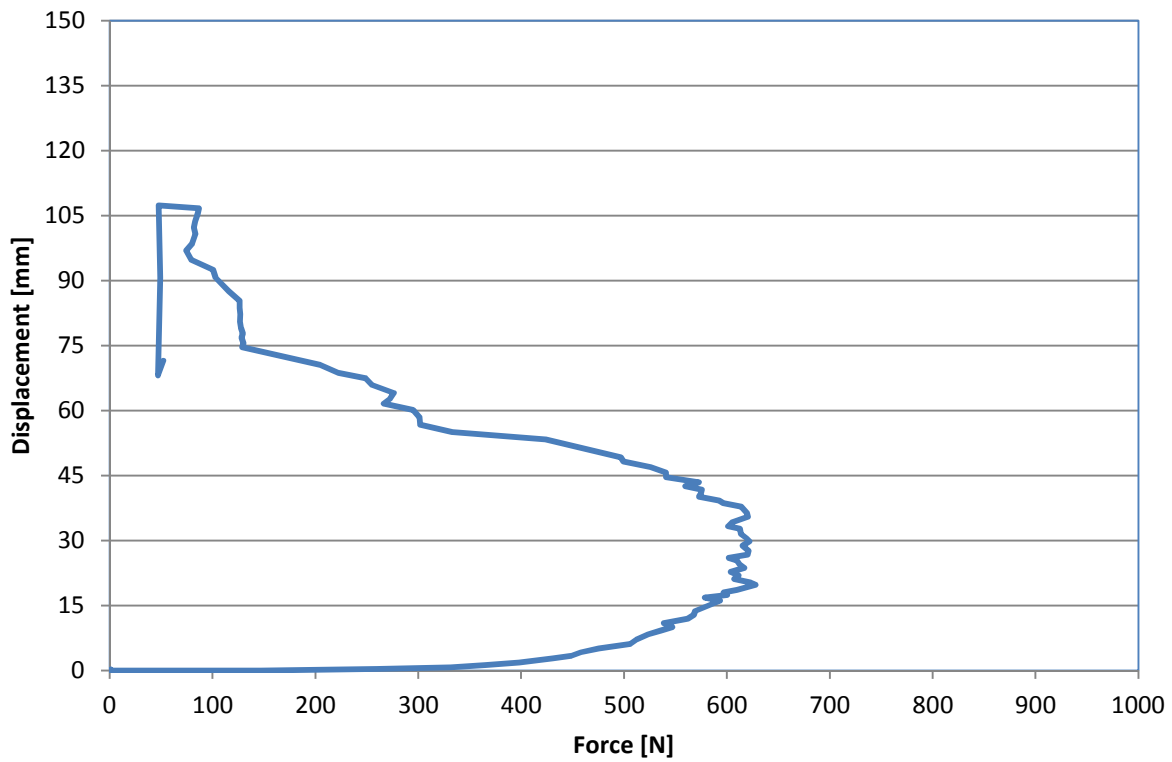
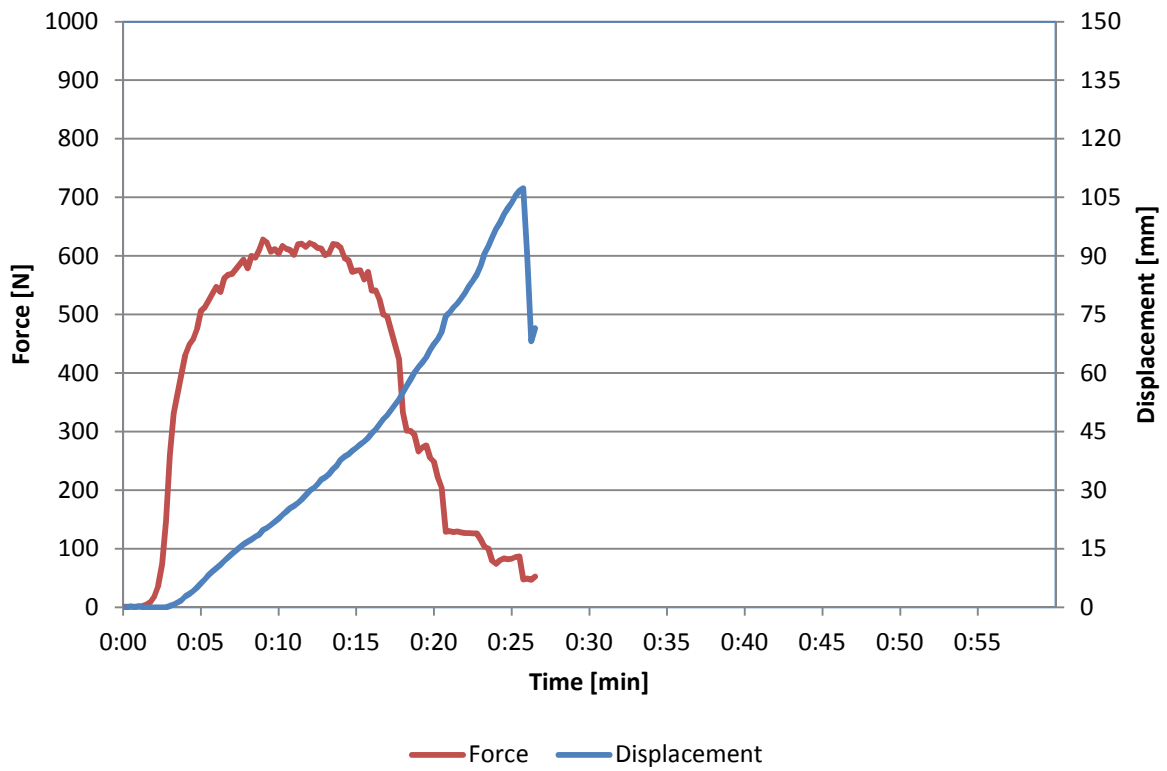
Date: 10-04-2013
 Time: 14:18



33

Location: N
 Section: 6
 Number: 18

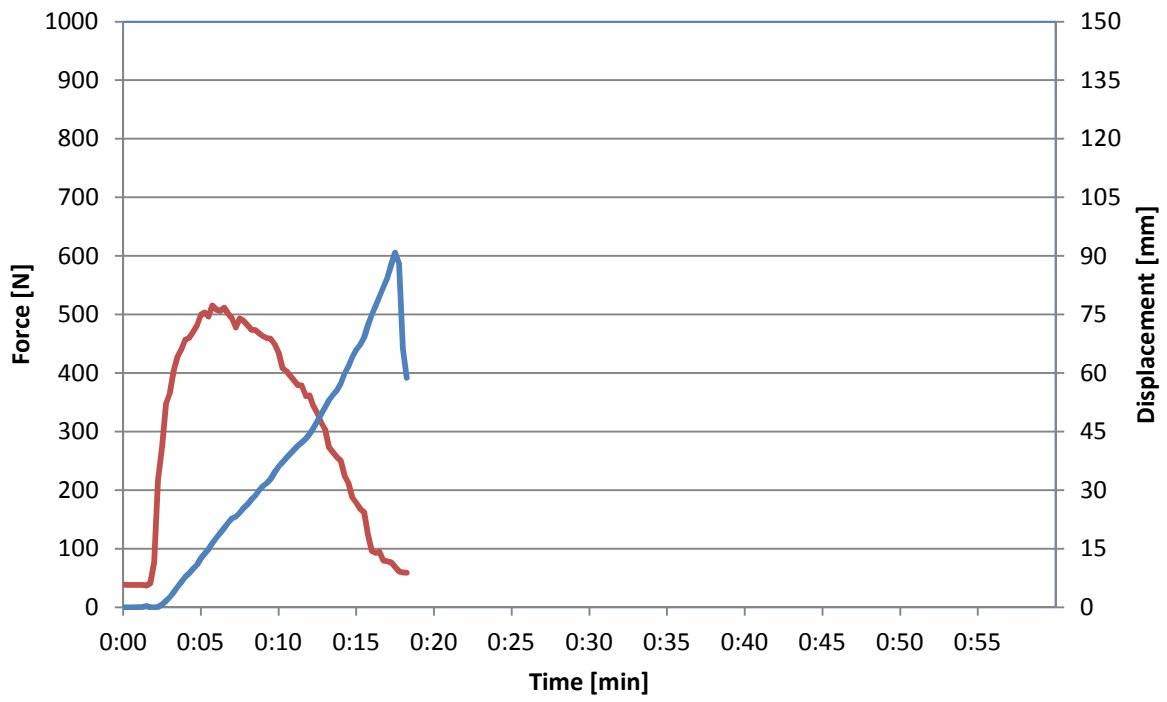
Date: 10-04-2013
 Time: 14:33



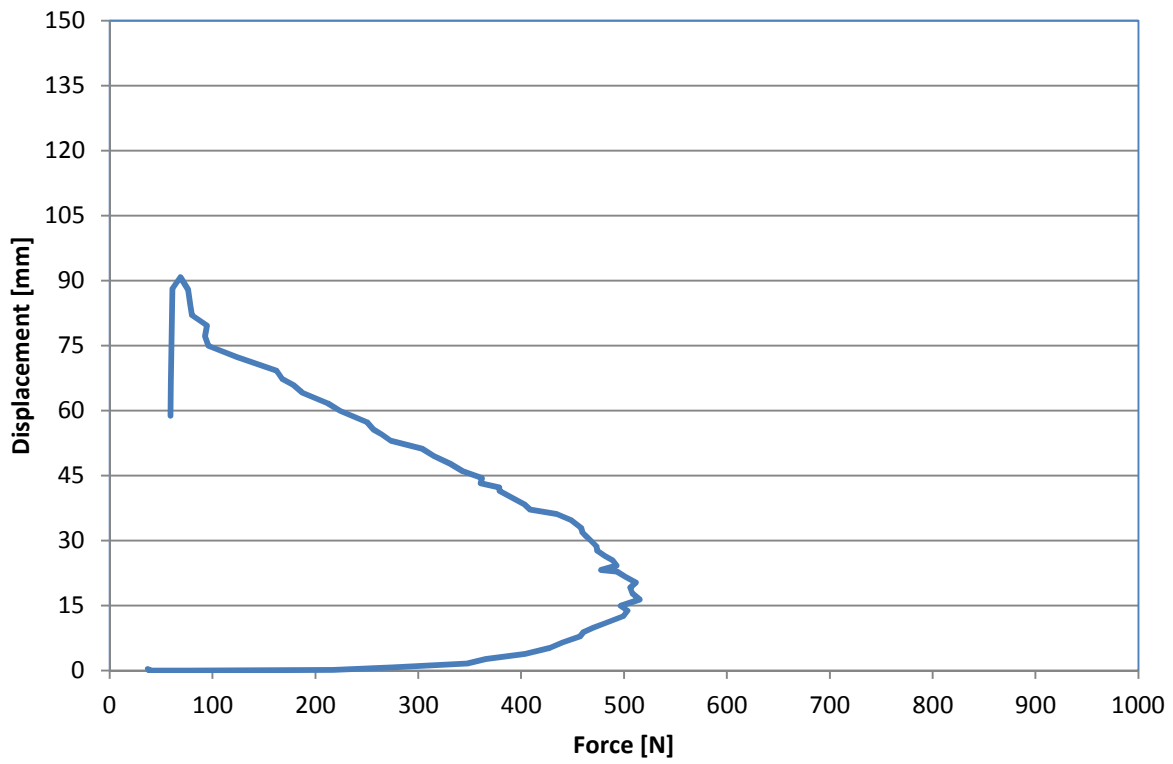
34

Location: N
 Section: 5
 Number: 13

Date: 10-04-2013
 Time: 15:23



— Force — Displacement



35

Location: N
 Section: 5
 Number: 14

Date: 10-04-2013
 Time: 15:31